Synthesis, Catalysis and Theoretical Investigations on Ru(II) and Ru(III)-NHC Complexes

A THESIS

Submitted in partial fulfilment of the

requirements for the award of the degree

of

DOCTOR OF PHILOSOPHY

By

NAVDEEP SRIVASTAVA

DEPARTMENT OF CHEMISTRY
INDIAN INSTITUTE OF TECHNOLOGY INDORE
SEPTEMBER 2024

INDIAN INSTITUTE OF TECHNOLOGY INDORE

CANDIDATE'S DECLARATION

I hereby certify that the work which is being presented in the thesis entitled **SYNTHESIS, CATALYSIS AND THEORETICAL INVESTIGATIONS ON Ru(II) AND Ru(III)-NHC COMPLEXES** in the partial fulfilment of the requirements for the award of the degree of **DOCTOR OF PHILOSOPHY** and submitted in the **DEPARTMENT OF CHEMISTRY, INDIAN INSTITUTE OF TECHNOLOGY INDORE**, is an authentic record of my own work carried out during the time period from July 2018 to September 2024 under the supervision of **Dr. Amrendra Kumar Singh**, Associate Professor, Department of Chemistry, Indian Institute of Technology Indore and **Dr. Ajay Kumar Kushwaha**, Associate Professor, Department of Metallurgical Engineering & Materials Science (MEMS), Indian Institute of Technology Indore .

The matter presented in this thesis has not been submitted by me for the award of any other degree of this or any other institute.

Navdeep Srivastava **15/09/2024**

Signature of the student with date
(NAVDEEP SRIVASTAVA)

This is to certify that the above statement made by the candidate is correct to the best of my/our knowledge.

A Singh 15/09/2024

Signature of Thesis Supervisor with date
(Dr. AMRENDRA KUMAR SINGH)

15-09-2024

Signature of Thesis Supervisor with date
(Dr. AJAY KUMAR KUSHWAHA)

NAVDEEP SRIVASTAVA has successfully given his/her Ph.D. Oral Examination held on 5/5/2025

A Singh 5/5/2025

Signature of Thesis Supervisor with date
(Dr. AMRENDRA KUMAR SINGH)

05.05.2025

Signature of Thesis Supervisor with date
(Dr. AJAY KUMAR KUSHWAHA)

ACKNOWLEDGEMENTS

I would like to express my sincere gratitude to my supervisor Dr. Amrendra Kumar Singh for his valuable guidance and constant support through my Ph.D. journey. I want to thank him for providing research facilities with freedom to work independently to develop new the research ideas. He always encouraged me to come out of my comfort zone and said go ahead to try new things. Also, I sincerely want to thank him for providing opportunities to present my work in various national and international conferences. The scope provided by him to develop my own research goals and to participate in projects within the lab have been helpful in my growth through these years. I would like to thank my co-supervisor Dr. Ajay Kumar Kushwaha for his valuable suggestions and guidance throughout this journey.

I also thank my PSPC members, Prof. Sanjay Kumar Singh, Prof. Rajneesh Misra and Dr. Abhijit Ghosh, for their constructive suggestions and comments to improve the work.

I extend my thanks to all the faculties, staff members and technicians at the Department of Chemistry, IIT Indore, for their guidance and support during my course work, department-related activities, and documentations. I am grateful to the staff members at SIC, Mr. Kinny, Mr. Ghanshyam, Mr. Atul for their help to perform various characterizations.

I also thank IIT Indore, for providing research fellowship.

I would like to extend my sincere thanks to all my current and past lab members for their warm support during these years.

I would like to thank Dr. Dibya, Shambhu Nath, Nida, Rahul, Ekta, Achena, Naveen, Ashu, Vishal, Rohitash, Manan and Priya. I would also like to thank Dr. Shilpi Mishra for her constant motivation and support throughout this journey.

I want to offer thanks to my friends Sandeep, Shivendu, Nirmiti and Shivendra for their support throughout the journey. I also want to extend my special thanks to my wife Dr. Neha Choudhary who has always been there though the ups & downs of the journey. She motivated me and gave me mental support during the hard times. Without her, I cannot imagine this journey possible.

Finally, I would like to thank my parents who has unconditionally supported me and allowed me to pursue my career despite all hurdles. My mother Mrs. Archana Srivastava and my father Mr. Dinesh Kumar Srivastava always encouraged me to be independent and go for further studies. My younger brother Navneet Srivastava was there to take care of the family so that I could focus on my research. They have given me enough freedom to take my decisions and motivated me to keep going. Words are not enough to explain their contribution in this journey and in my life. I owe them a lot. Lastly, I extend my sincere gratitude to everyone who has directly or indirectly contributed to my educational life.

NAVDEEP SRIVASTAVA

Dedicated to my family

ABSTRACT

The investigation embodied in the thesis entitled "**SYNTHESIS, CATALYSIS AND THEORETICAL INVESTIGATIONS ON Ru(II) AND Ru(III)-NHC COMPLEXES**" was initiated in July 2018 in the Department of Chemistry, Indian Institute of Technology Indore. The objectives of this thesis are synthesizing new Ru(II)-NHC complexes bearing the protic and classical NHC in one molecule and study their structural electronic and catalytic application. The theoretical investigation on Ru(III)-NHC precursor complexes utilized in the synthesis of Ru(II)-NHC complexes. The focal points of the thesis are as follows-

1) Design and synthesis of ligands precursors having possibility of protic- and classical-NHC in one molecule.

2) Synthesis of transition metal complexes with CNC-pincer ligand platform having protic- and classical-NHC in same molecule.

3) To compare the structural and electronic properties of protic & classical-NHC and compare the catalytic activity of complexes.

4) Theoretical investigations on our synthetic work of Ru(III)-NHC complexes.

This thesis includes five chapters, and it starts with the general introduction of pincer complexes followed by a discussion about N-heterocyclic carbenes (NHCs) and protic-NHC as ancillary ligands (**Chapter 1**). This is followed by **Chapter 2,** which involves the structural and electronic study of the phosphine-based Ru-CNC pincer complex with protic- or anionic- and classical-NHC in the same molecule in a nearly identical environment. Further, **Chapter 3** includes the Ru-based phosphine-free CNC pincer complexes having mixed protic- and classical-NHC which were used for

oxidant-free dehydrogenation of benzyl alcohols to benzoic acid. **Chapter 4** shows the role of ion-pairs in the synthesis of Ru(III)-NHC complexes. In **Chapter 5,** the conversion of Ru(III)-aNHC to Ru(III)-NHC has been studied computationally. Finally, the thesis concludes with the future outlook focusing on the utilization of protic-NHC complexes for small molecule activation (**Chapter 6**). The contents of each chapter included in the thesis are discussed as follows:

Chapter 1 includes a general introduction about pincer complexes and their importance, followed by a brief discussion about N-heterocyclic carbenes (NHCs) and their bonding with metal. This discussion succeeded by comparing NHC and phosphine as spectator ligands in homogeneous catalysis. Furthermore, the protic-NHC complexes and their role in metal-ligand cooperation are described.

In **Chapter 2**, the first set of pincer complexes with the general formula $[Ru(CNC)(PPh_3)_2Cl]Cl$ having a protic- and classical-NHC in the same molecule and nearly identical environments were synthesized. For this purpose, unsymmetrical imidazolium and benzimidazolium salts of CNC-pincer ligand precursors were synthesized and reacted with $RuCl_2(PPh_3)_3$ precursor. Further, protic-NHC complex was deprotonated to give anionic-NHC complex. A direct comparison between classical-NHC with protic- and anionic-NHC could be possible. The study of the molecular structure of complexes suggested that the bond length for metal carbene bond for the anionic-NHC> protic-NHC> classical-NHC. When compared for these complexes, the electron donation tendency was found to be anionic-NHC> protic-NHC and classical-NHC> protic-NHC. The cooperation between metal and ligand was observed by the reaction of anionic-NHC complex with H_2 gas at 1 atm. pressure which resulted in the heterolytic cleavage of H_2 molecule to give protic Ru-hydride complex.

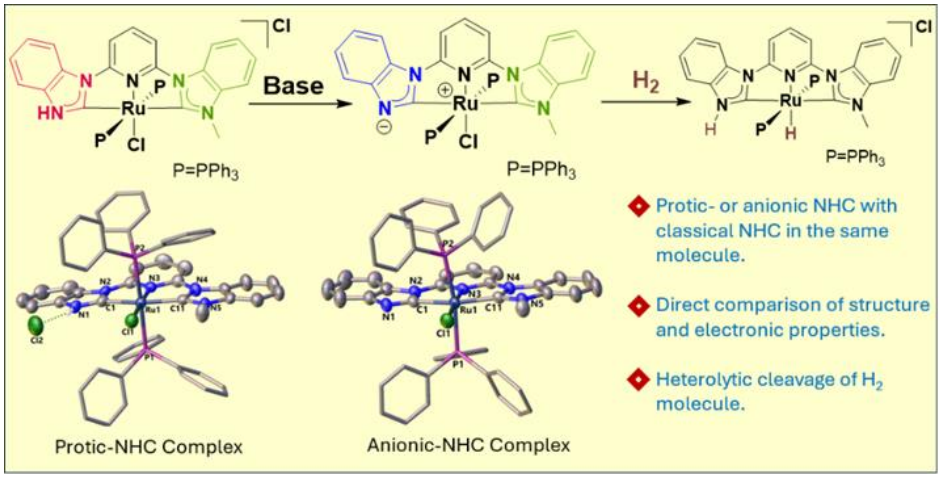

Figure 1. Schematic display of complexes bearing protic-NHC and anionic-NHC with classical-NHC in same molecule and in nearly identical environment.

In **Chapter 3**, new Ru-based phosphine free CNC pincer complexes ([Ru($C^{H}NC^{Me}$)(CN^{Me})I]PF_6, [Ru($C^{H}NC^{Me}$)($CN^{i\text{-}Pr}$)I]PF_6, [Ru($C^{H}NC^{Ad}$)(CN^{Me})I]PF_6, [Ru($C^{H}NC^{Ad}$)($CN^{i\text{-}Pr}$)I]PF_6 with mixed protic- and classical-NHC were synthesized. For this purpose, initially the unsymmetrical imidazolium salts of CNC-pincer ligands precursors were synthesized. The ligands precursors were reacted with the in-house synthesized Ru(III)-NHC precursors to give the desired complexes. The complexes were characterized by various spectroscopic techniques like ^{1}H-NMR, ^{31}P-NMR, ^{13}C-NMR, and HRMS. The molecular structure of complex was determined using a single-crystal X-ray diffraction technique. These complexes were utilized for the oxidant-free, acceptorless dehydrogenation of benzyl alcohols to give the corresponding benzoic acid products. The catalytic activity for these phosphine-free complexes was also compared with the activity of our previously reported [Ru(CNC)(PPh_3)$_2$Cl]Cl complexes. The catalytic activity of the superior catalyst was screened for various aromatic, heteroaromatic, and aliphatic substrates. Mechanistic investigations conducted suggest the formation of

some crucial intermediates. The TON value could go up to 20,000, which is greater than several ruthenium complexes.

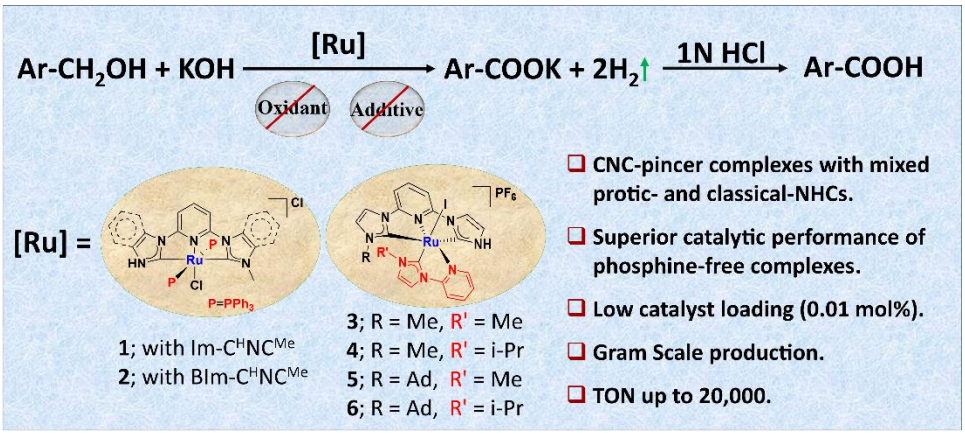

Figure 2. Schematic display of complexes (1-6) with the oxidant-free, acceptorless dehydrogenation of benzyl alcohol.

In **Chapter 4**, the role and effect of contact ion pairs in the synthesis of our in-house reported Ru(III)-NHC complexes has been described. During the synthesis of the Ru(III)-NHC precursor complex, an unusual reactivity was observed. In the presence of Cl^- as counteranion, no product was observed, while in the presence of Br^- as counteranion, mixed halide product was obtained. In the presence of I^- as counteranion, pure product was obtained. To study the role of counteranion, DFT study was performed. The three halides were compared for the electrophilic C-H bond activation during the synthesis of the complex. The NMR and UV-vis spectroscopy indicated the existence of ion pairs in the ligand precursors. DFT modelling suggests two possible pathways for the formation of the product, i.e., halide coordinated pathway and ion-pair pathway. The ion pair pathway was feasible for the Cl^- and I^-, while for the Br^-, the halide coordination pathway lead to a mixed halide complex. The ion-pair mechanism was found to follow the concerted-metalation-deprotonation (CMD) route. In the case of Cl^-, a greater stabilization of the intermediate than the transition state was

observed due to halide coordination or hydrogen bonding with Cl^- ions, which is responsible for the higher activation barrier. The conclusion of the DFT study was validated by the successful synthesis complex by the reaction of corresponding imidazolium precursor salt with Cl^- ion and $RuCl_3 \cdot 3H_2O$ in dioxane solvent at 100 ºC.

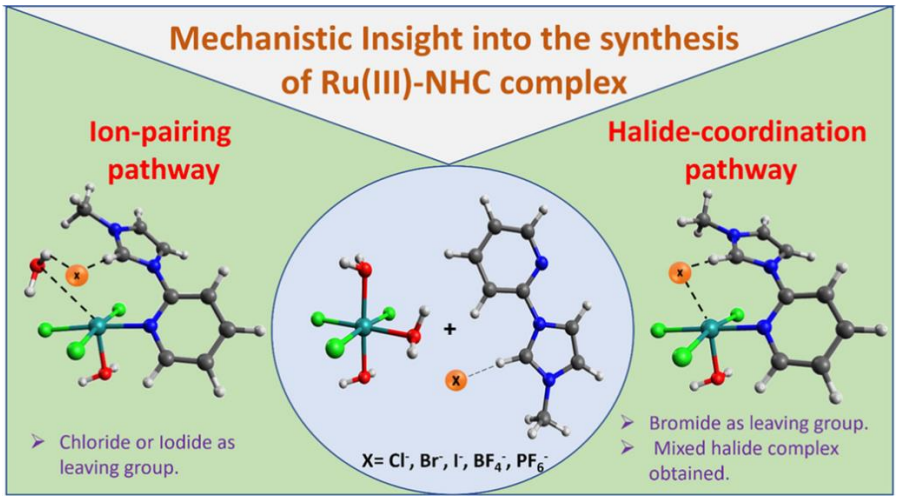

Figure 3. Schematic display of halide coordination pathway and ion-pair pathway for the different counteranion.

Chapter 5 contains the mechanistic investigation on the conversion of Ru(III)-aNHC to Ru-NHC. During the synthesis of Ru(III)-aNHC complex, it has been observed that the Ru(III)-aNHC complex converts to Ru(III)-NHC complex. Therefore, to study the mechanism of this conversion DFT study was performed. The suitable intermediates and transition states were optimized in gases states and their energies corrected for solvation in water. Three possible routes were proposed, i.e., pyridine roll-over (oxidative-addition), pyridine roll-over (halide-assisted), and water-assisted pathway. The pyridine roll-over path involved the proton transfer from pyridine-C3 to the imidazolium-C5. When this proton transfer occurred via the metal centre, it required very high energy. When the same proton transfer happened via chloride, the required energy was lowered. When the proton

transfer took place from the water coordinated to ruthenium instead of pyridine, the pathway called as water-assisted pathway. This pathway required lower energy than the pyridine roll-over pathway; hence, the pathway was found to be feasible for the conversion of Ru(III)-aNHC to Ru(III)-NHC.

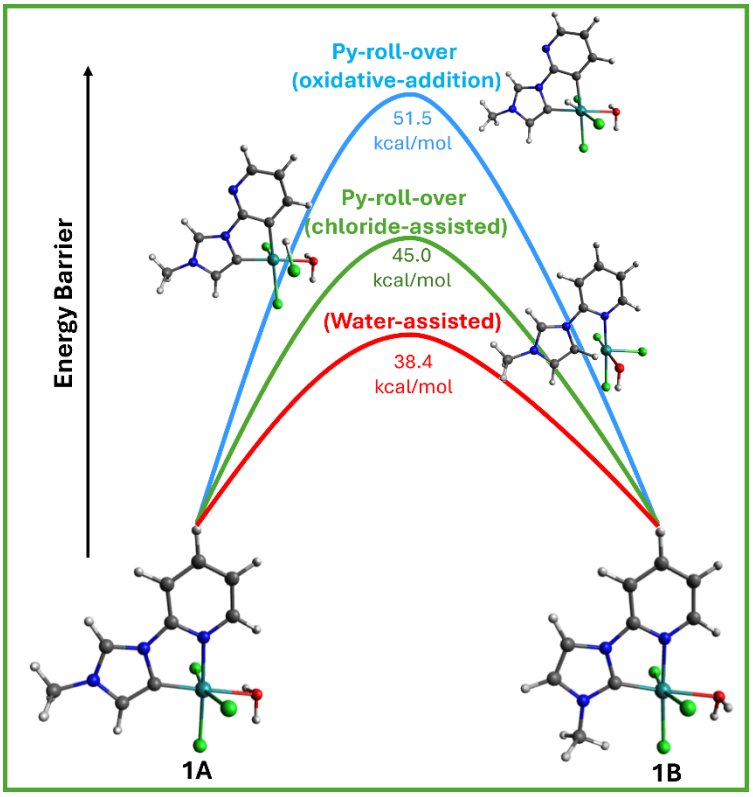

Figure 4. Schematic display of the routes for the conversion of Ru(III)-aNHC (1A) into Ru(III)-NHC (1B)

Chapter 6 includes the conclusion and the future scope of the work.

LIST OF PUBLICATIONS

1. **Srivastava, N**.; Shahid, N.; Singh, A. K.* Insight into the effect of contact ion pairs on C-H bond activation for the synthesis of Ru(III)-NHC complexes: A combined experimental and computational study. *J. Organomet. Chem.,* 2023**, 998**, 122802. Impact Factor: 2.1. DOI: 10.1016/j.jorganchem.2023.122802

2. **Srivastava, N**.; Singh, A. K.* Protic- or anionic-NHCs with classical-NHC in a single [Ru(CNC)(PPh_3)$_2$Cl]Cl pincer complex: Direct comparison of structure & electronic properties and heterolytic H_2 splitting. *Dalton Trans*., 2024, **53**, 6870-6874. Impact factor: 3.5. DOI: 10.1039/d4dt00623b

3. **Srivastava, N**.; Meena, R.; Singh, A. K.* Phosphine-free Ru(II)-CNC pincer complexes with mixed protic- and classical-NHCs in the same molecule for hydrogen production via oxidant-free benzyl alcohol dehydrogenation to benzoic acids. *New J. Chem*., 2024, **48**, 17071-17082. Impact Factor: 2.7 DOI: 10.1039/D4NJ03172E

4. **Srivastava, N**.; Singh, A. K.* Ru(III)-aNHC to Ru(III)-NHC conversion: A computational study. *(Manuscript under preparation).*

Other Publications

1. Shahid, N.; Singh, R.K.; **Srivastava, N**.; Singh, A. K.* Base-Free Synthesis of Benchtop Stable Ru(III)-NHC Complexes from $RuCl_3 \cdot 3H_2O$ and Their Use as Precursors for Ru(II)-NHC Complexes. *Dalton Trans.*, 2023**, 52**, 4176. Impact Factor: 3.5

Conferences/Workshop/Oral/Poster presentation

Poster presentation

1. Presented poster in the 19th International Conference on **"Modern Trends in Inorganic Chemistry (MTIC XIX)- 2022"** organized by Department of Chemistry, Banaras Hindu University, Varanasi on December 15-17, 2022.

2. Presented poster in #RSCPoster twitter conference-2023 on February 28 - March 1, 2023

3. Presented poster and won the best poster award in the International symposium on "**Frontiers in Sustainable Catalysis and Organometallic (FISCO-2024)**" during July 11-12, 2024 organized by Department of Chemistry, Malaviya National Institute of Technology Jaipur.

Oral presentation

4. Won the best oral-presentation award in the "***In-House Symposium CHEM-2020***" organized by Department of Chemistry, IIT-Indore, India on March, 06, 2023.

5. Won the best paper presentation award in the National Seminar on "**Frontiers in Chemical Research: Exploring New Horizons (FCRENH-2024)**" organized by Department of Chemistry, Ram Jaipal College, Chapra on November 29-30, 2024.

Webinar/workshops attended

1. Attended national workshop on "Workshop on NMR & Mass" on December 2019 at CSIR-CDRI Lucknow.

TABLE OF CONTENTS

Chapter 2

Protic- or anionic-NHCs with classical-NHC in a single [Ru(CNC)(PPh_3)$_2$Cl]Cl pincer complex: Direct comparison of structure & electronic properties and heterolytic H_2 splitting

Chapter 3

Phosphine-free Ru(II)-CNC pincer complexes with mixed protic- and classical-NHCs in the same molecule for hydrogen production via oxidant-free benzyl alcohol dehydrogenation to benzoic acids

Chapter 4

Insights into the effect of contact ion-pairs on C-H bond activation for the synthesis of Ru(III)-NHC complexes: A combined experimental and computational study

Chapter 5

Ru(III)-aNHC to Ru(III)-NHC conversion: A Computational Study

Chapter 6

Conclusions and Future Scope

LIST OF SCHEMES

LIST OF FIGURES

LIST OF TABLES

NOMENCLATURE

α	Alpha (angle)
β	Beta (angle)
υ	Gamma (angle)
Å	Angstrom
Λ	Wavelength
M	Micro
σ	Sigma
δ	Delta
Π	Pi
J	Coupling constant
Hz	Hertz
MHz	Mega hertz
K	Kelvin
D	Density
V	Volume
mM	Milli Molar
Cm	Centimeter
μL	Microliter
mL	Milliliter

ACRONYMS

DFT	Density Functional Theory
CO	Carbon Mono Oxide
CO_2	Carbon Dioxide
KOH	Potassium Hydroxide
NaOH	Sodium Hydroxide
MeOH	Methanol
DCM	Dichloromethane
ACN	Acetonitrile
RT	Room Temperature
℃	Degree Celsius
◦	Degree
K	Kelvin
pH	Potential Of Hydrogen
min	Minutes
h	Hour
nm	Nanometer
mmol	Millimole
Conv.	Conversion
Atm	Atmosphere (pressure)
a.u.	Arbitrary Unit
eV	Electron Volt
GC-MS	Gas Chromatography–Mass Spectrometry
NMR	Nuclear Magnetic Resonance
UV-vis	UV-visible Spectroscopy
ESI-MS	Electrospray Ionization- Mass Spectrometry
TLC	Thin Layer Chromatography

SCXRD	Single crystal X-ray Diffraction
GOF	Goodness of fit
Ar	Argon
O_2	Oxygen
H_2	Dihydrogen
N_2	Nitrogen
o	*ortho*
m	*meta*
p	*para*
Ru	Ruthenium
Ir	Iridium
Os	Osmium
NHC	*N*-heterocyclic carbene
PPh_3	Triphenylphosphine
AAD	Acceptorless Alcohol Dehydrogenation
s	Singlet
d	Doublet
t	Triplet
q	Quartet
m	Multiplet
r.t.	Room temperature
TON	Turnover number
TOF	Turnover frequency

CHAPTER 1

Introduction

1.1 Pincer Ligands

In 1976, Moulten and Shaw reported for the first time a tridentate chelating moiety 2,6-bis(di-t-butylphosphino) methylphenyl.[1,2] This diphosphine ligand and its corresponding complexes remained unnoticed for a decade. Later, after observing their extraordinary property of thermal stability, these tridentate complexes again came into the picture.[3] The pincer ligands provide high thermal stability to the complexes, making them a robust catalyst. The word pincer was coined by Van Koton in 1989 from a Dutch word *tang*, which means wrench or spanner in that language.[4][5] Pincer ligands are tridentate ligands that provide strong bonding and high stability to metal and allow meridional geometry around the metal center.[6] The selectivity of pincer complexes for meridional geometry differs from that of tripodal ligands, which prefer facial arrangement around the metal center.[6] It is the modular nature of the pincer ligand that makes it essential. The steric and electronic properties of pincer ligands can be fine-tuned without significantly modifying the coordination sphere (Figure 1.1).[7,8]

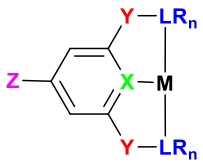

GROUP	EFFECTS OF VARIATION
LRn (L=P,N,S,O,As)	Electroni control by variation of L Steric control by variation of R
Y (Y=O, NH, (CH2)n	Control of reactivity: Introduction of chirality
X (X=N, C, B)	Electronic effect majorly trans-influence
Z (Halogen, R, OR)	Distant control of electron density

Figure 1.1. Variable parameters that regulate the steric and electronic properties of pincer ligands.

1.2 N-Heterocyclic Carbenes (NHCs)

Carbenes, ever since their discovery, have proved to play a vital role in organic synthesis by adding a single carbon atom to a molecule. Carbenes are neutral species with a divalent carbon and $6e^-$ in the valence shell. The incomplete octet makes the carbenes unstable and highly reactive. Carbenes are categorized as singlets or triplets, as shown in Figure 1.2.[9]

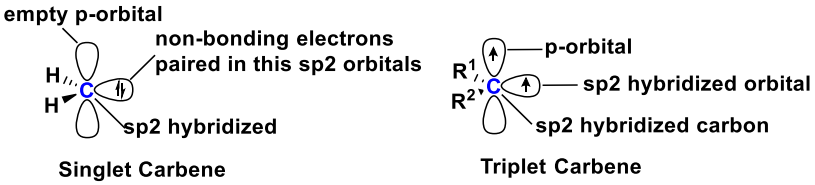

Figure 1.2. Geometry and hybridization of carbene: Single head arrow indicates electron.

The first introduction of carbenes in inorganic and organometallic chemistry was made in 1964 by Fisher and his coworkers.[10] After the discovery of the first metal-carbene complexes **1**, Ofele[11] and Wanzlick[12] *et al.* described complexes **2** and **3** containing N-heterocyclic carbenes (Figure 1.3).

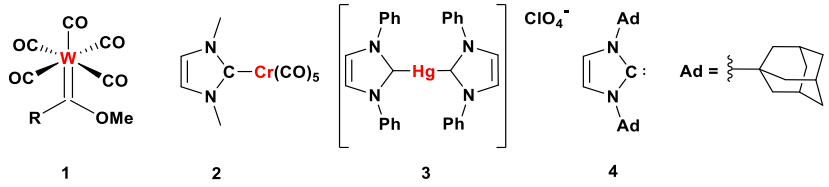

Figure 1.3. Early examples of carbene and NHC complexes.

Arduengo *et al.* in 1991 reported an isolable and bottleable first N-heterocyclic carbene (NHC), 1,3-di(adamantyl)imidazol-2-ylidene **4**[13], which further led to synthesis and theoretical studies on a series of new NHCs.

1.3 General properties and structural study of NHC

NHCs can be defined as heterocyclic species bearing a carbene carbon and at least one hetero atom within the ring structure.[14,15] N-heterocyclic carbenes are far less reactive when bound to metals than Schrock carbenes and Fischer carbenes, the two main families of carbene ligands.[16] NHCs are regarded as spectator ligands in comparison to these two categories of ligands.[16] Unlike many other reactions commonly associated with metal carbenes, NHCs do not undergo cyclopropanations or metathesis reactions.[17] N-heterocyclic carbenes are electron-rich nucleophilic species, unlike other carbenes, which are typically electrophilic.[17] The exceptional stability of the carbene center can be partially explained by the combined electronic and steric impact of the structural characteristics. The general representative structure of the NHC, as given by the first isolated compound given by Arduengo *et al.,* is shown in Figure 1.4. Since NHCs typically have bulky substituents (adamantyl group in **4**) next to the carbene carbon, which sterically disfavor dimerization to the corresponding olefin, they help kinetically stabilize the species (the Wanzlick equilibrium).

NHCs, in contrast to classical carbenes, have a singlet ground-state electronic configuration with an unoccupied p-orbital at the C2 carbon and a formally sp2-hybridized lone pair at the highest occupied molecular orbital (HOMO) and lowest unoccupied molecular orbital (LUMO), respectively (Figure 1.4 b). The adjacent nitrogen heteroatom stabilizes the structure due to its σ-electron withdrawing tendency, which lowers the energy of σ-orbitals inductively, and by π-electron donating tendency, which increases the electron density into the empty p-orbital mesomerically. NHCs are cyclic, which forces the carbene carbon into a bent, more sp2-like structure, favoring the singlet state.

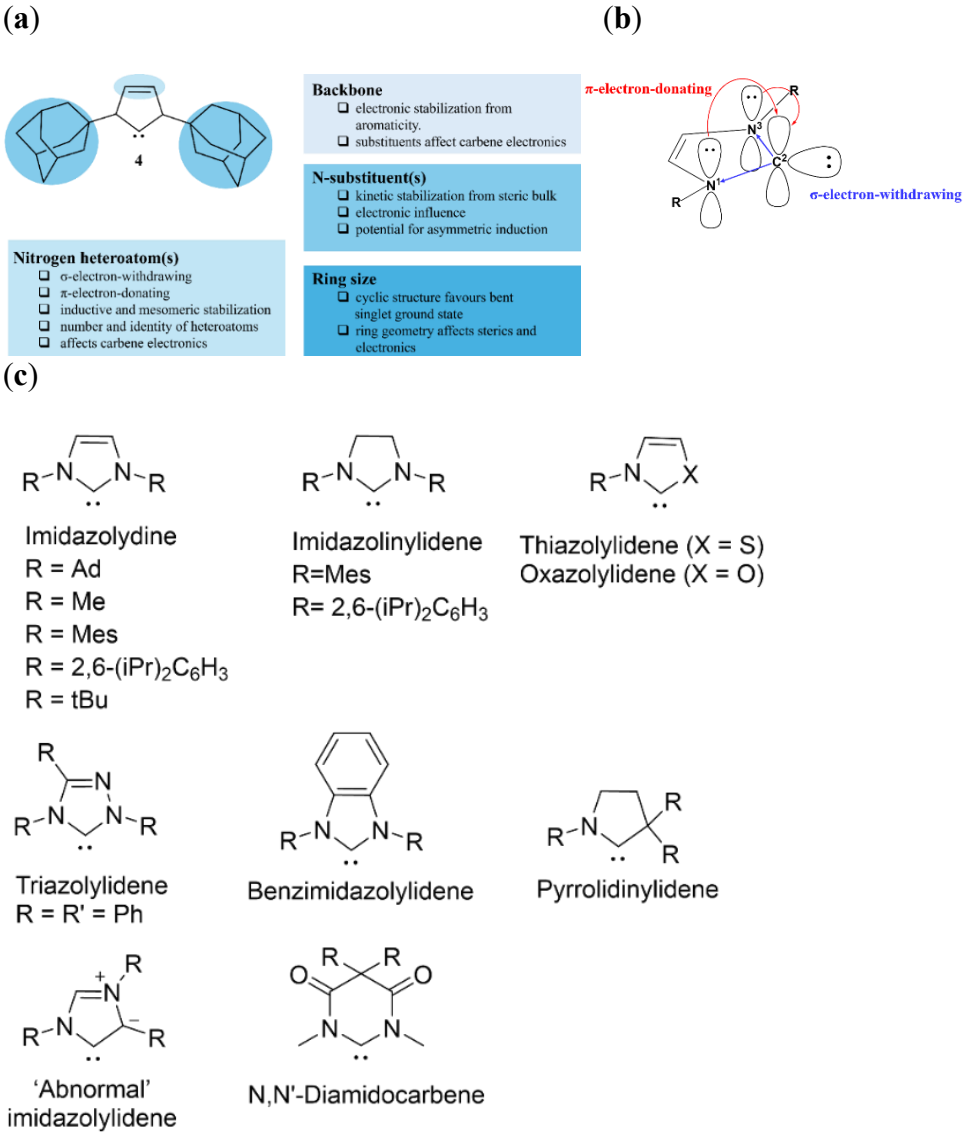

Figure 1.4. Structural features of NHC. (**a**) The general structure of **4** describes the effect of backbone, nitrogen substituents, ring size, and nitrogen heteroatoms on the stability and reactivity of the NHC. (**b**) The general structure of imidazole-2-ylidine, where the σ-withdrawing and π-donating nature of nitrogen atoms are the reasons for the stability of the singlet carbene structure. (**c**) Some examples of different classes of NHC. Ad = adamantyl; Me = methyl; Mes = mesityl; tBu = tert-Butyl; iPr = iso-Propyl; Ph = phenyl.

The ground-state structure is represented in the C2-N bond lengths (1.37Å) found in, which indicate that the C2 nitrogen bonds have partial double bond character and fall between those of the equivalent imidazolium salt (1.32Å)[13] and its C2 saturated counterpart (1.49 Å) (Figure 1.5**)** [18].

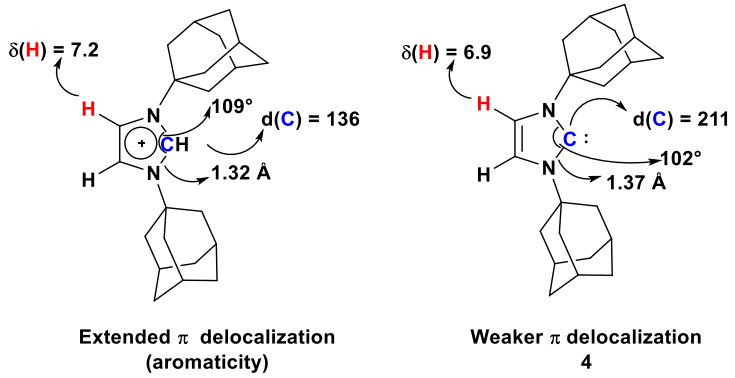

Extended π delocalization (aromaticity)

Weaker π delocalization 4

Figure 1.5. Geometric and spectroscopic parameters of the first isolated free carbene **4** and the corresponding imidazolium ion.

Although the proportional relevance of each effect varies from compound to compound, these broad principles of carbene stabilization apply to all classes of NHC (Figure 1.4c). The partial aromaticity of NHCs produced from heteroaromatic compounds provides a higher level of stability. This effect permits a lower requirement for proximal steric bulk, which is why the simple methyl-substituted NHC 1,3-di(methyl)imidazol-2-ylidene is persistent in solution.[19] It has been estimated to be approximately 25 kcal/mol for model imidazol-2-ylidenes.[20] When the carbene center is generated at places other than C2, the species stabilized by a single nitrogen atom may arise (Figure 1.6). In general, these mesoionic or "abnormal" carbenes are more electron-donating than their "normal" analogs and can exhibit a wide range of behaviors.[21,22] It is impossible to construct a neutral, non-zwitterionic carbene resonance structure for them.

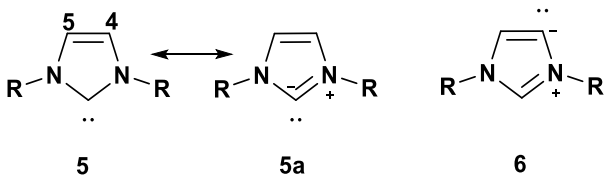

Figure 1.6. Normal-NHC (NHC) and Abnormal-NHC (aNHC).

1. 4 Electronic properties of NHCs

The successful isolation of (1,3-bis(adamantyl)imidazol-2-ylidene) by the deprotonation of the corresponding imidazolium chloride precursor has been a key event in the history of NHCs (Scheme 1.1).[13] The investigation of the characteristics and reactivity of this class of compounds was possible due to the continuous synthesis and isolation of stable NHCs. DFT study[23], ^{13}C NMR[24] and X-ray photoelectron spectroscopic investigations[25] were conducted. The investigation suggests the carbonic structure instead of the ylidic structure. In imidazolylidenes, the HOMO is the lone pair located on the carbene carbon, whereas, in silylenes and germylenes, HOMOs are the π-orbitals concentrating closer to the center of Si or Ge as the atomic number increases.[26]

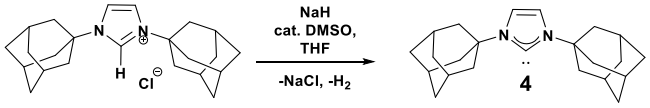

Scheme 1.1. Synthesis of the first isolated NHC **4** from imidazolium chloride precursor.

Electron density mapping on model carbene by Arduengo *et al.* revealed that the low reactivity of NHCs towards nucleophiles was caused by a significant electron density on the nitrogen atoms in addition to the expected electron density of the singlet carbene.[27] This electron mapping study also indicated little or no contribution from the ylidic resonance. Further study about the electronic nature of NHC suggested that the electron mapping method may not be appropriate for this purpose.[28] Experimental and theoretical studies were performed to study the electron delocalization

in imidazolylidenes and imidazolidinylidenes.[20,28] The study concludes that imidazolylidenes have a partial aromatic character that provides extra stability, whereas the imidazolidinylidenes do not have such aromatic character (Figure 1.7).[29]

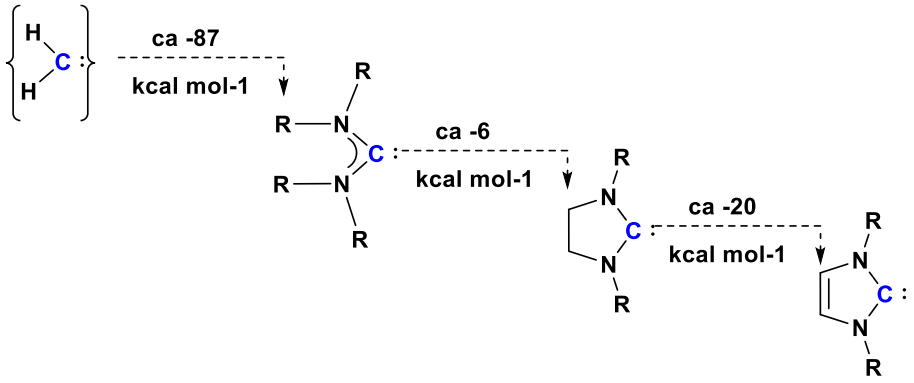

Figure 1.7. A downhill energy pathway leads from methylene to isolable heterocyclic carbenes.

The DFT calculations indicated carbene stabilization by adjacent nitrogen atoms because of their electron-withdrawing tendency along the σ-bond and the electron-donating tendency through which the lone pair of nitrogen is donated to the empty p-orbitals on carbenes. The stability of the carbene is decreased when the orientation of the nitrogen orbitals does not align with the empty p-orbital on the carbene.[30]

1.5 Stability of NHC

The study of steric and electronic properties can help understand the stability of NHCs and related species.[15] The unstable NHC tends to undergo dimerization by forming a double bond between the C2-centers (Figure 1.8).[31] The energy gap between singlet and triplet states of carbenes has been explained to be the reason behind the phenomenon of dimerization.[32,33] It is the long-lived singlet carbene preferred over the unstable triplet carbene ($t_{1/2}$ up to *ca.* 1 h at most)[34] in modern chemistry applications. The enthalpy of dimerization (E_{dim}) calculated by DFT predicted the stability of NHC. The estimated values of E_{dim} could also

predict the experimental behavior of NHC, i.e., when $E_{dim} \leq -20$ kcal/mol, the NHC is stable in the form of a dimer, whereas when the $E_{dim} \geq 0$ kcal/mol, the NHC is stable in the form of a monomer. For the between values, the NHCs exist as an equilibrium mixture between monomer and dimer.

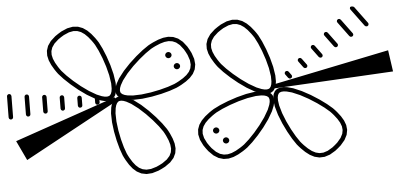

Figure 1.8. Transition state geometry for the dimerization of singlet carbenes.

The σ-electron withdrawing group on carbene increases the energy gap between the π orbital and σ-orbital, favoring the singlet carbene, while the π-electron donating group stabilizes the carbene via interaction, resulting in bent carbenes (NHC belongs to this class). The π-electron withdrawing substituents favor linear singlet carbenes by breaking the p_x/p_y degeneracy. The two effects are combined when the substituents are π-electron withdrawing and π-electron donating groups, stabilizing the carbene and favoring the singlet state. Bertrand displayed the impact of π-electron donating and π-electron withdrawing groups on the stability of carbene (Figure 1.9).[15] Triplet carbenes are generally more inclined toward a bent geometry (where the p_x and p_y orbitals are degenerate) than singlet carbenes are toward a linear geometry.

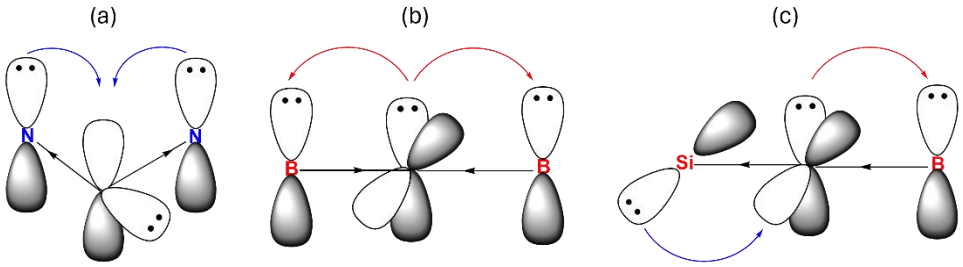

Figure 1.9. Examples of singlet carbenes stabilized by (a) two π-electron-donating substituents, (b) two π-electron-withdrawing substituents, and (c) a π-electron-donating substituent and a π-electron-withdrawing substituent.

1.6 The nature of bonds of NHCs

The ligand-metal bonding in the case of NHC is more complicated than that of phosphines. The contribution of σ- and π-bonding to metal centers in the case of NHCs has always been a subject of interest, while the phosphines involve the bonding to metal through σ-donation and π-backbonding. Tulloch *et al.* observed a shorter bond length for Cu-$C_{carbene}$ in copper-NHC complexes than the average Cu-C σ-bond distances.[35] A significant π-interaction between the carbene p-π orbitals and d_{xz} and d_{yz}-orbitals of the metal center in (NHC)Ag complexes was observed by Hu *et al*. Theoretical investigations further support these interactions and suggest a 15-30 % contribution of the overall orbital interaction energy.[36] Further, crystallographic evidence showed a lengthening of the N–$C_{carbene}$ distance in bis(NHC) (**7-9**) complexes as the metal centers became more electron-rich, allowing them to participate more in π-back bonding (Figure 1.10).

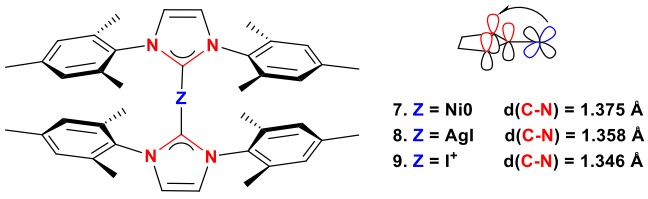

Figure 1.10. The effect of metal center electron density on the N–$C_{carbene}$ distance in some NHC–metal complexes.

The π-donation tendency of NHC to metal was shown by Covallo and coworkers. DFT calculations were performed on complexes **10** and **11**, reported by Nolan and coworkers.[37] The DFT calculations and crystallographic study indicate different Ir-C bond lengths for both carbenes (Figure 1.11). This difference in the bond length may be attributed to the partial π-donation into the d-orbitals of the metal center. Further, a study was performed on the series of NHC complexes with d-electrons from d0-d10.[38] When species with a low d-electron count are considered, both π-donation and π-backbonding contribute; when species with more d-electron counts are considered, π-backbonding dominates.

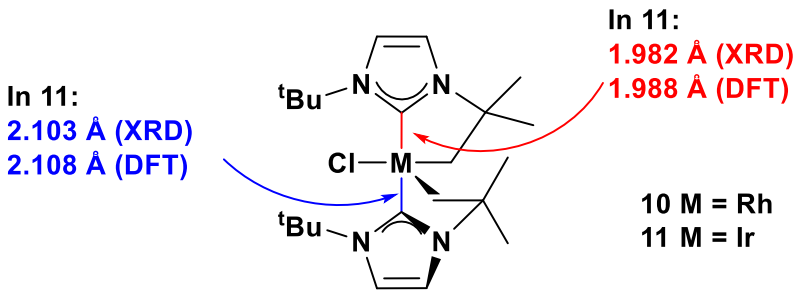

Figure 1.11. The bis(NHC) complexes reported by Nolan *et al.* and the DFT study performed by Covallo *et al*.

1.7 Quantitative measures for steric and electronic properties

It has been known that a ligand's combined steric and electronic properties are responsible for the lone pair's availability on the carbene.[39] Nolan, Cavallo, and coworkers developed buried volume parameters (%V_{bur}), which could be used to quantify the steric properties of NHC conveniently.[40] %V_{bur} represents the proportion of the sphere occupied by the ligand after it has coordinated with the metal in its center in an NHC (Figure 1.12). Metal–carbene bond distances of 2 Å and sphere radius diameters of 3Å or 3.5Å are commonly used for higher %V_{bur} values to indicate that the ligand exerts a more significant steric influence on the metal center. The %V_{bur} can be calculated using theoretical calculations or

crystallographic data. Azolium salt precursor, free-NHC, or several metal-NHC complexes can be used as suitable data sources.

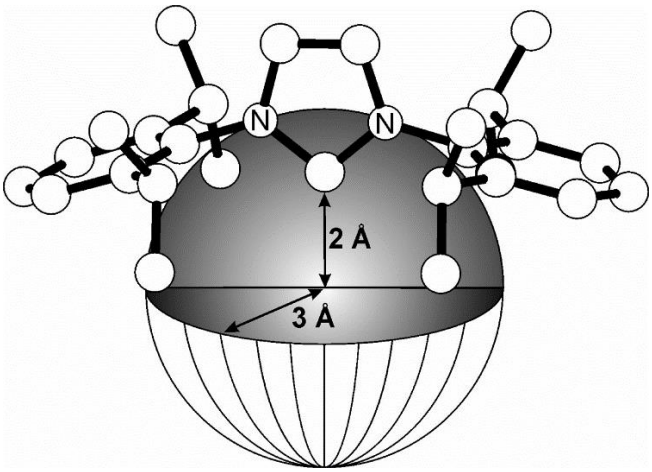

Figure 1.12. Sphere dimensions for steric parameter determination (%V_{Bur}) of NHC ligands.[40]

Tolman electronic parameter (TEP) describes the electronic properties of NHCs.[41] In particular, TEP measures the infrared stretching frequencies of carbonyl ligands to assess a ligand's capacity to donate electrons. As the tendency for ligand donation increases, the metal center becomes more electron-rich, increasing the degree of π-backbonding into the carbonyl ligands, reducing their bond order and infrared stretching frequency (Figure 1.13). The greater the electron tendency of ligands, the lower the stretching frequency of carbonyl ligands. TEP was initially developed for phosphines, where [$LNi(CO)_3$] based complexes were employed as initial model species for calculation. In contrast to absolute electron density at the metal, the TEP measures the p-donating ability of the metal center. As a result of differences in ligand-metal bonding, e.g., between imidazolylidenes and imidazolidinylidenes, the TEP may not be the best indicator of ligand-donating properties.[26]

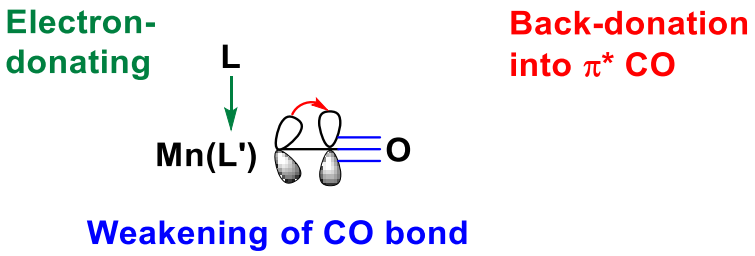

Figure 1.13. Representation of metal carbonyl complexes, used to determine the electronic properties of NHC by IR spectroscopy.

Crabtree and coworkers reported "abnormal" imidazolylidene **12** and "normal" imidazolylidene **13**, **14** & **15** and evaluated their Tollman electronic parameter (TEP) (Figure 1.14).[42] It has been shown that the abnormal-based imidazolidine has a greater electron donation tendency than the normal-based imidazolidine.

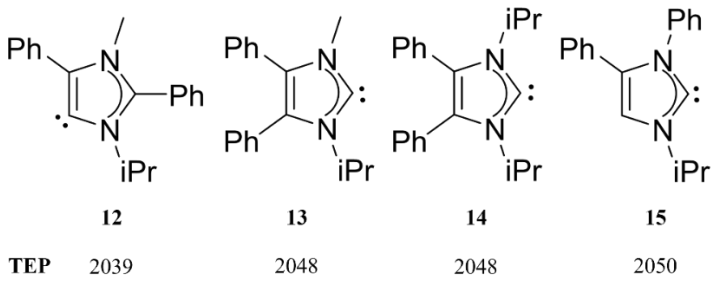

Figure 1.14. Electronic properties of previously reported imidazolylidenes.

1.8 Advantages of N-heterocyclic carbenes (NHC) over phosphine as a spectator ligand

NHCs have come to replace phosphines in many organometallic and organic reactions for several reasons[43]-

- NHCs have mostly comparable or superior activity to phosphines.
- NHCs tend to donate electrons more than phosphines.
- NHCs are easy to make on a large scale.

- The salts of the carbenes are stable without decomposition in air (phosphines degrade at higher temperatures and oxidize upon exposure to air).

Milstein *et al.* reported phosphine-based Ru-PNN pincer catalyst **16** for ester hydrogenation with low TOF.[44] Later, Song *et al.* reported NHC-based Ru-CNN pincer catalysts **17** and **18,** utilized for ester hydrogenation with significantly higher TOF values (Figure 1.15).[45]

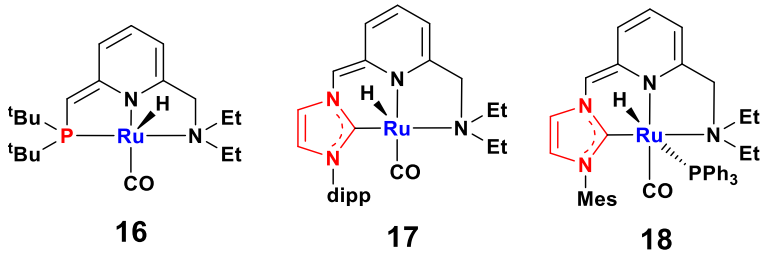

Figure 1.15. Ruthenium catalyst for ester hydrogenation.

1.9 General route for the synthesis of NHC complexes

N-substituted azolium salts are typically the first step in manufacturing NHC complexes. The two synthetic pathways that lead to these precursors are usually complementary: [46] (i) nucleophilic substitution, which begins at the imidazole heterocycle (figure 1.16),[47–49] and (ii) a multi-component reaction (figure 1.17)[29,50,51] that builds up the heterocycle with the necessary substituents in a single step.

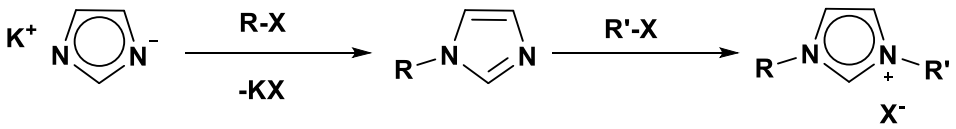

Figure 1.16. Synthesis of imidazolium salt from imidazole.

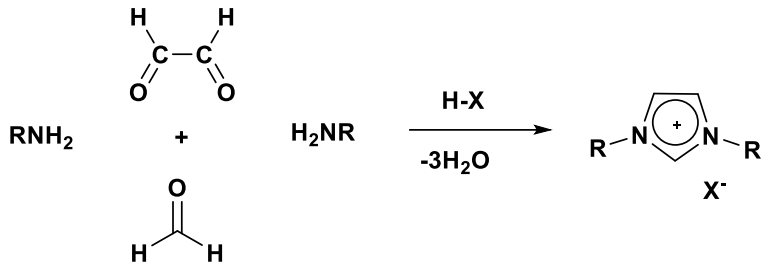

Figure 1.17. Synthesis of imidazolium salt *via* ring formation.

The transition metal NHC complexes can be synthesized from imidazolium salts through various methods, including (i) proton abstraction using bases (e.g., BuLi) before metalation (free carbene route),[19,52–54], (ii) metalation with a basic metal precursor such as $Pd(OAc)_2$ and $[Ir(COD)(OEt)]_2$ (direct metalation),[55–57] (iii) metal exchange commencing from silver carbenes (transmetalation),[58,59] and (iv) oxidative addition of carbon-halogen bonds to low-valent metal precursors.[60,61] Direct base-free activation of C-H bonds, analogous to arene mercuration.[62] The most common method for the metalation of NHC is *in situ* deprotonation of the imidazolium precursor.

Among the three, the *in situ* deprotonation pathway is the most followed method for synthesizing NHC complexes. The imidazolium C2-H proton, being acidic, requires a basic anion for the deprotonation. The basic anion on the metal precursor or the azolium salt may lead to deprotonation and, hence, complexation. Figure 1.18 shows an example of the *in situ* deprotonation by metal precursor.[11]

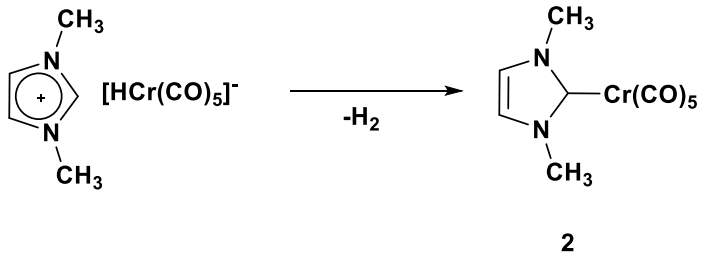

Figure 1.18. Example of *in situ* deprotonation by basic metalates.

In the case of counteranion as basic anion, the C2-H bond activation takes place by the hydrogen bonding interaction between the C2-H proton and the anion. This cation-anion pair is called the contact ion pair.[63] Recent research has demonstrated that the acidity of the C2-in imidazolium ionic liquids is contingent upon the character of the counteranion, in addition to the cationic moiety.[64] Thus, the rate of deprotonation may be substantially influenced by the counteranion's basicity in conjunction with its hydrogen-accepting capacity.

In the past decade, reports have shown that halides are essential for forming transition metal complexes with the protonated precursor of the mesoionic-NHC.[65–68] In some cases, adding a halide from outside simulated the formation of complexes.[69,70] C-H bond polarization with halides has been observed to follow the order $Cl^- > Br^- > I^-$.[71] However, with bulkier non-coordinating anions like BF_4^- and PF_6^-, poor C-H bond activation due to relatively weaker hydrogen bonding was observed.[71]

1.10 Ruthenium-NHC complexes as catalysts

NHCs are advantageous as ligands because of their strong σ-donor and weak σ-acceptor characteristics, which frequently aid intramolecular C-H bond activation and result in highly stable cyclometallated complexes.[72–75] In the last three decades, Ru-complexes have been found to be valuable in organometallic chemistry and catalysis. Ru-NHC complexes are remarkably versatile in catalytic applications, offering effective ways to transform renewable resources and produce valuable products.[22,74,76–80] These complexes are effective in various processes, including C-H activation, metathesis, cross-coupling reactions, and (de)hydrogenation.[81–88] The distinct electronic and steric characteristics of NHC ligands and the tunable reactivity of ruthenium enable them to participate in various bond activations and transformations. Ru-NHC complexes are highly versatile tools in synthetic chemistry, especially when used as phosphine-free catalysts. Conventional transition metal catalysts

frequently use phosphine ligands to stabilize the metal center and control reactivity; nevertheless, using phosphine ligands can have some disadvantages, such as toxicity, sensitivity to oxygen and moisture, and restricted ligand tunability.[89–92] Among other advantageous characteristics, the well-established effectiveness of NHC–Ru complexes can be attributed to ruthenium's extraordinarily broad variety of oxidation states and coordination geometries. Some of the commonly known classes of Ru-NHC complexes are-

1.10.1 Ru-NHC hydride and phenyl complexes-

The Ru-NHC hydride (**19-22**) and phenyl (**23**) complexes can be found in the hydrogenation [93,94] and isomerization [95] processes of functionalized unsaturated substrates or alkenes. They can also occur as reactive intermediates during hydrogenations catalyzed by Ru-alkylidene complexes [96].

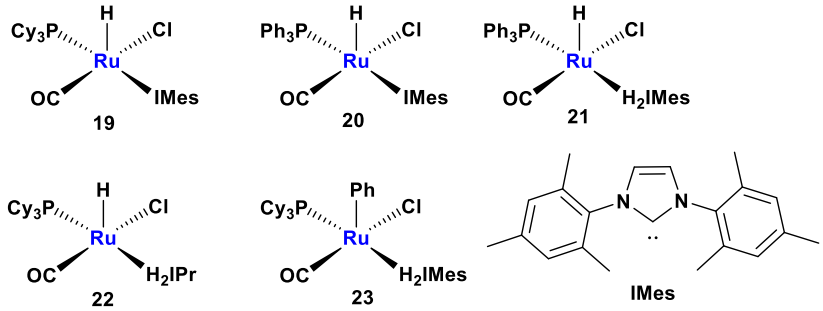

Figure 1.19. Examples of Ru-NHC-based hydride and phenyl complexes.

1.10.2 NHC–Ru arene complexes

The easy accessibility of the commercially available [(*p*-cymene)$RuCl_2$]$_2$ enables the synthesis of new Ru-NHC-based arene complexes (**24, 25**) using imidazolin-2-ylidene ligands. These complexes were utilized in the metathesis and radical reactions.[97,98]

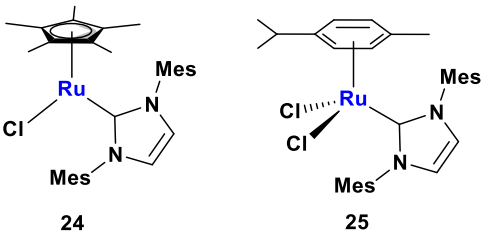

Figure 1.20. Examples of Ru-NHC-based arene complexes.

1.10.3 Ru-NHC alkylidene complexes

The complex **26-28** developed by Grubbs belongs to this NHC class.[99–102]

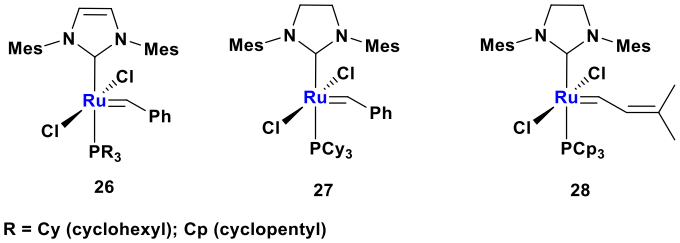

Figure 1.21. Examples of Ru-NHC-based alkylidene complexes.

1.10.4 Ru-NHC vinylidene and indenylidene complexes

Despite the steric complexation in **29** and **30**, these complexes have shown high reactivity in the atom transfer radical polymerization (ATRP) type reactions.

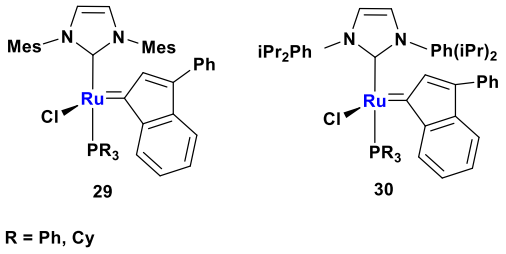

Figure 1.22. Examples of Ru-NHC-based vinylidene and indenylidene complexes.

1.10.5 Ru-NHC Schiff-base complexes

The complex **31a-f** showed promising results for ATRP of vinyl monomers.[103]

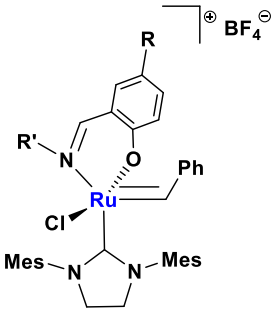

31a-f

a: R = H, R' = Me
b: R = NO_2, R' = Me
c: R = H, R' = 2,6-Me-4-Br-C_6H_2
d: R = NO_2, R' = 2,6-Me-4-Br-C_6H_2
e: R = H, R' = 2,6-iPrC_6H_3
f: R = NO_2, R' = 2,6-iPrC_6H_3

Figure 1.23. Examples of Ru-NHC-based Schiff-base complexes.

1.11 Protic-NHC ligands

The NHCs have always been an area of interest due to their electronic and steric tunability.[26,40] The substituents at the nitrogen atoms and the carbon backbone of the heterocyclic skeleton can alter the strong σ-donor characteristics of NHCs. Bulky groups on the ring-nitrogen atoms do have an extra effect on the steric requirement of NHCs in the coordination sphere of a metal atom, which affects the catalytic activity and selectivity of NHC complexes. A sterically less demanding hydrogen atom can replace one N-substituent at an NHC, adding new aspects to the ligand's coordination chemistry and behavior. The terms NH-NHCs, NR, NH-stabilized carbenes, NH-functionalized NHCs, and so forth have been used to describe NHCs with one or two NH wingtips. This subclass of NHCs is called protic N-heterocyclic carbenes (pNHCs).[104] In contrast to the nonprotic (N-alkylated) classical NHCs, the free pNHC is less stable than the equivalent azole isomer due to an NH group adjacent to the nucleophilic carbene carbon atom (Figure 1.24).[33,105,106] However, coordination with a metal center may change the relative stability of the tautomers.[107]

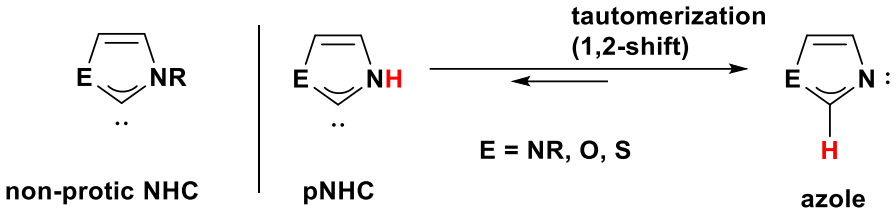

Figure 1.24. Comparison between Nonprotic and Protic N-Heterocyclic

The traditional synthetic route for synthesizing protic NHC complexes has been shown in Figure 1.25. Acid-induced tautomerization of imidazole, a synthetic technique exclusive to the production of pNHC complexes, was utilized by Sundberg and Taube in 1972 to accomplish the first synthesis of a complex containing a pNHC ligand (Figure 1.25 a).[108] The reversible deprotonation and creation of hydrogen bonding interactions with counterions in specific crystal structures soon revealed the Brønsted-acidic nature of the wingtip NH group in these complexes.[109] The development of base-induced N-functionalization of pNHC complexes by Angelici and colleagues was also influenced by the NH group's acidic nature. Protonation of azolyl complexes gives rational access to pNHC complexes, as predicted from acid-base chemistry (Figure 1.25 b).[110] Conversely, isocyanide ligands have been acknowledged as valuable constituents for synthesizing pNHCs on metal templates, beginning with the Fehlhammer group's groundbreaking 1974 work on the cyclization of functionalized isocyanides (Figure 1.25c).[111] Angelici, in 1979, showed that nucleophilic substitution of Fischer carbene complexes also provides an annulation route to the pNHC complexes (Figure 1.25d).[112] Another alternative approach for the protic-NHC involves the removal of the deprotecting group on the masked NHC (Figure 1.25e).[113]

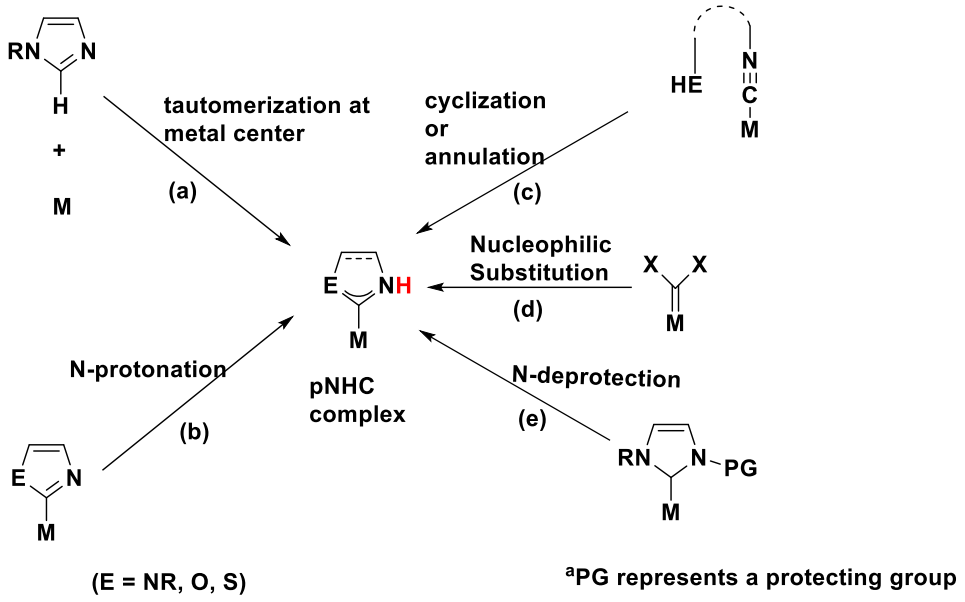

Figure 1.25. Representative synthetic strategies to access pNHC complexes.

1.12 Metal−Ligand Cooperation (MLC) Involving pNHC Complexes

A lot of attention has been focused on the direct involvement of ligands in substrate recognition, activation, and transformation through a variety of secondary interactions, including hydrogen bonding and proton transfer in the coordination sphere, to understand the function of metalloenzymes better and create new transition-metal catalysts.

The NH wingtip was first used by Hahn and Waldvogel in 2007 to identify substrates, enabling the chemoselective catalytic hydrogenation of an ester-functionalized olefin over an unfunctionalized one (Figure 1.26a).[114] Due to the pNHC's proton-responsive characteristics, bond activation and catalysis through metal-pNHC cooperation were further developed.[74]

Kuwata and Ikariya (2008) utilized a bifunctional technique to report C-O bond cleavage in allyl alcohol under moderate and neutral circumstances (Figure 1.26 b).[104] This strategy was then applied to the

catalytic dehydrogenative coupling of an allyl alcohol and an imidazole.[104] The Lewis acid/Brønsted base cooperation of a (imidazolyl)iridium complex allowed Grotjahn to demonstrate the heterolytic cleavage of dihydrogen (Figure 1.26c).[115] The application of p-NHC ligands in bifunctional catalysis has increased in recent years.

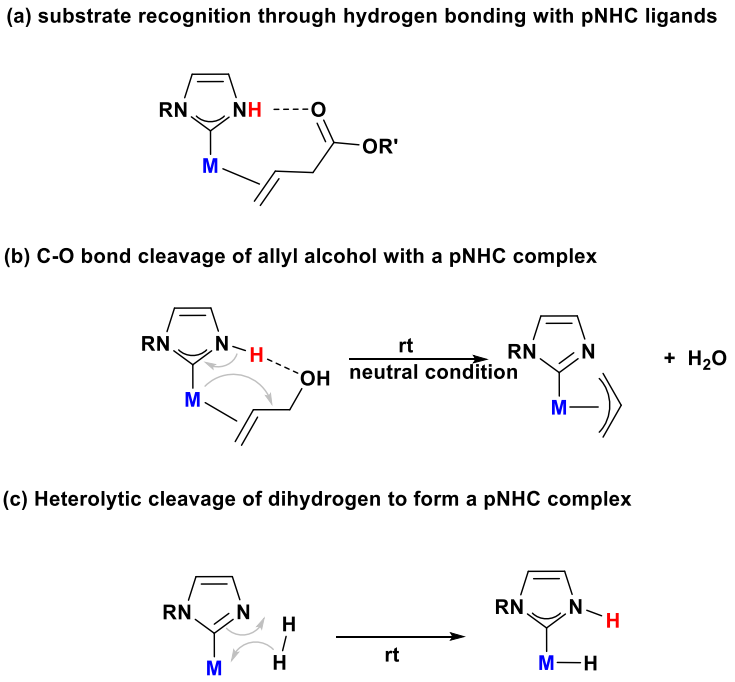

Figure 1.26. Examples of MLC involving pNHC.

1.13 Deprotonation of protic-NHC

The protic-NHC complexes, upon deprotonation, give a nucleophilic species defined as an azolyl complex or an anionic N-deprotonated NHC complex (Figure 1.27).

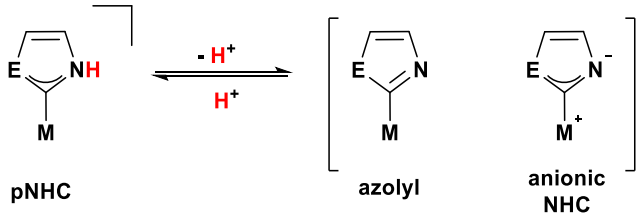

Figure 1.27. N-Deprotonation of pNHC complexes.

The deprotonated NHC has been shown to activate the dihydrogen or H-X in a concerted stepwise manner. The resulting protic ligand can subsequently transfer the nucleophilic X to the unsaturated substrate (Figure 1.28).[116,117]

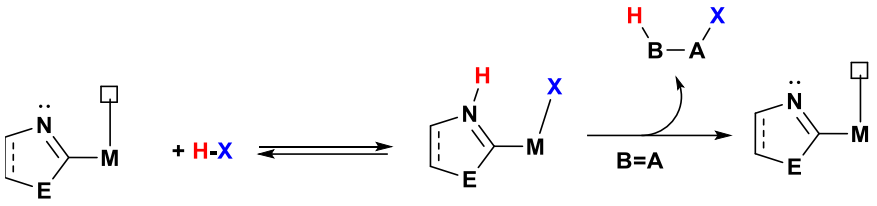

Figure 1.28. Bond activation and MLC by anionic-NHC.

1.14 Structural comparison of pNHC and anionic-NHC complexes

The crystallographic and ^{13}C NMR spectroscopic data of some previously reported pNHC and its corresponding anionic NHC pair complexes have been shown in Figure 1.29.[104,118–120] These complexes establish the carbenic nature of deprotonated NHC.

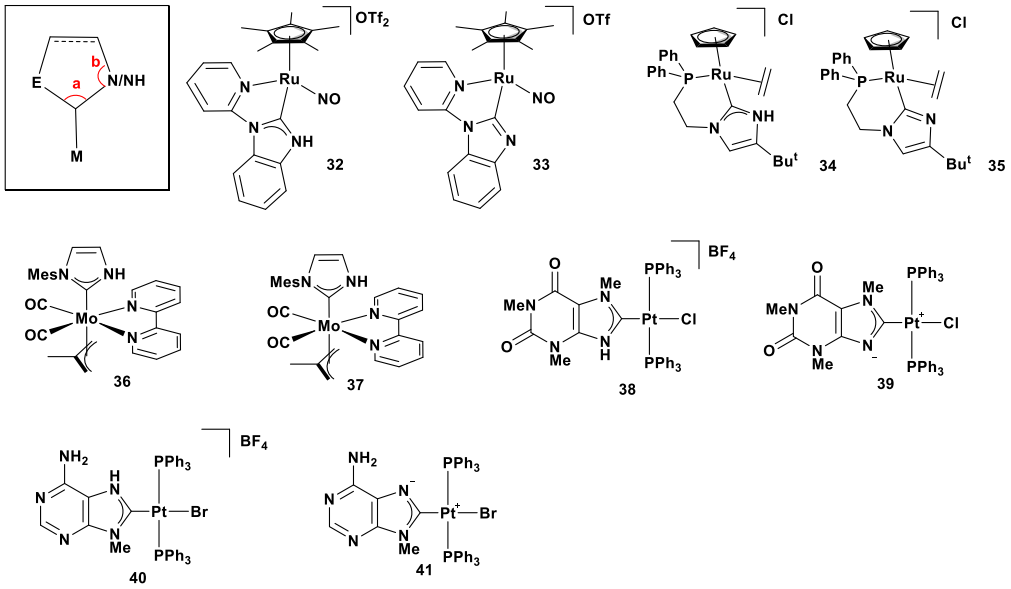

Entry	Complex	Type	M-C (Å)	C-N:/N-H (Å)	C-E (Å)	α (°)	β (°)	^{13}C δc
1	32	NH	2.060(5)	1.332(7)	1.396(6)	106.5(4)	110.5(4)	182.2
2	33	N:	2.048(4)	1.297(6)	1.417(4)	111.4(3)	106.4(3)	*na*
3	34	NH	2.061(4)	1.360(5)	1.351(5)	103.7(3)	112.8(3)	166.7
4	35	N:	2.0715(17)	1.342(2)	1.383(2)	108.31(14)	107.05(13)	156.4
5	36	NH	2.224(3)	1.358(4)	1.368(3)	102.9(2)	112.8(2)	188.2
6	37	N:	2.236(8)	1.299(9)	1.497(9)	108.0(7)	103.2(7)	184.5
7	38	NH	1.967(3)	1.373(3)	1.343(3)	106.0(2)	109.9(2)	*na*
8	39	N:	1.980(3)	1.352(3)	1.360(3)	110.6(2)	104.8(2)	150.3
9	40	NH	1.976(6)	1.345(8)	1.352(8)	107.1(5)	109.8(5)	155.2
10	41	N:	1.996(2)	1.323(3)	1.385(3)	111.70(19)	105.32(19)	149.9

Figure 1.29. Structural and Spectral Comparison of pNHC and Azolyl (Anionic NHC) Complexes. *na* = not assigned.

It has been observed that upon deprotonation, the N−C−N angle α increases, and the C−N−C angle β decreases. The $C_{carbene}$-N bond length also differs significantly upon deprotonation. The ^{13}C NMR resonance for the pNHC carbon atom observes an upfield shift upon N-deprotonation of pNHC.

1.15 Application of NHC-Complexes in Homogeneous Catalysis

There are limited homogeneous transition metal catalysts in which both steric and electrical effects can be precisely regulated through minor alterations in ligand structure within the series. Phosphines have been predominantly utilized in this context, facilitated by the accessibility of the Tolman map of electronic and steric effects.[121] N-heterocyclic carbenes (NHCs), formed by substituting the proton at C-2 in an imidazolium salt with a metal, have been recognized for years. NHC complexes have been widely explored in the field of homogeneous catalysis.[12,122] The NHCs, due to their nucleophilic nature, react efficiently with several electrophiles. Pincer carbene complexes have been the most beneficial catalytic system,

as the pincer framework provides thermal stability, and NHCs are known to be strong electron donors. Pincer ligands featuring N-heterocyclic carbenes (NHCs) are the most sought-after molecules due to their exceptional stability and pronounced chelate action, resulting in a stable class of compounds with notable catalytic properties.[67] The transition metal NHC complexes have been widely utilized for catalytic applications like hydrogenation/dehydrogenation reactions, coupling reactions, etc.[123–125]

We are more interested in the acceptorless dehydrogenation of benzyl alcohol to benzoic acid derivatives. The well-established method of synthesizing carboxylic acids involves oxidizing benzyl alcohols with a metal-based oxidant.[126,127] However, this process requires powerful, toxic oxidants or TEMPO in combination with a stoichiometric quantity of sodium hypochlorite, which reduces its atom efficiency.[128] Alternatively, benzoic acid can also be prepared by dehydrogenation of benzyl alcohol. Alcohol can be investigated as a hydrogen storage compound using an alcohol dehydrogenation process. This atom-economic method produces the required carboxylic acid and hydrogen gas, a potential fuel. The dehydrogenation of benzyl alcohol to benzoic acid is investigated at high temperatures in organic solvents or a high concentration of base in water.

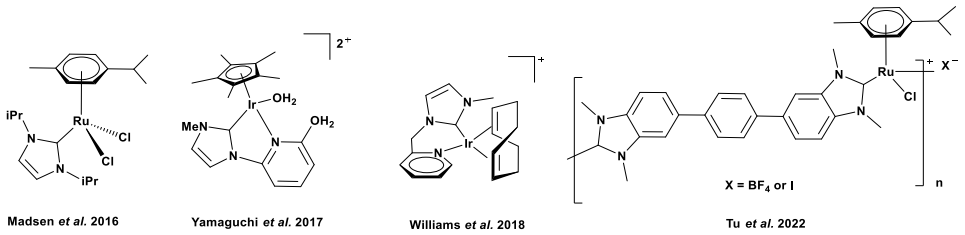

Figure 1.30. NHC-based complexes for acceptorless dehydrogenation of benzyl alcohol to benzoic acid.

In recent years, the NHCs have been a highly sustainable alternative for spectator ligands over the traditional phosphine-based ligands in organometallic catalysis. Some previously reported NHC-based transition

metal complexes for dehydrogenating benzyl alcohols to benzoic acid have been shown in Figure 1.30. Madsen *et al.* in 2016 reported half sandwich Ru-NHC complex [(p-cymene)$RuCl_2$(IiPr)] (where IiPr = 1,3-diisopropyl-2,3-dihydro-1H-imidazole) which shows dehydrogenation of alcohol to acid in the presence of additives (PCy_3 and HBF_4) in the presence of toluene solvent at reflux temperature (110 ºC) in 6 h.[129] Yamaguchi *et al.* reported a dicationic complex based on Cp*Ir(III), which features a highly electron-donating N-heterocyclic carbene (NHC) ligand and a bidentate ligand derived from α-hydroxypyridine moiety[130]. Williams *et al.* in 2018 reported Ir(III) complex [Ir(2-$PyCH_2(C_4H_5N_2)$)(COD)]OTf bearing NHC ligand for the catalytic transformation of benzyl alcohol to benzoic acid in the presence of base (KOH) in toluene solvent at 140 ºC.[131] In 2022, Tu *et al.* reported acceptorless dehydrogenation of aromatic and aliphatic primary alcohol to carboxylic acid by a self-supported NHC-Ru single-site catalyst under mild conditions.[132]

1.16 Research Gap

The study of phosphines as spectator ligands in a pincer framework has been widely used and explored. However, phosphines have had several disadvantages, such as poor stability in air and moisture and limited tunability.[90] Therefore, the NHCs as ligands were used to replace the phosphines, increasing the stability and enhancing steric and electronic tunability.[133] Further, the metal and ligand cooperation was observed upon introducing a special class of NHC ligands, i.e., protic-NHC (pNHC) ligands.[104] These pNHC ligands provided the formation of hydrogen bonds to selected substrates, which helped with substrate recognition, selection, and orientation. The deprotonation of the protic NH wingtip resulted in anionic NHC complexes, which have been shown to activate small molecules like H_2, CO_2, CO, etc.[134]

However, the comparison between protic and classical NHCs has mostly been based on catalytic activity. For the structural and electronic comparison, no example has been reported that could provide a direct comparison between protic- or anionic- with classical-NHC. We found this research gap and designed our complexes to incorporate the protic-NHC and classical-NHC ligands in a single molecule and a nearly identical environment. These complexes provide a direct comparison of structural and electronic properties between protic- and classical-NHC ligands. Initially, we synthesized our complexes using a very common phosphine-based ruthenium precursor ($RuCl_2(PPh3)_3$), which was later replaced by our in-house reported Ru(III)-NHC precursor. This replacement of the precursor resulted in new phosphine-free ruthenium complexes having mixed protic and classical-NHC ligands in one molecule. We could also establish the role of halides and ion-pairing in the C-H bond activation mediated by the Lewis acidic metal center. We also report the mechanism for in situ conversion of abnormal-NHC to normal-NHC for the first time.

1.17 Objectives of thesis

NHCs have drawn attention due to their strong donation tendency and greater metal carbene bond strength. Protic-NHC complexes have not been much explored, and the examples of complexes with protic- and classical-NHC in one molecule are very limited.

1. Design and synthesis of ligand precursors having the possibility of protic- and classical-NHC in one molecule.

2. Synthesis of transition metal complexes with CNC-pincer ligand platform having protic- and classical-NHC in the same molecule.

3. To compare the structural and electronic properties of protic & classical-NHC and the catalytic activity of complexes.

4. Theoretical investigations on our synthetic work of Ru(III)-NHC complexes.

1.18 Organization of thesis

This chapter includes five chapters describing the synthesis, catalysis, and theoretical investigations of Ru-NHC complexes.

Chapter 1 presents the general introduction of pincer complexes, followed by a discussion about N-heterocyclic carbenes (NHCs) and protic-NHC as ancillary ligands.

In **Chapter 2,** the structural and electronic study of the phosphine-based Ru-CNC pincer complex with protic- or anionic- and classical-NHC in the same molecule in a nearly identical environment has been extensively studied.

In **Chapter 3,** Ru-based phosphine-free CNC pincer complexes with mixed protic- and classical-NHC used for oxidant-free dehydrogenation of benzyl alcohols to benzoic acid have been studied.

In **Chapter 4,** the role of ion pairs in synthesizing our in-house reported Ru(III)-NHC precursor complexes has been extensively explored.

In **Chapter 5,** the conversion of our in-house synthesized and reported Ru(III)-aNHC to Ru(III)-NHC has been studied computationally.

1.19. References

[1] C. J. Moulton, B. L. Shaw, Transition metal–carbon bonds. Part XLII. Complexes of nickel, palladium, platinum, rhodium and iridium with the tridentate ligand 2,6-bis[(di-t-butylphosphino)methyl]phenyl, J. Chem. Soc. Dalton Trans. 0 (1976) 1020–1024. https://doi.org/10.1039/DT9760001020.

[2] G. van Koten, K. Timmer, J. G. Noltes, A. L. Spek, A novel type of Pt–C interaction and a model for the final stage in reductive elimination processes involving C–C coupling at Pt; synthesis and molecular geometry of [1, N , N ′-η-2,6-bis{(dimethylamino)methyl}-toluene]iodoplatinum(II) tetrafluoroborate, J. Chem. Soc. Chem. Commun. 0 (1978) 250–252. https://doi.org/10.1039/C39780000250.

[3] D. Morales-Morales, Pincer Complexes: Applications in Catalysis, Rev. Soc. Quím. México 48 (2004) 338–346.

[4] G. van Koten, Tuning the reactivity of metals held in a rigid ligand environment, Pure Appl. Chem. 61 (1989) 1681–1694. https://doi.org/10.1351/pac198961101681.

[5] P.A. Chase, R.A. Gossage, G. van Koten, Modern Organometallic Multidentate Ligand Design Strategies: The Birth of the Privileged "Pincer" Ligand Platform, in: G. van Koten, R.A. Gossage (Eds.), Privileged Pincer-Met. Platf. Coord. Chem. Appl., Springer International Publishing, Cham, 2016: pp. 1–15. https://doi.org/10.1007/3418_2015_131.

[6] E. Peris, R.H. Crabtree, Key factors in pincer ligand design, Chem. Soc. Rev. 47 (2018) 1959–1968. https://doi.org/10.1039/C7CS00693D.

[7] J. Choi, A.H.R. MacArthur, M. Brookhart, A.S. Goldman, Dehydrogenation and Related Reactions Catalyzed by Iridium Pincer Complexes, Chem. Rev. 111 (2011) 1761–1779. https://doi.org/10.1021/cr1003503.

[8] Q.-H. Deng, R.L. Melen, L.H. Gade, Anionic Chiral Tridentate N-Donor Pincer Ligands in Asymmetric Catalysis, Acc. Chem. Res. 47 (2014) 3162–3173. https://doi.org/10.1021/ar5002457.

[9] S. Saha, A. Manna, Carbene, BoD – Books on Demand, 2022.

[10] On the Existence of a Tungsten Carbonyl Carbene Complex - Fischer - 1964 - Angewandte Chemie International Edition in English - Wiley Online Library, (n.d.). https://onlinelibrary.wiley.com/doi/abs/10.1002/anie.196405801 (accessed September 13, 2024).

[11] K. Öfele, 1,3-Dimethyl-4-imidazolinyliden-(2)-pentacarbonylchrom ein neuer übergangsmetall-carben-komplex, J. Organomet. Chem. 12 (1968) P42–P43. https://doi.org/10.1016/s0022-328x(00)88691-x.

[12] H.-W. Wanzlick, H.-J. Schönherr, Direct Synthesis of a Mercury Salt-Carbene Complex, Angew. Chem. Int. Ed. Engl. 7 (1968) 141–142. https://doi.org/10.1002/anie.196801412.

[13] A.J.A. III, R.L. Harlow, M. Kline, A stable crystalline carbene, ACS Publ. (2002). https://doi.org/10.1021/ja00001a054.

[14] P. de Frémont, N. Marion, S.P. Nolan, Carbenes: Synthesis, properties, and organometallic chemistry, Coord. Chem. Rev. 253 (2009) 862–892. https://doi.org/10.1016/j.ccr.2008.05.018.

[15] D. Bourissou, O. Guerret, F.P. Gabbaï, G. Bertrand, Stable Carbenes, Chem. Rev. 100 (2000) 39–92. https://doi.org/10.1021/cr940472u.

[16] C.M. Crudden, D.P. Allen, Stability and reactivity of *N*-heterocyclic carbene complexes, Coord. Chem. Rev. 248 (2004) 2247–2273. https://doi.org/10.1016/j.ccr.2004.05.013.

[17] C.J. P, Priciples and Applications of Organotransition Metal Chemistry, Univ. Sci. Books 324 (1987). https://cir.nii.ac.jp/crid/1571417124701557504 (accessed August 8, 2024).

[18] J.W. Runyon, O. Steinhof, H.V.R. Dias, J.C. Calabrese, W.J. Marshall, A.J. Arduengo, Carbene-Based Lewis Pairs for Hydrogen Activation,

Aust. J. Chem. 64 (2011) 1165–1172. https://doi.org/10.1071/CH11246.

[19] A.J.A. III, H.V.R. Dias, R.L. Harlow, M. Kline, Electronic stabilization of nucleophilic carbenes, ACS Publ. (2002). https://doi.org/10.1021/ja00040a007.

[20] C. Heinemann, T. Müller, Y. Apeloig, H. Schwarz, On the Question of Stability, Conjugation, and “Aromaticity” in Imidazol-2-ylidenes and Their Silicon Analogs, J. Am. Chem. Soc. 118 (1996) 2023–2038. https://doi.org/10.1021/ja9523294.

[21] E. Aldeco-Perez, A.J. Rosenthal, B. Donnadieu, P. Parameswaran, G. Frenking, G. Bertrand, Isolation of a C5-Deprotonated Imidazolium, a Crystalline "Abnormal" N-Heterocyclic Carbene, Science 326 (2009) 556–559. https://doi.org/10.1126/science.1178206.

[22] O. Schuster, L. Yang, H.G. Raubenheimer, M. Albrecht, Beyond Conventional N-Heterocyclic Carbenes: Abnormal, Remote, and Other Classes of NHC Ligands with Reduced Heteroatom Stabilization, Chem. Rev. 109 (2009) 3445–3478. https://doi.org/10.1021/cr8005087.

[23] D.A. Dixon, A.J.A. III, Electronic structure of a stable nucleophilic carbene, ACS Publ. (2002). https://doi.org/10.1021/j100164a003.

[24] A.J.A. III, D.A. Dixon, K.K. Kumashiro, C. Lee, W.P. Power, K.W. Zilm, Chemical Shielding Tensor of a Carbene, ACS Publ. (2002). https://doi.org/10.1021/ja00093a041.

[25] A.J.A. III, H. Bock, H. Chen, M. Denk, D.A. Dixon, J.C. Green, W.A. Herrmann, N.L. Jones, M. Wagner, R. West, Photoelectron Spectroscopy of a Carbene/Silylene/Germylene Series, ACS Publ. (2002). https://doi.org/10.1021/ja00094a020.

[26] D. J. Nelson, S. P. Nolan, Quantifying and understanding the electronic properties of N-heterocyclic carbenes, Chem. Soc. Rev. 42 (2013) 6723–6753. https://doi.org/10.1039/C3CS60146C.

[27] Electron Distribution in a Stable Carbene | Journal of the American Chemical Society, (n.d.). https://pubs.acs.org/doi/pdf/10.1021/ja00094a040 (accessed August 10, 2024).

[28] C. Boehme, G. Frenking, Electronic Structure of Stable Carbenes, Silylenes, and Germylenes, J. Am. Chem. Soc. 118 (1996) 2039–2046. https://doi.org/10.1021/ja9527075.

[29] W.A. Herrmann, C. Köcher, N-Heterocyclic Carbenes, Angew. Chem. Int. Ed. Engl. 36 (1997) 2162–2187. https://doi.org/10.1002/anie.199721621.

[30] M.S. Collins, E.L. Rosen, V.M. Lynch, C.W. Bielawski, Differentially Substituted Acyclic Diaminocarbene Ligands Display Conformation-Dependent Donicities, Organometallics 29 (2010) 3047–3053. https://doi.org/10.1021/om1004226.

[31] R.W. Alder, M.E. Blake, L. Chaker, J.N. Harvey, F. Paolini, J. Schütz, When and How Do Diaminocarbenes Dimerize?, Angew. Chem. Int. Ed. 43 (2004) 5896–5911. https://doi.org/10.1002/anie.200400654.

[32] Relation between singlet-triplet gaps and bond energies | The Journal of Physical Chemistry, (n.d.). https://pubs.acs.org/doi/pdf/10.1021/j100278a006 (accessed August 18, 2024).

[33] C. Heinemann, W. Thiel, Ab initio study on the stability of diaminocarbenes, Chem. Phys. Lett. 217 (1994) 11–16. https://doi.org/10.1016/0009-2614(93)E1360-S.

[34] T. Itoh, Y. Nakata, K. Hirai, H. Tomioka, Triplet Diphenylcarbenes Protected by Trifluoromethyl and Bromine Groups. A Triplet Carbene Surviving a Day in Solution at Room Temperature, J. Am. Chem. Soc. 128 (2006) 957–967. https://doi.org/10.1021/ja056575j.

[35] A.A.D. Tulloch, A.A. Danopoulos, S. Kleinhenz, M.E. Light, M.B. Hursthouse, G. Eastham, Structural Diversity in Pyridine-N-

Functionalized Carbene Copper(I) Complexes, Organometallics 20 (2001) 2027–2031. https://doi.org/10.1021/om010014t.

[36] X. Hu, I. Castro-Rodriguez, K. Olsen, K. Meyer, Group 11 Metal Complexes of N-Heterocyclic Carbene Ligands: Nature of the MetalCarbene Bond, Organometallics 23 (2004) 755–764. https://doi.org/10.1021/om0341855.

[37] R. Dorta, E.D. Stevens, N.M. Scott, C. Costabile, L. Cavallo, C.D. Hoff, S.P. Nolan, Steric and Electronic Properties of N-Heterocyclic Carbenes (NHC): A Detailed Study on Their Interaction with Ni(CO)4, J. Am. Chem. Soc. 127 (2005) 2485–2495. https://doi.org/10.1021/ja0438821.

[38] H. Jacobsen, A. Correa, C. Costabile, L. Cavallo, π-Acidity and π-basicity of *N*-heterocyclic carbene ligands. A computational assessment, J. Organomet. Chem. 691 (2006) 4350–4358. https://doi.org/10.1016/j.jorganchem.2006.01.026.

[39] A.J. Arduengo III, R. Krafczyk, Auf der Suche nach Stabilen Carbenen, Chem. Unserer Zeit 32 (1998) 6–14. https://doi.org/10.1002/ciuz.19980320103.

[40] A.C. Hillier, W.J. Sommer, B.S. Yong, J.L. Petersen, L. Cavallo, S.P. Nolan, A Combined Experimental and Theoretical Study Examining the Binding of N-Heterocyclic Carbenes (NHC) to the Cp*RuCl (Cp* = η5-C5Me5) Moiety: Insight into Stereoelectronic Differences between Unsaturated and Saturated NHC Ligands, Organometallics 22 (2003) 4322–4326. https://doi.org/10.1021/om034016k.

[41] Steric effects of phosphorus ligands in organometallic chemistry and homogeneous catalysis | Chemical Reviews, (n.d.). https://pubs.acs.org/doi/pdf/10.1021/cr60307a002 (accessed August 27, 2024).

[42] A.R. Chianese, A. Kovacevic, B.M. Zeglis, J.W. Faller, R.H. Crabtree, Abnormal C5-Bound N-Heterocyclic Carbenes: Extremely Strong Electron Donor Ligands and Their Iridium(I) and Iridium(III)

Complexes, Organometallics 23 (2004) 2461–2468. https://doi.org/10.1021/om049903h.

[43] R.H. Crabtree, NHC ligands versus cyclopentadienyls and phosphines as spectator ligands in organometallic catalysis, J. Organomet. Chem. 690 (2005) 5451–5457. https://doi.org/10.1016/j.jorganchem.2005.07.099.

[44] J. Zhang, G. Leitus, Y. Ben-David, D. Milstein, Efficient Homogeneous Catalytic Hydrogenation of Esters to Alcohols, Angew. Chem. Int. Ed. 45 (2006) 1113–1115. https://doi.org/10.1002/anie.200503771.

[45] Y. Sun, C. Koehler, R. Tan, V. T. Annibale, D. Song, Ester hydrogenation catalyzed by Ru-CNN pincer complexes, Chem. Commun. 47 (2011) 8349–8351. https://doi.org/10.1039/C1CC12601F.

[46] T. Weskamp, V.P.W. Böhm, W.A. Herrmann, N-Heterocyclic carbenes: state of the art in transition-metal-complex synthesis, J. Organomet. Chem. 600 (2000) 12–22. https://doi.org/10.1016/S0022-328X(00)00035-8.

[47] B.K.M. Chan, N. Chang, M.R. Grimmett, The synthesis and thermolysis of imidazole quaternary salts, Aust. J. Chem. 30 (1977) 2005–2013. https://doi.org/10.1071/ch9772005.

[48] M.R. Haque, M. Rasmussen, Ambident heterocyclic reactivity: Alkylation of 2-substituted-4-methylbenzimidazoles, Tetrahedron 50 (1994) 5535–5554. https://doi.org/10.1016/S0040-4020(01)80708-0.

[49] M.R. Grimmett, Imidazole and Benzimidazole Synthesis, Academic Press, 1997.

[50] W.A. Herrmann, L.J. Gooβen, M. Spiegler, Functionalized imidazoline-2-ylidene complexes of rhodium and palladium, J. Organomet. Chem. 547 (1997) 357–366. https://doi.org/10.1016/S0022-328X(97)00434-8.

[51] T. Weskamp, V.P.W. Böhm, W.A. Herrmann, *N*-Heterocyclic carbenes: state of the art in transition-metal-complex synthesis, J. Organomet. Chem. 600 (2000) 12–22. https://doi.org/10.1016/S0022-328X(00)00035-8.

[52] W.A. Herrmann, M. Elison, J. Fischer, C. Köcher, G.R.J. Artus, N-Heterocyclic Carbenes: Generation under Mild Conditions and Formation of Group 8–10 Transition Metal Complexes Relevant to Catalysis, Chem. – Eur. J. 2 (1996) 772–780. https://doi.org/10.1002/chem.19960020708.

[53] R.E. Douthwaite, D. Haüssinger, M.L.H. Green, P.J. Silcock, P.T. Gomes, A.M. Martins, A.A. Danopoulos, Cationic Nickel(II) Complexes of Chelating N-Heterocyclic Carbenes, Organometallics 18 (1999) 4584–4590. https://doi.org/10.1021/om990398b.

[54] U. Kernbach, M. Ramm, P. Luger, W.P. Fehlhammer, A Chelating Triscarbene Ligand and Its Hexacarbene Iron Complex, Angew. Chem. Int. Ed. Engl. 35 (1996) 310–312. https://doi.org/10.1002/anie.199603101.

[55] C. Köcher, W.A. Herrmann, Heterocyclic carbenes. One-pot synthesis of rhodium and iridium carbene complexes, J. Organomet. Chem. 532 (1997) 261–265. https://doi.org/10.1016/S0022-328X(96)06732-0.

[56] J.C.C. Chen, I.J.B. Lin, The first dicarbene double helical mercury complex, J. Chem. Soc. Dalton Trans. (2000) 839–840. https://doi.org/10.1039/B000971G.

[57] E. Peris, J. A. Loch, J. Mata, R. H. Crabtree, A Pd complex of a tridentate pincer CNC bis-carbene ligand as a robust homogenous Heck catalystElectronic supplementary information (ESI) available: synthesis details and NMR data. See http://www.rsc.org/suppdata/cc/b0/b008038l/, Chem. Commun. 0 (2001) 201–202. https://doi.org/10.1039/B008038L.

[58] D.S. McGuinness, K.J. Cavell, Donor-Functionalized Heterocyclic Carbene Complexes of Palladium(II): Efficient Catalysts for C−C

Coupling Reactions, Organometallics 19 (2000) 741–748. https://doi.org/10.1021/om990776c.

[59] D.J. Nielsen, K.J. Cavell, B.W. Skelton, A.H. White, A pyridine bridged dicarbene ligand and its silver(I) and palladium(II) complexes: synthesis, structures, and catalytic applications, Inorganica Chim. Acta 327 (2002) 116–125. https://doi.org/10.1016/S0020-1693(01)00677-6.

[60] D.S. McGuinness, K.J. Cavell, B.F. Yates, B.W. Skelton, A.H. White, Oxidative Addition of the Imidazolium Cation to Zerovalent Ni, Pd, and Pt: A Combined Density Functional and Experimental Study, J. Am. Chem. Soc. 123 (2001) 8317–8328. https://doi.org/10.1021/ja010628p.

[61] M.S. Viciu, G.A. Grasa, S.P. Nolan, Catalytic Dehalogenation of Aryl Halides Mediated by a Palladium/Imidazolium Salt System, Organometallics 20 (2001) 3607–3612. https://doi.org/10.1021/om010332s.

[62] M. Albrecht, G. van Koten, Platinum Group Organometallics Based on "Pincer" Complexes: Sensors, Switches, and Catalysts, Angew. Chem. Int. Ed. 40 (2001) 3750–3781. https://doi.org/10.1002/1521-3773(20011015)40:20<3750::AID-ANIE3750>3.0.CO;2-6.

[63] A. Macchioni, Ion Pairing in Transition-Metal Organometallic Chemistry, Chem. Rev. 105 (2005) 2039–2074. https://doi.org/10.1021/cr0300439.

[64] S. Tsuzuki, H. Tokuda, K. Hayamizu, M. Watanabe, Magnitude and Directionality of Interaction in Ion Pairs of Ionic Liquids: Relationship with Ionic Conductivity, J. Phys. Chem. B 109 (2005) 16474–16481. https://doi.org/10.1021/jp0533628.

[65] E.C. Keske, O.V. Zenkina, R. Wang, C.M. Crudden, Synthesis and Structure of Silver and Rhodium 1,2,3-Triazol-5-ylidene Mesoionic Carbene Complexes, Organometallics 31 (2012) 456–461. https://doi.org/10.1021/om201104f.

[66] V. Karthik, V. Gupta, G. Anantharaman, Synthesis of Imidazole-Based Functionalized Mesoionic Carbene Complexes of Palladium: Comparison of Donor Properties and Catalytic Activity toward Suzuki–Miyaura Coupling, Organometallics 33 (2014) 6218–6222. https://doi.org/10.1021/om5009023.

[67] Y. Wang, B. Zhang, S. Guo, Transition Metal Complexes Supported by N-Heterocyclic Carbene-Based Pincer Platforms: Synthesis, Reactivity and Applications, Eur. J. Inorg. Chem. 2021 (2021) 188–204. https://doi.org/10.1002/ejic.202000911.

[68] Y. Wei, A. Petronilho, H. Mueller-Bunz, M. Albrecht, Mesoionic Triazolylidene Nickel Complexes: Synthesis, Ligand Lability, and Catalytic C–C Bond Formation Activity, Organometallics 33 (2014) 5834–5844. https://doi.org/10.1021/om500593s.

[69] H. Sivaram, J. Tan, H.V. Huynh, Syntheses, Characterizations, and a Preliminary Comparative Cytotoxicity Study of Gold(I) and Gold(III) Complexes Bearing Benzimidazole- and Pyrazole-Derived N-Heterocyclic Carbenes, Organometallics 31 (2012) 5875–5883. https://doi.org/10.1021/om300444c.

[70] J.C. Bernhammer, H.V. Huynh, Pyrazolin-5-ylidene Palladium(II) Complexes: Synthesis, Characterization, and Application in the Direct Arylation of Pentafluorobenzene, Organometallics 31 (2012) 5121–5130. https://doi.org/10.1021/om300464b.

[71] H.V. Huynh, T.T. Lam, H.T.T. Luong, Anion influences on reactivity and NMR spectroscopic features of NHC precursors, RSC Adv. 8 (2018) 34960–34966. https://doi.org/10.1039/C8RA05839C.

[72] K.R. Balinge, P.R. Bhagat, Palladium–N-heterocyclic carbene complexes for the Mizoroki–Heck reaction: An appraisal, Comptes Rendus Chim. 20 (2017) 773–804. https://doi.org/10.1016/j.crci.2017.03.003.

[73] A. Ortiz, P. Gómez-Sal, J.C. Flores, E. de Jesús, Highly Recoverable Pd(II) Catalysts for the Mizoroki–Heck Reaction Based on N-

Heterocyclic Carbenes and Poly(benzyl ether) Dendrons, Organometallics 37 (2018) 3598–3610. https://doi.org/10.1021/acs.organomet.8b00295.

[74] E. Peris, Smart N-Heterocyclic Carbene Ligands in Catalysis, Chem. Rev. 118 (2018) 9988–10031. https://doi.org/10.1021/acs.chemrev.6b00695.

[75] H.V. Huynh, Electronic Properties of N-Heterocyclic Carbenes and Their Experimental Determination, Chem. Rev. 118 (2018) 9457–9492. https://doi.org/10.1021/acs.chemrev.8b00067.

[76] F.E. Hahn, M.C. Jahnke, Heterocyclic Carbenes: Synthesis and Coordination Chemistry, Angew. Chem. Int. Ed. 47 (2008) 3122–3172. https://doi.org/10.1002/anie.200703883.

[77] S. Díez-González, N. Marion, S.P. Nolan, N-Heterocyclic Carbenes in Late Transition Metal Catalysis, Chem. Rev. 109 (2009) 3612–3676. https://doi.org/10.1021/cr900074m.

[78] H. Jacobsen, A. Correa, A. Poater, C. Costabile, L. Cavallo, Understanding the M(NHC) (NHC = N-heterocyclic carbene) bond, Coord. Chem. Rev. 253 (2009) 687–703. https://doi.org/10.1016/j.ccr.2008.06.006.

[79] A. Udvardy, F. Joó, Á. Kathó, Synthesis and catalytic applications of Ru(II)-phosphaurotropine complexes with the use of simple water-soluble Ru(II)-precursors, Coord. Chem. Rev. 438 (2021) 213871. https://doi.org/10.1016/j.ccr.2021.213871.

[80] T. Ishizuka, H. Sugimoto, S. Itoh, T. Kojima, Recent progress in oxidation chemistry of high-valent ruthenium-oxo and osmium-oxo complexes and related species, Coord. Chem. Rev. 466 (2022) 214536. https://doi.org/10.1016/j.ccr.2022.214536.

[81] C.K. Prier, D.A. Rankic, D.W.C. MacMillan, Visible Light Photoredox Catalysis with Transition Metal Complexes: Applications in Organic Synthesis, Chem. Rev. 113 (2013) 5322–5363. https://doi.org/10.1021/cr300503r.

[82] P. Nareddy, F. Jordan, M. Szostak, Recent Developments in Ruthenium-Catalyzed C–H Arylation: Array of Mechanistic Manifolds, ACS Catal. 7 (2017) 5721–5745. https://doi.org/10.1021/acscatal.7b01645.

[83] G.A. Filonenko, E. Cosimi, L. Lefort, M.P. Conley, C. Copéret, M. Lutz, E.J.M. Hensen, E.A. Pidko, Lutidine-Derived Ru-CNC Hydrogenation Pincer Catalysts with Versatile Coordination Properties, ACS Catal. 4 (2014) 2667–2671. https://doi.org/10.1021/cs500720y.

[84] Acceptorless dehydrogenation and dehydrogenative coupling of alcohols catalysed by protic NHC ruthenium complexes, Org. Biomol. Chem. 15 (2017) 3466–3471. https://doi.org/10.1039/c7ob00542c.

[85] C.A. Urbina-Blanco, A. Leitgeb, C. Slugovc, X. Bantreil, H. Clavier, A.M.Z. Slawin, S.P. Nolan, Olefin Metathesis Featuring Ruthenium Indenylidene Complexes with a Sterically Demanding NHC Ligand, Chem. – Eur. J. 17 (2011) 5045–5053. https://doi.org/10.1002/chem.201003082.

[86] A. Kajetanowicz, K. Grela, Nitro and Other Electron Withdrawing Group Activated Ruthenium Catalysts for Olefin Metathesis Reactions, Angew. Chem. Int. Ed. 60 (2021) 13738–13756. https://doi.org/10.1002/anie.202008150.

[87] C.M. Boudreaux, N.P. Liyanage, H. Shirley, S. Siek, D.L. Gerlach, F. Qu, J.H. Delcamp, E.T. Papish, Ruthenium(II) complexes of pyridinol and N-heterocyclic carbene derived pincers as robust catalysts for selective carbon dioxide reduction, Chem. Commun. 53 (2017) 11217–11220. https://doi.org/10.1039/c7cc05706g.

[88] Q. Zhao, G. Meng, S.P. Nolan, M. Szostak, N-Heterocyclic Carbene Complexes in C–H Activation Reactions, Chem. Rev. 120 (2020) 1981–2048. https://doi.org/10.1021/acs.chemrev.9b00634.

[89] I.P. Beletskaya, A.V. Cheprakov, The Heck Reaction as a Sharpening Stone of Palladium Catalysis, Chem. Rev. 100 (2000) 3009–3066. https://doi.org/10.1021/cr9903048.

[90] Y.-M. He, Q.-H. Fan, Phosphine-free chiral metal catalysts for highly effective asymmetric catalytic hydrogenation, Org. Biomol. Chem. 8 (2010) 2497–2504. https://doi.org/10.1039/B925199P.

[91] Efficient and phosphine-free bidentate N-heterocyclic carbene/ruthenium catalytic systems for the dehydrogenative amidation of alcohols and amines, Org. Chem. Front. 6 (2019) 563–570. https://doi.org/10.1039/c8qo00902c.

[92] J. Malineni, H. Keul, M. Möller, A green and sustainable phosphine-free NHC-ruthenium catalyst for selective oxidation of alcohols to carboxylic acids in water, Dalton Trans. 44 (2015) 17409–17414. https://doi.org/10.1039/C5DT01358E.

[93] H.M. Lee, Smith Dale C., Z. He, E.D. Stevens, C.S. Yi, S.P. Nolan, Catalytic Hydrogenation of Alkenes by the Ruthenium−Carbene Complex HRu(CO)Cl(PCy3)(IMes) (IMes = Bis(1,3-(2,4,6-trimethylphenyl)imidazol-2-ylidene), Organometallics 20 (2001) 794–797. https://doi.org/10.1021/om000882a.

[94] D. Banti, J.C. Mol, Degradation of the ruthenium-based metathesis catalyst [RuCl2(CHPh)(H2IPr)(PCy3)] with primary alcohols, J. Organomet. Chem. 689 (2004) 3113–3116. https://doi.org/10.1016/j.jorganchem.2004.07.033.

[95] U.L. Dharmasena, H.M. Foucault, E.N. dos Santos, D.E. Fogg, S.P. Nolan, N-Heterocyclic Carbenes as Activating Ligands for Hydrogenation and Isomerization of Unactivated Olefins, Organometallics 24 (2005) 1056–1058. https://doi.org/10.1021/om049041k.

[96] A. Fürstner, L. Ackermann, B. Gabor, R. Goddard, C.W. Lehmann, R. Mynott, F. Stelzer, O.R. Thiel, Comparative Investigation of Ruthenium-Based Metathesis Catalysts Bearing N-Heterocyclic

Carbene (NHC) Ligands, Chem. – Eur. J. 7 (2001) 3236–3253. https://doi.org/10.1002/1521-3765(20010803)7:15<3236::AID-CHEM3236>3.0.CO;2-S.

[97] A. W. Stumpf, E. Saive, A. Demonceau, A. F. Noels, Ruthenium-based catalysts for the ring opening metathesis polymerisation of low-strain cyclic olefins and of functionalised derivatives of norbornene and cyclooctene, J. Chem. Soc. Chem. Commun. 0 (1995) 1127–1128. https://doi.org/10.1039/C39950001127.

[98] C. Zhao, Transition metal-catalyzed diazo compounds decomposition for the catalytic enantioselective synthesis of new cyclopropanic scaffolds, phdthesis, Normandie Université, 2024. https://theses.hal.science/tel-04615718 (accessed September 14, 2024).

[99] M. Scholl, T.M. Trnka, J.P. Morgan, R.H. Grubbs, Increased ring closing metathesis activity of ruthenium-based olefin metathesis catalysts coordinated with imidazolin-2-ylidene ligands, Tetrahedron Lett. 40 (1999) 2247–2250. https://doi.org/10.1016/S0040-4039(99)00217-8.

[100] J. Huang, E.D. Stevens, S.P. Nolan, J.L. Petersen, Olefin Metathesis-Active Ruthenium Complexes Bearing a Nucleophilic Carbene Ligand, J. Am. Chem. Soc. 121 (1999) 2674–2678. https://doi.org/10.1021/ja9831352.

[101] A.K. Chatterjee, R.H. Grubbs, Synthesis of Trisubstituted Alkenes via Olefin Cross-Metathesis, Org. Lett. 1 (1999) 1751–1753. https://doi.org/10.1021/ol991023p.

[102] S.B. Garber, J.S. Kingsbury, B.L. Gray, A.H. Hoveyda, Efficient and Recyclable Monomeric and Dendritic Ru-Based Metathesis Catalysts, J. Am. Chem. Soc. 122 (2000) 8168–8179. https://doi.org/10.1021/ja001179g.

[103] B.D. Clercq, F. Verpoort, Synthesis and evaluation of a new class of ruthenium-based catalytic systems for atom transfer radical addition

and enol ester synthesis, J. Organomet. Chem. 672 (2003) 11–16. https://doi.org/10.1016/S0022-328X(03)00055-X.

[104] K. Araki, S. Kuwata, T. Ikariya, Isolation and Interconversion of Protic N-Heterocyclic Carbene and Imidazolyl Complexes: Application to Catalytic Dehydrative Condensation of N-(2-Pyridyl)benzimidazole and Allyl Alcohol, Organometallics 27 (2008) 2176–2178. https://doi.org/10.1021/om800285n.

[105] S. Karmakar, A. Datta, Tunneling Assists the 1,2-Hydrogen Shift in N-Heterocyclic Carbenes, Angew. Chem. 126 (2014) 9741–9745. https://doi.org/10.1002/ange.201404368.

[106] T.L. Amyes, S.T. Diver, J.P. Richard, F.M. Rivas, K. Toth, Formation and Stability of N-Heterocyclic Carbenes in Water: The Carbon Acid pKa of Imidazolium Cations in Aqueous Solution, J. Am. Chem. Soc. 126 (2004) 4366–4374. https://doi.org/10.1021/ja039890j.

[107] G. Sini, O. Eisenstein, R.H. Crabtree, Preferential C-Binding versus N-Binding in Imidazole Depends on the Metal Fragment Involved, Inorg. Chem. 41 (2002) 602–604. https://doi.org/10.1021/ic010714q.

[108] R. Sundburg, R. Shepherd, H. Taube, Carbon-bound imidazolium ylides as ligands in ruthenium(II) and ruthenium(III) complexes, J. Am. Chem. Soc. 94 (1972) 6558–6559. https://doi.org/10.1021/ja00773a600.

[109] Nitrogen-bound and carbon-bound imidazole complexes of ruthenium ammines | Journal of the American Chemical Society, (n.d.). https://pubs.acs.org/doi/10.1021/ja00809a011 (accessed September 14, 2024).

[110] L.K. Johnson, R.J. Angelici, Synthesis of aminooxycarbene complexes of iron with N-alkyl, -allyl, and -carbamoyl groups, Inorg. Chem. 26 (1987) 973–976. https://doi.org/10.1021/ic00254a002.

[111]K. Bartel, W.P. Fehlhammer, Modes of Reaction of 2- and 3-Hydroxyalkyl Isocyanides with Metal Compounds; Oxazolidinylidene and Perhydrooxazinylidene Complexes of Palladium, Platinum, and

Gold, Angew. Chem. Int. Ed. Engl. 13 (1974) 599–600. https://doi.org/10.1002/anie.197405992.

[112] Synthesis of cyclopentadienyldicarbonyl(dithiocarbene)iron cations and their reactions with amines | Inorganic Chemistry, (n.d.). https://pubs.acs.org/doi/10.1021/ic50195a011 (accessed September 14, 2024).

[113] S. Burling, M.F. Mahon, R.E. Powell, M.K. Whittlesey, J.M.J. Williams, Ruthenium Induced C−N Bond Activation of an N-Heterocyclic Carbene: Isolation of C- and N-Bound Tautomers, J. Am. Chem. Soc. 128 (2006) 13702–13703. https://doi.org/10.1021/ja065582k.

[114] N. Meier, F.E. Hahn, T. Pape, C. Siering, S.R. Waldvogel, Molecular Recognition Utilizing Complexes with NH,NR-Stabilized Carbene Ligands, Eur. J. Inorg. Chem. 2007 (2007) 1210–1214. https://doi.org/10.1002/ejic.200601258.

[115] V. Miranda-Soto, D.B. Grotjahn, A.G. DiPasquale, A.L. Rheingold, Imidazol-2-yl Complexes of Cp*Ir as Bifunctional Ambident Reactants, J. Am. Chem. Soc. 130 (2008) 13200–13201. https://doi.org/10.1021/ja804713u.

[116] S. Kuwata, T. Ikariya, Metal–ligand bifunctional reactivity and catalysis of protic N-heterocyclic carbene and pyrazole complexes featuring β-NH units, Chem. Commun. 50 (2014) 14290–14300. https://doi.org/10.1039/C4CC04457F.

[117] S. Kuwata, T. Ikariya, β-Protic Pyrazole and N-Heterocyclic Carbene Complexes: Synthesis, Properties, and Metal–Ligand Cooperative Bifunctional Catalysis, Chem. – Eur. J. 17 (2011) 3542–3556. https://doi.org/10.1002/chem.201003296.

[118] V. Miranda-Soto, D.B. Grotjahn, A.L. Cooksy, J.A. Golen, C.E. Moore, A.L. Rheingold, A Labile and Catalytically Active Imidazol-2-yl Fragment System, Angew. Chem. 123 (2011) 657–661. https://doi.org/10.1002/ange.201005100.

[119] M. Brill, J. Díaz, M.A. Huertos, R. López, J. Pérez, L. Riera, Imidazole to NHC Rearrangements at Molybdenum Centers: An Experimental and Theoretical Study, Chem. – Eur. J. 17 (2011) 8584–8595. https://doi.org/10.1002/chem.201101390.

[120] D. Brackemeyer, A. Hervé, C. Schulte to Brinke, M.C. Jahnke, F.E. Hahn, A Versatile Methodology for the Regioselective C8-Metalation of Purine Bases, J. Am. Chem. Soc. 136 (2014) 7841–7844. https://doi.org/10.1021/ja5030904.

[121] C.A. Tolman, Steric effects of phosphorus ligands in organometallic chemistry and homogeneous catalysis, Chem. Rev. 77 (1977) 313–348. https://doi.org/10.1021/cr60307a002.

[122] D. J. Cardin, B. Cetinkaya, E. Cetinkaya, M. F. Lappert, E. W. Randall, E. Rosenberg, Carbene complexes. Part III. Carbon-13 nuclear magnetic resonance studies of carbene complexes of 1,3-diorganoimidazolidin-2-ylidenes, J. Chem. Soc. Dalton Trans. 0 (1973) 1982–1985. https://doi.org/10.1039/DT9730001982.

[123] G. G. Zámbó, J. F. Schlagintweit, R. M. Reich, F. E. Kühn, Organometallic 3d transition metal NHC complexes in oxidation catalysis, Catal. Sci. Technol. 12 (2022) 4940–4961. https://doi.org/10.1039/D2CY00127F.

[124] M.K. Pandey, J. Choudhury, Ester Hydrogenation with Bifunctional Metal–NHC Catalysts: Recent Advances, ACS Omega 5 (2020) 30775–30786. https://doi.org/10.1021/acsomega.0c04819.

[125] X. Cai, X. Wei, M. Huang, Recent Developments of Transition-Metal-Catalyzed Cross-Coupling of Nitriles and Alcohols, ChemistrySelect 9 (2024) e202402955. https://doi.org/10.1002/slct.202402955.

[126] F. Freeman, Chromic Acid, in: Encycl. Reag. Org. Synth., John Wiley & Sons, Ltd, 2001. https://doi.org/10.1002/047084289X.rc164.

[127] J.M. Galvin, E.N. Jacobsen, M. Palucki, M.O. Frederick, Sodium Hypochlorite, in: Encycl. Reag. Org. Synth., John Wiley & Sons, Ltd, 2013. https://doi.org/10.1002/047084289X.rs084.pub3.

[128] L. Que, W.B. Tolman, Biologically inspired oxidation catalysis, Nature 455 (2008) 333–340. https://doi.org/10.1038/nature07371.

[129] C. Santilli, I.S. Makarov, P. Fristrup, R. Madsen, Dehydrogenative Synthesis of Carboxylic Acids from Primary Alcohols and Hydroxide Catalyzed by a Ruthenium N-Heterocyclic Carbene Complex, J. Org. Chem. 81 (2016) 9931–9938. https://doi.org/10.1021/acs.joc.6b02105.

[130] K. Fujita, R. Tamura, Y. Tanaka, M. Yoshida, M. Onoda, R. Yamaguchi, Dehydrogenative Oxidation of Alcohols in Aqueous Media Catalyzed by a Water-Soluble Dicationic Iridium Complex Bearing a Functional N-Heterocyclic Carbene Ligand without Using Base, ACS Catal. 7 (2017) 7226–7230. https://doi.org/10.1021/acscatal.7b02560.

[131] V. Cherepakhin, T.J. Williams, Iridium Catalysts for Acceptorless Dehydrogenation of Alcohols to Carboxylic Acids: Scope and Mechanism, ACS Catal. 8 (2018) 3754–3763. https://doi.org/10.1021/acscatal.8b00105.

[132] S. Yin, Q. Zheng, J. Chen, T. Tu, Acceptorless dehydrogenation of primary alcohols to carboxylic acids by self-supported NHC-Ru single-site catalysts, J. Catal. 408 (2022) 165–172. https://doi.org/10.1016/j.jcat.2022.02.018.

[133] V. Dragutan, I. Dragutan, L. Delaude, A. Demonceau, NHC–Ru complexes—Friendly catalytic tools for manifold chemical transformations, Coord. Chem. Rev. 251 (2007) 765–794. https://doi.org/10.1016/j.ccr.2006.09.002.

[134] S. Nath, E. Yadav, A. Raghuvanshi, A.K. Singh, Ru(II) Complexes with Protic- and Anionic-Naked-NHC Ligands for Cooperative

Activation of Small Molecules, Chem. – Eur. J. 29 (2023) e202301971. https://doi.org/10.1002/chem.202301971.

CHAPTER 2

Protic- or anionic-NHCs with classical-NHC in a single [Ru(CNC)(PPh_3)$_2$Cl]Cl pincer complex: Direct comparison of structure & electronic properties and heterolytic H_2 splitting

2.1. Introduction

Proton-responsive ligands are known to provide a better insight into understanding metal-ligand cooperation.[1–9] They can show non-covalent interaction, which facilitates the substrate binding to the metal, hence activation followed by transformation.[10] Protic-NHC ligands are a special class of proton-responsive ligands that provide the metal with proton delivering site at the β-position.[11] This β-proton functionality may provide hydrogen bonding for recognition and orientation of substrates at the metal center.[12] Deprotonation of the N-H wingtip of the protic-NHC ligand forms anionic-NHC, which has been shown to activate small molecules like H_2, CO_2, etc.[12–17]

Synthesis of protic-NHC complexes has been achieved through multiple routes.[18] There are few reports where a comparison between protic and classical NHCs has been made, mainly based on catalytic activity.[19,20] For the structural comparison, two different molecules containing a protic- or classical-NHC ligand have generally been considered. These molecules may crystallize into different space groups or have different lattice parameters, thereby not giving a clear picture for direct comparison. Hahn in 2016 reported a Rh-based unsymmetrical complex that features protic and classical NHC in a single molecule.[21] A few examples of recently reported ruthenium-based pincer complexes with protic-NHCs are shown in Figure 2.1.[11,17,22]

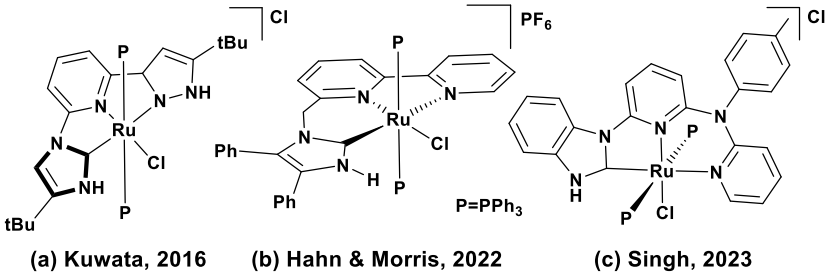

Figure 2.1. Some representative examples of Ru-pincer complexes with protic-NHC ligands.

CNC-pincer complexes based on a " pyridine-dicarbene" ligand platform have been developed by many groups and found to give robust complexes with two NHCs in the pincer platform. Figure 2.2 shows some previously reported Ru-CNC pincer complexes that are structurally similar to the complexes reported here.[23–26]

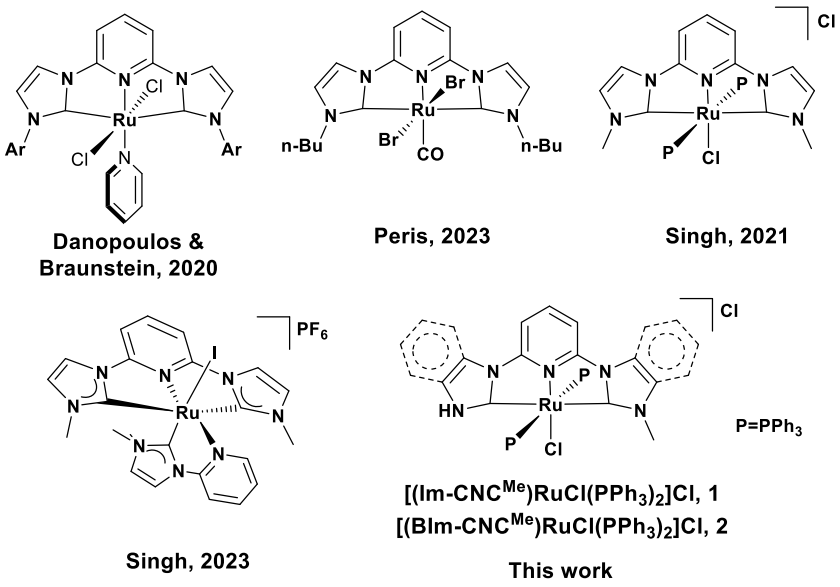

Figure 2.2. Some representative examples of Ru-CNC complexes.

Our group had reported Ru(II)-CNC pincer complexes, which inspired us to design new Ru(II)-CNC pincer complexes, which enabled us to study structural and electronic changes due to protic *vs.* classical NHCs. In this chapter, we describe a simple and easy-to-synthesize first set of ruthenium-based pincer complexes bearing protic and classical NHC within the same molecule. This pincer platform provides a direct comparison between protic and classical NHCs.

2.2 Results and Discussion

The design of complexes was inspired by the previously reported analogous classical NHC complexes by our group.[25] The suitable ligand precursor salts **L^1·HI** and **L^2·HI** have been synthesized with 92% and 86% yield, respectively, by selective methylation at the nitrogen atom of one of the imidazole/benzimidazole of the palindromic ligand 2,6-di(1H-imidazol-1-yl)pyridine[27] and 2,6-bis(1H-benzo[d]imidazol-1-yl)pyridine[28] (Scheme 2.1) and confirmed by NMR.

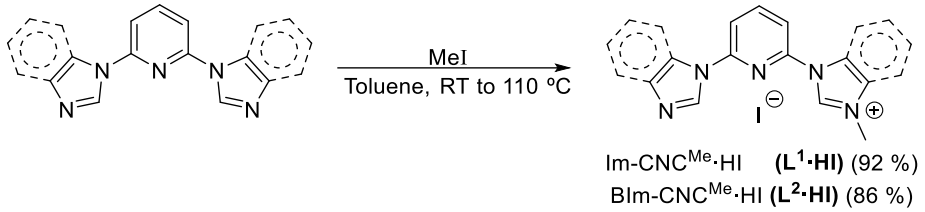

Scheme 2.1. Synthesis ligands (**L^1·HI**) and (**L^2·HI**)

The azolium salts, when reacted with Ag_2O in methanol for 12 h, give silver-carbene complex, which further undergoes an in-situ transmetallation with Ru precursor. The reaction of $RuCl_2(PPh_3)_3$ for 24 h at 70 °C with the in-situ generated silver carbene complexes of **L^1·HI/L^2·HI** ligands leads to the formation of cyclometallated [(Im/BIm)-Ru(C^HNC^{Me})(PPh_3)$_2$Cl]Cl protic-NHC complexes **1** and **2** with 45% and 60% yield respectively **(**Scheme 2.2). These complexes were characterized by LCMS, HRMS, multinuclear NMR, and single-crystal XRD techniques. The disappearance of C2-H peaks of azolium in ^{1}H and ^{13}C{^{1}H} NMR indicates the generation of carbene during the complex formation.

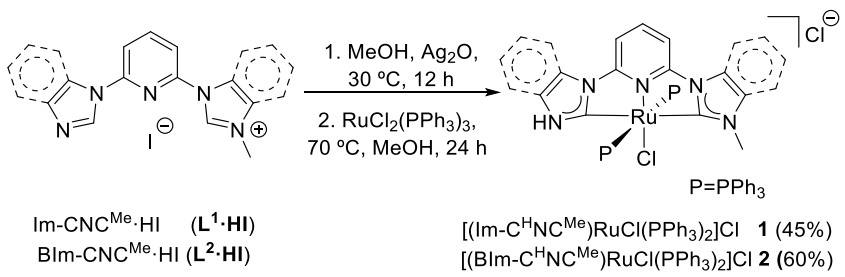

Scheme 2.2. Synthesis of complexes **1** and **2**.

The ^{1}H NMR spectrum of complexes **1** and **2** shows a downfield singlet peak at δ= 13.27 ppm and 14.42 ppm for protic-N-H protons**,** respectively. $^{31}P\{^{1}H\}$ NMR spectra show a singlet peak at δ= 29.78 ppm and 27.08 ppm for **1** and **2,** respectively, indicating the two-phosphine are trans to each other. In $^{13}C\{^{1}H\}$ NMR, the chemical shift for carbene peaks in complex **1** and **2** appears at δ= 189.7 ppm, 187.8 ppm and 202.6 ppm, 201.3 ppm respectively. The HRMS (ESI^{+}) for complexes **1** & **2** show the m/z peaks for $[M\text{-}Cl]^{+}$ fragments at 886.1578 (886.1573 calculated for $C_{48}H_{41}ClN_5P_2Ru$) and 986.1902 (986.1889 calculated for $C_{56}H_{45}ClN_5P_2Ru$) with ruthenium isotopic fingerprint pattern.

The molecular structures of **1** and **2** have been confirmed by single crystal X-ray diffraction analysis. Complex **1** (Figure 2.3) and **2** (Figure 2.4) crystallized in a monoclinic system with P21/c space group. The molecular structures show a distorted octahedral geometry around ruthenium, bound by an unsymmetrical CNC-based tridentate pincer ligand in a meridional position. The two PPh_3 groups are trans to each other, and Cl occupies the 6^{th} coordination site of ruthenium.

In the case of complex **1**, the Ru-C1 and Ru1-C11 bond distances are 2.109(7) Å and 2.059(8) Å, respectively, indicating a stronger bonding interaction of Ru with the classical-NHC compared to the protic-NHC. The bond length of C1-N1 and C11-N5 is 1.276(9) and 1.358(9) respectively. The shorter C1-N1 bond length than C11-N5 indicates a more double bond character in the case of the protic-NHC, while the classical-NHC bonds are more delocalized. The chlorido ligand is located trans to pyridine, and the bond distances for Ru1-N3 and Ru1-Cl1 are 2.032(6) Å and 2.457(2) Å, respectively. The free chloride is found hydrogen bonded to protic-NH (N-H---Cl) at a distance 2.324 Å from hydrogen and a bond angle of 155.63°. The bite angle between C1-Ru1-C11 formed by the CNC pincer ligand occupying the meridional site is 155.4(3)°.

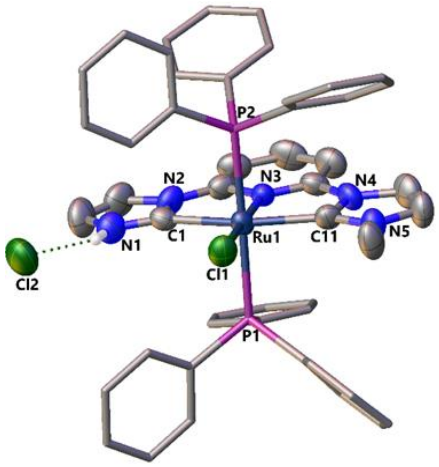

Figure 2.3. Single-crystal X-ray diffraction structure of **1**. One solvent H_2O molecule and hydrogen atoms (except for NH) are omitted for clarity. Phenyl rings of the phosphine ligand are drawn in tube form for clarity. Selected bond lengths (Å) and bond angles (°): Ru1-C1= 2.109(7) Å, Ru1-C11= 2.059(8) Å, N1-C1= 1.276(9) Å, N5-C11= 1.358(9) Å, N2-C1=1.404(9) Å, N4-C11= 1.372(9) Å, N1-C1-N2= 104.7(6)°, N5-C11-N4= 103.5(6)°.

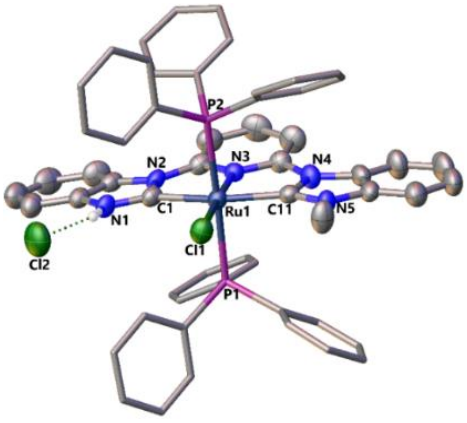

Figure 2.4. Single-crystal X-ray diffraction structure of **2**. One DMSO solvent molecule and hydrogen atoms (except for NH) are omitted for clarity. Phenyl rings of the phosphine ligand are drawn in tube form for clarity. Selected bond lengths (Å) and bond angles (°): Ru1-C1= 2.056(6) Å, Ru-C11= 2.027(6) Å, N1-C1= 1.331(7) Å, N5-C11= 1.344(7) Å, N2-C1=1.404(9) Å, N4-C11= 1.412(7) Å, N1-C1-N2= 103.5(5)°, N5-C11-N4= 103.6(5)°.

Similarly, in the case of complex **2**, the Ru1-C1 bond length is 2.056(6) Å, while the Ru1-C11 bond length is 2.027(6) Å (Figure 2.4), indicating, again, a stronger bond between Ru and classical-NHC. The bond lengths of N1-C1 and N5-C11 bonds are found to be comparable, perhaps due to more delocalization possible in the benzimidazolylidene units. The ruthenium carbene bonds in the case of complex **2** are shorter than complex **1**, perhaps due to the slightly better π-acceptor ability of benzimidazolydiene than imidazolydiene carbenes. Comparison of Ru-C(pNHC) bond of complex **1** and **2** with previously reported complexes has been listed in Table 2.1.

Table 2.1. Comparison of relevant properties of **1** & **2** with reported pNHC complexes shown in Figure 2.1.

ENTRY	1	2	A	B	C
Ru-C (Å)	2.109(7)	2.056(6)	2.077(6)	1.993(3)	1.960(7)
C-N(H) (Å)	1.276(9)	1.331(7)	1.348(8)	1.359(3)	1.351(8)
N-C-N(H) (°)	104.7(6)	103.5(5)	103.4(5)	103.1(2)	104.5(6)
$^{*}E_{1/2}$	0.97	1.09	0.44	-	-

*** Oxidation potential vs $Fc^{0/+}$ in Volts.**

The electron donation tendencies of protic-NHC and classical-NHC ligands were compared by electrochemical investigations, for which the anion was exchanged from Cl to PF_6 in complexes (Scheme 2.3). The reversible one-electron oxidation for complex **1-PF_6** and **1a-PF_6** appear at 0.97 V (vs. $Fc^{0/+}$) and 0.73 V (vs $Fc^{0/+}$), respectively (Figure 2.5). The more negative potential of **1a-PF_6** than **1-PF_6** suggests more electron donation tendency of the classical-NHC ligand than the protic-NHC ligand. Another oxidation peak at 1.07 V (vs. $Fc^{0/+}$) in the case of **1a-PF_6** is referred to as halide dissociated species identified by mass and NMR study in our previous report.[25] Similarly, the complex **1-PF_6** oxidises at a lower potential than **2-PF_6** (1.09 V vs. $Fc^{0/+}$), indicating more electron donation in the case of imidazoline-2-ylidene compared to benzimidazoline-2-ylidene (Figure

2.6). Comparison of oxidation potential (vs $Fc^{0/+}$) of complex **1** and **2** with previously reported complexes has been shown in Table 2.1.

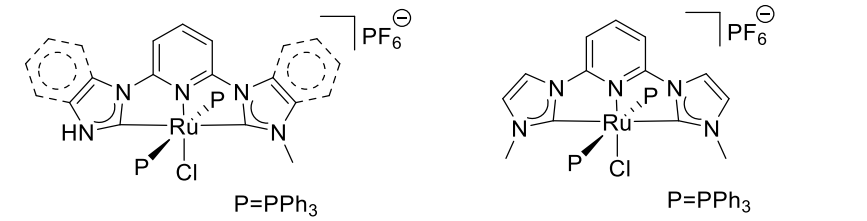

$[(Im\text{-}C^{H}NC^{Me})RuCl(PPh_3)_2]PF_6$ **1-PF6**
$[(BIm\text{-}C^{H}NC^{Me})RuCl(PPh_3)_2]PF_6$ **2-PF6**

$[(Im\text{-}C^{Me}NC^{Me})RuCl(PPh_3)_2]PF_6$ **1a-PF6**

Scheme 2.3. Complexes for electronic comparison

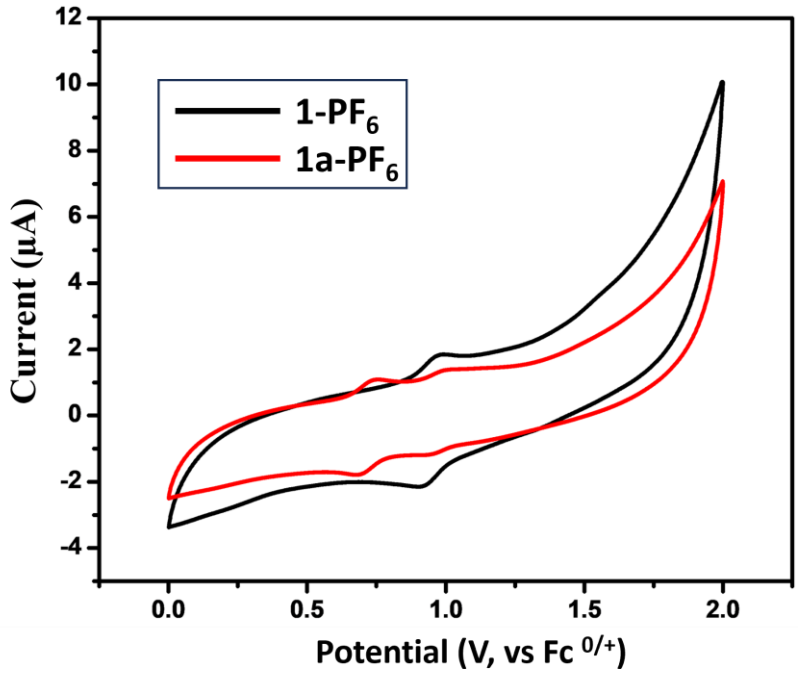

Figure 2.5. Comparison of CV-plot of complex **1-PF6** and **1a-PF6**.

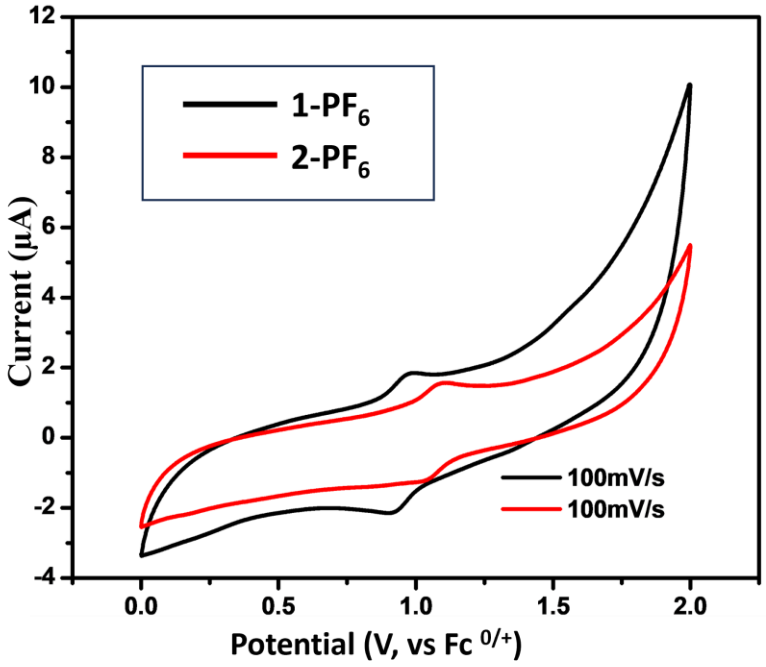

Figure 2.6. Comparison of CV-plot of complex **1-PF$_6$** and **2-PF$_6$.**

In the case of complex **2**, the deprotonated complex could be isolated only upon the reaction of KHMDS with complex **2** in toluene solvent at room temperature under nitrogen atmosphere in the glove box (Scheme 2.4). The deprotonated complex **2'** was characterized by ESI$^+$-MS, multinuclear NMR, and single crystal x-ray diffraction techniques.

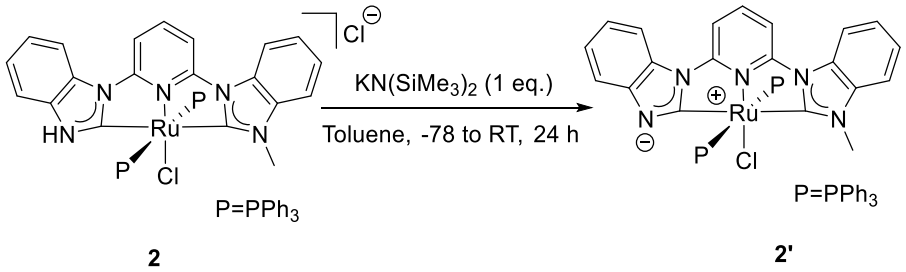

2 **2'**

Scheme 2.4. Deprotonation of protic N-H wingtip of **2**.

The ^{1}H-NMR spectrum of complex **2'** recorded in DMSO-d6 solvent shows the disappearance of the protic N-H signal at δ= 14.42 ppm. The ^{31}P{^{1}H} spectrum shows a singlet at δ= 31.41 ppm downfield to complex **2** (δ= 27.08 ppm). The carbene peaks in the ^{13}C{^{1}H} spectra of **2'** appear slightly different for samples of isolated

2' complex and in situ deprotonation of **2** in the NMR tube. In the case of in situ generated **2'**, signals at δ= 210.8 ppm and 202.6 ppm are obtained for the anionic- and classical-NHC, respectively, indicating the coordination of K^+ to the deprotonated nitrogen atom. However, in case of $^{13}C\{^1H\}$-NMR data of isolated **2'**, signals at δ= 193.7 ppm and 206.6 ppm are obtained for the anionic- and classical-NHC, respectively, indicating no K···N ion-pair as confirmed by the solid-state structures obtained from X-ray diffraction data. The complex **2'** is a neutral complex and is identified in LCMS as $[M+H]^+$ at 986.1966. The crystals for determining molecular structure were grown in two different sets of solvents. The first structure (**2'-MeOH**) was obtained from the diffraction of crystals formed by the layering of diethyl ether on methanol, whereas another structure was obtained from the diffraction of crystals formed by layering of ether on toluene (Figure 2.6). The complex **2'** crystallized in a monoclinic system with P21/n space group (Figure 2.7).

A distorted octahedral geometry around ruthenium with CNC-pincer ligand occupying the meridional position, two PPh_3 are trans to each other, and chloride trans to the pyridine group. When comparing the bond lengths for the metal carbene arm between complexes **2** and **2'**, it is observed that the Ru-C1 bond length increases upon deprotonation, as reported in some previous cases.[18,29,30] The bond angle formed by N1-C1-N2 increases from δ= 103.5(5)° to 108.75(14)° upon deprotonation. The bond length of the N1-C1 bond becomes shorter than the N5-C11 bond, which was comparable in the case of protic-NHC complex **2**.

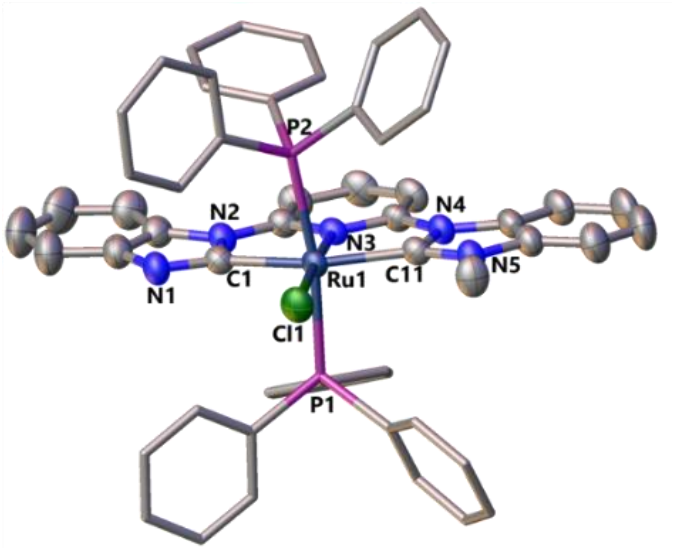

Figure 2.7. Single-crystal X-ray diffraction structure of **2'** (hydrogen atoms and diethyl ether solvent molecule have been omitted for clarity). Phenyl rings of the phosphine ligand are drawn in tube form for clarity. Selected bond lengths (Å) and bond angles (°): Ru1-C1= 2.0796(16) Å, Ru-C11= 2.0590(16) Å, N1-C1= 1.312(2) Å, N5-C11= 1.349(2) Å, N2-C1= 1.441(2) Å, N4-C11= 1.409(2) Å, N1-C1-N2= 108.75(14)°, N5-C11-N4= 103.95(13)°.

Further, electrochemical study on the protic-NHC complex **2-PF_6** and the anionic-NHC complex **2'** was performed, and their cyclic voltammogram were compared (Figure 2.8). A reversible oxidation peak at 0.91 V and a non-reversible oxidation peak at 1.18 V were observed in the plots. The appearance of two oxidation peaks can be understood in terms of an equilibrium between the Cl^- coordinated and dissociated forms in the case of anionic-NHC complex **2'**. Upon electrochemical oxidation, the Cl^- binding tendency increases, and only the Ru(III) complex with Cl^- coordinated form exists in the solution. Therefore, a reversible oxidation for the Cl^- bound form is observed, but not for the Cl^- dissociated form. The comparison of CV spectra of complex **2-PF_6** and **2'** indicated a more electron-donating tendency of anionic-NHC than protic-NHC.

(**a**)

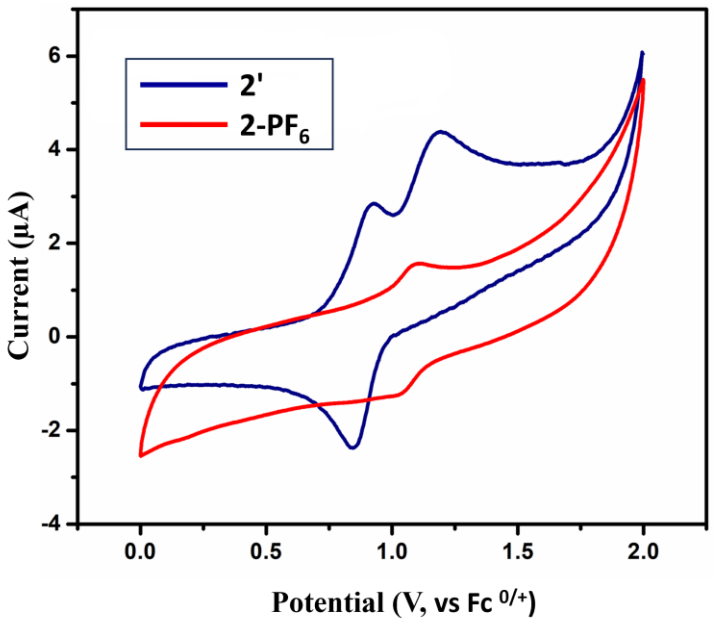

(**b**)

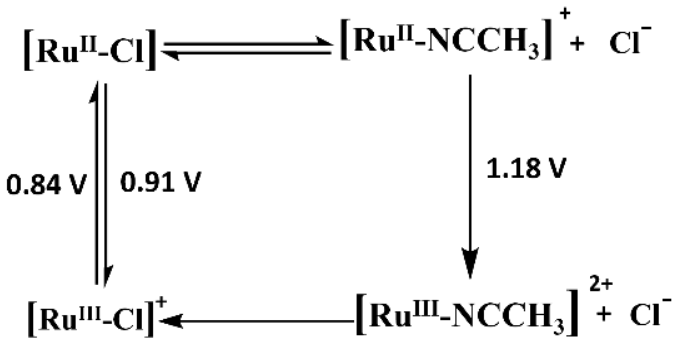

Figure 2.8. (**a**) Comparison of CV-plot of complex **2-PF$_6$** and **2'**. (**b**) Electrochemical oxidation-reduction of complex **2'**.

Further, to examine the cooperative nature of the proton-responsive ligand, H_2 splitting has been performed with complex **2'**. The deprotonated complex **2'** in toluene solvent was purged with H_2 gas and heated for 24 h at 110 °C (Scheme 2.5). The resulting product shows the formation of hydride complex **3** via heterolytic cleavage of H_2. The Ru-H complex **3** is found stable at laboratory benchtop conditions in air. The formation of complex **3** was confirmed by the ^{1}H and ^{31}P{^{1}H} NMR spectroscopy and ESI$^+$-MS. The ^{1}H NMR of complex **3** displays a hydride signal at δ= -8.50 ppm as a triplet and a

protic N-H signal at δ= 12.67 ppm as a singlet. The $^{31}P\{^{1}H\}$ NMR shows a new peak at δ= 51.36 ppm. The shifts in the $^{31}P\{^{1}H\}$ well as the protic-NHC signal in ^{1}H NMR, upon formation of the hydride complex **3,** are similar to our recent study.[17] The HRMS spectra show a peak $[M]^{+}$ peak at 952.2225.

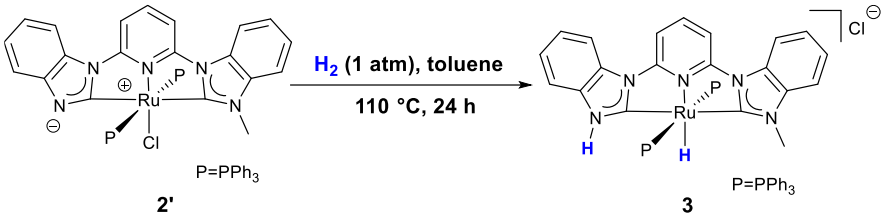

Scheme 2.5. Heterolytic cleavage of H_2 molecule.

2.3 Conclusions

In this chapter, first ruthenium-based CNC pincer complexes **1** and **2,** having the protic and classical NHC within the same complexes and in nearly identical environment, have been described. To the best of our knowledge, this is the first report that directly compares protic and classical NHC ligands in a CNC-pincer complex. The structural study shows that the bond length of Ru-C(pNHC) > Ru-C(classical). The electrochemical study indicates that the classical-NHC ligand has more electron donation tendency than the protic-NHC ligand. Upon deprotonation, the bond length of the Ru1-C1 bond of the anionic-NHC increases, and the carbene bond angle formed by the adjacent nitrogen atom of anionic-NHC also increases. Although the solid-state structure of complex **2'** suggests a sizable contribution of the C-imidazolyl structure, the $^{13}C\{^{1}H\}$-NMR data indicate a carbene-like signal. The chemical shift (δ 193.7) doesn't show a drastic upfield shift expected for the C-atom if the extra negative charge is transferred to this C-atom. Further, a downfield shift of the chemical shift (δ 210.8) for in situ deprotonation in DMSO-d6 is described as resulting from the formation of K···N ion-pair which pulls the electron density away from the carbenic carbon. The CV study of the anionic NHC complex **2'** indicates a more electron donation tendency of anionic-NHC than

protic-NHC ligand. Cooperation between metal and ligand was shown by the reaction of **2'** with H_2 to give complex **3**.

2.4 Experimental Section and Characterization

2.4.1 Materials and characterization methods

All the reactions and modifications were performed under an inert (dinitrogen unless otherwise stated) atmosphere using standard Schlenk line and glove box techniques. The glasswares were oven-dried over 200 °C overnight and cooled under vacuum. The solvents, i.e., dimethyl sulfoxide (DMSO), dichloromethane (DCM), toluene ($C_6H_5CH_3$), methanol (CH_3OH), and diethyl ether ($C_2H_5OC_2H_5$) were purchased from S. D. Fine-Chem Limited and further used after purification by distillation under N_2 atmosphere. Azoles (1-H-imidazole and 1-H-benzimidazole) and $RuCl_3 \cdot 3H_2O$ were purchased from Sisco Research Laboratories Pvt. Ltd. (SRL)-India and Sigma-Aldrich respectively. $RuCl_3 \cdot 3H_2O$ was used as the metal salt for the synthesis of metal precursor $RuCl_2(PPh_3)_3$ following literature procedure.[29] Deuterated solvents, DMSO-d_6 and $CDCl_3$ were purchased from Eurisotop and distilled using calcium hydride (CaH_2). 2,6-dibromopyridine was purchased from Sigma-Aldrich and used as starting material for the synthesis of ligand precursors $\mathbf{L^1}$ and $\mathbf{L^2}$ (2,6-bis((benz)imidazolyl)pyridine).[30,31] Electrospray ionization mass spectrometry (ESI-MS) spectrogram was recorded using Bruker Daltonik-Micro-TOF-QII spectrometer for exact mass and true isotopic measurement and solutions were prepared using analytical grade methanol or acetonitrile. NMR was obtained using a Bruker Avance (III) spectrometer operating at 400 MHz (^{1}H), 162 MHz (^{31}P), and 100 MHz (^{13}C) and Bruker Avance NEO spectrometer operating at 500 MHz (^{1}H), 202 (^{31}P), and 126 MHz (^{13}C).

2.4.2 Electrochemical and photophysical study

The electrochemical properties of the complexes **1-PF_6**, **1a-PF_6**, **2-PF_6** and **2'** were assessed using cyclic voltammetry, utilizing a standard

three-electrode set up comprising a glassy carbon as a working electrode, Pt wire as a counter electrode, and Ag/AgCl as a reference electrode. Analyte with 0.1 M tetrabutylammonium hexafluorophosphate ($[nBu_4N]PF_6$) in dry-degassed acetonitrile were utilized. All data were collected at scan rates of 100 mVs^{-1} and referenced to a [Ferrocene]/[Ferrocenium ion] redox couple internal standard, followed by conversion to SCE. Before each measurement, the electrochemical cell containing samples were deaerated by bubbling nitrogen gas. A photophysical study was attempted to compare the protic and classical NHC ligands in complexes **1-PF$_6$** and **1a-PF$_6$**, but no significant difference was observed in the UV spectra (figure 2.9). The electronic absorption spectra were recorded in a quartz cuvette using a Varian UV-vis spectrophotometer.

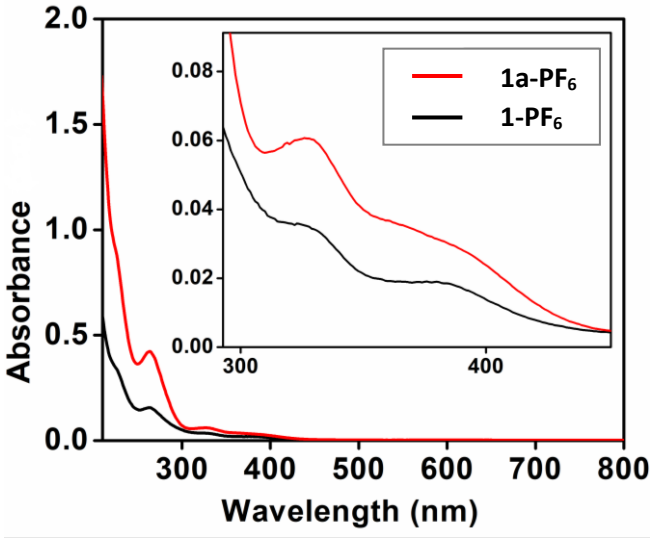

Figure 2.9. Comparison of UV-plot of complex **1-PF$_6$** and **1a-PF$_6$**

2.4.3 Synthesis of Ligand Precursor L^1/L^2- The ligand **L^1/L^2** was synthesized following the previously reported literature procedure.

2.4.4 Synthesis of Ligand (L^1·HI/L^2·HI)

An oven dried 100 ml two neck round bottle flask with magnetic bead was connected to reflux condenser in Schlenk line and then cooled under vacuum. The R.B flask was charged with L^1/L^2, methyl iodide (1 eq. in case of L^1 and 5 eq. in case of L^2) and dry toluene under N_2

atmosphere. The temperature increased from room temperature to reflux for 18 hours, allowing precipitate to settle. After cooling to room temperature, the precipitate was filtered, washed with toluene, DCM, and diethyl ether. The pure product was obtained after crystallization in methanol solvent.

2.4.4 (i) Characterization of L^1·HI-

^{1}H NMR (500 MHz, DMSO-d6) δ 10.26 (s, 1H), 8.85 (s, 1H), 8.69 (d, 0H), 8.39 (t, *J* = 8.1 Hz, 1H), 8.21 (s, 1H), 8.02 (d, *J* = 8.1 Hz, 1H), 7.95 (d, *J* = 7.9 Hz, 1H), 7.20 (s, 1H), 4.00 (s, 2H). **^{13}C{^{1}H} NMR** (126 MHz, DMSO-d6) δ 147.8, 145.2, 144.1, 136.0, 135.9, 130.7, 125.0, 119.1, 117.0, 114.2, 113.0, 111.0, 36.5

2.4.4 (ii) Characterization of L^2·HI

^{1}H NMR (500 MHz, DMSO-d6) δ 10.58 (s, 1H), 9.17 (s, 1H), 8.55 (d, *J* = 8.1 Hz, 1H), 8.41 (d, *J* = 8.4 Hz, 1H), 8.27 (d, *J* = 7.9 Hz, 2H), 8.20 (d, *J* = 8.4 Hz, 1H), 8.04 (d, *J* = 8.1 Hz, 1H), 7.85 – 7.75 (m, 3H), 7.37 (s, 2H), 4.26 (s, 3H). **^{13}C{^{1}H} NMR** (126 MHz, DMSO-d6) δ 148.9, 145.6, 144.0, 143.5, 142.8, 142.2, 132.0, 131.3, 129.0, 127.6, 127.0, 124.1, 123.3, 120.0, 115.0, 114.35, 113.9, 113.6, 33.7.

2.4.5 Synthesis of Complex 1 and 2

A 100 ml Schlenk tube with magnetic bead was cooled under vacuum and purged with nitrogen gas. The Schlenk tube was charged with **L^1·HI/L^2·HI** (1 equivalent) and dried under vacuum at 100 °C for 1 hour and then cooled to room temperature under nitrogen atmosphere. Dry methanol 10 ml was added followed by addition of Ag_2O (1 equivalent). The reaction mixture was stirred at room temperature for 12 hours under dark resulting in formation of white precipitate. After that 1 equivalent of $RuCl_2(PPh_3)_3$ was added and the reaction temperature was increased to 70 °C for 24 hours. The reaction mixture was filtered through a pad of celite. the filtrate was concentrated to 2 ml under reduced pressure followed by addition of 10 ml of diethyl

ether. X-ray quality crystals were obtained by layering of diethyl ether on the methanolic solution of complex at -18 °C.

2.4.5 (i) Characterizaion of complex 1

Yield (45%) **^{1}H NMR** (500 MHz, DMSO-d6) δ 13.27 (s, 1H), 8.32 (d, *J* = 2.4 Hz, 2H), 7.90 (d, *J* = 2.4 Hz, 1H), 7.46 (s, 1H), 7.43 – 7.31 (m, 2H), 7.26 (t, *J* = 7.4 Hz, 10H), 7.19 – 7.06 (m, 20H), 6.72 (d, *J* = 8.2 Hz, 1H), 3.23 (s, 3H). **^{31}P{^{1}H} NMR** (202 MHz, DMSO-d6) δ 29.78 (s). **^{13}C{^{1}H} NMR** (101 MHz, DMSO-d6) δ 189.7, 187.9, 152.2, 152.2, 136.0, 133.5, 133.4, 133.1, 133.0, 132.7, 129.8, 129.2, 128.9, 128.8, 127.9, 127.9, 127.8, 125.6, 121.8, 117.7, 116.4, 115.61, 105.3, 105.0, 36.1. HRMS (ESI+) m/z calcd for $C_{48}H_{41}ClN_5P_2Ru$ $[M\text{-}Cl]^+$ 886.1578, found 886.1573. Anal. Calcd for ($C_{48}H_{41}Cl_2N_5P_2Ru$) C, 62.54; H, 4.48; N, 7.60. Found C, 62.61; H, 4.25; N, 7.84.

2.4.5 (ii) Characterizaion of complex 2

Yield (60%) **^{1}H NMR** (500 MHz, DMSO-d6) δ 14.40 (s, 1H), 8.27 (d, 1H), 7.93 (d, *J* = 8.1 Hz, 1H), 7.73 (d, *J* = 7.8 Hz, 10H), 7.65 (d, *J* = 8.4 Hz, 1H), 7.63 – 7.48 (m, 4H), 7.38 (d, *J* = 7.7 Hz, 2H), 7.25 – 7.17 (m, 6H), 7.09 – 7.04 (m, 23H), 3.52 (s, 2H). **^{31}P{^{1}H} NMR** (202 MHz, DMSO-d6) δ 27.18 (s). **^{13}C{^{1}H} NMR** (101 MHz, DMSO-d6) δ 202.6, 201.3, 152.4, 137.1, 136.6, 135.7, 132.6, 132.5, 132.5, 132.3, 132.1, 130.6, 130.1, 129.4, 127.8, 127.9, 124.8, 124.5, 124.4, 123.6, 112.3, 111.7, 111.2, 110.8, 106.8, 106.5, 33.8. HRMS (ESI+) m/z calcd for $C_{56}H_{45}ClN_5P_2Ru$, $[M\text{-}Cl]^+$ 986.1901, found 986.1889. Anal. Calcd for ($C_{56}H_{45}Cl_2N_5P_2Ru$) C, 65.82; H, 4.44; N, 6.85. Found C, 65.91; H, 4.30; N, 6.98.

2.4.6 Synthesis of Complex 1a

To a solution of **1** (100 mg, 0.11 mmol) in THF, NH_4PF_6 was added and stirred for 30 min at room temperature. A precipitate of NH_4Cl comes out of the solution. The solution was filtered, and filtrate was

vacuum dried. The residue was washed with diethyl ether and collected over filter paper.

2.4.7 Synthesis of Complex 2a

To a solution of **1** (100 mg, 0.10 mmol) in methanol, NH_4PF_6 was added and stirred for 30 min at room temperature. A precipitate of 2a slowly comes out, and on cooling at 0 °C, some more precipitation happens. Precipitate was filtered, washed with diethyl ether.

2.4.8 Synthesis of Complex 2' by KHMDS

A solution of KHMDS (356 µL, 0.10 mmol) is added to complex 2 (100 mg, 0.10 mmol) in toluene at -78 ºC and allowed to stir at room temperature for 24 hours in glove box. The solution was filtered, and filtrate was dried under vacco. Subsequent recrystallization by Methanol/diethyl ether or toluene/diethyl ether afforded complex **2'**. Yield (72%) **^{1}H NMR** (500 MHz, DMSO-d6) δ 8.23 (d, *J* = 9.0 Hz, 1H), 7.64 – 7.58 (m, 2H), 7.56 (t, *J* = 5.3 Hz, 2H), 7.48 (d, *J* = 7.8 Hz, 1H), 7.41 (dd, *J* = 6.5, 12.8 Hz, 5H), 7.32 (dt, *J* = 7.9, 14.7 Hz, 3H), 7.24 (d, *J* = 3.8 Hz, 2H), 7.13 (q, *J* = 7.4 Hz, 15H), 6.94 (t, *J* = 7.6 Hz, 10H), 6.61 (d, *J* = 8.2 Hz, 1H), 3.36 (s, 3H)). **^{31}P{^{1}H} NMR** (202 MHz, DMSO-d6) δ 31.41 (s). **^{13}C{^{1}H} NMR** (126 MHz, DMSO-d6) δ 210.8, 202.6, 152.4, 137.2, 136.6, 135.7, 132.6, 132.6, 132.5, 132.3, 132.2, 132.0, 131.5, 131.4, 130.6, 130.1, 129.4, 128.80, 128.7, 124.8, 124.6, 124.5, 123.7, 112.3, 111.5, 111.2, 110.8, 106.8, 106.4, 33.8. Anal. Calcd for ($C_{56}H_{44}ClN_5P_2Ru$) C, 68.25; H, 4.50; N, 7.11. Found C, 68.32; H, 4.33; N, 7.28.

2.4.9 Heterolytic cleavage of H_2 (1 atm) at 110 °C by 2' to give 3

Complex **2'** (50 mg, 0.05 mmol) in toluene solvent was purged with hydrogen gas and heated for 24 hours at 110 °C. After the reaction the precipitate was filtered, dried and washed with diethyl ether to give complex **3**. Yield (45%) **^{1}H NMR** (500 MHz, DMSO-d6) δ 12.76 (s, 1H), 8.22 (d, *J* = 8.2 Hz, 1H), 8.03 (s, 1H), 7.78 (d, *J* = 8.2 Hz, 1H),

7.62 (t, *J* = 6.3 Hz, 1H), 7.38 (d, *J* = 7.2 Hz, 2H), 7.31 – 7.25 (m, 2H), 7.21 (d, *J* = 8.0 Hz, 2H), 7.19 – 7.10 (m, 6H), 7.01 (q, *J* = 3.2 Hz, 24H), 2.90 (s, 3H), -8.50 (t, *J* = 24.5 Hz, 1H). **$^{31}P\{^{1}H\}$ NMR** (202 MHz, DMSO-d6) δ 51.36.

2.4.10 X-ray data collection

The X-ray diffraction, of a single crystal acquired by crystallization of complexes, was performed and data obtained by using dual-core Agilent technologies (Oxford Diffraction) Super Nova CCD System equipped with micro focus Mo and Cu sources. Data was recorded at 293(2) K using graphite-mono chromated Mo Kα radiation source (λ_α = 0.71073 Å). The crystal data was collected using CrysAlisPro CCD and was further reduced using CrysAlisPro RED software. The structure with intrinsic phasing was solved using the SHELXT1[32] software, and the entire matrix least-squares on F^2 was refined using the SHELXL1[33] program within the Olex2[34] program for graphical interface. Anisotropic refinement was performed on all non-hydrogen atoms.

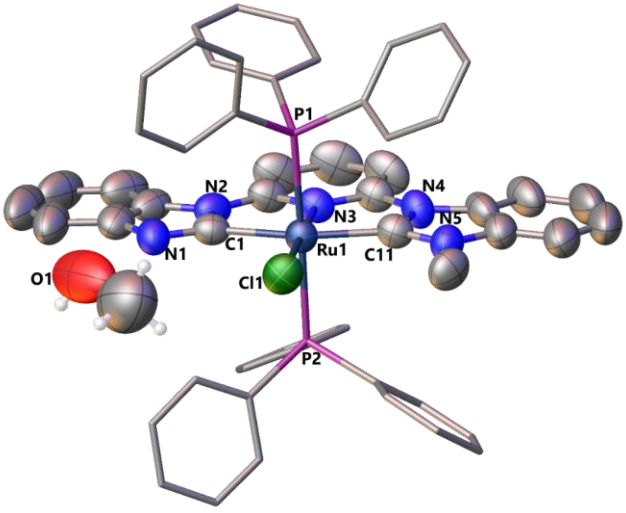

Figure 2.10. Single-crystal X-ray diffraction structure of **2'-MeOH** (hydrogen atoms except for CH_3OH solvent molecule are omitted and diethyl ether molecule has also been omitted for clarity). Phenyl rings of phosphine ligand drawn in tube form for clarity.

Table 2.2. Important crystallographic parameters with selected bond lengths and angle

Crystals	**1**	**2**	**2'-MeOH**	**2'**
Empirical formula	$C_{48}H_{43}Cl_2N_5OP_2Ru$	$C_{58}H_{51}Cl_2N_5OP_2RuS$	$C_{61}H_{58}ClN_5O_2P_2Ru$	$C_{56}H_{44}ClN_5P_2Ru$
Formula weight	939.78	1100.01	1091.58	985.42
Temperature/K	293(2)	293(2)	293(2)	300
Crystal system	Monoclinic	Monoclinic	Monoclinic	Monoclinic
Space group	$P2_1/c$	$P2_1/c$	$P2_1/n$	$P2_1/n$
a/Å	11.9308(2)	9.7331(3)	13.1379(4)	16.6067(2)
b/Å	17.8608(2)	23.3559(8)	24.4204(6)	18.5906(2)
c/Å	21.5668(5)	23.4710(8)	17.1734(3)	19.4595(3)
α/°	90	90	90	90
β/°	104.447(2)	101.886(3)	93.432(2)	114.968(2)
γ/°	90	90	90	90
Volume/$Å^3$	4450.42(14)	5221.2(3)	5499.9(2)	5446.24(15)
Z	4	4	4	4
$\rho_{calc}g/cm^3$	1.403	1.399	1.318	1.202
μ/mm^{-1}	0.586	0.550	0.439	0.434
F(000)	1928.0	2264.0	2264	2024.0
Crystal size/mm^3	0.31 × 0.18 × 0.17	0.17 × 0.07 × 0.04	0.33 × 0.29 × 0.2	0.43 × 0.34 × 0.17
Radiation	Mo Kα (λ = 0.71073)	Mo Kα (λ = 0.71073)	Mo Kα (λ = 0.71073)	Mo Kα (λ = 0.71073)
2Θ range for data collection/°	3.9 to 50.698	6.062 to 50.052	4.354 to 52.042	3.482 to 58.366
Index ranges	$-14 \le h \le 14$, $-21 \le k \le 21$, $-25 \le l \le 25$	$-11 \le h \le 11$, $-27 \le k \le 27$, $-27 \le l \le 27$	$-15 \le h \le 16$, $-28 \le k \le 30$, $-21 \le l \le 21$	$-21 \le h \le 22$, $-25 \le k \le 25$, $-24 \le l \le 26$
Reflections collected	81376	95237	56057	67182
Independent reflections	8144 [R_{int} = 0.1053, R_{sigma} = 0.0507]	9224 [R_{int} = 0.2046, R_{sigma} = 0.1057]	10821 [R_{int} = 0.1022, R_{sigma} = 0.0635]	13643 [R_{int} = 0.0468, R_{sigma} = 0.0328]
Data/restraints/parameters	8144/0/536	9224/0/634	10821/0/654	13643/0/587
Goodness-of-fit on F^2	1.165	1.040	1.076	1.029
Final R indexes	R_1 = 0.0801,	R_1 = 0.0683,	R_1 = 0.0621,	R_1 = 0.0324,

[I>=2σ (I)]	wR_2 = 0.1513	wR_2 = 0.1325	wR_2 = 0.1546	wR_2 = 0.0804
Final R indexes [all data]	R_1 = 0.1209, wR_2 = 0.1774	R_1 = 0.1229, wR_2 = 0.1551	R_1 = 0.0854, wR_2 = 0.1715	R_1 = 0.0399, wR_2 = 0.0857
Largest diff. peak /hole/ e $Å^{-3}$	1.96/-0.67	1.64/-0.84	0.71/-0.58	0.54/-0.61

Table 2.3. Important bond lengths and angles

Structures	**Bond length**	**Bond Angles**
1	Ru1-N3 = 2.032(6)	N3-Ru1-C1 = 78.7(3)
	Ru1-C11 = 2.059(8)	N3-Ru1-C11 = 76.8(3)
	Ru1-C1 = 2.109(7)	C11-Ru1-C1 = 155.4(3)
	Ru1-Cl1 = 2.457(2)	P1-Ru1-Cl1 = 91.10(7)
	Ru1-P1 = 2.376(2)	P2-Ru1-Cl1 = 86.05(7)
	Ru1-P2 = 2.371(2)	P2-Ru1-P1 = 177.12(7)
	N5-C11 = 1.358(9)	N5-C11-N4 = 103.5(6)
2	Ru1-N3 = 1.997(4)	N3-Ru1-C1 = 78.3(2)
	Ru1-C11 = 2.027(6)	N3-Ru1-C11 = 78.9(2)
	Ru1-C1 = 2.056(6)	C11-Ru1-C1 = 157.0(2)
	Ru1-Cl1 = 2.4487(14)	P1-Ru1-Cl1 = 88.76(5)
	Ru1-P1 = 2.3847(16)	P2-Ru1-Cl1 = 87.76(6)
	Ru1-P2 = 2.3820(17)	P2-Ru1-P1 = 176.37(6)
	N1-C1 = 1.331(7)	N1-C1-N2 = 103.5(5)
	N5-C11 = 1.344(7)	N5-C11-N4 = 103.6(5)
2'-MeOH	Ru1-N3 = 1.989(3)	N3-Ru1-C1 79.27(16)

	Ru1-C11 2.031(5)	N3-Ru1-C11 = 78.67(16)
	Ru1-C1 2.076(5)	C11-Ru1-C1 = 157.93(17)
	Ru1-Cl1 2.4448(11)	P1-Ru1-Cl1 88.15(4)
	Ru1-P1 2.3720(11)	P2-Ru1-Cl1 = 88.52(4)
	Ru1-P2 2.3703(12)	P2-Ru1-P1 176.59(4)
	N1-C1 1.318(6)	N1-C1-N2 108.6(4)
	N5-C11 1.352(6)	N5-C11-N4 103.4(4)
2'	Ru1-N3 1.9993(12)	N3-Ru1-C1 78.91(6)
	Ru1-C11 2.0590(16)	N3-Ru1-C11 78.43(6)
	Ru1-C1 2.0796(16)	C11-Ru1-C1 157.28(6)
	Ru1-Cl1 2.4780(4)	P1-Ru1-Cl1 = 90.373(16)
	Ru1-P1 2.3753(4)	P2-Ru1-Cl1 = 88.011(16)
	Ru1-P2 2.3716(5)	P2-Ru1-P1 = 171.245(15)
	N1-C1 1.312(2)	N1-C1-N2 = 108.75(14)
	N5-C11 1.349(2)	N5-C11-N4 = 103.95(13)

2.5. Spectral data of ligands and complexes (NMR and MS data)

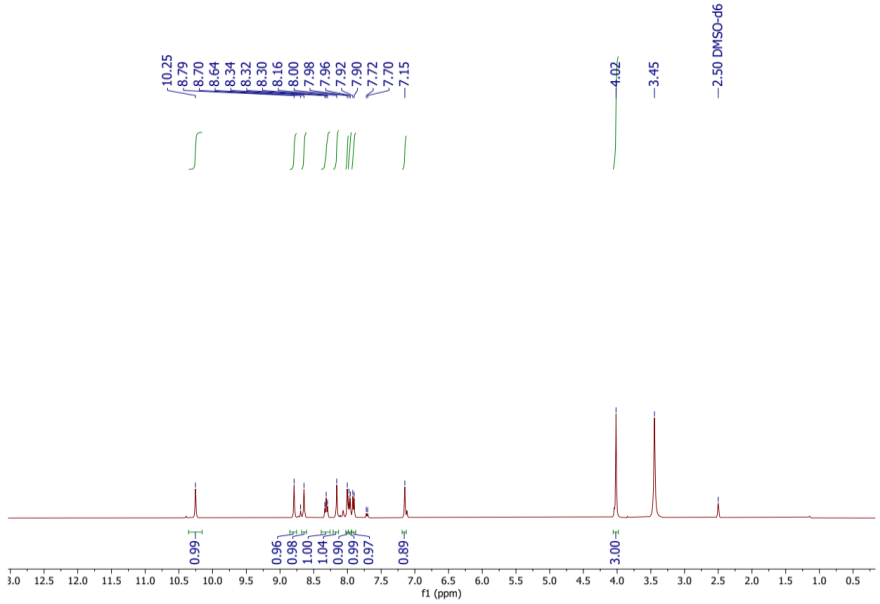

Figure 2.11.1. ^{1}H NMR spectrum of **L^{1}·HI** in DMSO-d6**.**

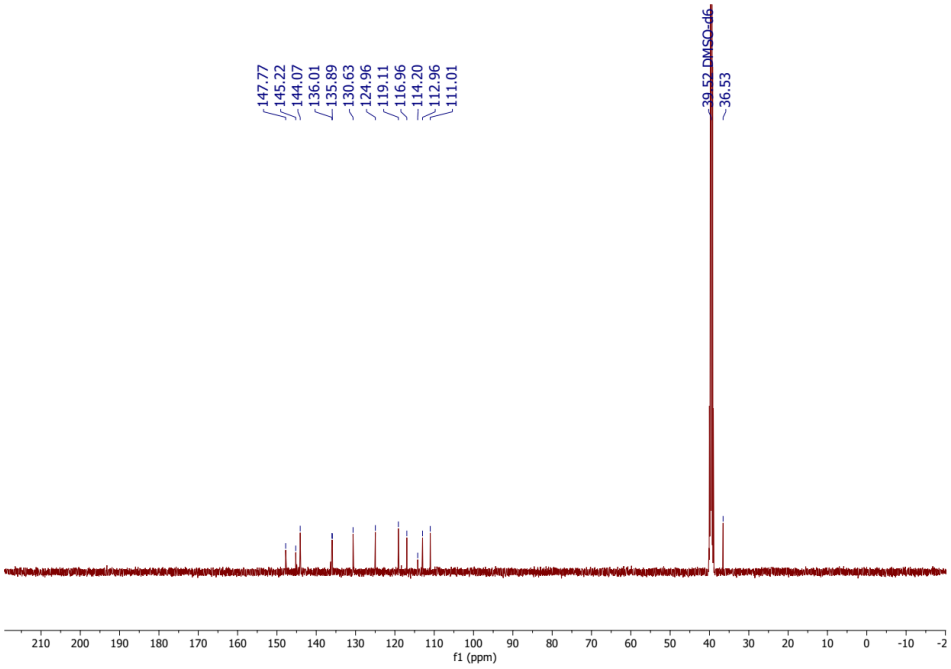

Figure 2.11.2. ^{13}C{^{1}H} NMR spectrum of **L^{1}·HI** in DMSO-d6**.**

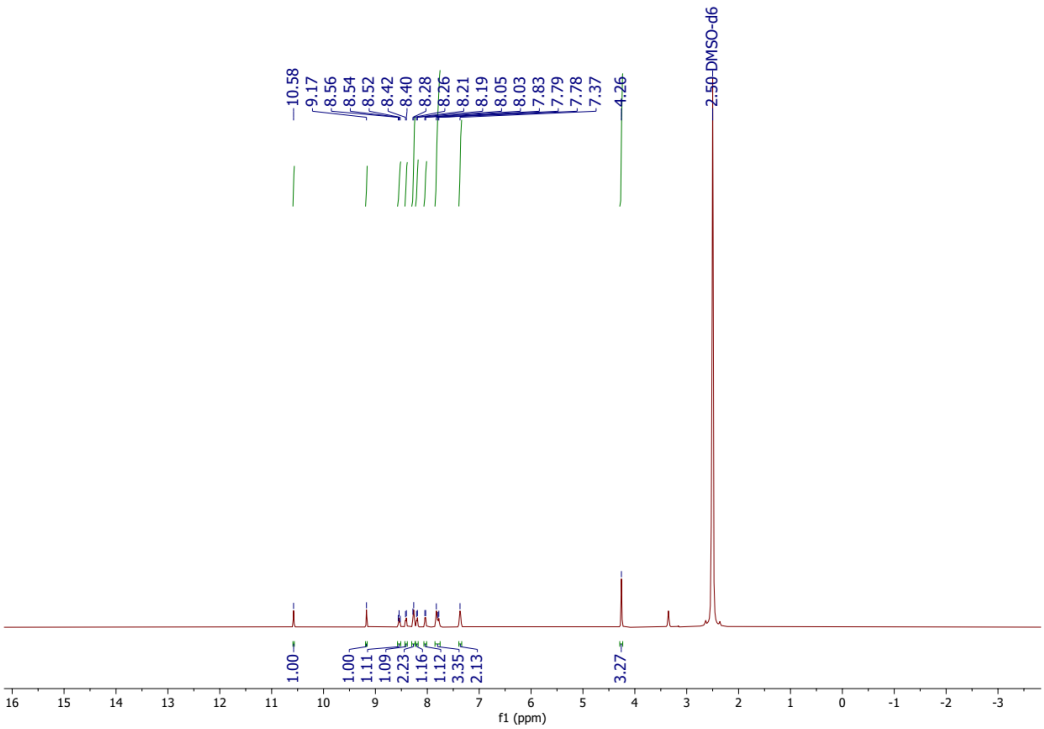

Figure 2.11.3. $^{13}C\{^{1}H\}$ NMR spectrum of **L^2·HI** in DMSO-d6**.**

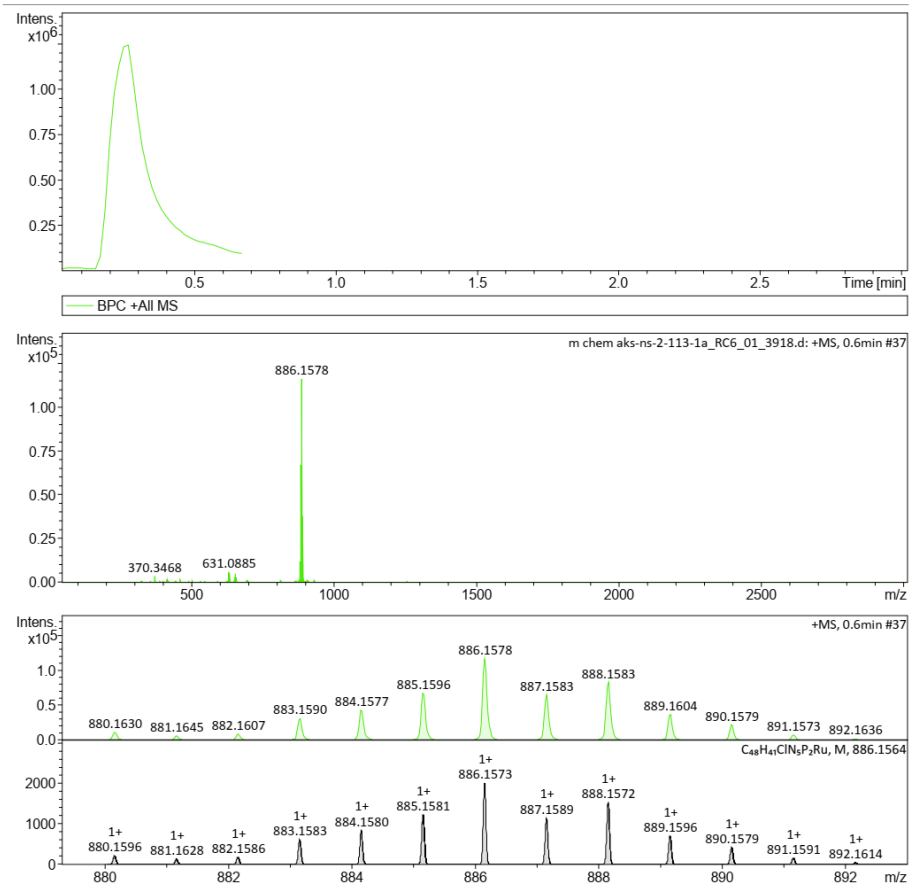

Figure 2.11.4. HRMS of complex **1.**

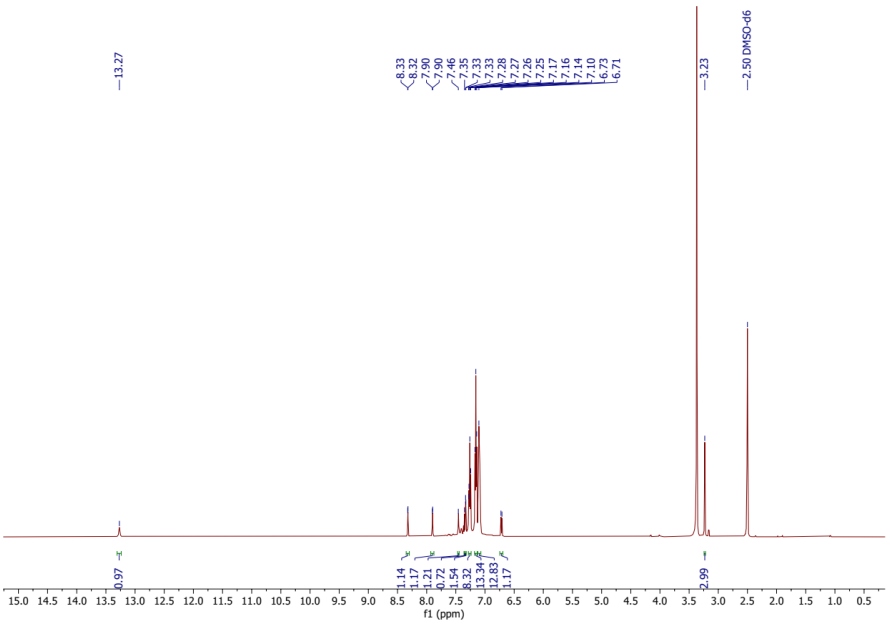

Figure 2.11.5. ^{1}H NMR spectrum of **1** in DMSO-d6**.**

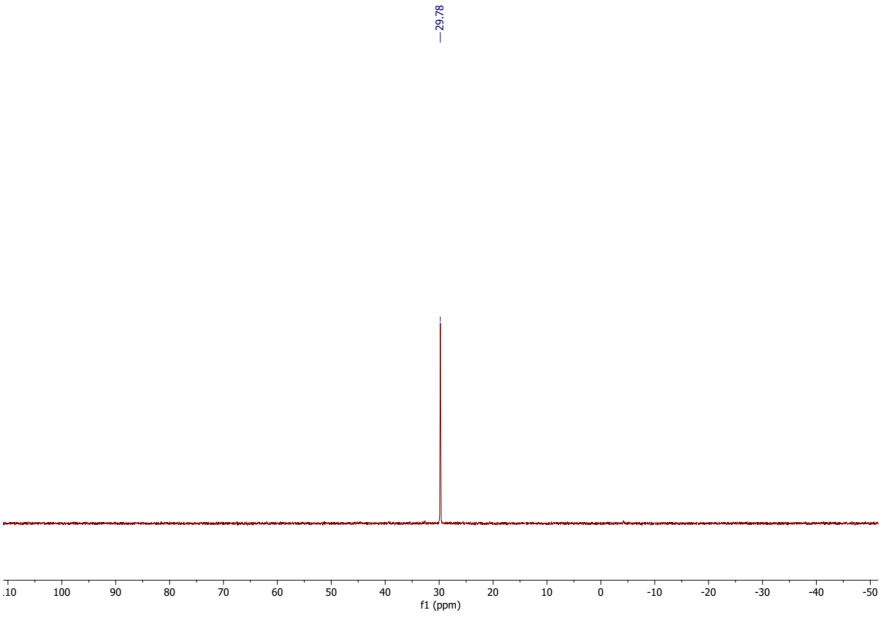

Figure 2.11.6. $^{31}P\{^{1}H\}$ NMR spectrum of **1** in DMSO-d6**.**

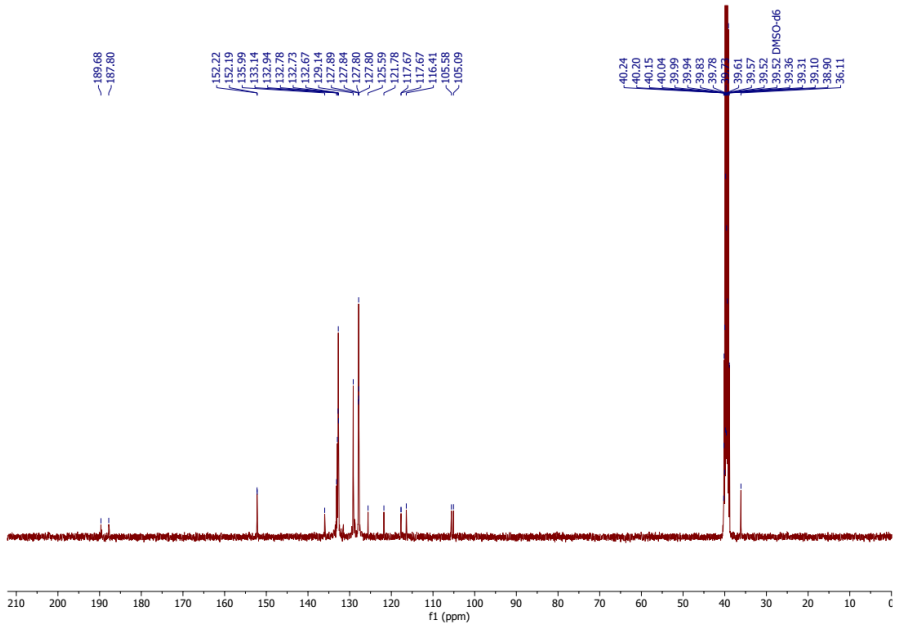

Figure 2.11.7. $^{13}C\{^{1}H\}$ NMR spectrum of **1** in DMSO-d6.

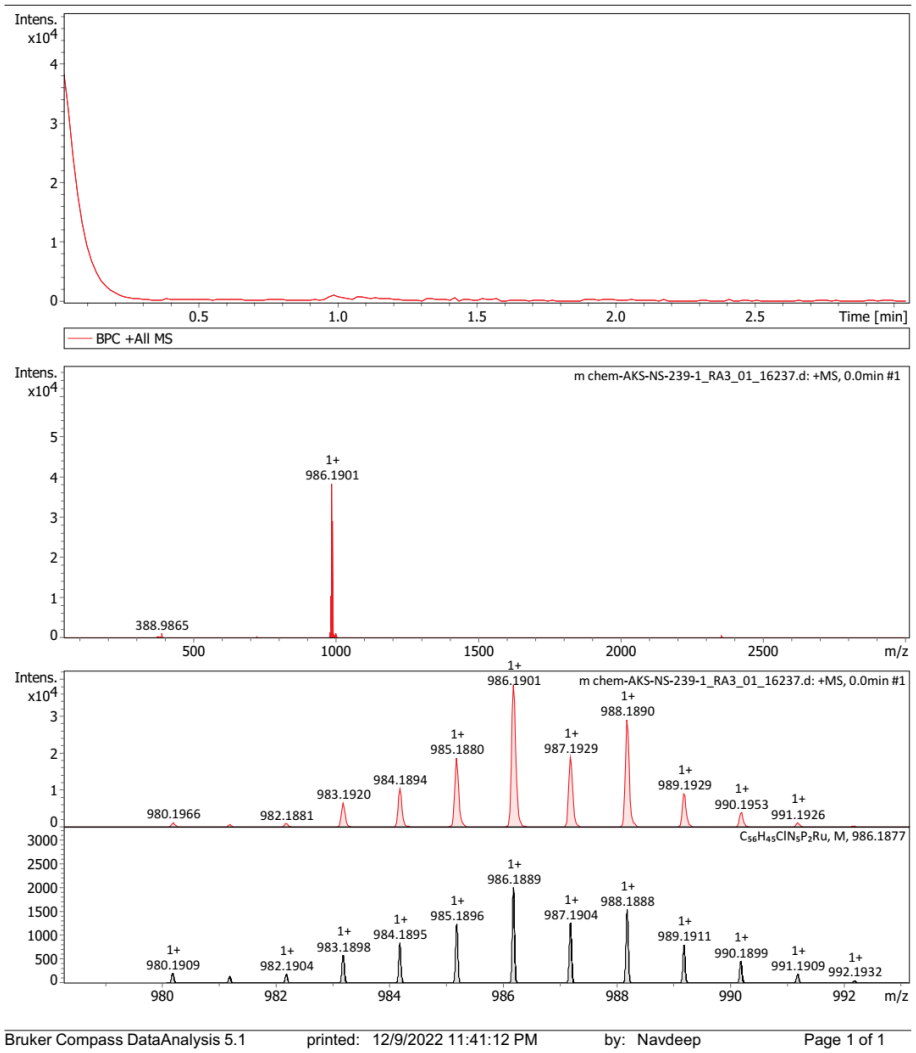

Figure 2.11.8. LCMS of complex 2.

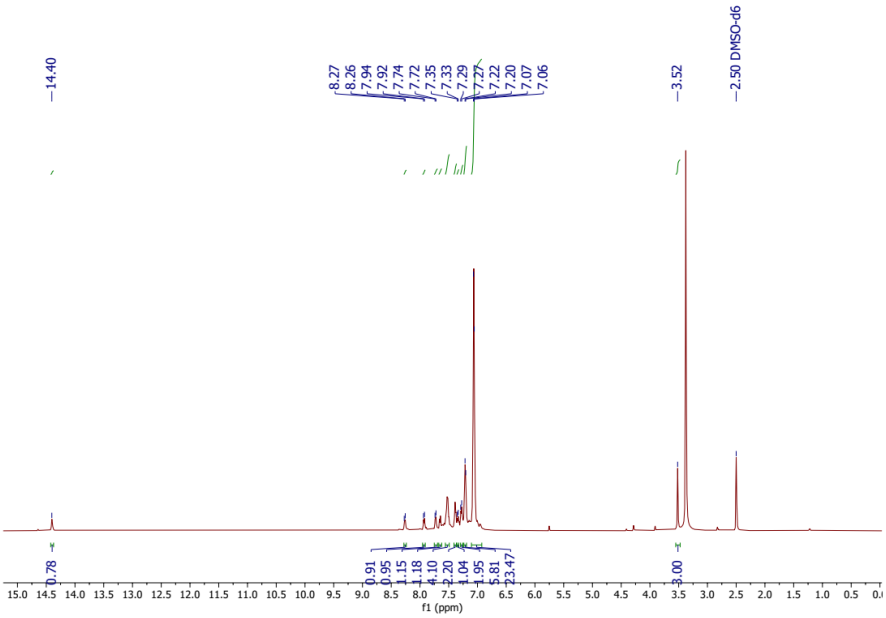

Figure 2.11.9. ^{1}H NMR spectrum of **2** in DMSO-d6**.**

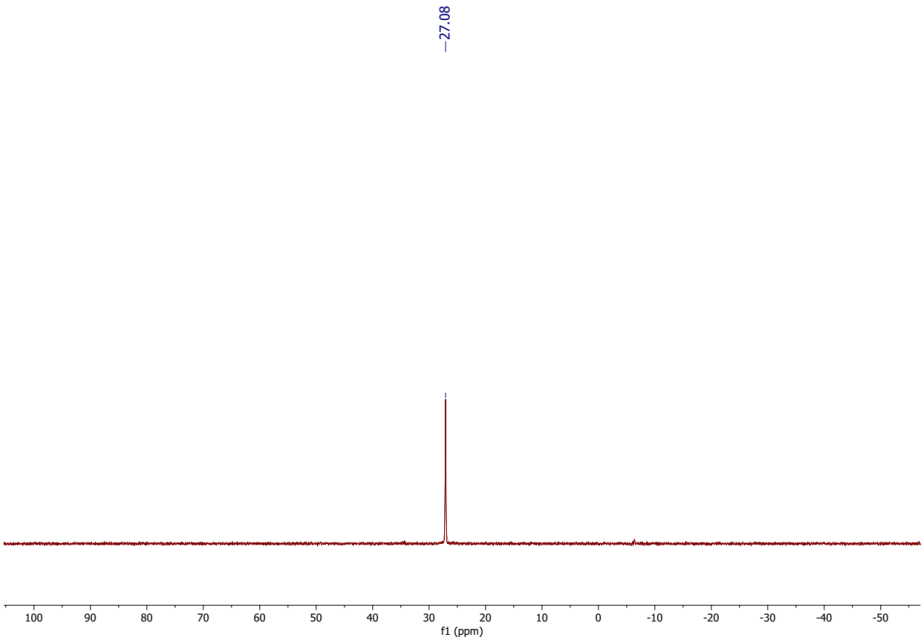

Figure 2.11.10. $^{31}P\{^{1}H\}$ NMR spectrum of **2** in DMSO-d6**.**

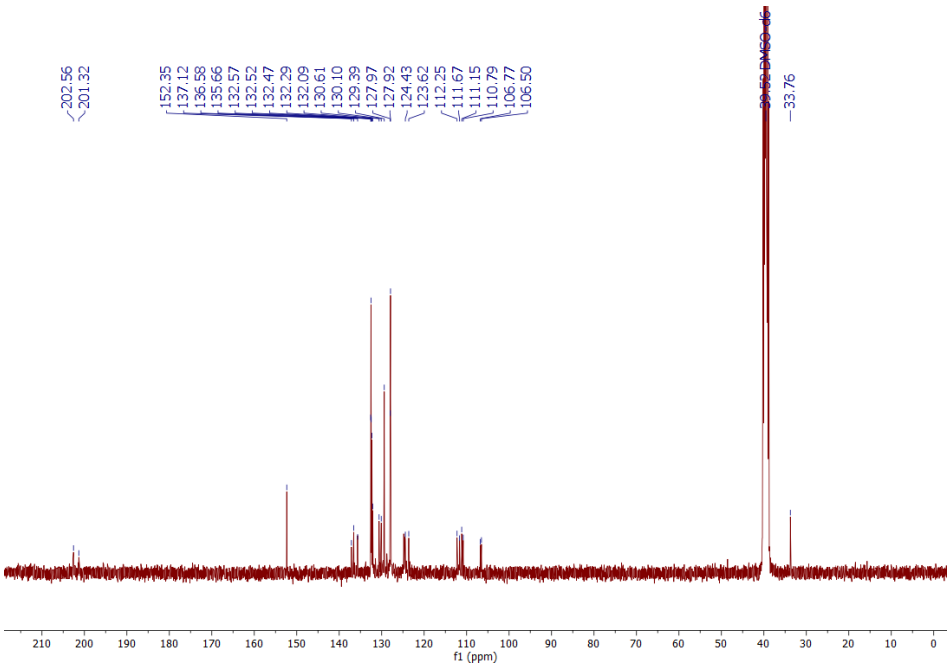

Figure 2.11.11. $^{13}C\{^{1}H\}$ NMR spectrum of **2** in DMSO-d6**.**

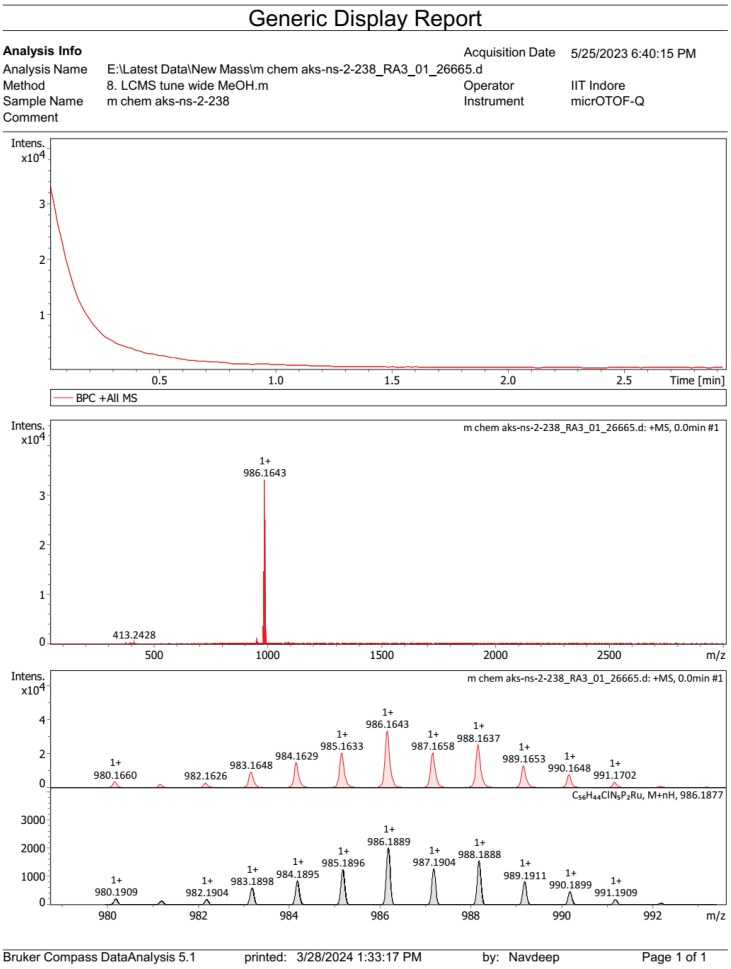

Figure 2.11.12. LCMS of complex **2'**

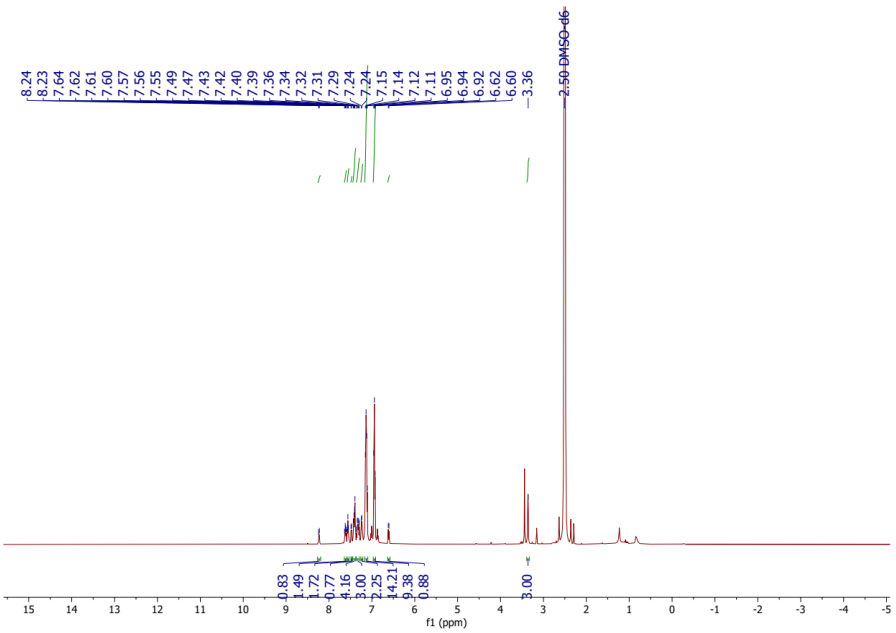

Figure 2.11.13. ^{1}H NMR spectrum of **2'** in DMSO-d6.

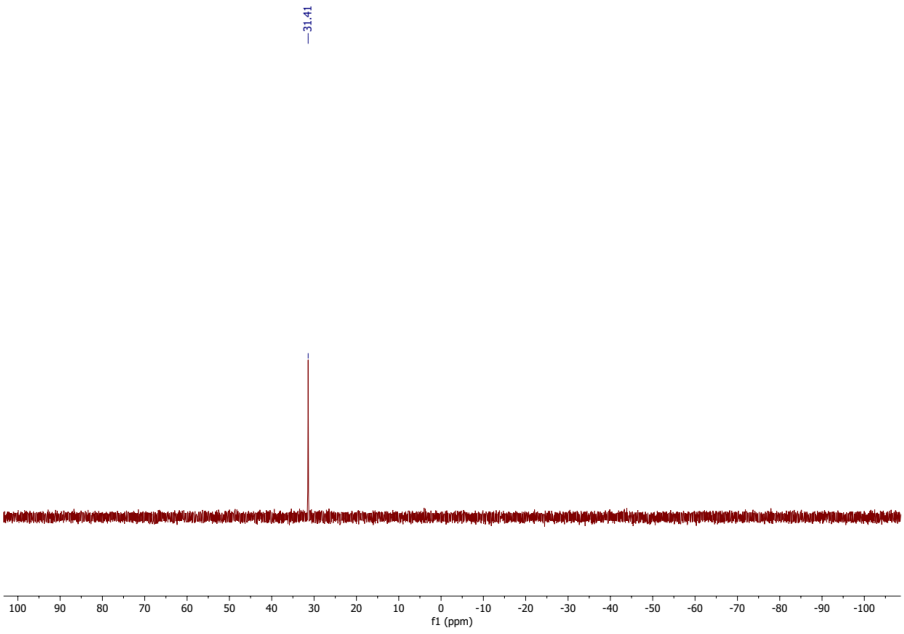

Figure 2.11.14. $^{31}P\{^{1}H\}$ NMR spectrum of **2'** in DMSO-d6.

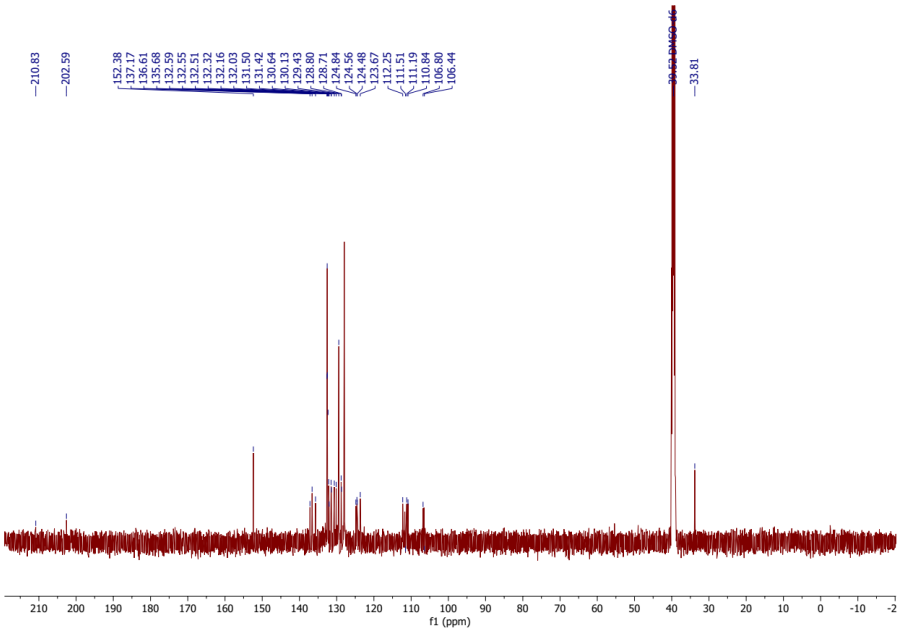

Figure 2.11.15. $^{13}C\{^{1}H\}$ NMR spectrum of in-situ deprotonated (**2'**) in DMSO-d6**.**

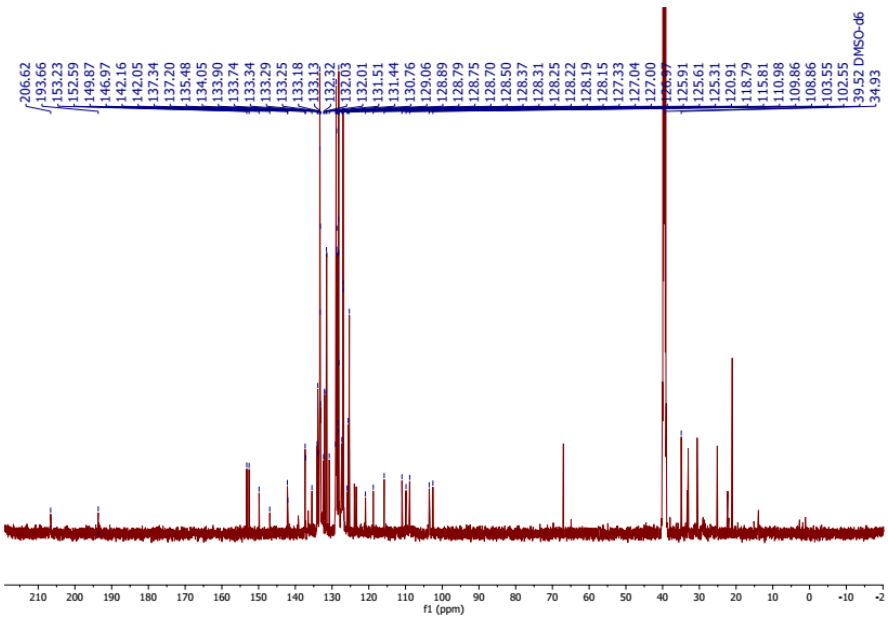

Figure 2.11.16. $^{13}C\{^{1}H\}$ NMR spectrum of isolated **2'**.

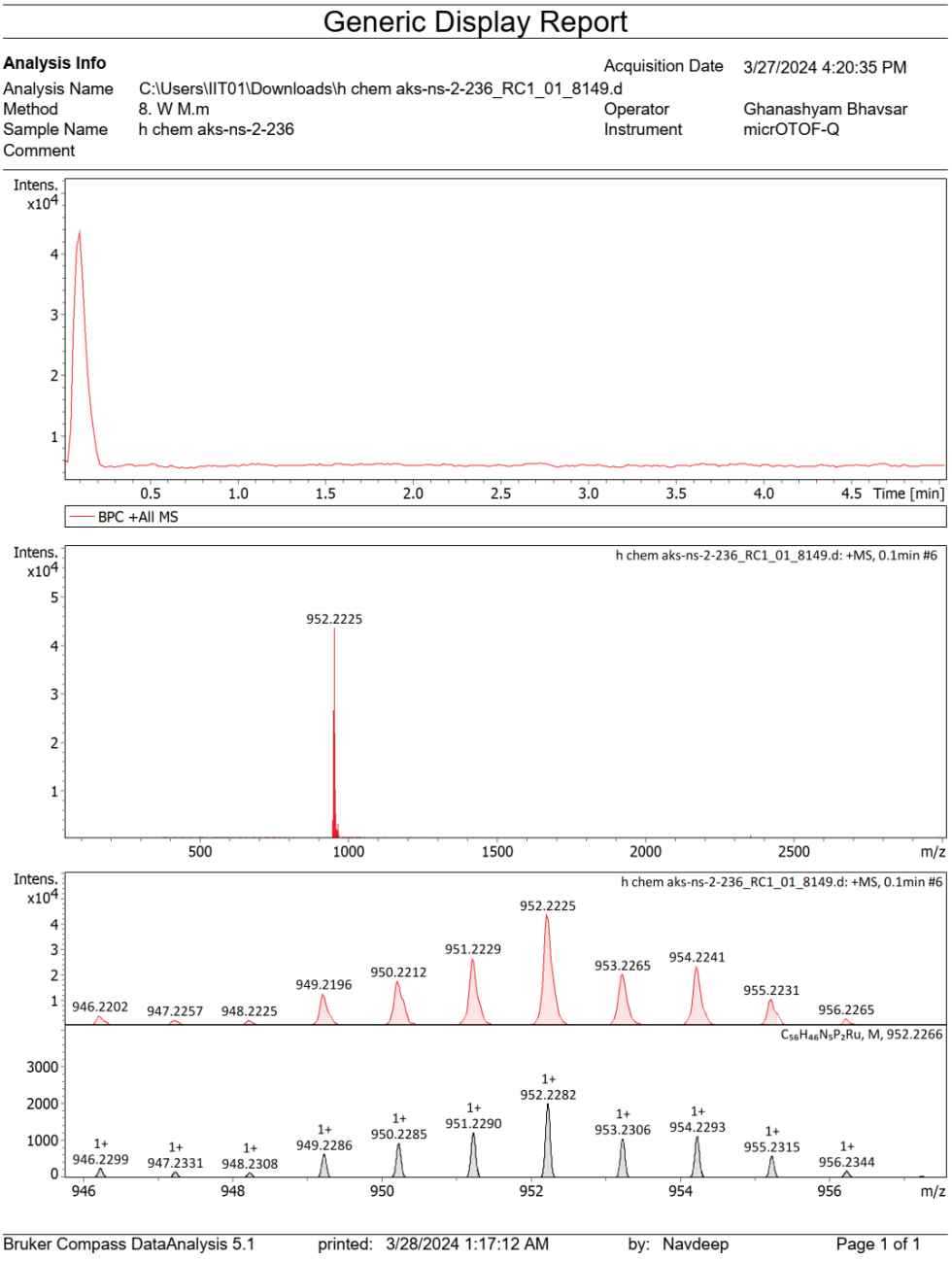

Figure 2.11.17. HRMS of complex **3.**

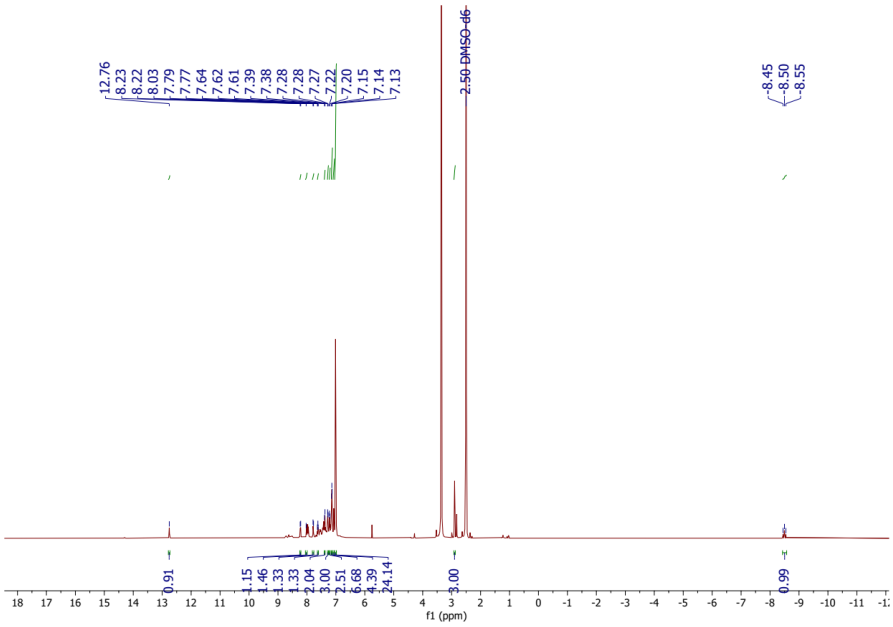

Figure 2.11.18. ^{1}H NMR of complex **3**.

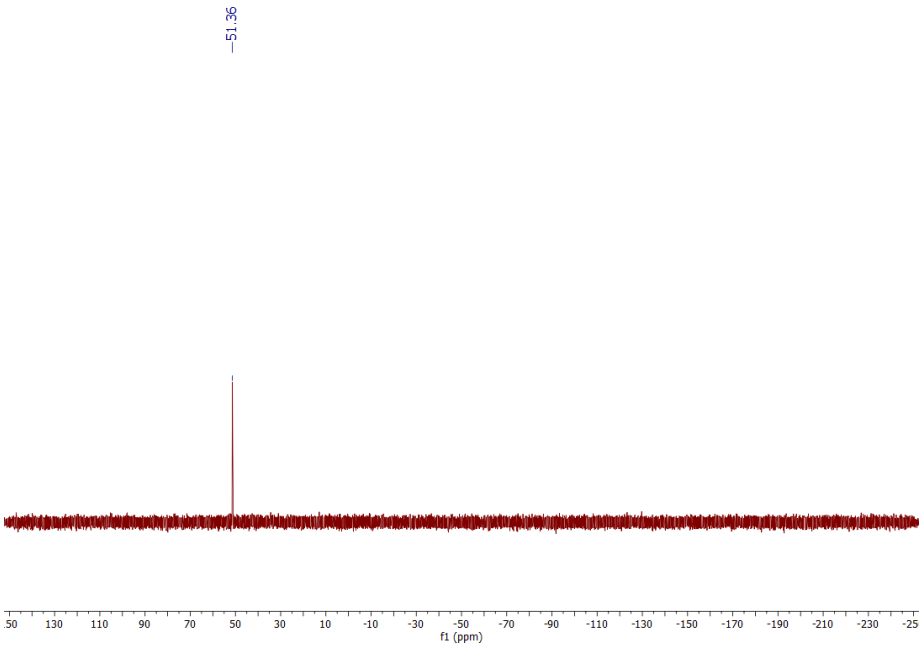

Figure 2.11.19. ^{31}P{^{1}H} NMR spectrum of **3.**

2.6. References

[1] C.B. van Beek, N.P. van Leest, M. Lutz, S.D. de Vos, R.J.M.K. Gebbink, B. de Bruin, D.L. J. Broere, Combining metal–metal cooperativity, metal–ligand cooperativity and chemical non-innocence in diiron carbonyl complexes, Chem. Sci. 13 (2022) 2094–2104. https://doi.org/10.1039/D1SC05473B.

[2] G. Van Koten, K. Kirchner, M.-E. Moret, eds., Metal-Ligand Co-operativity: Catalysis and the Pincer-Metal Platform, Springer International Publishing, Cham, 2021. https://doi.org/10.1007/978-3-030-68916-2.

[3] J.R. Khusnutdinova, D. Milstein, Metal–Ligand Cooperation, Angew. Chem. Int. Ed. 54 (2015) 12236–12273. https://doi.org/10.1002/anie.201503873.

[4] T. Higashi, S. Kusumoto, K. Nozaki, Cleavage of Si–H, B–H, and C–H Bonds by Metal–Ligand Cooperation, Chem. Rev. 119 (2019) 10393–10402. https://doi.org/10.1021/acs.chemrev.9b00262.

[5] D.L. DuBois, Development of Molecular Electrocatalysts for Energy Storage, Inorg. Chem. 53 (2014) 3935–3960. https://doi.org/10.1021/ic4026969.

[6] L. Alig, M. Fritz, S. Schneider, First-Row Transition Metal (De)Hydrogenation Catalysis Based On Functional Pincer Ligands, Chem. Rev. 119 (2019) 2681–2751. https://doi.org/10.1021/acs.chemrev.8b00555.

[7] M.R. Elsby, R.T. Baker, Strategies and mechanisms of metal–ligand cooperativity in first-row transition metal complex catalysts, Chem. Soc. Rev. 49 (2020) 8933–8987. https://doi.org/10.1039/D0CS00509F.

[8] J.I. van der Vlugt, J.N.H. Reek, Neutral Tridentate PNP Ligands and Their Hybrid Analogues: Versatile Non-Innocent Scaffolds for Homogeneous Catalysis, Angew. Chem. Int. Ed. 48 (2009) 8832–8846. https://doi.org/10.1002/anie.200903193.

[9] C. Gunanathan, D. Milstein, Metal–Ligand Cooperation by Aromatization–Dearomatization: A New Paradigm in Bond Activation and "Green" Catalysis, Acc. Chem. Res. 44 (2011) 588–602. https://doi.org/10.1021/ar2000265.

[10] B. de Bruin, P. Gualco, N.D. Paul, Redox Non-innocent Ligands, in: Ligand Des. Met. Chem., John Wiley & Sons, Ltd, 2016: pp. 176–204. https://doi.org/10.1002/9781118839621.ch7.

[11] T. Toda, A. Yoshinari, T. Ikariya, S. Kuwata, Protic N-Heterocyclic Carbene Versus Pyrazole: Rigorous Comparison of Proton- and Electron-Donating Abilities in a Pincer-Type Framework, Chem. – Eur. J. 22 (2016) 16675–16683. https://doi.org/10.1002/chem.201602552.

[12] F.E. Hahn, Substrate Recognition and Regioselective Catalysis with Complexes Bearing NR,NH-NHC Ligands, ChemCatChem 5 (2013) 419–430. https://doi.org/10.1002/cctc.201200567.

[13] T. Kösterke, J. Kösters, E.-U. Würthwein, C. Mück-Lichtenfeld, C. Schulte to Brinke, F. Lahoz, F.E. Hahn, Synthesis of Complexes Containing an Anionic NHC Ligand with an Unsubstituted Ring-Nitrogen Atom, Chem. – Eur. J. 18 (2012) 14594–14598. https://doi.org/10.1002/chem.201202973.

[14] V. César, N. Lugan, G. Lavigne, A Stable Anionic N-Heterocyclic Carbene and Its Zwitterionic Complexes, J. Am. Chem. Soc. 130 (2008) 11286–11287. https://doi.org/10.1021/ja804296t.

[15] S. T. Liddle, I. S. Edworthy, P. L. Arnold, Anionic tethered N -heterocyclic carbene chemistry, Chem. Soc. Rev. 36 (2007) 1732–1744. https://doi.org/10.1039/B611548A.

[16] M.Y. Leow, C.C. Ho, M.G. Gardiner, A.C. Bissember, Non-Classical Anionic Naked N-Heterocyclic Carbenes: Fundamental Properties and Emerging Applications in Synthesis and Catalysis, Catalysts 8 (2018) 620. https://doi.org/10.3390/catal8120620.

[17] S. Nath, E. Yadav, A. Raghuvanshi, A.K. Singh, Ru(II) Complexes with Protic- and Anionic-Naked-NHC Ligands for

Cooperative Activation of Small Molecules**, Chem. – Eur. J. 29 (2023) e202301971. https://doi.org/10.1002/chem.202301971.

[18] S. Kuwata, F.E. Hahn, Complexes Bearing Protic N-Heterocyclic Carbene Ligands, Chem. Rev. 118 (2018) 9642–9677. https://doi.org/10.1021/acs.chemrev.8b00176.

[19] C. Mühlen, J. Linde, L. Rakers, T.T.Y. Tan, F. Kampert, F. Glorius, F.E. Hahn, Synthesis of Iron(0) Complexes Bearing Protic NHC Ligands: Synthesis and Catalytic Activity, Organometallics 38 (2019) 2417–2421. https://doi.org/10.1021/acs.organomet.9b00260.

[20] S. Nath, E. Yadav, A. Raghuvanshi, A. K. Singh, Mechanistic insights and comparative analysis of Ru(ii)–NNC pincer complexes with anionic-, protic-, and classical-NHCs for transfer hydrogenation of ketones, Catal. Sci. Technol. 13 (2023) 7085–7099. https://doi.org/10.1039/D3CY01383A.

[21] F. Aznarez, P.J. Sanz Miguel, T.T.Y. Tan, F.E. Hahn, Preparation of Rhodium(III) Di-NHC Chelate Complexes Featuring Two Different NHC Donors via a Mild NaOAc-Assisted C–H Activation, Organometallics 35 (2016) 410–419. https://doi.org/10.1021/acs.organomet.5b00993.

[22] B.T.H. Tsui, M.M.H. Sung, J. Kinas, F.E. Hahn, R.H. Morris, A Ruthenium Protic N-Heterocyclic Carbene Complex as a Precatalyst for the Efficient Transfer Hydrogenation of Aryl Ketones, Organometallics 41 (2022) 2095–2105. https://doi.org/10.1021/acs.organomet.2c00228.

[23] A.A. Danopoulos, P. Braunstein, J. Saßmannshausen, D. Pugh, J.A. Wright, “Pincer” Pyridine–Dicarbene–Iridium and -Ruthenium Complexes and Derivatives Thereof, Eur. J. Inorg. Chem. 2020 (2020) 3359–3369. https://doi.org/10.1002/ejic.202000429.

[24] M. Poyatos, J.A. Mata, E. Falomir, R.H. Crabtree, E. Peris, New Ruthenium(II) CNC-Pincer Bis(carbene) Complexes: Synthesis and Catalytic Activity, Organometallics 22 (2003) 1110–1114. https://doi.org/10.1021/om020817w.

[25] D. Yadav, S. Misra, D. Kumar, S. Singh, A.K. Singh, Cationic ruthenium(II)–NHC pincer complexes: Synthesis, characterisation and catalytic activity for transfer hydrogenation of ketones, Appl. Organomet. Chem. 35 (2021) e6287. https://doi.org/10.1002/aoc.6287.

[26] R.K. Singh, D. Yadav, A.K. Singh, Cationic ruthenium(II)-CNC pincer complexes as phosphine-free catalysts for nitrile hydration to amides in aqueous medium, Mol. Catal. 549 (2023) 113523. https://doi.org/10.1016/j.mcat.2023.113523.

[27] A. Raba, M.R. Anneser, D. Jantke, M. Cokoja, W.A. Herrmann, F.E. Kühn, Facile and scalable preparation of 2-imidazolylpyridines, Tetrahedron Lett. 54 (2013) 3384–3387. https://doi.org/10.1016/j.tetlet.2013.04.060.

[28] C.J. Clarke, P.J. Morgan, J.P. Hallett, P. Licence, Linking the Thermal and Electronic Properties of Functional Dicationic Salts with Their Molecular Structures, ACS Sustain. Chem. Eng. 9 (2021) 6224–6234. https://doi.org/10.1021/acssuschemeng.0c08564.

[29] P.S. Hallman, T.A. Stephenson, G. Wilkinson, Tetrakis(triphenylphosphine)dichlororuthenium(II) and Tris(triphenylphosphine)dichlororuthenium(II), in: Inorg. Synth., John Wiley & Sons, Ltd, 1970: pp. 237–240. https://doi.org/10.1002/9780470132432.ch40.

[30] A. Raba, M.R. Anneser, D. Jantke, M. Cokoja, W.A. Herrmann, F.E. Kühn, Facile and scalable preparation of 2-imidazolylpyridines, Tetrahedron Lett. 54 (2013) 3384–3387. https://doi.org/10.1016/j.tetlet.2013.04.060.

[31] C.J. Clarke, P.J. Morgan, J.P. Hallett, P. Licence, Linking the Thermal and Electronic Properties of Functional Dicationic Salts with Their Molecular Structures, ACS Sustain. Chem. Eng. 9 (2021) 6224–6234. https://doi.org/10.1021/acssuschemeng.0c08564.

[32] G.M. Sheldrick, SHELXT – Integrated space-group and crystal-structure determination, Acta Crystallogr. Sect. Found. Adv. 71 (2015) 3–8. https://doi.org/10.1107/S2053273314026370.

[33] G.M. Sheldrick, Experimental phasing with SHELXC/D/E: combining chain tracing with density modification, Acta Crystallogr. D Biol. Crystallogr. 66 (2010) 479–485. https://doi.org/10.1107/S0907444909038360.

[34] O.V. Dolomanov, L.J. Bourhis, R.J. Gildea, J. a. K. Howard, H. Puschmann, OLEX2: a complete structure solution, refinement and analysis program, J. Appl. Crystallogr. 42 (2009) 339–341. https://doi.org/10.1107/S0021889808042726.

Chapter 3

Phosphine-free Ru(II)-CNC pincer complexes with mixed protic- and classical-NHCs in the same molecule for hydrogen production via oxidant-free benzyl alcohol dehydrogenation to benzoic acids

3.1 Introduction

N-heterocyclic cyclic carbenes (NHCs) are cyclic species that bear a carbene carbon and have at least one nitrogen atom within the ring.[1,2] Protic-NHC (p-NHC) is a special class of cyclic carbenes ligands that are stabilized by two heterocyclic atoms with at least one NH group.[3,4] In recent years, NHCs have been preferred over phosphines for ancillary ligands as phosphines have disadvantages like toxicity, poor air and moisture stability, and limited tunability. On the other hand NHCs show high stability towards oxygen and moisture.[5] NHCs also have more electron donation tendency than phosphines, which makes the metal-ligand bond thermodynamically stronger; hence, more bond dissociation energy and shorter bond length are observed in NHC complexes than their corresponding phosphine complex.[6] Ru-NHC complexes have been widely studied and explored in the field of homogeneous catalysis. The distinctive steric & electronic properties of NHC and the tunable reactivity of ruthenium make the Ru-NHC complexes an excellent catalyst.[7–11] Ru-NHC complexes have been employed in various catalytic applications like (de)hydrogenation, bond metathesis, cross-coupling reactions, and bond activation, etc.[12–19]

The selective oxidation of benzyl alcohol to benzoic acid is a fundamental textbook reaction but is essential for academic and industrial production.[20–23] Traditionally, the stoichiometric amount of hazardous

(in)organic oxidants[24,25] or hydrogen acceptor reagents[26–29] are required to complete this reaction. This process has a low atom economy and generates high metal waste, which is not suitable for the environment. In recent years, an alternative route for synthesizing carboxylic acid has been employed, which involves the dehydrogenation of benzyl alcohols. In the process of dehydrogenation, the catalyst facilitates the production of hydrogen gas along with carboxylic acid product, making it an atom economic reaction as hydrogen gas is the sole by-product.[30] This hydrogen gas can be used as potential fuel; hence, this process opens the door to the possibility of using alcohols as hydrogen storage compounds. With the recent discovery of new catalytic conditions, some enabling the reaction under very comfortable circumstances (25-120 °C, 1 atm), carboxylate synthesis via acceptorless dehydrogenation presents a graceful approach. The catalytic dehydrogenation of alcohol has been widely explored using Ru,[31–43] Rh,[44] Ir,[45,46] Mn,[47,48] Fe,[47] Ni[49] based catalysts, but the problem with these reactions was that it required high catalyst loading, high base concentrations in aqueous medium of organic solvent and the reaction required high temperature (>110 ºC).

Alcohols can be readily dehydrogenated to equivalent aldehydes or ketones with the help of different noble metal catalysts;[50–55] however, the direct dehydrogenative transformation of alcohols into carboxylic acids/carboxylates without the need for an oxidant has received comparatively less attention. The first example of this reaction was given by Milstein et al. in 2013 where Ru-PNN catalyst was used.[31] This work was followed by other ruthenium complexes like Ru-PNP[34] complex in 2014 and Ru-NHC[39] complex in 2015. The catalytic systems typically have significant drawbacks such as high metal loadings (up to 5 mol%), low turnover numbers (TON), long reaction periods (40 h), etc.[33,42,45,56] Recent reports show improved results for dehydrogenation of benzyl alcohol to carboxylic acid.

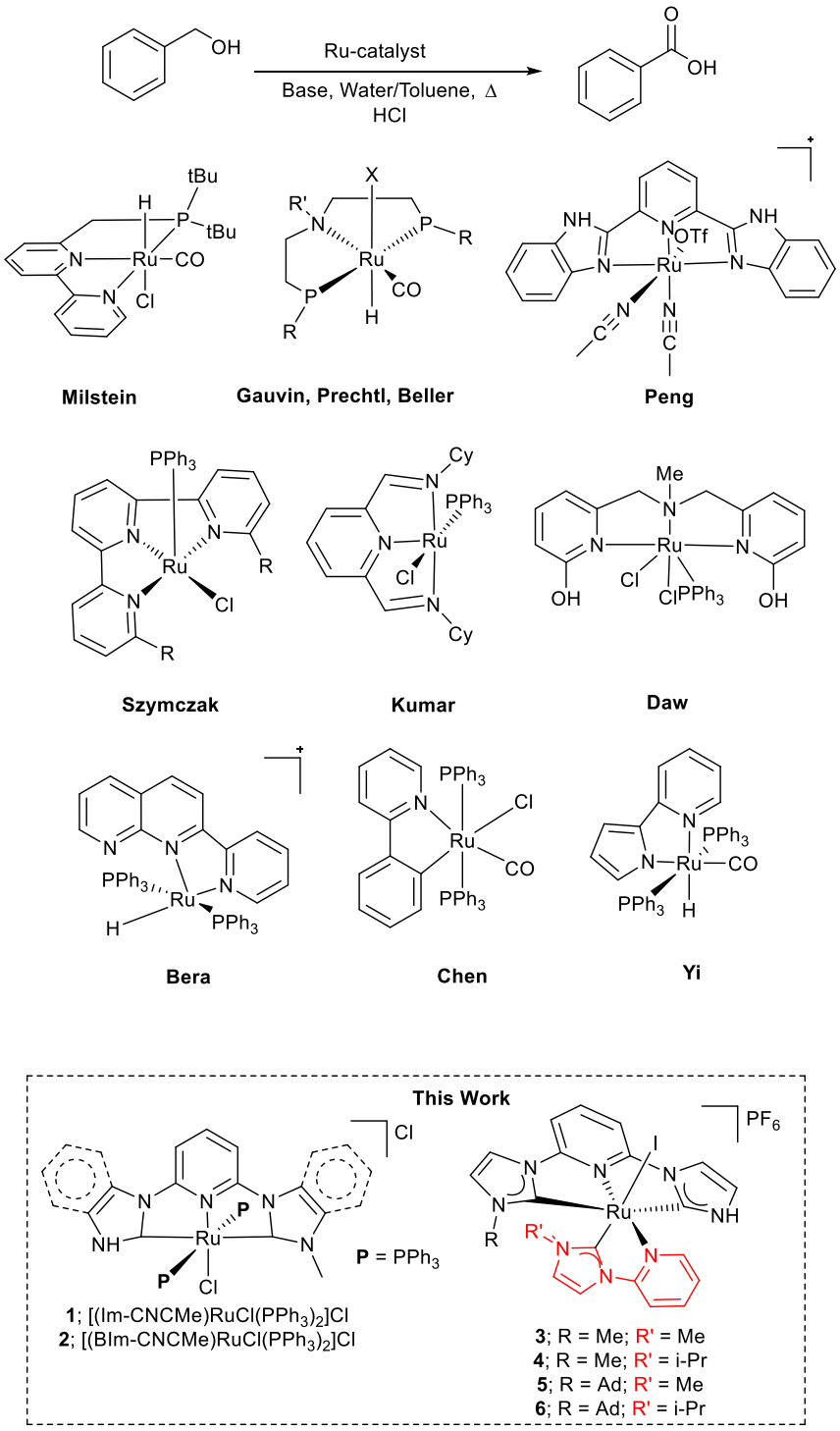

Figure 3.1. Some previously reported Ru-catalyst for Dehydrogenation of Benzyl Alcohol to Benzoic Acids.

Bera et al. in 2017 reported Ru-hydride catalyst having an N, N-type bidentate ligand for the acceptorless dehydrogenation of alcohol to acid aqueous solution under highly basic conditions.[40] Peng et al. in 2017 also reported Ru(II)-NNN pincer complex for neat alcohol dehydrogenation at high temperature (150 ºC).[36] Szymczak et al. reported dehydrogenative oxidation 0.2 mol% of catalyst at 120 ºC for 18 h.[57] Chen et al. in 2019 reported Ru(II)-NC bidentate complex for alcohol dehydrogenation using 0.5 mol % of catalyst toluene solvent.[43] Yi et al. in 2022 reported *cis*-pyr-Ru-H Ru(pp)H(CO)(PPh_3)$_2$] complex (where Hpp = 2-(1H-pyrrol-2-yl) pyridine) used for acceptorless dehydrogenation of benzyl alcohol using 0.1 mol% of catalyst in 12 hours.[58] Daw et al. in 2023 reported NNN-Ru catalyst for dehydrogenation benzyl alcohol to benzoic acid.[59] Kumar et al. in 2023 also reported (^{Cy2}NNN)$RuCl_2(PPh_3)$ pincer complexes used for the transformation of benzyl alcohols to corresponding acids products.[60] Some previously reported Ru-complexes for oxidant free dehydrogenation of benzyl alcohol to carboxylic acid have been shown in Figure 3.1.

Our group reported Ru(III)-NHC complexes [Ru($CN^{R'}$)(H_2O)$(Cl)_3$] (R'=Me (**P1**), *i*-Pr (**P2**)),[61] which were further used as precursors for the synthesis of Ru(II)-NHC based phosphine free complexes.[62] These phosphine-free complexes were utilized to nitrile hydration to amides in an aqueous medium.[62] In our previous chapter, we have shown the use of suitably substituted CNC ligand precursors for the preparation of complexes of general formula [Ru(CNC)(PPh_3)$_2$Cl]Cl, **1** and **2**, bearing protic and classical NHC in the same molecule, and studied their structural and electronic properties. In this chapter, we report the use of this strategy starting from our in-house Ru(III)-NHC complexes **P1**, **P2** as precursors for the preparation of new electron-rich phosphine-free complexes [Ru(CNC)(CN)I]PF_6 (**3**-**6**) with multiple carbene ligands having protic- and classical-NHCs in the same molecule. These complexes have been further explored for acceptorless dehydrogenation of aromatic, heteroaromatic and aliphatic alcohols under oxidant-free conditions.

3.2 Results and Discussion

3.2.1 Synthesis and characterization of ligands and Ru(II)-CNC based protic NHC complexes

The synthesis of complexes **1** and **2** has been described in our previous chapter. The ligand precursor for this work was prepared following the previously reported literature procedure with slight modification. Initially, the commercially available 2,6-dibromopyridine was reacted with an excess of imidazole in the presence of CuI to give a symmetric bis-NHC pincer ligand, i.e., 2,6-di(1H-imidazol-1-yl)pyridine (**L1**) *via* Ullmann's coupling.[63] The unsymmetrical CNC-pincer ligands **L1·HI**, **L2·HBr** were prepared by the selective alkylation of one of the imidazole of the palindromic ligand (Scheme 3.1). The ligands were confirmed by HRMS, ^{1}H, and $^{13}C\{^{1}H\}$ NMR spectroscopic techniques. In the case of **L1·HI,** the imidazolium-C2 proton and carbon appears in ^{1}H & $^{13}C\{^{1}H\}$ at δ= 10.25 ppm and 147.77 ppm, respectively, whereas the imidazole-C2 proton and carbon in ^{1}H & $^{13}C\{^{1}H\}$ positions at δ= 8.79 ppm and 145.22 ppm respectively. Several attempts were made to synthesize ligand **L2·HBr** by varying the solvent and temperature; the successful synthesis was achieved under solvent-free conditions when the reaction was performed at 160 °C for 24 h. This synthesis was supported by ^{1}H, $^{13}C\{^{1}H\}$ NMR, where the imidazolium C2-H proton appears at δ= 10.05 ppm and imidazolium C2 carbon appears at 147.48 ppm in the respective NMR spectra. In addition, HRMS (ESI^{+}) also indicated the formation of **L2·HBr** with the corresponding peak for $[M\text{-}Br]^{+}$ at m/z = 346.2018 (calculated for $C_{21}H_{24}N_5$; 346.2026).

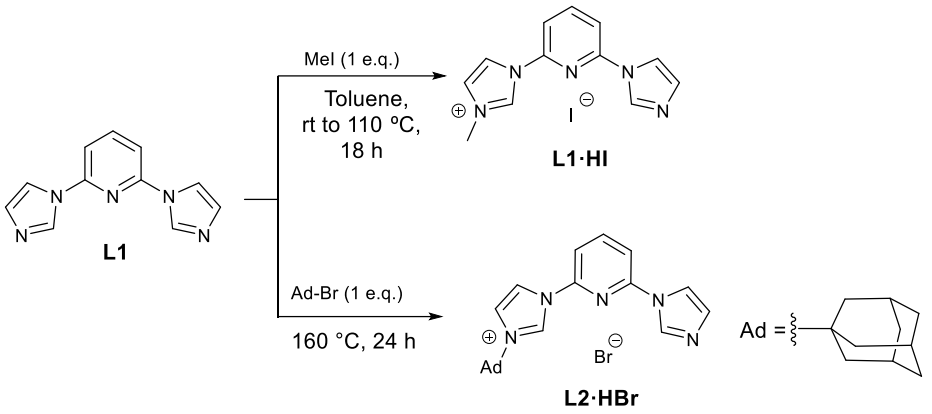

Scheme 3.1. Synthesis of ligands

Further ruthenium precursors **P1** and **P2**, where $[Ru(CN^{R'})(H_2O)(Cl)_3]$ (R'=Me (**P1**), *i*-Pr (**P2**)), were prepared following the previously reported literature procedures.[61] The desired Ru(II) complexes were obtained by the reaction of Ru(III) bidentate precursor (**P1**/**P2**) with unsymmetrical CNC-pincer ligands (**L1·HI**/**L2·HBr**) in ethylene glycol solvent at 200 °C in the presence of an excess of NaI, followed by anion exchange with aqueous NH_4PF_6 (Scheme 3.2). Excess sodium iodide prevents the synthesis of complexes with other halides in the coordination sphere.[64] The complexes obtained are $[Ru(C^{H}NC^{Me})(CN^{Me})I]PF_6$ (**3**), $[Ru(C^{H}NC^{Me})(CN^{i\text{-}Pr})I]PF_6$ (**4**), $[Ru(C^{H}NC^{Ad})(CN^{Me})I]PF_6$ (**5**), $[Ru(C^{H}NC^{Ad})(CN^{i\text{-}Pr})I]PF_6$ (**6**) which has two classical NHC and one protic NHC framework in the system (Scheme 3.2). The unsymmetrically substituted CNC pincer ligand and a bidentate CN-type ligand result in the formation of a racemic mixture of chiral-at-the-metal complexes from achiral starting material. However, at this stage, we have not attempted to separate the enantiomerically pure isomers. These complexes (**3-6**) were characterized by multinuclear NMR (^1H, $^{31}P\{^1H\}$, $^{13}C\{^1H\}$) and HRMS techniques. The solid-state structure of complex **6** has been determined using single crystal X-ray diffraction technique.

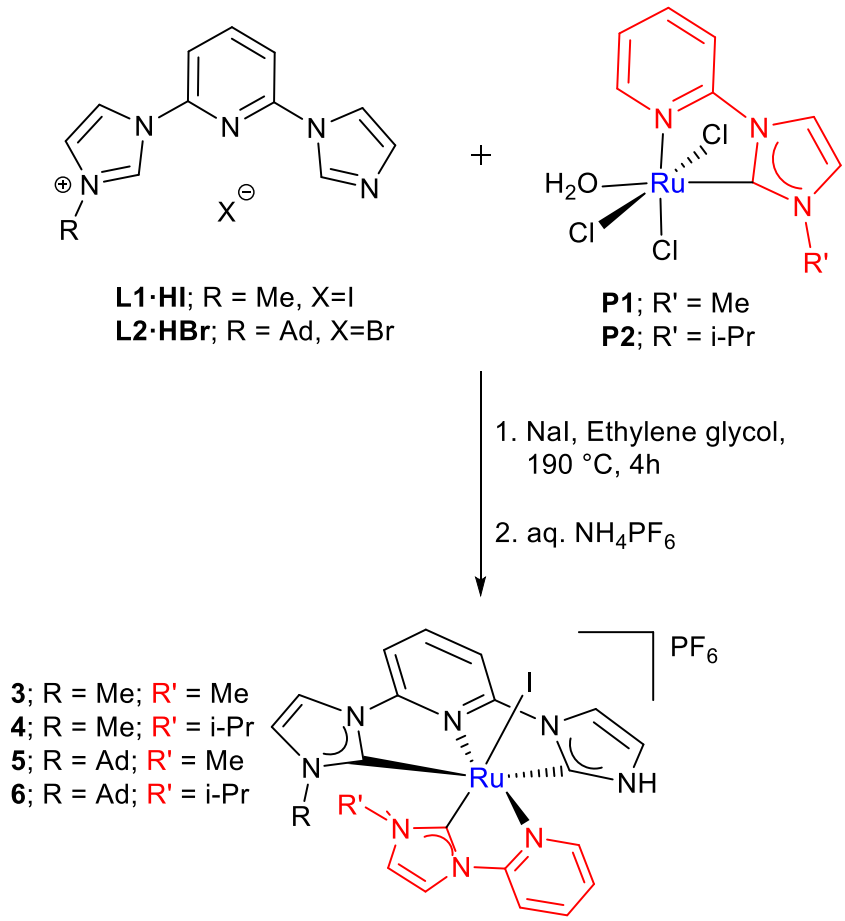

Scheme 3.2. Synthesis of complexes (**3-6)**

The ^{1}H NMR spectra of complexes **3-6** in DMSO-d6 show two sets of signals for each proton. The formation of two sets of signals in the NMR peaks was also observed in the recently reported complexes of our lab, which was due to the halide substitution by nucleophilic DMSO-d6.[62] The ^{1}H-NMR of complex **3** shows two protic signals at δ= 12.96 ppm and 12.28 ppm, respectively, corresponding to complex **3** and the DMSO-d6 coordinated species **3'**. The chemical shift for 2-pyridyl-H atom of the bidentate ligand for **3** and in situ generated **3'** appear at δ= 10.16 ppm (downfield shifted due to iodide) and 9.70 ppm, respectively, as a doublet. The four singlet peaks in the aliphatic region represent the four methyl groups of the complexes **3** and **3'**. In the ^{13}C{^{1}H} NMR spectrum, the carbene peaks for CNC^{Me} pincer appear at δ= 187.7 ppm, 186.2 ppm, and

for the bidentate CN^{Me} appears at δ= 184.0 ppm in complex **3** The $^{31}P\{^{1}H\}$ NMR spectrum shows a septate peak at δ= -144.24 ppm, corresponding to PF_6^- counter anion, and the splitting into septet occurs due to the presence of ^{19}F nuclei. HRMS (ESI^+) signal for complex **3** in methanol appears at m/z 612.9898 (612.9899 for $C_{21}H_{20}IN_8Ru$) corresponding to $[M\text{-}PF_6]^+$.

Complex **4** differs from complex **3** in having an isopropyl group, instead of methyl, at the nitrogen atom of the bidentate CN^R ligand. The ^1H NMR of complex **4** and **4'** shows the protic signals at δ= 13.00 ppm and 12.31 ppm, respectively, similar to complex **3**. The 2-pyridyl-H atom for the DMSO-d6 coordinated complex appears at δ= 9.69 ppm, while the same for the halide coordinated species appears at 10.18 ppm. In the $^{13}C\{^{1}H\}$ NMR spectrum, the carbene signals for CNC^{Me} pincer appear at δ= 187.8 ppm and 186.4 ppm for protic and classical NHC, respectively, and the peak corresponding to bidentate $CN^{i\text{-}Pr}$ appears at δ= 182.0 ppm. The $^{31}P\{^{1}H\}$ NMR spectrum shows a septate peak at -144.24 ppm, corresponding to PF_6^- counter anion. The HRMS (ESI^+) signal for complex **4** appears at m/z 641.0237 (641.0212 for $C_{23}H_{24}IN_8Ru$) corresponding to $[M\text{-}PF_6]$.

Complexes **5** and **6** contain the same CNC^{Ad} but differ in the alkyl group on bidentate CN, i.e., methyl group for **5** and isopropyl group for **6**. Complex **5** and **5'** have a protic signal at δ= 12.80 ppm and 11.96 ppm, and the peak for the 2-pyridyl-H atom of bidentate appears at δ= 9.99 ppm and 8.51 ppm for iodide coordinated, and DMSO-d6 coordinated complex respectively. The $^{13}C\{^{1}H\}$ NMR for the carbene signals for classical, protic, and bidentate CN^{Me} NHC carbene appear at δ= 185.4 ppm, 184.4 ppm, and 178.7 ppm, respectively. In the $^{31}P\{^{1}H\}$ NMR, a peak at δ= 144.27 appears as a septet.

The HRMS (ESI^+) peak for complex **5** appears at m/z 733.0893, corresponding to $[M\text{-}PF_6]$. Similarly, for complex **6**, ^1H NMR shows protic signals at δ= 12.85 ppm and 11.97 ppm corresponding to iodide coordinated complex **6** and DMSO-d6 coordinated species **6'**, respectively. The 2

pyridyl H atom shows chemical shift at δ= 12.85 ppm and 11.97 ppm for the two species. The $^{13}C\{^{1}H\}$ NMR spectrum shows the three carbenes for protic-NHC, classical-NHC, and bidentate-NHC at δ= 191.6 ppm, 190.6, and 188.2 ppm, respectively. In the $^{31}P\{^{1}H\}$ NMR, a septet peak appears at 144.27 ppm. The HRMS (ESI^{+}) for complex 6 shows a signal for m/z at 761.1167 corresponding to [M-PF_6].

3.2.2. Description of the crystal structure

The molecular structure of the racemic mixture of complex **6** is confirmed using single crystal x-ray diffraction technique. The racemic mixture of complex **6** crystalized in a triclinic system with **P**$\bar{1}$ space group containing both the enantiomers in the unit cell. The crystal structure has a distorted octahedral geometry around the ruthenium center with coordination to two five-membered metallacycles of the CNC^{Ad} based pincer ligand, one five-membered metallacycle $CN^{i\text{-}Pr}$, and I^{-} occupying the sixth coordinate site of the ruthenium center. The electron residual map indicated the occupancy of iodine below 90%. The crystal data refines well upon consideration of a mixed halide position of iodide (85%) with chloride (15%). We expected the complex to have an abnormal NHC due to the bulkiness of the adamantly group so that we could have abnormal NHC, normal NHC, and protic NHC within the same system. However, the crystal structure indicates having normal NHC with adamantly group (Figure 3.2). The CNC pincer ligand has a tridentate chelating nature and coordinates with ruthenium in a meridional configuration.

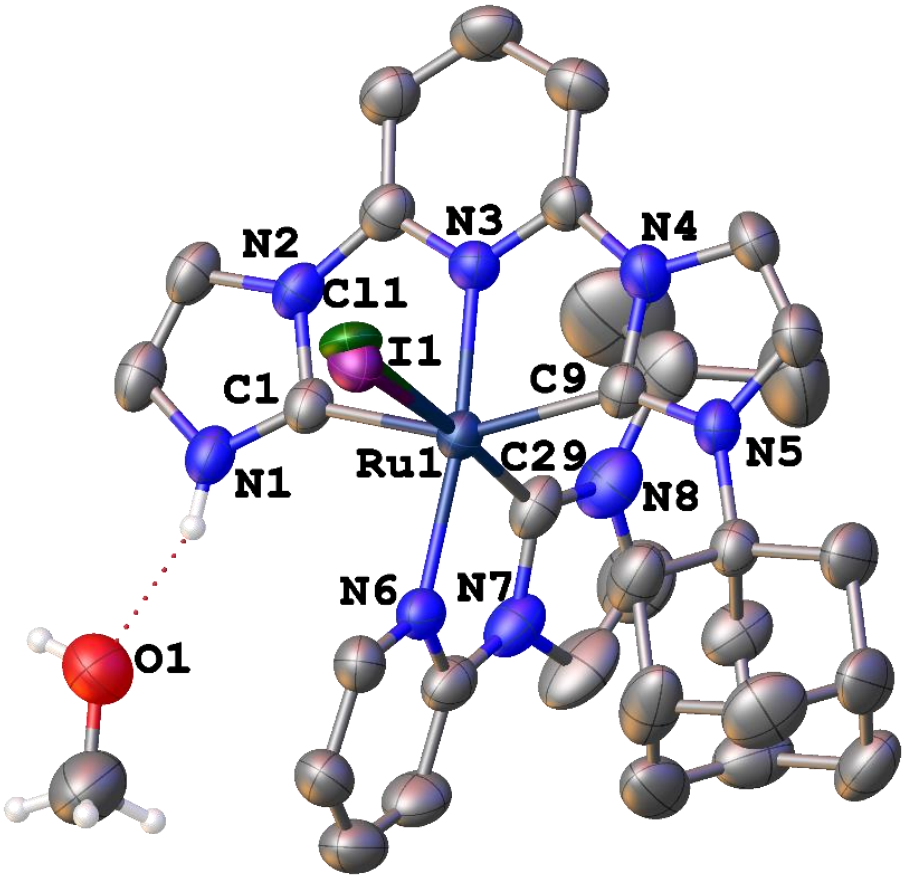

Figure 3.2. Single crystal diffracted structure of complex **6**. The hydrogen atom (except for protic-NH and methanol molecule) and PF_6 atom have been omitted for clarity. Selected bond lengths Ru1-C1= 2.031(3) Å , Ru1-C9= 2.119(3) Å, Ru1-C29= 1.972(4) Å, Ru1-N3= 2.007(3) Å, Ru1-N6= 2.121(3) Å, Ru1-I1= 2.7971(7) Å, Ru1-Cl1= 2.740(16) Å, C1-N1= 1.342(4) Å, C1-N2= 1.396(4) Å, C9-N5= 1.348(4) Å, C9-N4= 1.392(4) Å, C29-N8= 1.338(5) Å, C29-N7= 1.392(5) Å, C1-Ru1-C9= 155.79(14)º, C1-Ru1-N6= 92.74(12)º, C9-Ru1-N6= 111.47(12)º.

The bond length and bond angle formed by ruthenium with both carbene atoms of the pincer, i.e., Ru1-C1= 2.031(3) Å, Ru1-C9= 2.119(3) Å, C1-Ru1-C9= 155.79(14)º and the bite angle formed by C1-Ru1-N6= 92.74(12)º. The bidentate ligand $CN^{i\text{-}Pr}$ occupies two coordination sites to ruthenium with the bond angle between Ru1-C29= 1.972(4) Å and bite

angle N6-Ru1-C29= 78.27(15)º. The pyridine ring of the CNC^{Ad} pincer ligand is located trans to the pyridine of the bidentate $CN^{i\text{-}Pr}$ ligand. The bond length of the Ru1-I1 bond, trans to the carbene of the bidentate ligand, is 2.7971(7) Å, which is longer than the previously reported Ru-I bond length of 2.7671 Å. The bond length for the Ru-N bond of the pyridine is comparable to the previously reported complexes.

3.2.3. Catalytic applications in the dehydrogenation of benzyl alcohols

The general route for the catalytic conversion of benzyl alcohol to benzoic acid occurs in two steps, i.e., (i) the conversion of alcohol to aldehyde with the release of 1 equiv. of hydrogen (H_2) gas, (ii) conversion of this aldehyde into diols with the assistance of base, which again undergoes dehydrogenation with the release of 1 equiv. of H_2 gas gives the final carboxylic acid product (Figure 3.3). This conversion of alcohol to acid is considered to be an atom economic process as this reaction provides a quantitative yield of the carboxylic acid product with the release of two equivalents of H_2 gas (Figure 3.3). The catalytic performance of the synthesized complexes **1-6** was investigated for the acceptorless alcohol dehydrogenation to carboxylate/carboxylic acid using benzyl alcohol as model substrate.

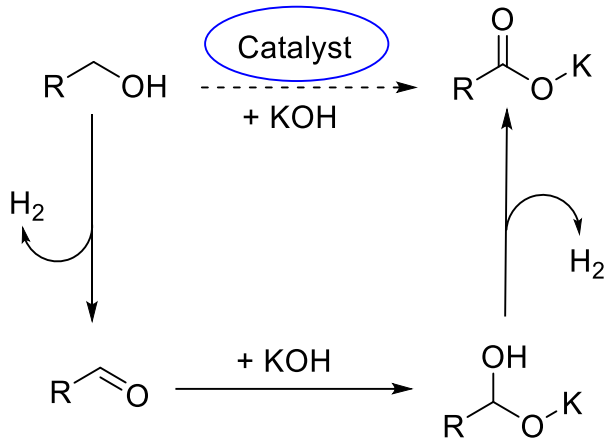

Figure 3.3 Catalytic approach in acceptorless dehydrogenation of alcohols

The initial attempt for dehydrogenation of benzyl alcohol was attempted by our previously reported [Ru(CNC)(PPh_3)$_2$Cl]Cl complexes **1** and **2** using KOH (1 mmol) as base and water as solvent at reflux temperature for 16 hours. Complexes **1** and **2** did not react under the given reaction conditions (Table 3.1, entry 1, 2). This poor reactivity may be attributed to the poor stability of complexes **1** and **2** in water. However, under the given reaction conditions in water, the phosphine-free catalysts (**3**-**6**) gave low to moderate yields of benzoic acid (Table 3.1, entry 3-6). Upon decreasing the catalytic loading from 1 mol % to 0.5 mol% percent in water, the yield of the benzoic acid decreases (Table 3.1, entry 7-10). When the solvent was changed to toluene, the catalytic activity of the complexes (**1**-**6**) increased drastically in the presence of base KOH (1 mmol). The catalysts **1** and **2** gave 60 % and 51 % yield of benzoic acid (Table 3.1, entry 11, 12), while the phosphine-free catalyst (**3**-**6**) had 97 %, >99 %, 96 %, 95 %, respectively (Table 3.1, entry 13-16). The more electron donation tendency of imidazoline-2-ylidene than benzimidazoline-2-ylidene is the reason for the more significant catalytic activity of complex **1** over **2**. This is the reason for the design of imidazole-based catalysts. The catalytic activity of phosphine-free catalysts (**3**-**6**) is better than complexes **1** and **2** because the bidentate-NHC has more electron donation tendency than phosphines and provides extra stability to the complexes.

Catalyst **4** shows superior activity for dehydrogenation of benzyl alcohol to benzoic acid than catalysts **3**, **5**, and **6** in water and toluene. This may be due to the presence of the isopropyl group on the CN-bidentate, which increases the electron density on ruthenium. Catalyst **6** shows lower reactivity due to the bulkiness of the adamantyl group. Decreasing the catalyst loading to 0.5 mol%, no significant decrease in isolated yield of benzoic acid in 12 hours was observed (Table 3.1, entry 17-20). Upon decreasing the catalyst loading to 0.1 mol%, >99 % in 12 hours and 94 % yield of benzoic acid could be obtained in 6 hours, while further reducing the catalyst loading to 0.01 mol%, the 94% yield is obtained in 24 hours

(Table 3.1, entry 21-23). Further, it was observed that in the presence of a stronger base, better yield was obtained, while with weaker base, a low yield of benzoic acid was obtained (Table 3.1, entry 24-26). KOH acts as a base and nucleophile during the catalytic reaction; therefore, upon decreasing the KOH amount, a lower yield of benzoic acid is obtained (Table 3.1, entry 27). The temperature decrease also lowers the benzoic acid yield (entry 28-30). The most favorable condition for dehydrogenation of benzyl alcohol to benzoic acid is entry 23, which has catalyst 4 (0.01 mol%), base KOH (1 equiv.), time 24 hours, and solvent toluene (3 ml).

Table 3.1. Screening of Catalysts **1-6** for Benzyl Alcohol Dehydrogenation[a].

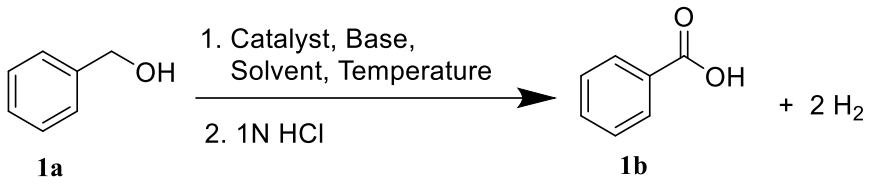

1a **1b**

Entry	Catalyst (mol %)	Solvent	Base (mmol)	Temp. (°C)	Time (h)	Isolated Yield (%)
1	1 (1)	Water	KOH	100	16	-
2	2 (1)	Water	KOH	100	16	-
3	3 (1)	Water	KOH	100	16	37
4	4 (1)	Water	KOH	100	16	54
5	5 (1)	Water	KOH	100	16	42
6	6 (1)	Water	KOH	100	16	40
7	3 (0.5)	Water	KOH	100	16	31
8	4 (0.5)	Water	KOH	100	16	50
9	5 (0.5)	Water	KOH	100	16	33
10	6 (0.5)	Water	KOH	100	16	30
11	1 (1)	Toluene	KOH	110	12	60
12	2 (1)	Toluene	KOH	110	12	51
13	3 (1)	Toluene	KOH	110	12	97
14	4 (1)	Toluene	KOH	110	12	>99
15	5 (1)	Toluene	KOH	110	12	96
16	6 (1)	Toluene	KOH	110	12	95

17	3 (0.5)	Toluene	KOH	110	12	95
18	4 (0.5)	Toluene	KOH	110	12	>99
19	5 (0.5)	Toluene	KOH	110	12	94
20	6 (0.5)	Toluene	KOH	110	12	91
21	4 (0.1)	Toluene	KOH	110	12	>99
22	4 (0.1)	Toluene	KOH	110	6	94[b]
23	4 (0.01)	Toluene	KOH	110	24	94
24	4 (0.01)	Toluene	NaOH	110	24	84
25	4 (0.01)	Toluene	K_2CO_3	110	24	5
26	4 (0.01)	Toluene	Na_2CO_3	110	24	<1
27	4 (0.01)	Toluene	KOH (0.5)	110	24	75
28	4 (0.01)	Toluene	KOH	100	24	88
29	4 (0.01)	Toluene	KOH	90	24	77
30	4 (0.01)	Toluene	KOH	70	24	62

[a]**Reaction condition**: benzyl alcohol (1 mmol), catalyst (1-0.01 mol %), base (1, 0.5 equiv.), solvent (3 mL), time (24-6 h). [b]46.3 ml (≈ 2 mmol) of H_2 gas collected by water displacement method (yield of H_2 gas, 100 %).

3.2.4 Substrate Screening

Further, the better catalyst, i.e., **4**, was used to screen a variety of substituted aromatic alcohol and aliphatic alcohol substrates for the acceptorless dehydrogenation of alcohol under the optimized reaction conditions (**4**-(0.01 mol%), KOH (1 equiv.), toluene (3ml), 110 ºC for 24 hours (Table 3.2). Complex **4** works as a precatalyst in converting the aromatic and aliphatic benzyl alcohols to the corresponding carboxylic acids. The substrates bearing an electron donating group or electron withdrawing group in the aryl group are found to react efficiently under the optimized reaction conditions, giving good to excellent yields. The effect of substituents at the ortho (*o*), meta (*m*), and para (*p*) positions on the corresponding carboxylic acid derivative product yield has also been observed. The carboxylic acid derivatives were isolated after workup and characterized by NMR spectroscopy. Dehydrogenation of benzylalcohol,

the model substrate, gave 94 % isolated yield of benzoic acid (4a). The alkoxy-substituted aryl groups like *p*-methoxybenzylalcohol, *m*-methoxybenzylalcohol, *o*-methoxybenzylalcohol, *m*,*p*-dimethoxybenzylalcohol, and (*p*-(benzyloxy)phenyl)methanol gave >99 %, 83 %, 88 %, 81 % and 96 % of the corresponding carboxylic acid products respectively (4b, 4c, 4d, 4e, 4f). Since the substitution of the alkoxy group at the ortho and para position donates more electron density to ruthenium than the meta-substituted alkoxy, a lower product yield in the case of meta-substituted benzylalcohol is observed. Similarly, *p*-methylbenzylalcohol, *m*-methylbenzylalcohol, *p*-*iso*propylbenzylalcohol, and *p*-*tert*butylbenzylalcohol gave the corresponding acid products in 85 %, 72 %, 82 %, and 78 %, yield respectively (4g, 4h, 4i, 4j). Here again, a decrease in yield upon substitution of methyl group at meta position is observed. In the case of the amino-aryl derivatives, i.e., *p*-aminobenzylalcohol and *m*-aminobenzylalcohol, the corresponding acid products were isolated in 84 % and 76 % yield, respectively (4k, 4l). However, *o*-aminobenzylalcohol showed no reactivity under the optimized reaction conditions (4m). The electron-withdrawing nitro group substituted at the meta position of benzyl alcohol gave a *m*-nitrobenzoic acid (4n) with a 65 % yield lower than the *m*-aminobenzoic acid yield (4l). Halogen substituted benzyl alcohols, i.e., *p*-florobenzylalcohol, *p*-chlorobenzylalcohol, *p*-bromobenzylalcohol, *p*-iodobenzylalcohol 81 %, 83 %, 78 %, 76 %, while *m*-florobenzylalcohol, *m*-chlorobenzylalcohol gave 52 %, 58 % product, and *o*-bromobenylalcohol gave 65 % yield of the corresponding carboxylic acid derivative (4o-4u). The o> p> m yield in the halo-substituted benzoic acid can be seen. Furfuryl alcohol, when reacted under the optimized reaction conditions, gives 65% of 2-furoic acid (4v), which is used as a preservative and a flavoring agent, where it imparts a sweet, earthy flavor. Another substrate, piperonyl alcohol, yields 80% of the corresponding piperonylic acid (4w) (a pharmaceutical drug to inhibit cancer cell growth and regulate immunity). In the case of aliphatic alcohols, catalyst **4** shows poor reactivity. The aliphatic alcohol

butan-1-ol gave a 55% yield (4x), while the other aliphatic alcohols, hexan-1-ol (4y) and 2-phenylethan-1-ol (4z), did not react under the optimized reaction conditions.

Table 3.2. Substrate Scope for Acceptorless Alcohol Dehydrogenation when Using catalyst **4**.[a]

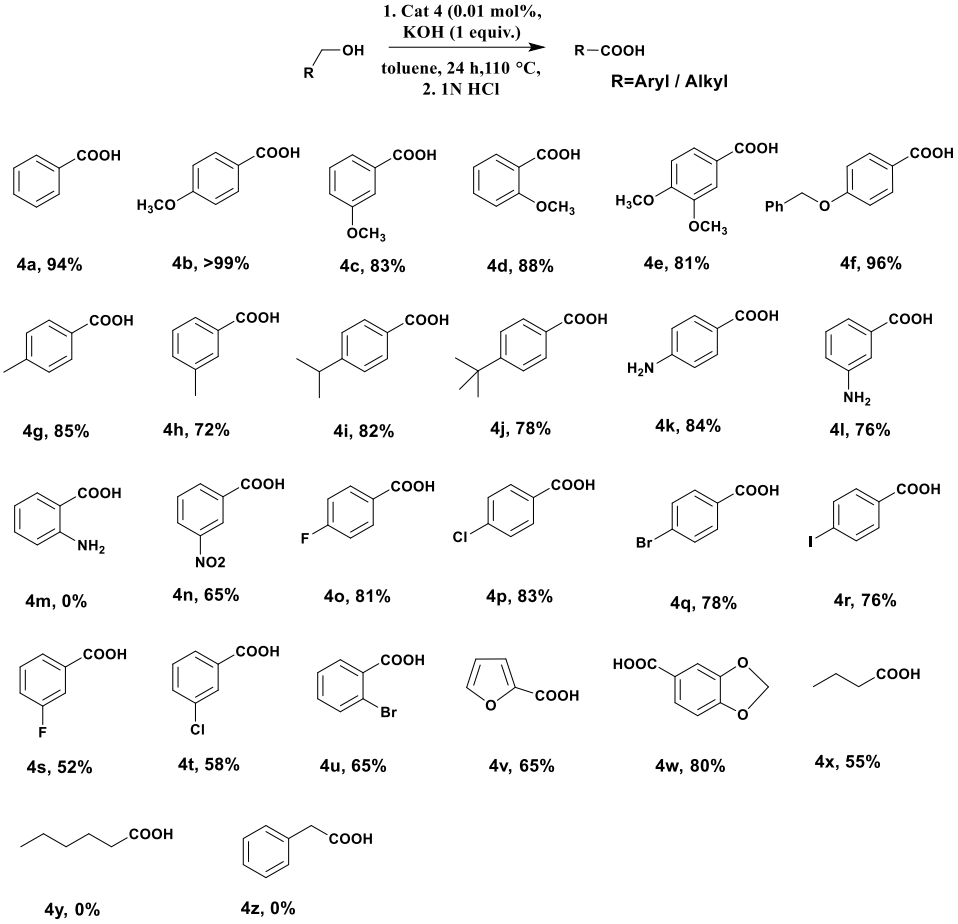

[a]**Reaction Conditions:** Alcohol (2 mmol), KOH (2 mmol), catalyst **4** (0.01 mol%), toluene (6 ml), time 24 hours, temperature 110 °C, followed by acidification with 1N HCl.

3.2.5 Bulk reaction for alcohol dehydrogenation and calculation of TON (TOF)

We further applied our catalytic system for gram-scale dehydrogenation of benzyl alcohol to synthesize carboxylic acid. For this purpose, 10 mmol of benzyl alcohol reacted with 10 mmol of KOH, and 0.1 mol % of catalyst **4** were reacted under optimized reaction conditions for 8 h, giving 1.2 g of benzoic acid with the release of *ca*. 20 equiv. of H_2 gas (yield = 100%). The catalyst loading could be reduced to 0.005 mol% and complete conversion was observed after 5 days (TON/ (TOF) = 20,000/ (167 h^{-1})) The TON and TOF values for catalyst **4** have been compared with some previously reported ruthenium complexes shown in Table 3.3.

Table 3.3. Comparative study for catalytic dehydrogenation of benzyl alcohol to benzoic acid

Entry	Cat- (mol %)	temp. (°C)	Time (h)	Base (equiv.)	Solvent	TON/ (TOF)
1.	This work 4 (**0.01**) 4 (**0.005**)	 110 110	 24 120	 KOH (1) KOH (1)	 toluene toluene	 10,000 (416 h^{-1}) 20,000 (167 h^{-1})
2.	Milstein et al. (**0.2**) 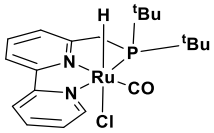	110	18	NaOH (1.1)	water	455/ ($25h^{-1}$)
3.	Peng et al. (**0.2**) 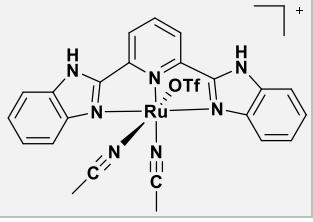	150	24	CsOH (1.0)	-	400/ ($17h^{-1}$)

4.	Bera etal. (**5.0**) 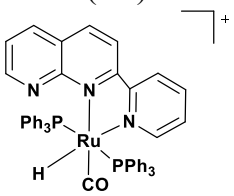	110	6	NaOH (18.5)	water	20/ ($3h^{-1}$)
5.	Szymczak et al. (**0.4**) 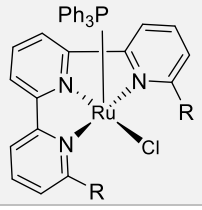	120	18	KOH (3)	toluene	250/ ($14h^{-1}$)
6.	Chen et al (**0.5**) 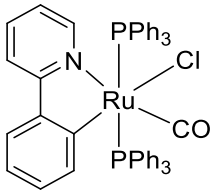	110	6	KOH (1.5)	toluene	200/ ($33h^{-1}$)
7.	Yi et al. (**0.1**) 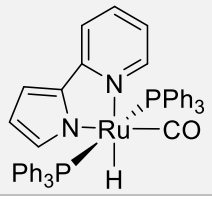	120	12	KOH (1.1)	toluene	4000/ ($333h^{-1}$)
8.	Daw (**1**) 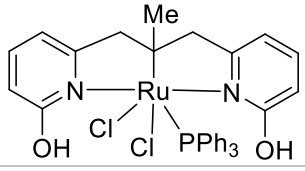	150	24	KOH (0.5)	Diglyme : H_2O (9:1)	400/ ($17h^{-1}$)

TON = [(Number of moles of substrate converted)/(Number of moles of catalyst)] at the end of the reaction. TOF = [(TON)/hour]

3.2.6 Mechanistic investigation

To understand the plausible pathway for the acceptorless dehydrogenation of alcohols to carboxylic acids, control experiments were conducted. Initially, deprotonation of the protic-NHC of the pincer ligand was observed when complex **4** was reacted with KOH (2 equiv.) at room temperature in toluene solvent for 1 h. This was observed in the mass spectrum by a peak at 533 for [M-PF_6-I-H]. The mass spectrum was recorded in methanol solvent; therefore, a peak for the methoxy-substituted complex was also indicated by a peak for[M-PF_6-I+OMe] After 2 h, the sample was analyzed and showed a peak for [M-PF_6-I+OH+H_2O] at 549. The deprotonation of protic N-H was also confirmed by ^{1}H-NMR when catalyst **4** was reacted with KOH (2 equiv.) in DMSO-d6 solvent.

Similarly, when complex **3** was reacted with KOH, deprotonated species [M-PF_6-I-H], as observed in the case of complex **4**, was observed at 485. The Ru-OMe and Ru-OH species for complex **3,** similar to the analogous complex **4,** were observed at 517 and 521, respectively. Similarly, when catalyst **3** was reacted in water solvent with KOH (1 mmol), peaks at 485 and 517 are observed in the mass spectra as observed in the toluene solvent. When 1 mmol of benzyl alcohol was added to the complex 3 and KOH reaction mixture in the toluene solvent, a mass peak at 627 indicated the coordination of Ph-C(OH)O- to the ruthenium center.

The catalytic dehydrogenation of benzyl alcohol to benzoic acid may proceed via aldehyde or ester intermediate. Experiments were conducted to differentiate between the two intermediates. When benzyl alcohol was reacted with base KOH in the presence of catalyst **3** at a temperature of 110 °C without any solvent, benzaldehyde was observed as the only product observed in GC. When the same reaction was performed in toluene solvent at 60 °C, similar benzaldehyde without any trace of formation of benzyl ester, this indicates that the reaction proceeds via the Cannizaro-like pathway and not with Tishchenko-like reaction pathway.

The aromatic aldehydes in the presence of base KOH are known to readily disproportionate into benzyl alcohol and benzoic acid. Also, when benzaldehyde (1 mmol) and KOH (1 mmol) are reacted for 1 h without a catalyst, the benzoic acid formed in 56 % with benzyl alcohol in 42 %. On the other hand, when reacted in the presence of the catalyst, the benzoic acid >99 % and with traces of benzyl alcohol formed. This suggests that the catalytic alcohol dehydrogenation pathway via benzaldehyde is responsible for benzylic alcohol derivatives.

Based on the experimental findings, a mechanistic pathway has been proposed using complex **3** (Scheme 3.3)**.** In the first step, catalyst **3** undergoes deprotonation in the presence of KOH to give a neutral complex **3-A**. Next, in the presence of base KOH, substrate benzyl alcohol was added, which coordinated to **3-A** as benzyloxy to give **3-B**. The alkoxy coordinated species are a very common intermediate in acceptorless dehydrogenation process of alcohols and have been invoked in several mechanistic and theoretical studies.[65–67] In the next step, the **3-B** undergoes β-hydride transfer from CH_2 of benzyloxy to give **3-D** *via* **3-C.** The incoming water molecule attacked the electrophilic carbon of aldehyde in 3-D to give **3-E**. Followed by the attack of water; in the next step, one equiv. of H_2 gas is liberated to give the **3-F**. In the next step, β-hydride transfer occurs in **3-F** to give ruthenium hydride complex **3-H** *via* **3-G**. Another equiv. of H_2 gas is released, resulting in **3-I** species. This **3-I** species, in the presence of KOH and benzyl alcohol, regenerates the active catalyst **3-C,** which continues the cycle.

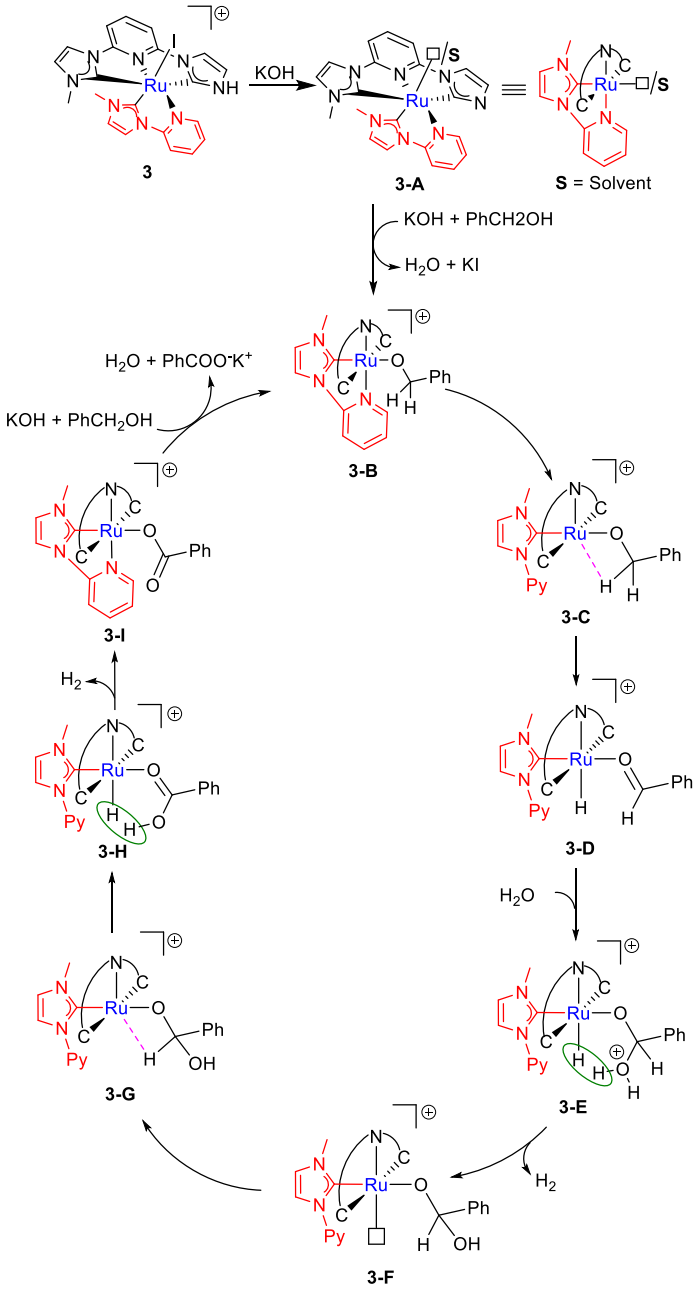

Scheme 3.3. Plausible Mechanistic pathway for the acceptorless dehydrogenation of benzyl alcohol to benzoic acid.

3.3 Conclusions

In this chapter, we report that we have synthesized and characterized unsymmetrical ligands **L1·HI** and **L2·HBr,** which were used for the synthesis of a series of new phosphine-free, moisture and air-stable complexes [Ru($C^{H}NC^{Me}$)(CN^{Me})I]PF_6 (**3**), [Ru($C^{H}NC^{Me}$)($CN^{i\text{-}Pr}$)I]PF_6 (**4**), [Ru($C^{H}NC^{Ad}$)(CN^{Me})I]PF_6 (**5**), [Ru($C^{H}NC^{Ad}$)($CN^{i\text{-}Pr}$)I]PF_6 (**6**). The unsymmetrically substituted CNC pincer ligand and a bidentae CN-type ligand result in the formation of a racemic mixture of chiral-at-the-metal complexes from achiral starting material. However, at this stage, we have not attempted to separate the enantiomerically pure isomers. The complexes were characterized by multinuclear NMR and HRMS techniques, and the molecular structure of complex **6** was determined using a single-crystal x-ray diffraction technique. The catalytic investigation of these complexes for oxidant-free acceptorless dehydrogenation of benzyl alcohol to corresponding acid derivative compound was performed and compared to the previously reported [Ru(CNC)(PPh_3)$_2$Cl]Cl complexes **1** and **2**. The catalytic activity of complex **1** > **2** because of the electron donation tendency of imidazoline-2-ylidene > benzimidazoline-2-ylidene. The phosphine-free catalysts (**3**-**6**) show higher catalytic activity than **1** and **2** due to the presence of NHC, which has more electron donation ability than phosphines. The best activity and performance for acceptorless dehydrogenation of benzyl alcohol to benzoic acid was shown by complex **4** due to the isopropyl group, which increases the electron density on ruthenium. Catalyst **6** has lower activity due to the bulkiness of the adamantyl group. Under the optimized reaction conditions, i.e., cat **4** (0.01 mol%) with 1 equiv. of KOH against 1 equiv. of benzyl alcohol substrate in toluene solvent at 110 ºC, 94 % yield of benzoic acid in 24 h with the production of 2 equivalent of H_2 gas. Catalyst **4** was utilized for the dehydrogenation of a wide range of aromatic, aliphatic, and heteroaromatic alcohols to their corresponding acid product. Catalyst **4** is also compatible

with large-scale reactions for converting benzyl alcohol into benzoic acid. A maximum TON of 20,000, greater than several previously reported ruthenium catalysts, was achieved using 0.005 mol% of catalyst **4**. The mechanistic investigation indicates that the reaction proceeds via the catalyst's deprotonation followed by Ru-OH species formation. This efficient system allows a simple and straightforward synthesis of carboxylic acids in good yields, and the only by-product is the H_2 gas, which uses a very low catalyst loading and low base loading.

3.4. Experimental Section and characterization data

3.4.1 General considerations

All reactions and modifications were performed under an inert atmosphere (dinitrogen unless otherwise stated) using the standard Schlenk line techniques. Solvents were purchased from S. D. Fine-Chem Limited and purified by distillation under an inert atmosphere. Azoles (1-H-imidazole and 1-H-benzimidazole) and $RuCl_3 \cdot 3H_2O$ were purchased from Sisco Research Laboratories Pvt. Ltd. (SRL)-India and Sigma-Aldrich respectively. Deuterated dimethyl sulphoxide (DMSO-d6), and deuterated chloroform ($CDCl_3$) were purchased either from EURISOtop or Sigma-Aldrich. NMR spectra were recorded on Bruker Avance (III) spectrometer and Bruker Avance NEO spectrometer operating at 400 and 500 MHz for ^{1}H, 162 and 202 MHz for ^{31}P, and 101 and 126 MHz for ^{13}C NMR, respectively. NMR chemical shifts are reported in ppm and referenced to the solvent peaks for ^{1}H ($CDCl_3$ δ 7.26 and DMSO-d6 δ 2.50 ppm) and ^{13}C (natural abundance of ^{13}C in $CDCl_3$ δ 77.16 and DMSO-d6 δ 39.52 ppm). ^{31}P NMR chemical shifts are referenced to an external 85% H_3PO_4 standard as 0 ppm. Multiplicities are given as s (singlet), d (doublet), t (triplet), and m (multiplet), and the coupling constants *J* are given in hertz. The mass chromatograms were recorded on Bruker-Daltonics-MicroTOF-QII mass spectrometer in HPLC grade methanol (catalytic samples) and acetonitrile (metal complexes). Elemental analysis was carried out on a Thermo Fischer

Scientific FLASH 2000 (formerly the Flash EA1112) CHNS-O elemental analyser.

3.4.2 synthesis of ligand precursors

The ligand precursors were prepared following the previously reported literature procedure by the reaction of 2,6-dibromopyridine, imidazole via Ullmann coupling.

3.4.3 Synthesis of ligand L1·HI

An oven dried 100 ml two neck round bottle flask with magnetic bead was connected to reflux condenser in Schlenk line and then cooled under vacuum. The R.B flask was charged with ligand precursor **L** (1055 mg, 5 mmol), methyl iodide (1 equiv.) and dry toluene (10 ml) under N_2 atmosphere. The temperature increased from room temperature to reflux (110 ºC) for 18 hours, allowing the white precipitate to settle. After cooling to room temperature, the precipitate was filtered, washed with toluene, DCM, and diethyl ether. The pure product was obtained after crystallization in methanol solvent. Yield= 1100 mg, 97 %. **^{1}H NMR** (500 MHz, DMSO-d6) δ 10.26 (s, 1H), 8.85 (s, 1H), 8.69 (d, 1H), 8.39 (t, *J* = 8.1 Hz, 1H), 8.21 (s, 1H), 8.02 (d, *J* = 8.1 Hz, 1H), 7.95 (d, *J* = 7.9 Hz, 1H), 7.20 (s, 1H), 4.00 (s, 2H). **^{13}C NMR** (126 MHz, DMSO-d6) δ 147.77, 145.22, 144.07, 136.01, 135.89, 130.63, 124.96, 119.11, 116.96, 114.20, 112.96, 111.01, 36.53.

3.4.4 Synthesis of ligand L2·HBr

An oven dried 100 ml ACE glass pressure tube with magnetic bead was cooled under vacuum and purged with nitrogen gas. The ligand precursor **L** (5 mmol, 1055 mg) was added to the pressure tube followed by 1-bromoadmantane (1075.65 mg, 5 mmol). The pressure tube was sealed and dipped in a pre-heated oil bath at 160 ºC and allowed to react for 24 h. After 24 h, the reaction was stopped, and the tube was cooled to room temperature. The precipitate was filtered and washed with DCM and diethyl

ether. Yield= 1620 mg , 94 %. 1H NMR (400 MHz, DMSO-d6) δ 10.05 (s, 1H), 9.08 (s, 1H), 8.85 (s, 1H), 8.40 (s, 2H), 8.32 (s, 1H), 8.16 (d, *J* = 7.9 Hz, 1H), 8.07 (d, *J* = 7.9 Hz, 1H), 7.30 (d, *J* = 20.7 Hz, 1H), 2.27 (s, 9H), 1.76 (s, 6H). ^{13}C NMR (126 MHz, DMSO-d6) δ 147.48, 145.27, 143.77, 133.12, 129.65, 120.69, 119.71, 114.97, 113.06, 112.03, 110.64, 60.52, 41.29, 34.81, 28.92. HRMS for $[M\text{-}Br]^+$ $C_{21}H_{24}N_5$ 346.2018 (found), 346.2018 (calculated).

3.4.5. General procedure for the synthesis of metal precursors

$[Ru(CN^{Me})(H_2O)Cl_3]$ (P1) and $[Ru(CN^{i\text{-}Pr})(H_2O)Cl_3]$ (P2) precursors were synthesized following the procedure reported by our research group using $RuCl_3 \cdot 3H_2O$ as starting materials.

3.4.6. General procedure for the synthesis of metal complexes

The complexes **1** and **2** were reported earlier by our group, and synthesis was performed following the previously reported procedure. Further for the synthesis of complexes **3-6,** an oven-dried schlenk tube with a magnetic stirring bar was charged with ligand precursor (1 equiv.), ruthenium precursor (1 equiv.), and NaI (0.149 g, 1mmol) in ethylene glycol (10 ml), the resulting mixture was refluxed under N_2 atmosphere for 4 h. After the reaction was completed, cooled to room temperature, and added an aqueous solution of NH_4PF_6 (0.184 g, 1 mmol, 10 ml water), then stirred for 2 min at room temperature. The desired complex was precipitated out, filtered the precipitate, washed with H_2O, and dried under vacuum.

3.4.7. synthesis of complex (3)

Complex **3** was prepared following the general procedure for complex synthesis, by the reaction of L1·HI (184 mg, 0.52 mmol) and $[Ru(CN^{Me})(H_2O)Cl_3]$ (P1) (200 mg, 0.52 mmol) to giving the product as red solid. Yield = 440 mg (58%). ^{1}H NMR (400 MHz, DMSO-d6) δ 12.96 (s, 1H), 12.29 (s, 1H), 10.17 (d, *J* = 5.9 Hz, 1H), 9.71 (d, *J* = 5.9 Hz, 1H), 8.54

– 8.48 (m, 3H), 8.42 (q, *J* = 4.5, 6.1 Hz, 5H), 8.30 – 8.20 (m, 4H), 8.10 (p, *J* = 8.0 Hz, 4H), 7.95 (t, *J* = 8.5 Hz, 2H), 7.66 – 7.53 (m, 3H), 7.45 – 7.35 (m, 2H), 7.31 – 7.26 (m, 1H), 7.15 – 7.07 (m, 1H), 3.13 (s, 3H), 2.98 (s,3H), 2.51 (s 3H), 2.47 (s, 2H). $^{13}C\{^{1}H\}$ NMR (101 MHz, DMSO-d6) δ 187.83, 186.39, 182.01, 153.57 (d, *J* = 3.1 Hz), 152.69, 152.09, 141.74, 138.59, 137.72, 125.60, 124.26, 121.91 (d, *J* = 16.4 Hz), 120.60 (d, *J* = 6.6 Hz), 119.93, 118.57, 118.33, 117.80 (d, *J* = 14.3 Hz), 116.88, 116.31 (d, *J* = 7.5 Hz), 112.27, 35.89, 21.96. $^{31}P\{^{1}H\}$ NMR (202 MHz, DMSO-d6) δ -144.24 ppm. HRMS for $C_{21}H_{20}N_8RuI$ calculated- 612.9899 found- 612.9198. Anal. Calcd. for $[C_{21}H_{20}N_8RuI]PF_6$ calculated- C, 33.30; H, 2.66; N, 14.80 Found- C, 33.62; H, 2.33; N,14.57.

3.4.8 synthesis of complex (4)

Complex **4** was prepared following the general procedure for complex synthesis, by the reaction of L1·HI (175 mg, 0.50 mmol) and $[Ru(CN^{i\text{-}Pr})(H_2O)Cl_3]$ (P2) (190 mg, 0.50 mmol) to giving the product as light red solid. Yield= 511 mg (65%). ^{1}H NMR (400 MHz, DMSO-d6) δ 13.00 (s, 1H), 12.31 (s, 1H), 10.19 (d, *J* = 7.8 Hz, 1H), 9.70 (d, *J* = 7.8 Hz, 1H), 8.54 (s, 3H), 8.44 (d, *J* = 15.3 Hz, 2H), 8.38 (s, 1H), 8.16 (d, *J* = 8.3 Hz, 3H), 7.96 (t, *J* = 10.5 Hz, 1H), 7.59 (d, *J* = 6.8 Hz, 4H), 7.38 (d, *J* = 20.3 Hz, 2H), 3.12 (s, 3H), 2.97 (s, 1H), 2.20 (s, 1H), 1.57 (s, 1H), 0.80 – 0.61 (m, 8H). $^{13}C\{^{1}H\}$ NMR (101 MHz, DMSO-d6) δ 187.83, 186.39, 182.00, 153.55, 152.69, 152.09, 141.74, 138.59, 125.59, 121.99, 121.83, 119.93, 118.32, 117.86, 117.72, 112.26, 107.78,107.50, 49.84, 35.88, 21.96. $^{31}P\{^{1}H\}$ NMR (202 MHz, DMSO-d6) δ -144.24 ppm. HRMS for $C_{23}H_{24}N_8RuI$ calculated- 641.0212 found- 641.0237. Anal. Calcd. for $[C_{23}H_{24}N_8RuI]PF_6$ calculated- C, 35.17; H, 3.08, N; 14.27 found- C, 35.48; H, 3.25; N, 14.10.

3.4.9 synthesis of complex (5)

The complex **5** was prepared following the general procedure for complex synthesis, by the reaction of L2·HI (222 mg, 0.52 mmol) and [Ru(CN^{Me})(H_2O)Cl_3] (P1) (200 mg, 0.52 mmol) to giving the product as red solid. Yield = 456 mg (52%). ^{1}H NMR (500 MHz, DMSO-d6) δ 12.80 (s, 1H), 11.96 (s, 1H), 9.99 (d, *J* = 5.7 Hz, 1H), 9.83 (d, *J* = 5.7 Hz, 1H), 8.52 (d, *J* = 2.7 Hz, 1H), 8.39 (s, 1H), 8.25 (d, *J* = 2.7 Hz, 4H), 8.22 – 8.06 (m, 1H), 7.92 (d, *J* = 8.0 Hz, 1H), 7.64 (d, *J* = 2.7 Hz, 1H), 7.46 (t, *J* = 6.7 Hz, 1H), 7.30 (s, 1H), 7.10 (d, *J* = 2.7 Hz, 1H), 2.47(s, 3H) 1.86 (d, *J* = 9.9 Hz, 4H), 1.74 (s, 4H), 1.35 (d, *J* = 12.2 Hz, 4H), 1.23 (s, 1H), 0.94 (d, *J* = 11.4 Hz, 4H). ^{13}C{^{1}H} NMR (126 MHz, DMSO-d6) δ 185.42, 184.39, 178.68, 154.73, 153.20, 153.04, 152.93, 152.43, 151.92, 126.33, 122.67, 122.19, 121.61, 118.06, 117.65, 116.03, 112.46, 107.98, 59.59, 58.61, 41.69, 34.57, 34.40, 28.93. ^{31}P{^{1}H} NMR (202 MHz, DMSO-d6) δ -144.24 ppm. HRMS for $C_{30}H_{32}N_8RuI$ calculated- 733.0840 found- 733.0893. Anal. Calcd. for [$C_{30}H_{32}N_8RuI$]PF_6 calculated- C, 41.06; H, 3.68; N, 12.77 found- C, 41.52; H, 3.75; N, 12.61.

3.4.10 Synthesis of complex (6)

Complex **3** was prepared following the general procedure for complex synthesis, by the reaction of L2·HI (222 mg, 0.52 mmol) and [Ru($CN^{i\text{-}Pr}$)(H_2O)Cl_3] (P2) (200 mg, 0.52 mmol) to giving the product as red solid. Yield = 498 mg (55%). ^{1}H NMR (400 MHz, DMSO-d6) δ 12.85 (s, 1H), 11.97 (s, 1H), 10.02 (d, *J* = 6.0 Hz, 1H), 9.84 (d, *J* = 6.0 Hz, 1H), 8.53 (s, 3H), 8.37 (d, *J* = 19.8 Hz, 5H), 8.29 – 8.25 (m, 1H), 8.15 (s, 4H), 8.12 (d, *J* = 14.3 Hz, 1H), 8.05 (s, 2H), 7.92 (d, *J* = 8.0 Hz, 2H), 7.64 (d, *J* = 8.5 Hz, 2H), 7.44 (s, 3H), 7.34 (d, *J* = 18.1 Hz, 4H), 1.85 (d, *J* = 11.8 Hz, 6H), 1.78 (s, 2H), 1.73 (s, 6H), 1.47 (d, *J* = 11.3 Hz, 7H), 1.35 (d, *J* = 12.3 Hz, 7H), 0.92 (d, *J* = 12.3 Hz, 7H) 0.65 (dd, *J* = 6.9, 21.7 Hz, 15H). ^{13}C{^{1}H} NMR (101 MHz, DMSO-d6) δ 191.59, 190.62, 188.15, 156.25, 153.09, 151.59, 151.35, 137.55, 136.57, 120.35, 118.68, 116.03, 115.87, 115.67, 110.95, 57.09, 49.04, 41.21, 34.41, 28.61, 21.39, 20.97. ^{31}P{^{1}H} NMR (202 MHz,

DMSO-d6) δ -144.24 ppm. HRMS for $C_{32}H_{36}N_8RuI$ calculated- 761.1154 found- 761.1167. Anal. Calcd. for $[C_{32}H_{36}N_8RuI]PF_6$ calculated- C, 42.44; H, 4.01 N, 12.37 found- C, 42.05; H, 4.22; N, 12.63.

3.4.11 X-ray data collection

The X-ray diffraction of a single crystal acquired by crystallization of complexes were performed, and data obtained by using dual-core Agilent technologies (Oxford Diffraction) Super Nova CCD System equipped with micro focus Mo and Cu sources. Data was recorded at 293(2) K using graphite-mono chromated Mo Kα radiation source (λ_α = 0.71073 Å). The crystal data was collected using CrysAlisPro CCD and was further reduced using CrysAlisPro RED software. The structure with intrinsic phasing was solved using the SHELXT software, and the entire matrix least-squares on F2 was refined using the SHELXL program within the Olex2 program for graphical interface. Anisotropic refinement was performed on all non-hydrogen atoms. CCDC Deposition Number 2367429 contains the supplementary data for complex **6**.

Table 3.4 Crystal data and structure refinement parameters of complex 6

Empirical formula	**$C_{33}H_{40}Cl_{0.14}F_6I_{0.85}N_8OPRu$**
Formula weight	**924.41**
Temperature/K	**293(2)**
Crystal system	**triclinic**
Space group	**P-1**
a/Å	**11.7722(3)**
b/Å	**12.5423(3)**
c/Å	**14.3998(4)**
α/°	**77.402(2)**
β/°	**69.513(2)**
γ/°	**71.130(2)**
Volume/Å^3	**1871.37(9)**

Z	**2**
ρ_{calc}g/cm^3	**1.641**
μ/mm^{-1}	**1.246**
F(000)	**926.0**
Crystal size/mm^3	**0.25 × 0.2 × 0.18**
Radiation	**MoKα (λ = 0.71073)**
2Θ range for data collection/°	**6.632 to 58.01**
Index ranges	**-15 ≤ h ≤ 15, -16 ≤ k ≤ 16, -18 ≤ l ≤ 14**
Reflections collected	**20121**
Independent reflections	**8714 [R_{int} = 0.0484, R_{sigma} = 0.0653]**
Data/restraints/parameters	**8714/1/474**
Goodness-of-fit on F^2	**1.044**
Final R indexes [I>=2σ (I)]	**R_1 = 0.0477, wR_2 = 0.1048**
Final R indexes [all data]	**R_1 = 0.0712, wR_2 = 0.1189**
Largest diff. peak/hole / e Å^{-3}	**0.77/-0.67**

Table 3.5 *Selected bond lengths and bond angles of complex* ***6****.*

Bond lengths (Å)		**Bond Angles (°)**	
Ru1-I1	2.7971(7)	N3-Ru1-I1	87.32(9)
Ru1-N3	2.007(3)	N3-Ru1-N6	170.60(11)
Ru1-N6	2.121(3)	N3-Ru1-C1	78.01(13)
Ru1-C1	2.031(3)	N3-Ru1-C9	77.80(12)
Ru1-C9	2.119(3)	N3-Ru1-C29	100.47(15)
Ru1-C29	1.972(4)	N6-Ru1-I1	94.36(9)
N1-C1	1.342(4)	N6-Ru1-C1	92.74(12)
N2-C1	1.396(4)	N6-Ru1-C9	111.47(12)
N5-C9	1.348(4)	N6-Ru1-C29	78.27(15)

N4-C9	1.392(4)	N1-C1-N2	103.0(3)
N8-C29	1.338(5)	N5-C9-N4	103.4(3)
N7-C29	1.392(5)	N8-C29-N7	103.2(4)
Ru1-Cl1	2.740(16)	N3-Ru1-Cl1	81.6(6)
-	-	N8-Ru1-Cl1	99.6(6)

3.4.12 General procedure for dehydrogenation of benzyl alcohol to benzoic acid

In an oven-dried and vacuum-cooled schlenk tube, **catalyst** (0.01 mol%) and potassium hydroxide KOH (2 mmol) toluene solvent (6 ml) under inert atmosphere were added. The reaction mixture allowed to stir at room temperature for 1 hour. Further, increased the reaction temperature to 110 °C and added benzyl alcohol (2 mmol). The mixture was then refluxed for 24 hours. After cooling to room temperature, the solution was evaporated under reduced pressure to produce crude potassium carboxylate salt. Deionized water (20 ml) was added to the crude reaction mixture to dissolve the potassium carboxylate, and the resulting aqueous solution, washed with DCM (3 x 20 mL). The final aqueous solution is then acidified with 1N HCl and extracted with ethyl acetate (3 x 20 mL). The combined organic phase was separated and dried over anhydrous Na_2SO_4 and evaporated to dryness under vacuum to provide the corresponding carboxylic acid.

3.4.13 Large-scale synthesis of benzoic acid

A mixture of catalyst **4** (0.01 mmol), base (560 mg, 10 mmol) and toluene 30 ml was added in a 100 ml two neck round bottom flask and allowed to stir at room temperature for 1 hour. Further, the temperature was elevated from room temperature to reflux temperature and then benzyl alcohol (1.08 g, 10 mmol) was added to the reaction mixture and r was dibbed in the

preheated oil bath. The reaction was allowed to reflux for 6 hours and then allowed to cool. The work up was performed following the usual procedure and pure carboxylic acid was received as white solid (1.20 g, 97%).

3.4.14 Volumetric estimation of H_2 gas evolved during synthesis of carboxylic acid

An oven dried, vacuum cooled schlenk tube was purged with nitrogen and charged with catalyst **4** (0.1 mol%), KOH (1 mmol) in 3 ml toluene solvent. The reaction mixture was stirred at room temperature for 1 hour and then the temperature of the oil-bath was increased to 120 °C. After the temperature reached, benzyl alcohol (1 mmol) was added to the reaction mixture. The schlenk tube was again purged with nitrogen and then its side arm was connected to a gas burette and headspace was closed tightly. The schlenk tube was then dipped in preheated oil bath and then reaction continued until evolution of H_2 gas ceased. The reaction was performed 3 times to get the consistent reading and the calculation for number of moles was done using ideal gas equation $n(H_2)= [(P_{atm} - P_{water})V]RT$. Vapour pressure of water (P_{water}) at 293 K = 17.5424 Torr. Atmospheric pressure (P_{atm}) at 293 K = 761.3126 Torr. R = 62.363 L Torr K^{-1} mol^{-1}, volume of gas displaced = 46.3 ml.

3.4.15 Reaction of benzaldehyde with KOH

Added benzaldehyde (1 mmol) and KOH (1 mmol) in 3 ml of dry toluene in an oven dried, vacuum cooled Schlenk tube and dipped in a preheated oil bath at 110 ºC. Allowed to reflux for 1 hour in N_2 atmosphere. The reaction allowed it to cool, and the solvent removed under vacuum. The solid remains weas washed several time with ethyl acetate and then filtered. The precipitate was dissolved in deionized water (30 ml) and extracted with ethyl acetate. The organic phase was dried over Na_2SO_4, and the solvent was removed under vacuum to give pure solid product of benzoic acid (68 mg, 56%).

3.4.16 Control Experiments

(a) A mixture of benzyl alcohol (1 mmol) and KOH (1 mmol) were added in a Schlenk tube and reacted at 110 ºC for 4 hours in N_2 atmosphere. The reaction was cooled and analyzed by GCMS. No indication for ester formation, but a peak for benzaldehyde was observed.

(b) A mixture of benzyl alcohol (1 mmol) and KOH (1 mmol) were mixed in toluene solvent (3 ml) and in a Schlenk tube and reacted at 110 ºC for 4 hours in N_2 atmosphere. The reaction was cooled and further analyzed by GCMS. No indication of ester formation but a peak for benzaldehyde was observed.

(c) Dehydrogenation of benzaldehyde to benzoic acid

Catalyst **4** (0.1 mol%), KOH (1 mmol) were mixed in dry toluene 3 ml in a schlenk tube and then stirred for 1 hour. After that the oil bath temperature was heated to 120 °C and benzaldehyde (1 mmol) was added to reaction mixture and schlenk tube was dipped in preheated oil bath under inert atmosphere. The reaction was stirred for 1 hour and cooled. The workup was followed as mentioned in the procedure. The product was analysed by ^{1}H-NMR showing formation of benzoic acid with traces of benzyl alcohol (Figure 3.4.19).

3.5 Spectral Data

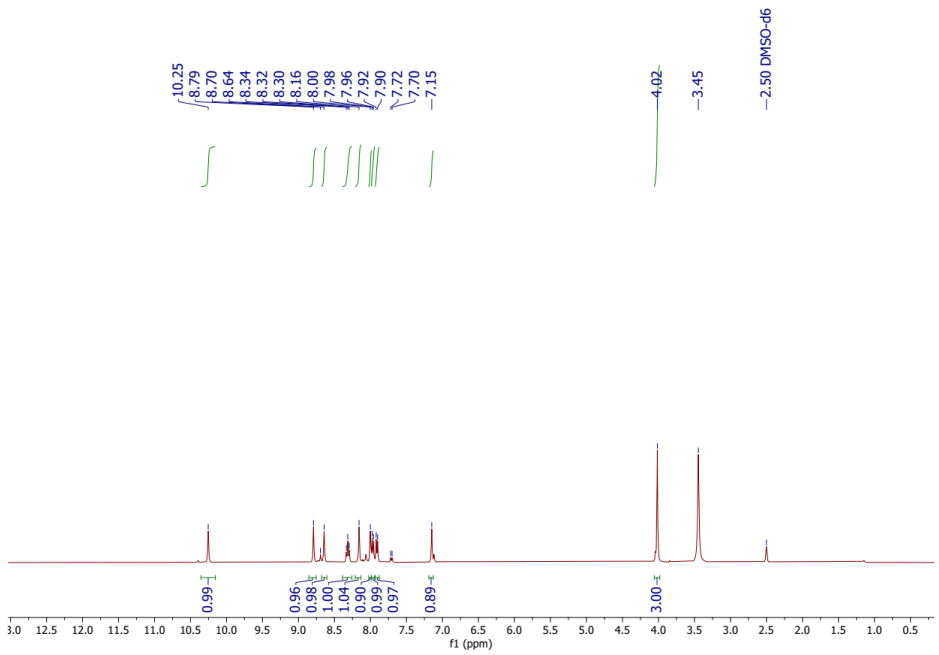

Figure 3.4.1 ^{1}H NMR spectrum of **L^{1}.HI.**

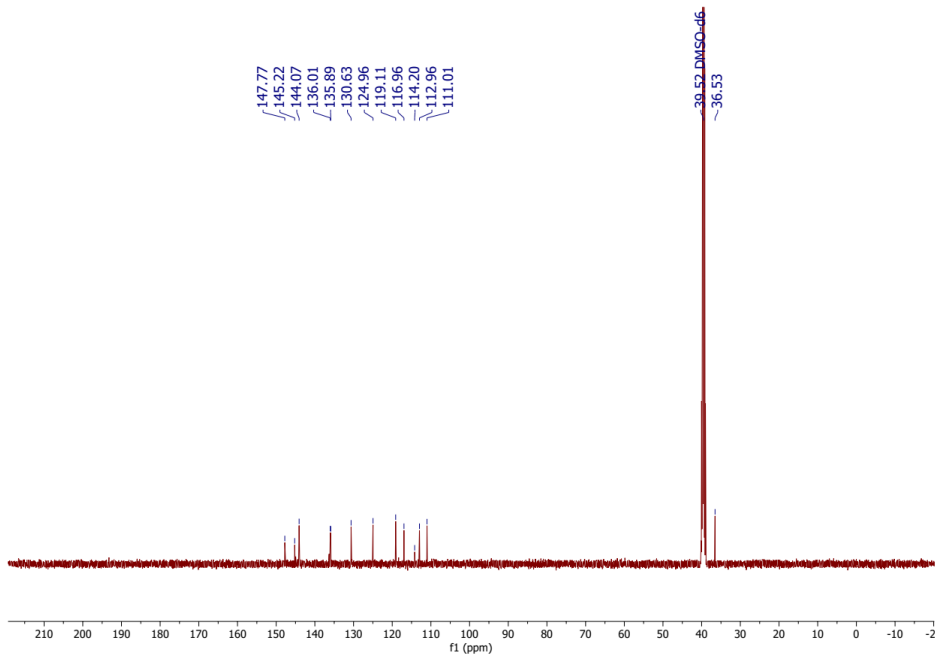

Figure 3.4.2 ^{13}C{^{1}H} NMR spectrum of **L^{1}·HI.**

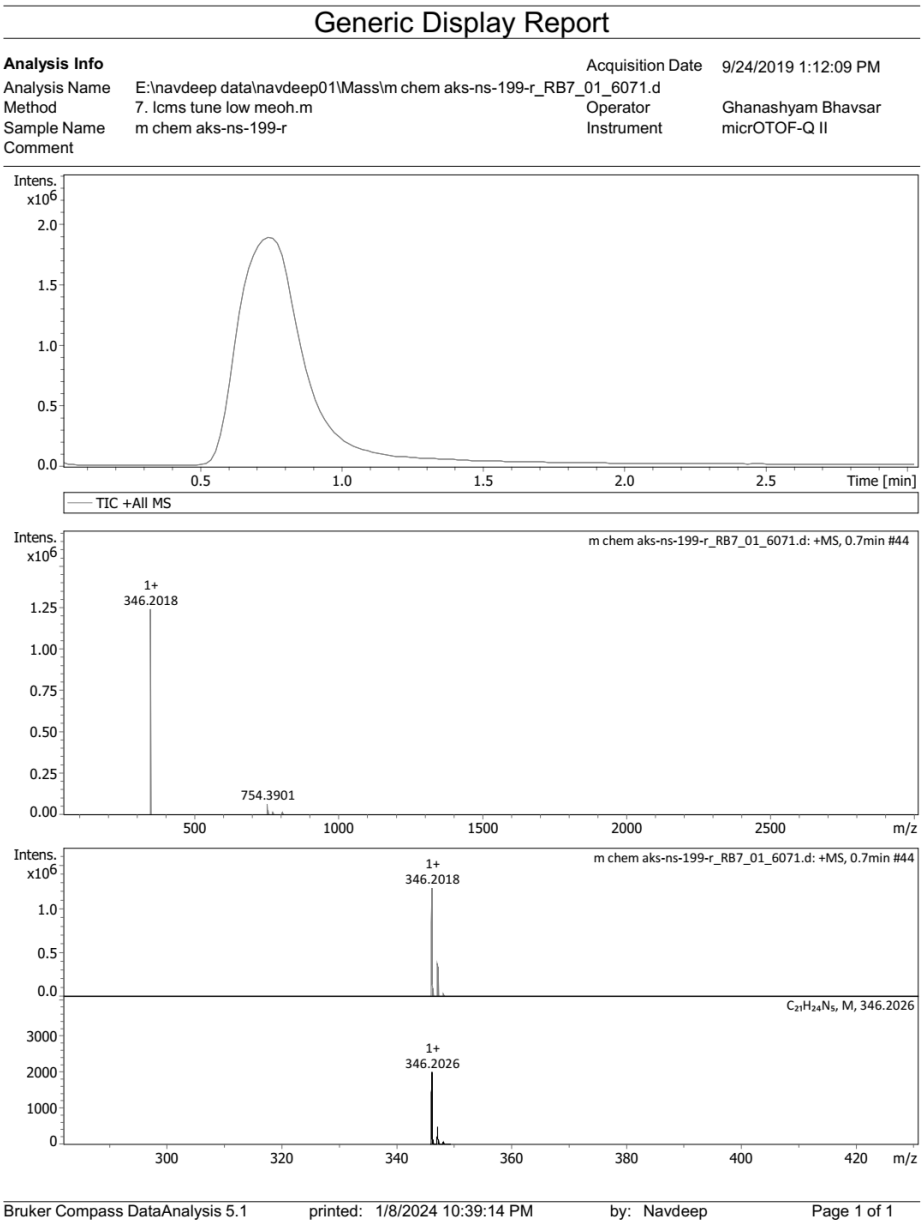

Figure 3.4.3 HRMS of L2·HBr ligand.

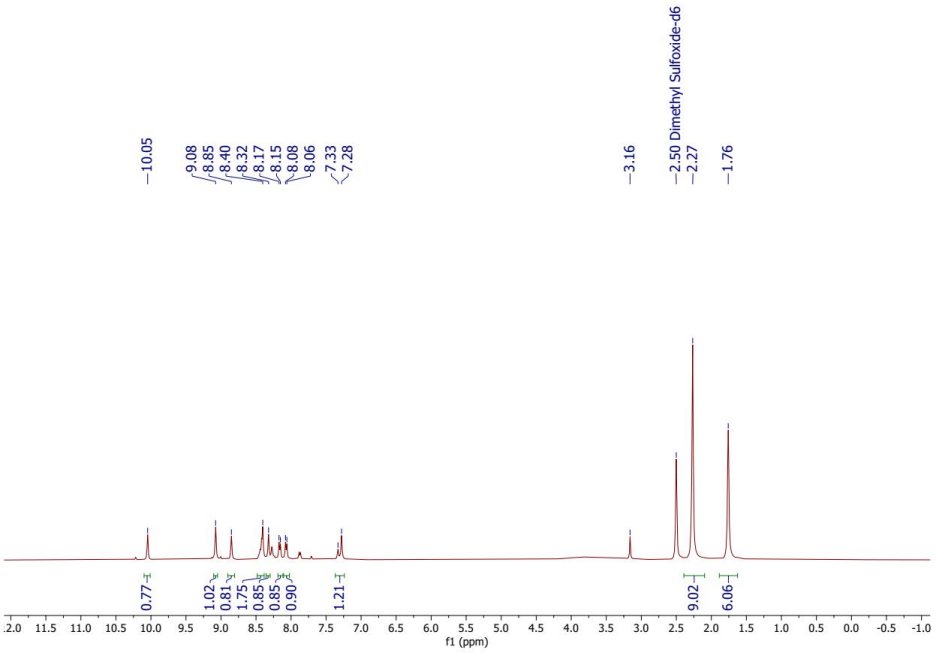

Figure 3.4.4 ^{1}H NMR of L2·HBr ligand.

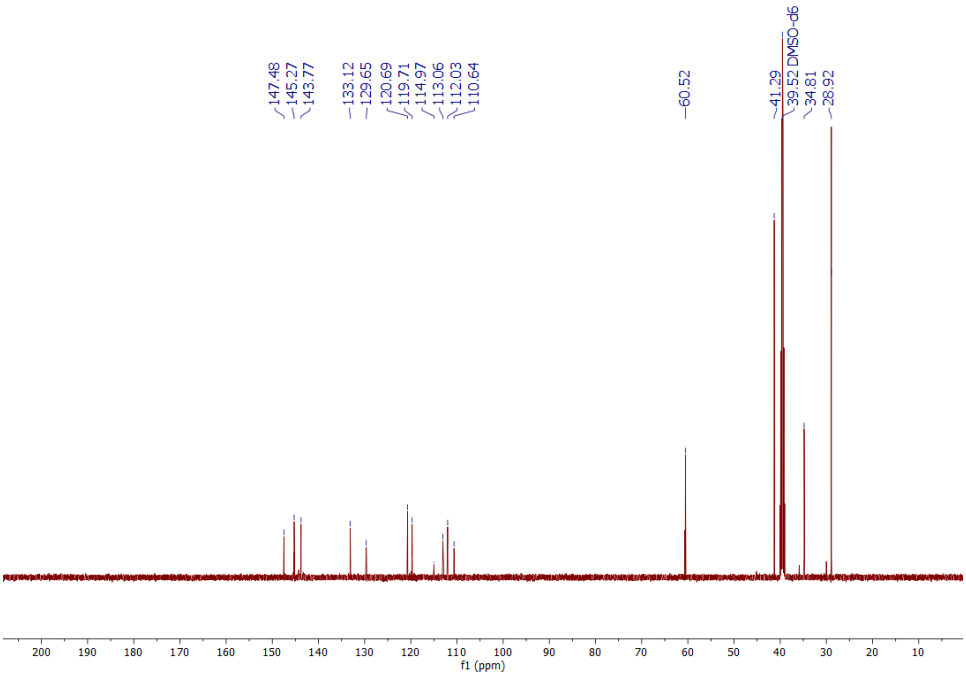

Figure 3.4.5 ^{13}C{^{1}H} NMR of L2·HBr ligand.

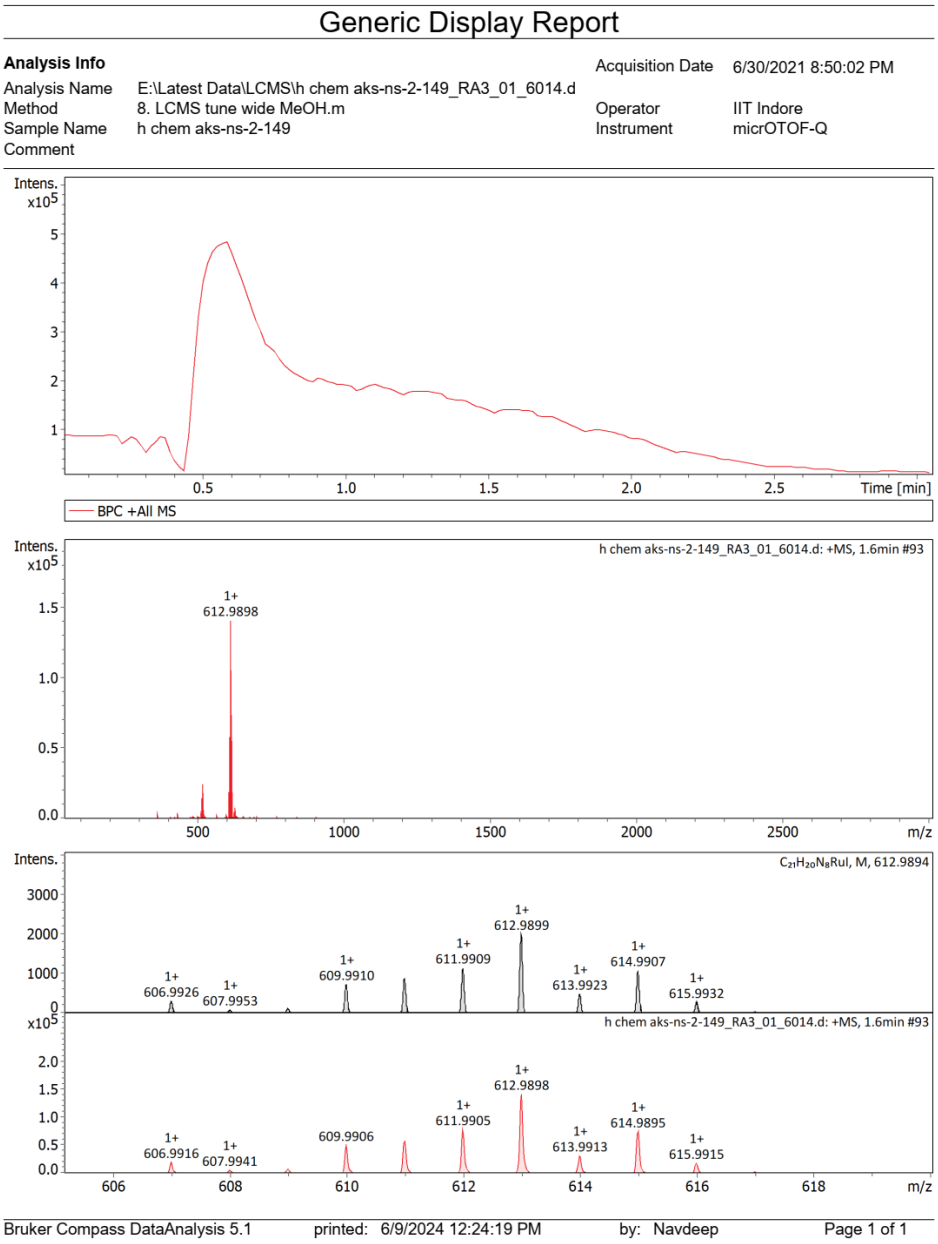

Figure 3.4.6 HRMS of complex **3.**

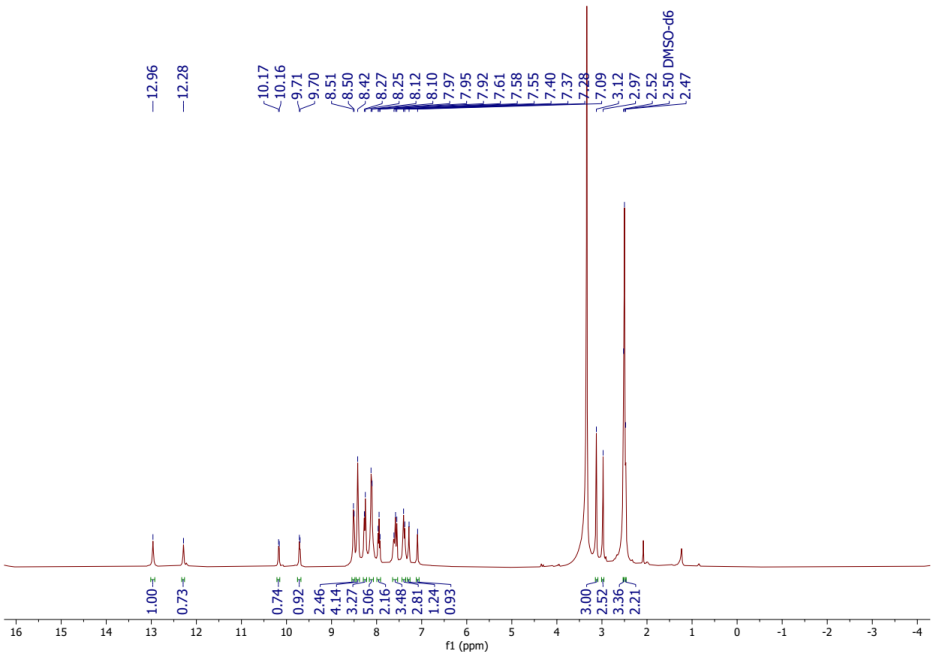

Figure 3.4.7 ^{1}H NMR of complex **3**

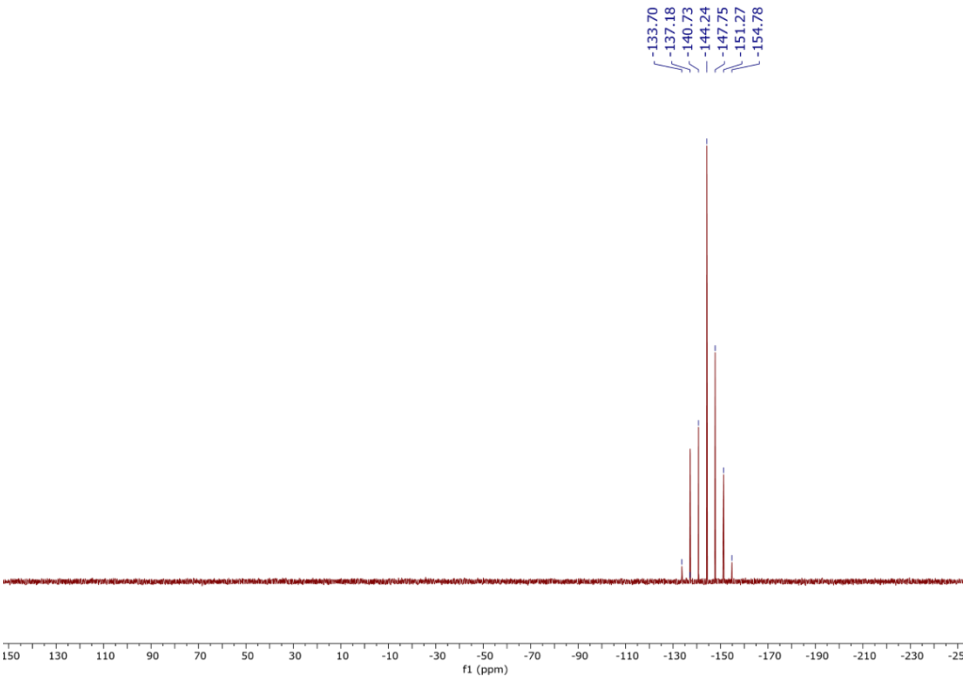

Figure 3.4.8 ^{31}P{^{1}H} NMR of complex **3**

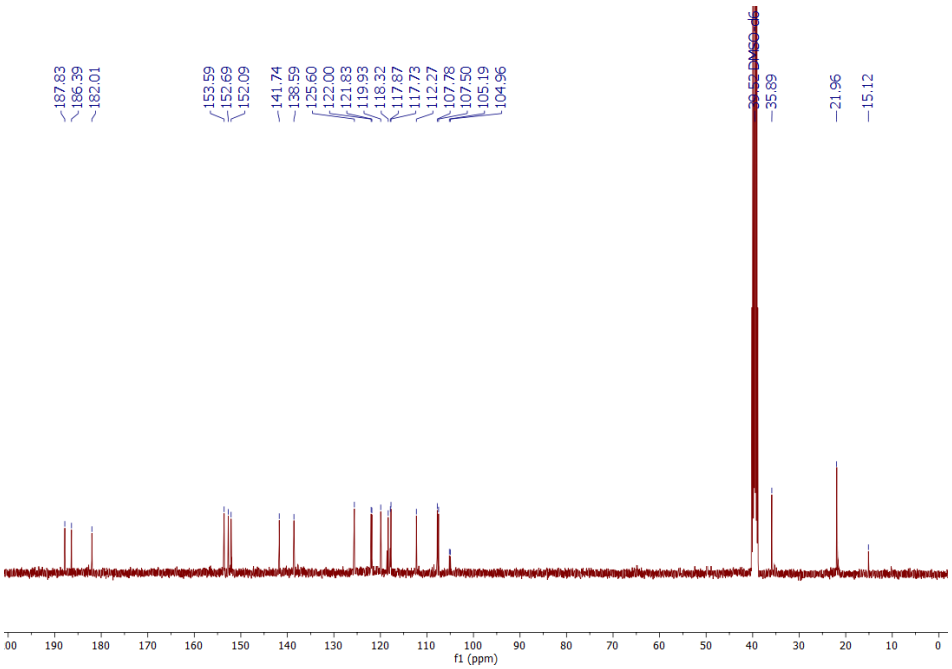

Figure 3.4.9 $^{13}C\{^{1}H\}$ NMR of complex **3**

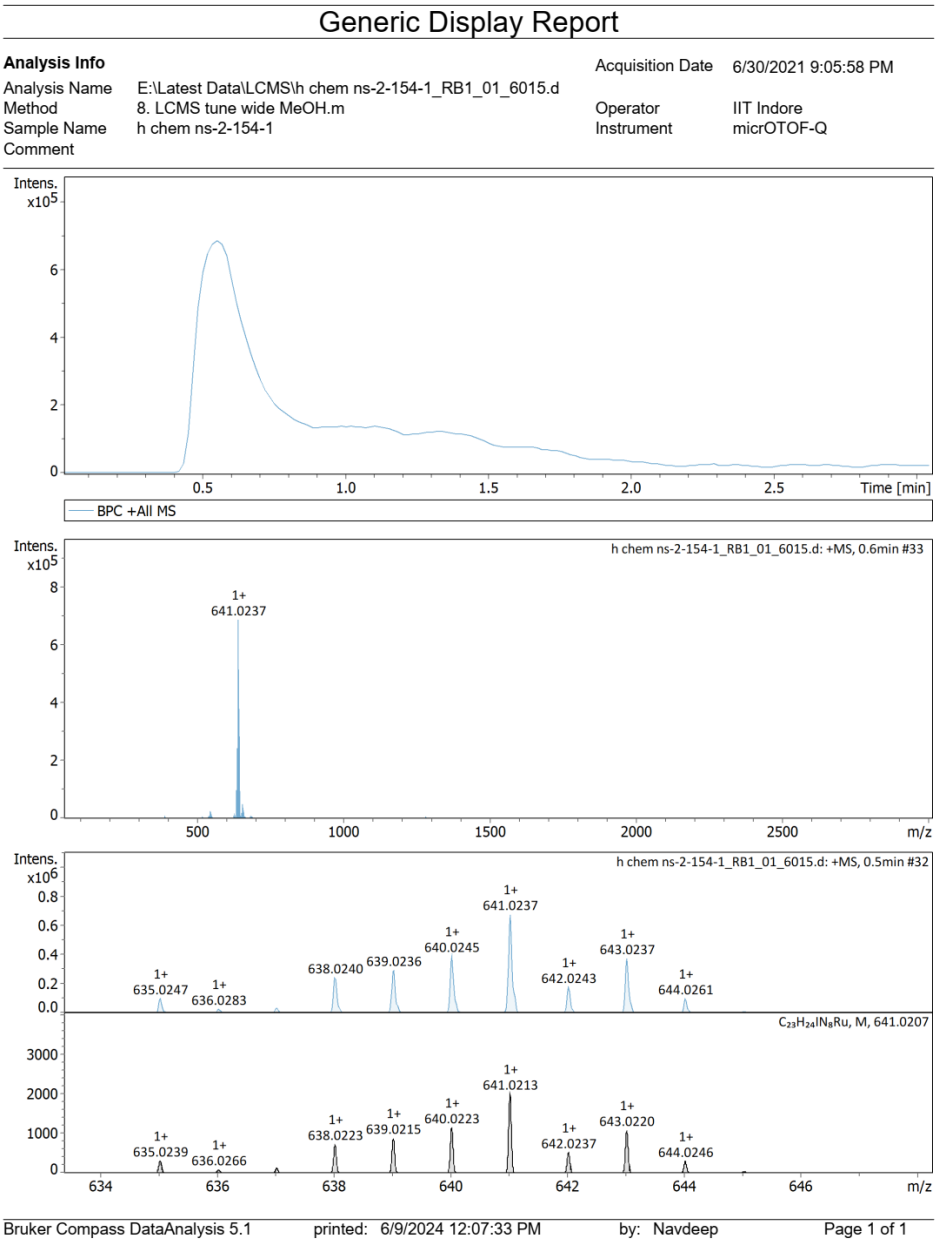

Figure 3.4.10 HRMS of complex **4**

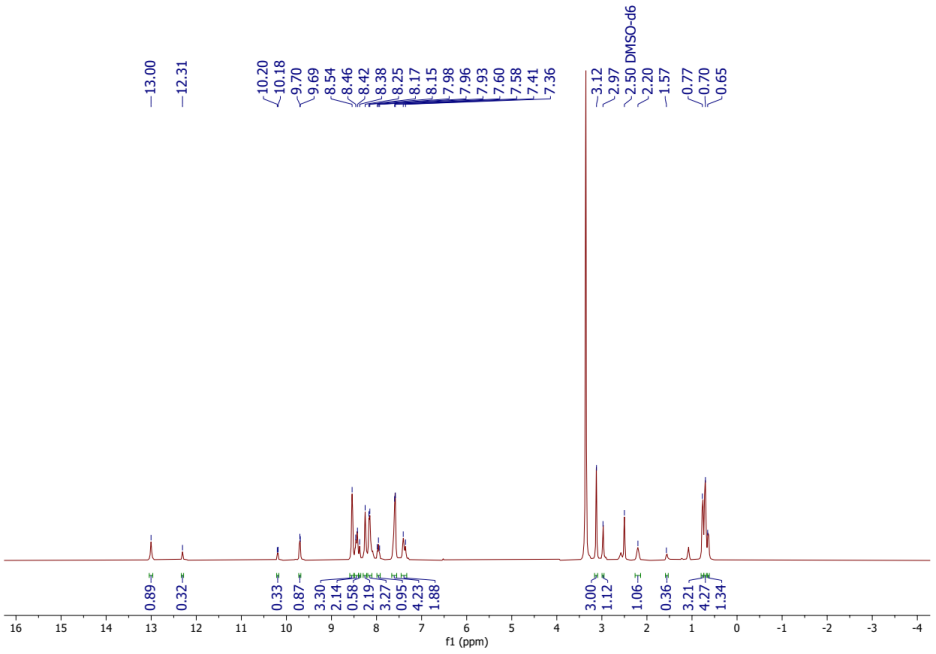

Figure 3.4.11 ^{1}H NMR of complex **4**

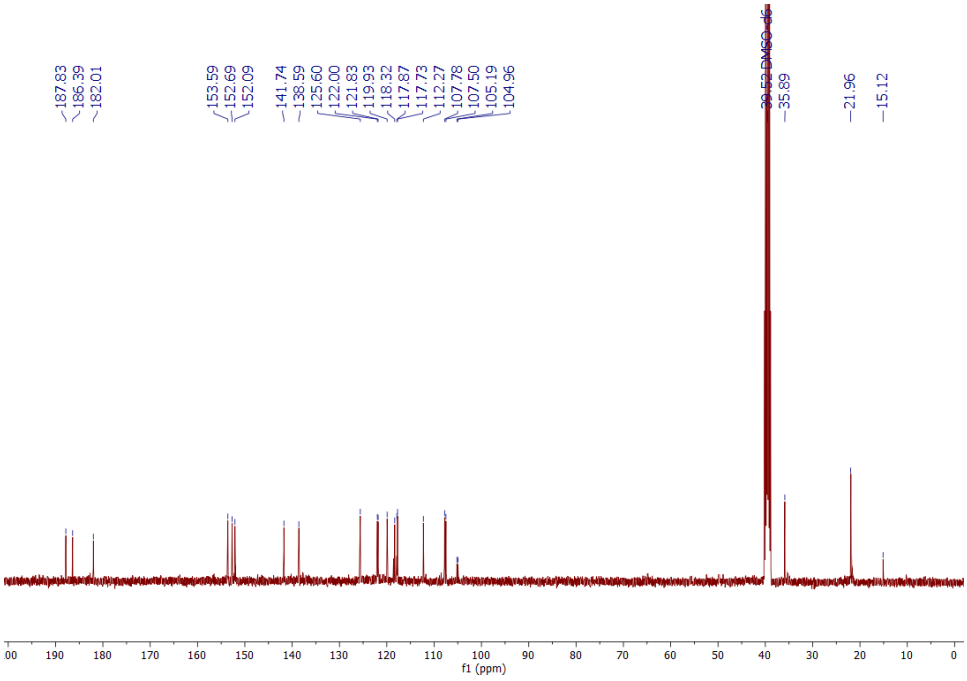

Figure 3.4.12 ^{31}C{H} NMR of complex **4**

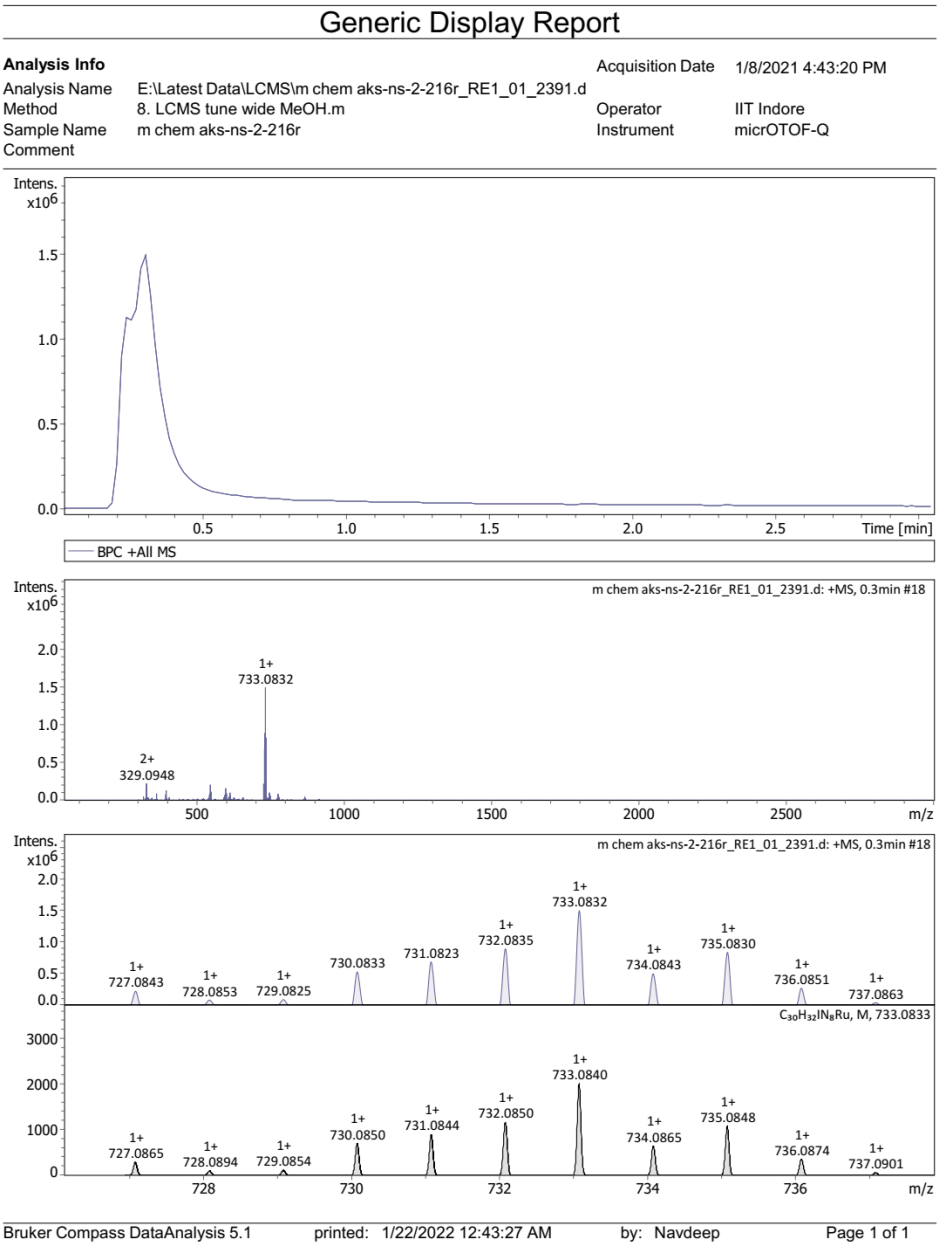

Figure 3.4.13 HRMS of complex **5**

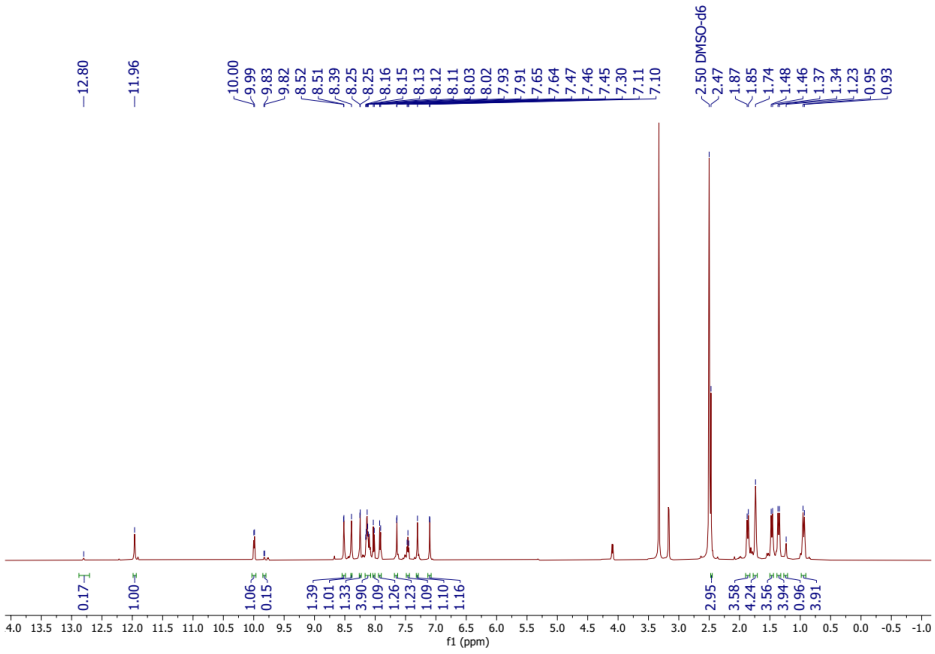

Figure 3.4.14 ^{1}H NMR of complex **5**

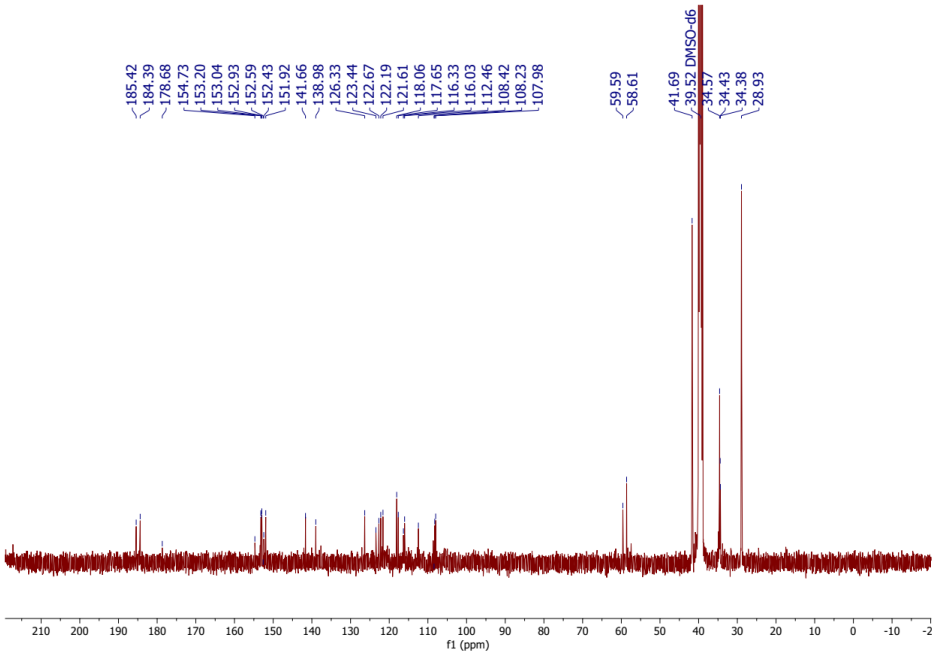

Figure 3.4.15 ^{13}C{^{1}H} NMR of complex **5**

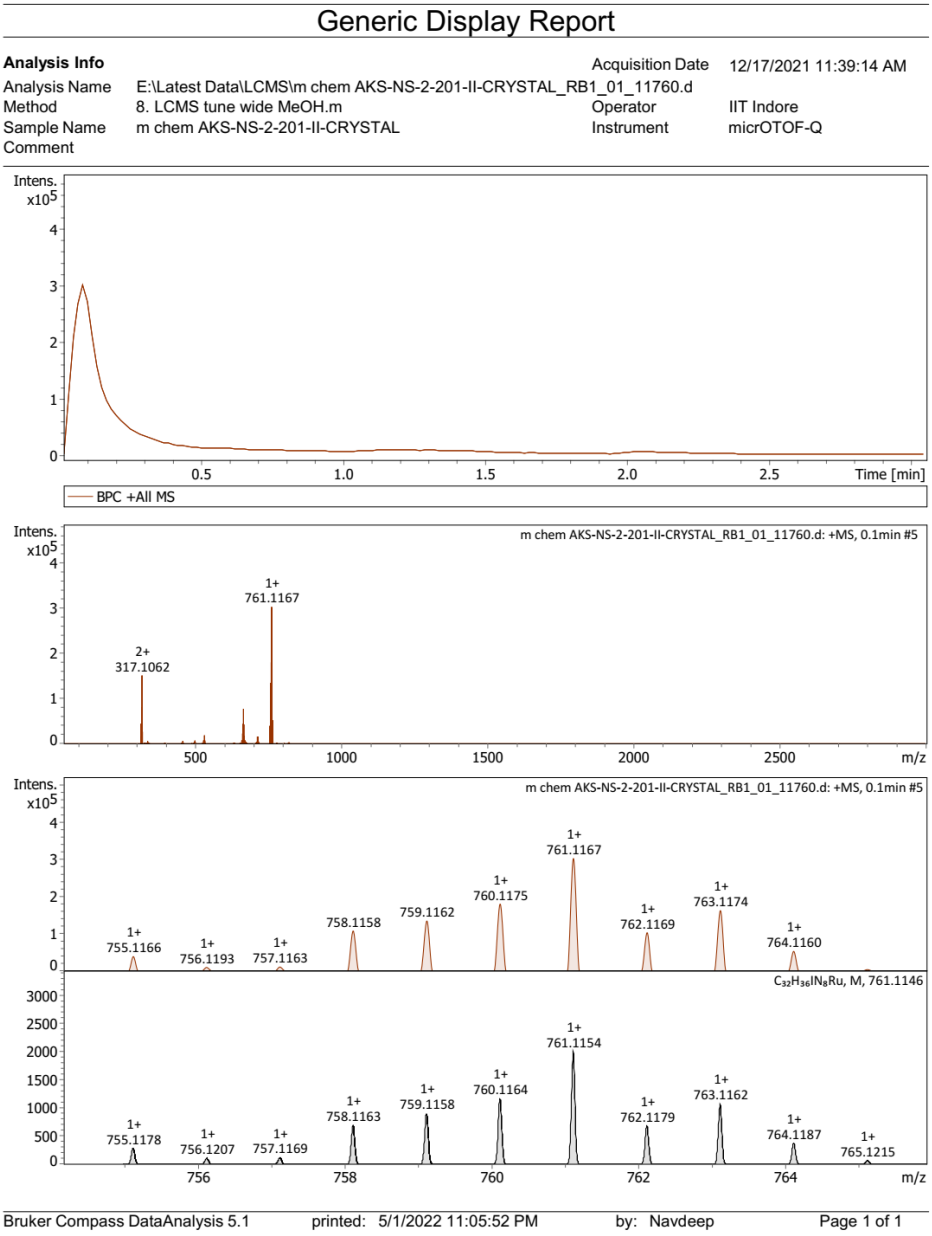

Figure 3.4.16 HRMS of complex **6**

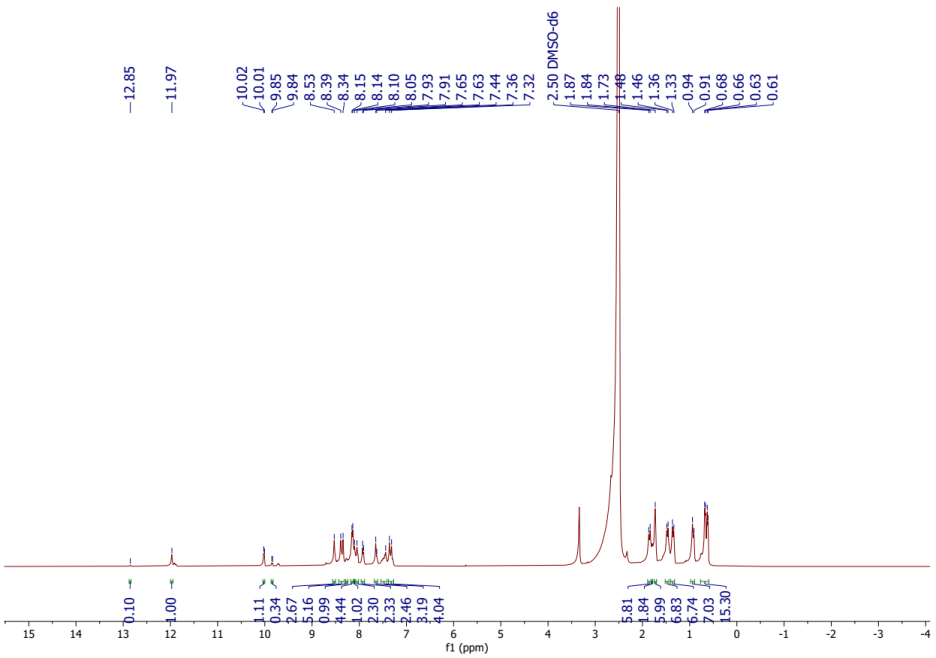

Figure 3.4.17 ^{1}H NMR of complex **6**

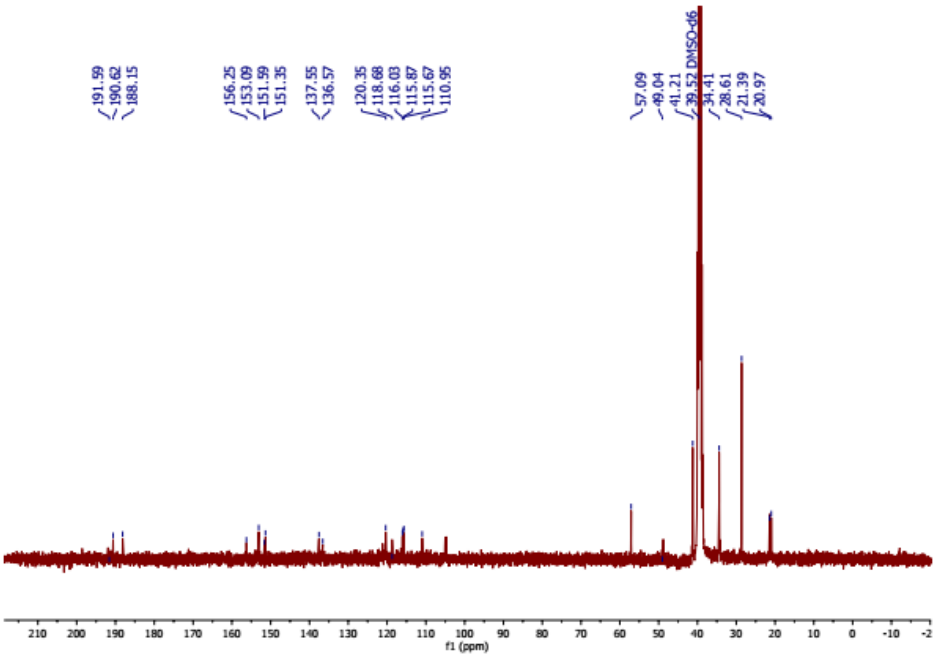

Figure 3.4.18 ^{13}C{^{1}H} NMR of complex **6**

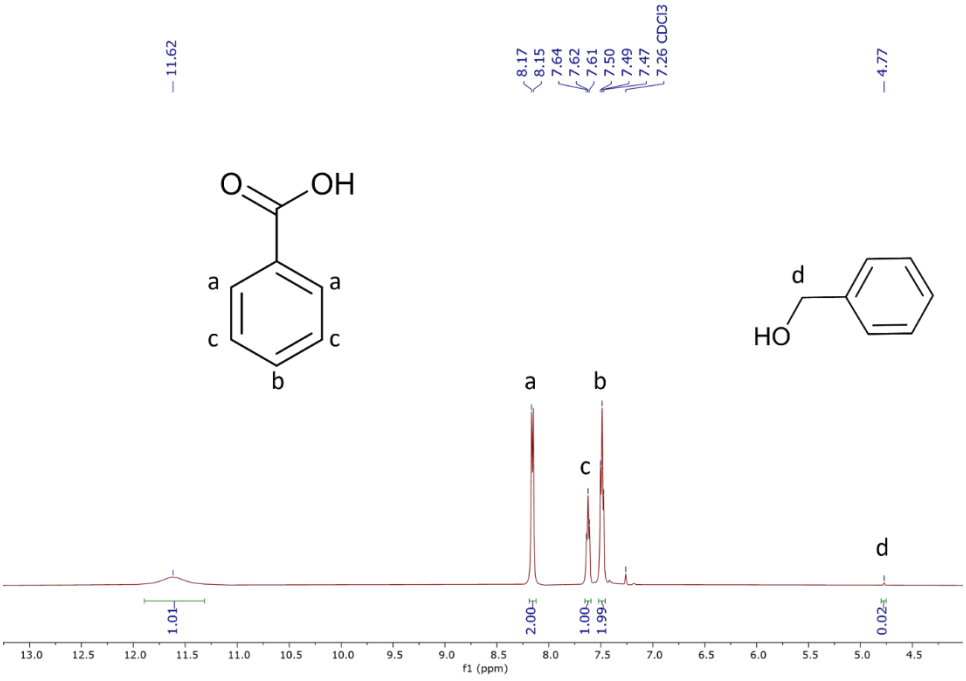

Figure 3.4.19 NMR spectra for dehydrogenation of benzaldehyde

3.5.1 NMR of carboxylic acid products after dehydrogenation of alcohol

(4a) Benzoic acid:

^{1}H NMR (500 MHz, $CDCl_3$) δ 11.67 (s, 1H), 8.14 (dd, *J* = 1.5, 8.4 Hz, 2H), 7.63 (t, *J* = 7.4 Hz, 1H), 7.49 (t, *J* = 7.8 Hz, 2H). ^{13}C{^{1}H} NMR (126 MHz, CDCl3) δ 172.18 (COOH), 133.72, 130.12, 129.20, 128.39.

(4b) p-Methoxy benzoic acid:

^{1}H NMR (500 MHz, $CDCl_3$) δ 6.39 (dd, *J* = 5.5, 8.9 Hz, 2H), 6.13 (t, *J* = 8.9 Hz, 2H), 2.94 (s, 3H). ^{13}C{^{1}H} NMR (126 MHz, $CDCl_3$) δ 167.18 (COOH), 163.01, 131.52, 123.14, 113.99, 55.62.

(4c) m-Methoxy benzoic acid

^{1}H NMR (500 MHz, $CDCl_3$) δ 7.72 (d, *J* = 7.6 Hz, 1H), 7.63 (s, 1H), 7.39 (t, *J* = 8.0 Hz, 1H), 7.17 (ddd, *J* = 1.0, 2.7, 8.3 Hz, 1H), 3.87 (s, 3H). ^{13}C{^{1}H}

NMR (126 MHz, $CDCl_3$) δ 171.69 (COOH), 159.77, 130.65, 129.69, 122.83, 120.63, 114.54, 55.62.

(4d) o-Methoxy benzoic acid

^1H NMR (500 MHz, $CDCl_3$) δ 8.06 (dd, *J* = 1.5, 8.3 Hz, 1H), 7.45 (td, *J* = 1.5, 7.5 Hz, 1H), 7.27 (m, 2H), 2.58 (s, 3H). $^{13}C\{^1H\}$ NMR (126 MHz, $CDCl_3$) δ 172.55 (COOH), 141.50, 133.09, 132.08, 131.71, 128.34, 126.00, 29.85.

(4e) m,p-dimethoxybenzoic acid

^1H NMR (500 MHz, $CDCl_3$) δ 7.78 (dd, *J* = 2.0, 8.4 Hz, 1H), 7.60 (d, *J* = 2.1 Hz, 1H), 6.92 (d, *J* = 8.5 Hz, 1H), 3.95 (d, *J* = 5.2 Hz, 6H). $^{13}C\{^1H\}$ NMR (126 MHz, $CDCl_3$) δ 171.71 (COOH), 153.86, 148.83, 124.73, 121.81, 112.45, 110.46, 56.16.

(4f) p-(benzyloxy)benzoic acid

^1H NMR (500 MHz, DMSO-d6) δ 12.62 (s, 1H), 7.92 – 7.86 (m, 2H), 7.46 (d, *J* = 7.1 Hz, 2H), 7.37 (dt, *J* = 7.4, 29.5 Hz, 3H), 7.09 (d, *J* = 8.1 Hz, 2H), 5.18 (d, *J* = 3.2 Hz, 2H). $^{13}C\{^1H\}$ NMR (126 MHz, DMSO-d6) δ 166.97 (COOH), 161.93, 136.54, 131.34, 128.50, 127.82, 114.62, 69.45.

(4g) p-Methyl benzoic acid:

^1H NMR (500 MHz, DMSO-d6) δ 7.83 (d, *J* = 8.1 Hz, 2H), 7.30 (d, *J* = 8.2 Hz, 2H), 2.37 (s, 3H). $^{13}C\{^1H\}$ NMR (126 MHz, DMSO-d6) δ 167.16 (COOH), 142.82, 129.16, 127.94, 20.96.

(4h) m-Methyl benzoic acid:

^1H NMR (500 MHz, DMSO-d6) δ 12.83 (s, 1H), 7.78 – 7.71 (m, 2H), 7.41 (dd, *J* = 7.7, 22.6 Hz, 2H), 2.36 (s, 3H). $^{13}C\{^1H\}$ NMR (126 MHz, DMSO-d6) δ 167.43, 137.91, 133.48, 130.73, 129.74, 128.47, 126.47, 20.83.

(4i) p-^{Iso}Propyl benzoic acid:

^{1}H NMR (500 MHz, $CDCl_3$) δ 8.04 (d, *J* = 6.3 Hz, 2H), 7.33 (d, *J* = 8.4 Hz, 2H), 3.04 – 2.93 (m, 1H) 1.27 (d, *J* = 17.1 Hz, 6H). ^{13}C{^{1}H} NMR (126 MHz, $CDCl_3$) δ 171.83, 155.40, 130.53, 127.16, 126.75, 34.49, 23.83.

(4j) p-^{tert}Butyl benzoic acid

^{1}H NMR (500 MHz, $CDCl_3$) δ 8.05 (d, *J* = 8.7 Hz, 2H), 7.49 (d, *J* = 8.7 Hz, 2H), 1.36 (s, 9H). ^{13}C{^{1}H} NMR (126 MHz, $CDCl_3$) δ 171.95, 157.73, 130.27, 126.65, 125.64, 35.35, 31.25.

(4k) p-Amino benzoic acid

^{1}H NMR (500 MHz, $CDCl_3$) δ 7.91 (d, *J* = 8.7 Hz, 2H), 6.66 (d, *J* = 8.7 Hz, 2H). ^{13}C{^{1}H} NMR (126 MHz, $CDCl_3$) δ 171.10 (COOH), 151.62, 132.53, 118.77, 113.93.

(4l) m-aminobenzoic acid

^{1}H NMR (500 MHz, DMSO-d6) δ 12.55 (s, 1H) 7.16 (s, 1H), 7.13 – 7.04 (m, 2H), 6.79 – 6.73 (m, 1H). ^{13}C{^{1}H} NMR (126 MHz, DMSO-d6) δ 167.90 (COOH), 148.85, 131.33, 128.89, 117.99, 116.64, 114.44.

(4m) o-aminobenzoic acid

No reaction

(4n) m- Nitro benzoic acid:

^{1}H NMR (500 MHz, DMSO-d6): δ 8.29 (d, *J* = 8.4 Hz, 1H), 8.16 (t, *J* = 8.5 Hz, 1H), 7.9 (d, *J* = 8.5 Hz, 1H), 7.3 (s, *J* = 8.5 Hz, 1H). ^{13}C{^{1}H}NMR (126 MHz, DMSO-d6) δ 192.83, 130.93, 130.73, 127.09, 123.74, 123.53, 123.35.

(4o) p-Fluoro benzoic acid:

^{1}H NMR (500 MHz, DMSO-d6) δ 8.00 (dd, *J* = 5.6, 8.9 Hz, 2H), 7.32 (t, *J* = 8.9 Hz, 2H). ^{13}C{^{1}H} NMR (126 MHz, DMSO-d6) δ 166.82, 131.87, 131.47, 130.30, 127.01.

(4p) p-Chloro benzoic acid:

^{1}H NMR (500 MHz, $CDCl_3$) δ 8.03 (d, *J* = 4.4 Hz, 2H), 7.45 (d, *J* = 9.0 Hz, 2H). ^{13}C{^{1}H} NMR (126 MHz, DMSO-D6) δ 166.82, 131.87, 131.47, 130.30, 127.01.

(4q) p-Bromo benzoic acid:

1H NMR (500 MHz, DMSO-d6) δ 7.86 (d, *J* = 8.5 Hz, 2H), 7.70 (d, *J* = 6.4 Hz, 2H). ^{13}C{^{1}H} NMR (126 MHz, DMSO-d6) δ 166.82, 131.87, 131.47, 130.30, 127.01.

(4r) p-Iodo benzoic acid:

^{1}H NMR (500 MHz, DMSO-d6) δ 8.03 (d, *J* = 4.4 Hz, 2H), 7.45 (d, *J* = 9.0 Hz, 2H).^{13}C{^{1}H} NMR (126 MHz, DMSO-d6) δ 166.82, 131.87, 131.47, 130.30, 127.01.

(4s) m-Floro benzoic acid:

^{1}H NMR (500 MHz, $CDCl_3$) δ 7.91 (d, *J* = 9.2 Hz, 1H), 7.46 (td, *J* = 5.5, 8.0 Hz, 2H), 7.32 (td, *J* = 2.7, 8.2 Hz, 1H). ^{13}C{^{1}H} NMR (126 MHz, $CDCl_3$) δ 170.50, 163.69, 161.73, 131.55 (d, *J* = 7.4 Hz), 130.35 (d, *J* = 3.7 Hz), 126.10 (d, *J* = 3.7 Hz), 121.08 (d, *J* = 21.1 Hz), 117.20 (d, *J* = 23.0 Hz).

(4t) m-Chloro benzoic acid:

^{1}H NMR (500 MHz, DMSO-d6) δ 13.26 (s, 1H), 7.92 (s, 1H), 7.70 (d, *J* = 8.0 Hz, 1H), 7.55 (d, *J* = 8.2 Hz, 1H). ^{13}C{^{1}H} NMR (126 MHz, DMSO-d6) δ 166.10 (COOH), 133.35, 132.95, 132.73, 130.68, 128.84.

(4u) o-Bromo benzoic acid:

^{1}H NMR (500 MHz, DMSO-d6) δ 7.72 (ddd, *J* = 1.8, 7.6, 11.4 Hz, 2H), 7.51 – 7.39 (m, 2H). ^{13}C{^{1}H} NMR (126 MHz, DMSO-d6) δ 167.42 (COOH), 133.77, 132.52, 127.74, 119.94.

(4v) Furan-2-Carboxylic acid:

^{1}H NMR (500 MHz, DMSO-d6) δ 8.74 (s, 1H), 7.63 (dd, *J* = 0.9, 1.8 Hz, 1H), 7.34 – 7.28 (m, 1H), 6.55 (dd, *J* = 1.8, 3.5 Hz, 1H). ^{13}C{1H} NMR (126 MHz, DMSO-d6) δ 163.62, 147.68, 144.36, 120.29, 112.62.

(4w) Piperonylic acid:

^{1}H NMR (500 MHz, DMSO-d6) δ 12.74 (s, 1H), 7.54 (dd, *J* = 1.8, 8.2 Hz, 1H), 7.36 (d, *J* = 1.8 Hz, 1H), 7.00 (d, *J* = 8.2 Hz, 1H), 6.12 (s, 2H). ^{13}C{1H} NMR (126 MHz, DMSO-d6) δ 166.64, 151.15, 147.49, 124.98, 124.67, 108.80, 108.09, 101.95.

(4x) Butyric acid:

^{1}H ^{1}H NMR (500 MHz, $CDCl_3$) δ 2.33 (t, *J* = 7.4 Hz, 2H), 1.66 (q, *J* = 7.5 Hz, 2H), 0.96 (d, *J* = 7.5 Hz, 3H). ^{13}C{^{1}H} NMR (126 MHz, $CDCl_3$) δ 179.52, 35.77, 18.04, 13.48.

(4y) Hexan-1-ol:

No reaction

(4z) Phenylethan-1-ol:

No reaction

3.6 References

[1] P. de Frémont, N. Marion, S.P. Nolan, Carbenes: Synthesis, properties, and organometallic chemistry, Coord. Chem. Rev. 253 (2009) 862–892. https://doi.org/10.1016/j.ccr.2008.05.018.

[2] D. Bourissou, O. Guerret, F.P. Gabbaï, G. Bertrand, Stable Carbenes, Chem. Rev. 100 (2000) 39–92. https://doi.org/10.1021/cr940472u.

[3] M.C. Jahnke, F.E. Hahn, Complexes with protic (NH,NH and NH,NR) N-heterocyclic carbene ligands, Coord. Chem. Rev. 293–294 (2015) 95–115. https://doi.org/10.1016/j.ccr.2015.01.014.

[4] S. Kuwata, F.E. Hahn, Complexes Bearing Protic N-Heterocyclic Carbene Ligands, Chem. Rev. 118 (2018) 9642–9677. https://doi.org/10.1021/acs.chemrev.8b00176.

[5] S. Yaşar, E.Ö. Karaca, Ç. Şahin, İ. Özdemir, O. Şahin, O. Büyükgüngör, Novel ruthenium(II)–N-heterocyclic carbene complexes; synthesis, characterization and catalytic application, J. Organomet. Chem. 789–790 (2015) 1–7. https://doi.org/10.1016/j.jorganchem.2015.04.012.

[6] M.N. Hopkinson, C. Richter, M. Schedler, F. Glorius, An overview of N-heterocyclic carbenes, Nature 510 (2014) 485–496. https://doi.org/10.1038/nature13384.

[7] C. Gunanathan, D. Milstein, Bond Activation and Catalysis by Ruthenium Pincer Complexes, Chem. Rev. 114 (2014) 12024–12087. https://doi.org/10.1021/cr5002782.

[8] E. Fogler, E. Balaraman, Y. Ben-David, G. Leitus, L. Shimon J.W., D. Milstein, New CNN-Type Ruthenium Pincer NHC Complexes. Mild, Efficient Catalytic Hydrogenation of Esters, Organometallics 30 (2011) 3826–3833. https://doi.org/10.1021/om200367j.

[9] H.A. Younus, N. Ahmad, W. Su, F. Verpoort, Ruthenium pincer complexes: Ligand design and complex synthesis, Coord. Chem. Rev. 276 (2014) 112–152. https://doi.org/10.1016/j.ccr.2014.06.016.

[10] Ruthenium Pincer Complexes: Synthesis and Catalytic Applications, Adv. Synth. Catal. 357 (2015) 283–330. https://doi.org/10.1002/adsc.201400777.

[11] Ruthenium complexes with an N-heterocyclic carbene NNC-pincer ligand: preparation and catalytic properties, Org. Chem. Front. 2 (2015) 936–941. https://doi.org/10.1039/c5qo00137d.

[12] C.K. Prier, D.A. Rankic, D.W.C. MacMillan, Visible Light Photoredox Catalysis with Transition Metal Complexes: Applications in Organic Synthesis, Chem. Rev. 113 (2013) 5322–5363. https://doi.org/10.1021/cr300503r.

[13] P. Nareddy, F. Jordan, M. Szostak, Recent Developments in Ruthenium-Catalyzed C–H Arylation: Array of Mechanistic Manifolds, ACS Catal. 7 (2017) 5721–5745. https://doi.org/10.1021/acscatal.7b01645.

[14] G.A. Filonenko, E. Cosimi, L. Lefort, M.P. Conley, C. Copéret, M. Lutz, E.J.M. Hensen, E.A. Pidko, Lutidine-Derived Ru-CNC Hydrogenation Pincer Catalysts with Versatile Coordination Properties, ACS Catal. 4 (2014) 2667–2671. https://doi.org/10.1021/cs500720y.

[15] Acceptorless dehydrogenation and dehydrogenative coupling of alcohols catalysed by protic NHC ruthenium complexes, Org. Biomol. Chem. 15 (2017) 3466–3471. https://doi.org/10.1039/c7ob00542c.

[16] C.A. Urbina-Blanco, A. Leitgeb, C. Slugovc, X. Bantreil, H. Clavier, A.M.Z. Slawin, S.P. Nolan, Olefin Metathesis Featuring Ruthenium Indenylidene Complexes with a Sterically Demanding NHC Ligand, Chem. – Eur. J. 17 (2011) 5045–5053. https://doi.org/10.1002/chem.201003082.

[17] A. Kajetanowicz, K. Grela, Nitro and Other Electron Withdrawing Group Activated Ruthenium Catalysts for Olefin Metathesis Reactions, Angew. Chem. Int. Ed. 60 (2021) 13738–13756. https://doi.org/10.1002/anie.202008150.

[18] C.M. Boudreaux, N.P. Liyanage, H. Shirley, S. Siek, D.L. Gerlach, F. Qu, J.H. Delcamp, E.T. Papish, Ruthenium(II) complexes of pyridinol and N-heterocyclic carbene derived pincers as robust catalysts for selective carbon dioxide reduction, Chem. Commun. 53 (2017) 11217–11220. https://doi.org/10.1039/C7CC05706G.

[19] Highly Active and Robust Ruthenium Complexes Based on Hemilability of Hybrid Ligands for C–H Oxidation, J. Org. Chem. 85 (2020) 4324–4334. https://doi.org/10.1021/acs.joc.0c00025.

[20] K.-N.T. Tseng, J.W. Kampf, N.K. Szymczak, Mechanism of N,N,N-Amide Ruthenium(II) Hydride Mediated Acceptorless Alcohol Dehydrogenation: Inner-Sphere β-H Elimination versus Outer-Sphere Bifunctional Metal–Ligand Cooperativity, ACS Catal. 5 (2015) 5468–5485. https://doi.org/10.1021/acscatal.5b00952.

[21] S. Chakraborty, P.E. Piszel, W.W. Brennessel, W.D. Jones, A Single Nickel Catalyst for the Acceptorless Dehydrogenation of Alcohols and Hydrogenation of Carbonyl Compounds, Organometallics 34 (2015) 5203–5206. https://doi.org/10.1021/acs.organomet.5b00824.

[22] J. Campos, L.S. Sharninghausen, M.G. Manas, R.H. Crabtree, Methanol Dehydrogenation by Iridium N-Heterocyclic Carbene Complexes, Inorg. Chem. 54 (2015) 5079–5084. https://doi.org/10.1021/ic502521c.

[23] M.A. Weber, P.C. Ford, Catalytic dehydrogenation of 1,2- and 1,3-diols, J. Mol. Catal. Chem. 416 (2016) 81–87. https://doi.org/10.1016/j.molcata.2016.02.018.

[24] T. Punniyamurthy, S. Velusamy, J. Iqbal, Recent Advances in Transition Metal Catalyzed Oxidation of Organic Substrates with Molecular Oxygen, Chem. Rev. 105 (2005) 2329–2364. https://doi.org/10.1021/cr050523v.

[25] S. Patel, B.K. Mishra, Chromium(VI) oxidants having quaternary ammonium ions: studies on synthetic applications and oxidation

kinetics, Tetrahedron 63 (2007) 4367–4406. https://doi.org/10.1016/j.tet.2007.02.073.

[26] M. Trincado, H. Grützmacher, F. Vizza, C. Bianchini, Domino Rhodium/Palladium-Catalyzed Dehydrogenation Reactions of Alcohols to Acids by Hydrogen Transfer to Inactivated Alkenes, Chem. – Eur. J. 16 (2010) 2751–2757. https://doi.org/10.1002/chem.200903069.

[27] S. Annen, T. Zweifel, F. Ricatto, H. Grützmacher, Catalytic Aerobic Dehydrogenative Coupling of Primary Alcohols and Water to Acids Promoted by a Rhodium(I) Amido N-Heterocyclic Carbene Complex, ChemCatChem 2 (2010) 1286–1295. https://doi.org/10.1002/cctc.201000100.

[28] S.P. Annen, H. Grützmacher, Nitrosobenzene as a hydrogen acceptor in rhodium catalysed dehydrogenation reactions of alcohols: synthesis of aldehydes and azoxybenzenes, Dalton Trans. 41 (2012) 14137–14145. https://doi.org/10.1039/C2DT31691A.

[29] T.L. Gianetti, S.P. Annen, G. Santiso-Quinones, M. Reiher, M. Driess, H. Grützmacher, Nitrous Oxide as a Hydrogen Acceptor for the Dehydrogenative Coupling of Alcohols, Angew. Chem. Int. Ed. 55 (2016) 1854–1858. https://doi.org/10.1002/anie.201509288.

[30] C. Gunanathan, D. Milstein, Applications of Acceptorless Dehydrogenation and Related Transformations in Chemical Synthesis, Science 341 (2013) 1229712. https://doi.org/10.1126/science.1229712.

[31] E. Balaraman, E. Khaskin, G. Leitus, D. Milstein, Catalytic transformation of alcohols to carboxylic acid salts and H2 using water as the oxygen atom source, Nat. Chem. 5 (2013) 122–125. https://doi.org/10.1038/nchem.1536.

[32] P. Hu, Y. Ben-David, D. Milstein, General Synthesis of Amino Acid Salts from Amino Alcohols and Basic Water Liberating H2, J. Am.

Chem. Soc. 138 (2016) 6143–6146. https://doi.org/10.1021/jacs.6b03488.

[33] L. Zhang, D.H. Nguyen, G. Raffa, X. Trivelli, F. Capet, S. Desset, S. Paul, F. Dumeignil, R.M. Gauvin, Catalytic Conversion of Alcohols into Carboxylic Acid Salts in Water: Scope, Recycling, and Mechanistic Insights, ChemSusChem 9 (2016) 1413–1423. https://doi.org/10.1002/cssc.201600243.

[34] J.-H. Choi, L. E. Heim, M. Ahrens, M.H. G. Prechtl, Selective conversion of alcohols in water to carboxylic acids by in situ generated ruthenium trans dihydrido carbonyl PNP complexes, Dalton Trans. 43 (2014) 17248–17254. https://doi.org/10.1039/C4DT01634C.

[35] P. Sponholz, D. Mellmann, C. Cordes, P.G. Alsabeh, B. Li, Y. Li, M. Nielsen, H. Junge, P. Dixneuf, M. Beller, Efficient and Selective Hydrogen Generation from Bioethanol using Ruthenium Pincer-type Complexes, ChemSusChem 7 (2014) 2419–2422. https://doi.org/10.1002/cssc.201402426.

[36] Z. Dai, Q. Luo, X. Meng, R. Li, J. Zhang, T. Peng, Ru(II) complexes bearing 2,6-bis(benzimidazole-2-yl)pyridine ligands: A new class of catalysts for efficient dehydrogenation of primary alcohols to carboxylic acids and H2 in the alcohol/CsOH system, J. Organomet. Chem. 830 (2017) 11–18. https://doi.org/10.1016/j.jorganchem.2016.11.038.

[37] E.W. Dahl, T. Louis-Goff, N.K. Szymczak, Second sphere ligand modifications enable a recyclable catalyst for oxidant-free alcohol oxidation to carboxylates, Chem. Commun. 53 (2017) 2287–2289. https://doi.org/10.1039/C6CC10206A.

[38] C. Santilli, I.S. Makarov, P. Fristrup, R. Madsen, Dehydrogenative Synthesis of Carboxylic Acids from Primary Alcohols and Hydroxide Catalyzed by a Ruthenium N-Heterocyclic Carbene Complex, J. Org. Chem. 81 (2016) 9931–9938. https://doi.org/10.1021/acs.joc.6b02105.

[39] J. Malineni, H. Keul, M. Möller, A green and sustainable phosphine-free NHC-ruthenium catalyst for selective oxidation of alcohols to carboxylic acids in water, Dalton Trans. 44 (2015) 17409–17414. https://doi.org/10.1039/C5DT01358E.

[40] A. Sarbajna, I. Dutta, P. Daw, S. Dinda, S.M.W. Rahaman, A. Sarkar, J.K. Bera, Catalytic Conversion of Alcohols to Carboxylic Acid Salts and Hydrogen with Alkaline Water, ACS Catal. 7 (2017) 2786–2790. https://doi.org/10.1021/acscatal.6b03259.

[41] G. Zeng, S. Sakaki, K. Fujita, H. Sano, R. Yamaguchi, Efficient Catalyst for Acceptorless Alcohol Dehydrogenation: Interplay of Theoretical and Experimental Studies, ACS Catal. 4 (2014) 1010–1020. https://doi.org/10.1021/cs401101m.

[42] M.K. Awasthi, S.K. Singh, Ruthenium Catalyzed Dehydrogenation of Alcohols and Mechanistic Study, Inorg. Chem. 58 (2019) 14912–14923. https://doi.org/10.1021/acs.inorgchem.9b02691.

[43] D. Gong, B. Hu, D. Chen, Bidentate Ru(ii)-NC complexes as catalysts for the dehydrogenative reaction from primary alcohols to carboxylic acids, Dalton Trans. 48 (2019) 8826–8834. https://doi.org/10.1039/C9DT01414D.

[44] X. Wang, C. Wang, Y. Liu, J. Xiao, Acceptorless dehydrogenation and aerobic oxidation of alcohols with a reusable binuclear rhodium(II) catalyst in water, Green Chem. 18 (2016) 4605–4610. https://doi.org/10.1039/C6GC01272H.

[45] K. Fujita, R. Tamura, Y. Tanaka, M. Yoshida, M. Onoda, R. Yamaguchi, Dehydrogenative Oxidation of Alcohols in Aqueous Media Catalyzed by a Water-Soluble Dicationic Iridium Complex Bearing a Functional N-Heterocyclic Carbene Ligand without Using Base, ACS Catal. 7 (2017) 7226–7230. https://doi.org/10.1021/acscatal.7b02560.

[46] V. Cherepakhin, T.J. Williams, Iridium Catalysts for Acceptorless Dehydrogenation of Alcohols to Carboxylic Acids: Scope and

Mechanism, ACS Catal. 8 (2018) 3754–3763. https://doi.org/10.1021/acscatal.8b00105.

[47] D.H. Nguyen, Y. Morin, L. Zhang, X. Trivelli, F. Capet, S. Paul, S. Desset, F. Dumeignil, R.M. Gauvin, Oxidative Transformations of Biosourced Alcohols Catalyzed by Earth-Abundant Transition Metals, ChemCatChem 9 (2017) 2652–2660. https://doi.org/10.1002/cctc.201700310.

[48] Z. Shao, Y. Wang, Y. Liu, Q. Wang, X. Fu, Q. Liu, A general and efficient Mn-catalyzed acceptorless dehydrogenative coupling of alcohols with hydroxides into carboxylates, Org. Chem. Front. 5 (2018) 1248–1256. https://doi.org/10.1039/C8QO00023A.

[49] Z. Dai, Q. Luo, H. Jiang, Q. Luo, H. Li, J. Zhang, T. Peng, Ni(II)–N′NN′ pincer complexes catalyzed dehydrogenation of primary alcohols to carboxylic acids and H2 accompanied by alcohol etherification, Catal. Sci. Technol. 7 (2017) 2506–2511. https://doi.org/10.1039/C7CY00432J.

[50] I. Dutta, A. Sarbajna, P. Pandey, S.M.W. Rahaman, K. Singh, J.K. Bera, Acceptorless Dehydrogenation of Alcohols on a Diruthenium(II,II) Platform, Organometallics 35 (2016) 1505–1513. https://doi.org/10.1021/acs.organomet.6b00085.

[51] K. Toyomura, K. Fujita, Synthesis of Coordinatively Unsaturated Iridium Complexes Having Functional 8-Quinolinolato Ligands: New Catalysts for Dehydrogenative Oxidation of Alcohols in Aqueous Media, Chem. Lett. 46 (2017) 808–810. https://doi.org/10.1246/cl.170166.

[52] Z. Wang, B. Pan, Q. Liu, E. Yue, G. A. Solan, Y. Ma, W.-H. Sun, Efficient acceptorless dehydrogenation of secondary alcohols to ketones mediated by a PNN-Ru(ii) catalyst, Catal. Sci. Technol. 7 (2017) 1654–1661. https://doi.org/10.1039/C7CY00342K.

[53] Q. Wang, H. Chai, Z. Yu, Dimeric Ruthenium(II)-NNN Complex Catalysts Bearing a Pyrazolyl-Pyridylamino-Pyridine Ligand for

Transfer Hydrogenation of Ketones and Acceptorless Dehydrogenation of Alcohols, Organometallics 36 (2017) 3638–3644. https://doi.org/10.1021/acs.organomet.7b00587.

[54] D. Sengupta, R. Bhattacharjee, R. Pramanick, S.P. Rath, N. Saha Chowdhury, A. Datta, S. Goswami, Exclusively Ligand-Mediated Catalytic Dehydrogenation of Alcohols, Inorg. Chem. 55 (2016) 9602–9610. https://doi.org/10.1021/acs.inorgchem.6b01310.

[55] H. Song, B. Kang, S.H. Hong, Fe-Catalyzed Acceptorless Dehydrogenation of Secondary Benzylic Alcohols, ACS Catal. 4 (2014) 2889–2895. https://doi.org/10.1021/cs5007316.

[56] V. Cherepakhin, T.J. Williams, Iridium Catalysts for Acceptorless Dehydrogenation of Alcohols to Carboxylic Acids: Scope and Mechanism, ACS Catal. 8 (2018) 3754–3763. https://doi.org/10.1021/acscatal.8b00105.

[57] E.W. Dahl, T. Louis-Goff, N.K. Szymczak, Second sphere ligand modifications enable a recyclable catalyst for oxidant-free alcohol oxidation to carboxylates, Chem. Commun. 53 (2017) 2287–2289. https://doi.org/10.1039/C6CC10206A.

[58] Z.-W. Chen, F. Ma, Y. Liu, X.-F. Mo, G. Chen, X. Peng, X.-Y. Yi, Geometrical isomerization and acceptorless dehydrogenative alcohol oxidation based on pyrrole-based Ru(II) complexes, Inorganica Chim. Acta 541 (2022) 121034. https://doi.org/10.1016/j.ica.2022.121034.

[59] S.T. Sahoo, A. Mohanty, R. Sharma, S.R. Rout, R. Dandela, P. Daw, A Bifunctional Ruthenium Catalyst for Effective Renewable Hydrogen Production from Biomass-Derived Sorbitol, Organometallics 42 (2023) 745–751. https://doi.org/10.1021/acs.organomet.3c00064.

[60] V. Arora, S. Dhole, A. Kumar, Reforming of ethanol to hydrogen and acetic acid catalyzed by pincer-ruthenium complexes, Catal. Sci. Technol. 13 (2023) 6699–6711. https://doi.org/10.1039/D3CY01107K.

[61] N. Shahid, R.K. Singh, N. Srivastava, A.K. Singh, Base-free synthesis of benchtop stable Ru(III)–NHC complexes from RuCl3·3H2O and their use as precursors for Ru(II)–NHC complexes, Dalton Trans. 52 (2023) 4176–4185. https://doi.org/10.1039/D3DT00243H.

[62] R.K. Singh, D. Yadav, A.K. Singh, Cationic ruthenium(II)-CNC pincer complexes as phosphine-free catalysts for nitrile hydration to amides in aqueous medium, Mol. Catal. 549 (2023) 113523. https://doi.org/10.1016/j.mcat.2023.113523.

[63] Z. Xi, F. Liu, Y. Zhou, W. Chen, CuI/L (L=pyridine-functionalized 1,3-diketones) catalyzed C–N coupling reactions of aryl halides with NH-containing heterocycles, Tetrahedron 64 (2008) 4254–4259. https://doi.org/10.1016/j.tet.2008.02.082.

[64] N. Srivastava, N. Shahid, A.K. Singh, Insights into the effect of contact ion-pairs on CH bond activation for the synthesis of Ru(III)-NHC complexes: A combined experimental and computational study, J. Organomet. Chem. 998 (2023) 122802. https://doi.org/10.1016/j.jorganchem.2023.122802.

[65] J. Luo, Q.-Q. Zhou, M. Montag, Y. Ben-David, D. Milstein, Acceptorless dehydrogenative synthesis of primary amides from alcohols and ammonia, Chem. Sci. 13 (2022) 3894–3901. https://doi.org/10.1039/D1SC07102E.

[66] J.A. Luque-Urrutia, M. Solà, D. Milstein, A. Poater, Mechanism of the Manganese-Pincer-Catalyzed Acceptorless Dehydrogenative Coupling of Nitriles and Alcohols, J. Am. Chem. Soc. 141 (2019) 2398–2403. https://doi.org/10.1021/jacs.8b11308.

[67] J. Masdemont, J.A. Luque-Urrutia, M. Gimferrer, D. Milstein, A. Poater, Mechanism of Coupling of Alcohols and Amines To Generate Aldimines and H2 by a Pincer Manganese Catalyst, ACS Catal. 9 (2019) 1662–1669. https://doi.org/10.1021/acscatal.8b04175.

Chapter 4

Insights into the effect of contact ion-pairs on C-H bond activation for the synthesis of Ru(III)-NHC complexes: A combined experimental and computational study

4.1 Introduction

Transition metal catalyzed C-H bond activation is one of the most widely investigated methods for converting petroleum feedstock into functionalized and value added chemicals.[1,2] Functionalization of hydrogen bond of methane is considered to be one of the major challenges in the field of chemistry.[3,4] In addition, C-H activation is also routinely utilised in various synthetic methodologies for the preparation of new compounds.[5–9] In general, C-H activation in organocatalysis is considered to be a step-economical process because of reduced functional group manipulations in substrates undergoing C-X (X = C, or other heteroatom) bond formation.[10–15] In this regard, understanding the selectivity and factors affecting C-H functionalization has been an important area of investigation in all fields of chemistry.[16–18] C-H activation is considered as the most straightforward path for the generation of N-heterocyclic carbenes[19–21] because of its efficiency in producing the least number of side products.[9,18,22–25]

In general, C-H bond activation by transition metal is proposed to involve the interaction between σ C-H bonding orbital and the vacant d-orbital of the transition metal. This interaction leads to synergic electron transfer between metal orbitals and C-H orbitals, which is accompanied by electron transfer from the filled d orbital of the metal to σ* antibonding orbital.[26–28] The different types of transition metal catalysed C-H bond activation mechanisms include oxidative addition, σ-bond metathesis,

electrophilic substitution, 1,2 addition, and concerted metalation deprotonation (CMD) pathway. The concerted metalation deprotonation (CMD) pathway, proposed by Winstein and Traylor in 1955 for the acetolysis of diphenyl mercury in acetic acid, is one of the most common ways to activate C-H bonds.[29] This process involves cleaving the C–H bond of the substrate and forming a new C–Metal bond through a single transition state using transition metals.[30,31] Transition states in CMD are influenced by various factors, such as agostic interactions, syndetic donations, noncovalent interactions, and so on. C–H bond activation has found extensive utilization of carboxylate ligands due to their ability to act as bases and spectator ligands. When acting as base[32], the carboxylates with electron electron-donating group are preferred, whereas when acting as spectator ligand[33], electron-deficient carboxylates are useful.[34]

It has been very well known for 1-2 decades that mesoionic NHCs (their protonated precursors, respectively) may not be metalated with any late transition metal without the presence of halide.[35–40] In some circumstances, an external ion source is used to stimulate the formation of metal complexes containing only one type of anion[41]. The presence of halide deshields the azolium proton due to the formation of a strong hydrogen bond.[42] This hydrogen bond further makes the azolium proton acidic and favors the formation of NHC complexes in the presence of late-transition metals.

C-H activation in ionic liquids (IL), based on azolium salts, can be affected by the cation-anion interactions through hydrogen bonding.[43,44] This hydrogen bonding in ionic liquids has been regarded as crucial in determining melting point as well as viscosities.[45] Owing to their importance in IL properties and structures, there have been many studies on the ion species dependence of hydrogen bonding strength.[46–50] However, ion pairs have not been extensively studied in regioselective or site-selective processes employing transition metals, because they are often

thought to lack the directionality required to obtain high degrees of positional control when compared to hydrogen bonds.[51–54]

Recent developments in organometallic chemistry have increased the importance of counteranion effects brought by ion-pairing.[55] In the imidazolium-based salts, the formation of H-bonds is primarily facilitated by the hydrogen atoms on the imidazolium ring.[56] The hydrogen atom at C2-H has been found to be more acidic than the hydrogen atom at C4/5-H, which points to the possibility of stronger H-bonds forming between donor C2-H and an anionic acceptor.[56–58] The C2-H/D exchange reactions have been shown to depend on the relative strength of hydrogen bonding with anions; the stronger the H-X interaction, the easier the C2-H/D exchange.[43,44,50] Huynh et al. reported that the external addition of halide ions is required for the activation of C2-H in [azolium][X] (X = BF_4^-, PF_6^-, and OTf^-) for the generation of carbene, even in the presence of Ag_2O as a base.[59–61] However, the role of such H-X interactions during the synthesis of transition metal-NHC complexes has not been thoroughly investigated until now.

Among the halides (Cl^-, Br^-, and I^-) and weakly coordinating bulkier anions (e.g., BF_4^- and PF_6^-) in ionic liquids, the rapid ease of C-H bond polarization followed the trend $Cl^- > Br^- > I^-$ followed by BF_4^- and PF_6^-.[43] However, ionic liquids bearing weakly coordinating anions (e.g., BF_4^- and PF_6^-) undergo poor C-H activation even under harsh reaction conditions, due to the lower acidity of C-H proton of the heterocyclic ring.[43] Recently, we reported the synthesis of Ru(III)-NHC complexes **1a** and **1b** (Figure 4.1) by the reaction of **$RuCl_3 \cdot H_2O$** with a bidentate $PyNHC^R$ ligand framework bearing R = Me and ^{i}Pr alkyl wingtips.[62] We observed that the anions of the azolium salts played an important role in the synthesis of complex.

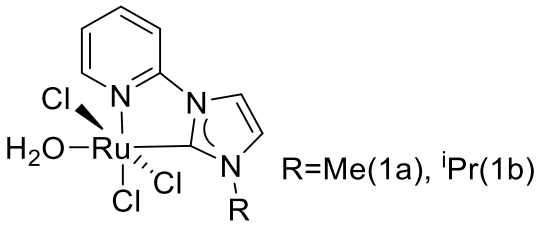

Figure 4.1. Recently reported Ru(III)-NHC complexes by our group

Our group had previously reported Ru(III)-NHC precursor complexes[62], which were used for the synthesis of our phosphine-free complexes in our previous chapter. During the synthesis of the Ru(III)-NHC precursor complex, usual reactivity was reported. In the presence of azolium salts with different counteranions, the product was affected. In case of Cl^- as counteranion no product was formed while with Br^- as counteranion, mixed halide product obtained. [62] Pure product with high yield was obtained in case of I^- as counteranion. [62] In this chapter we report the existence of ion-pairing between azolium cations and anions like halides and BF_4^-, PF_6^- in the imidazolium salts, by different spectroscopic techniques like NMR, UV-Vis spectroscopy and further supported by DFT analysis. The role and effect of ion pair in the reaction during the synthesis of complex **1a** and **1b** have been studied theoretically. Two possible pathways involving ion-pairing or halide coordination have been explored and suitable explanations can be provided for the experimental observations for the synthesis of these Ru(III)-NHC complexes.

4.2 Results and Discussion

4.2.1 Investigation of contact ion pairs in solution

The formation of contact ion pairs in numerous ionic liquids and their solutions has been previously studied using various tools, including conductivity measurements[63–65] and spectroscopic techniques, such as NMR,[66,67] UV-vis,[68,69] and IR[70,71]. As described in our recent work, the synthesis of Ru(III)-NHC complexes depends on the counterions

of azolium salts. The best yields, with no indication of mixed halide complexes, were obtained with iodide as the counter ion for synthesizing all three complexes. Therefore, to study the ion-pair interactions, ligand precursors were synthesized, and a systematic investigation was carried out with the ligand precursor, [PyIm^{iPr}·HX] with X = Cl^-, Br^-, I^-, PF_6^-, and BF_4^-, using NMR and UV-Vis spectroscopic techniques. Table 4.1 lists the ^1H and ^{13}C NMR chemical shifts of N*CH*N in $CDCl_3$ and λ_{max} observed in the UV-Vis spectra in acetonitrile solutions of imidazolium salts with different anions (figure 4.2).

Table 4.1. Spectral data for [3-isopropyl-1-(pyridine-2-yl)imidazolium]X (X = Cl, Br, I, BF_4) salts recorded at room temperature.

X	$\delta H_{(NC\underline{H}N)}$ $(D_{Cl})^a$	$\delta C_{(N\underline{C}N)}$ $(D_{Cl})^a$	λ_{max} [transitions]
Cl^-	11.56	148.82	266 [$\pi_{py}\rightarrow\pi^*_{py}$] 226 [$\pi_{Im}\rightarrow\pi^*_{Im}$]
Br^-	11.28 (0.28)	148.95 (-0.13)	266 [$\pi_{py}\rightarrow\pi^*_{py}$] 221 [$\pi_{Im}\rightarrow\pi^*_{Im}$]
I^-	10.94 (0.62)	149.05 (-0.23)	266(s) [$\pi_{py}\rightarrow\pi^*_{py}$] 244 [CTTS] 206 [$\pi_{Im}\rightarrow\pi^*_{Im}$]
BF_4^-	9.53 (2.03)	149.24 (-0.42)	266 [$\pi_{py}\rightarrow\pi^*_{py}$] 227 [$\pi_{Im}\rightarrow\pi^*_{Im}$]
PF_6^-	--[b]	--[b]	266 [$\pi_{py}\rightarrow\pi^*_{py}$] 227 [$\pi_{Im}\rightarrow\pi^*_{Im}$]

[a] Chemical shift difference from Cl^- analogue.

[b] NMR spectra could not be obtained due to its negligible solubility in $CDCl_3$.

The difference in the chemical shift of the imidazolium proton, NC*H*N, followed the order $Cl^- > Br^- > I^- > BF_4^-$ which reflects the strength of the cation-anion interactions and the formation of hydrogen bonds from Cl^- to BF_4^-. The data obtained were in accordance with previous reports on ion-pair formation in imidazolium salt solutions.[66,67] The imidazolium salt, [$PyIm^{iPr}$·HPF_6], could not be analysed through NMR spectroscopy due to its poor solubility in $CDCl_3$. The chemical shift change in ^{13}C NMR data is less pronounced (Table 4.1); however slight increase in δ C2 carbon from Cl^- to BF_4^- can be related to the basic nature of anion. The chemical shift of C2 follows the reverse trend in ^{13}C NMR ($BF_4^- > I^- > Br^- > Cl^-$) to that observed in ^1H NMR. As the basicity of anion increases, the tendency to form strong hydrogen bond with H2 proton also increases. The stronger base, Cl^-, strongly pulls the H2 proton via hydrogen bonding interactions, leaving the corresponding ligand scaffold with slightly increased electron density on the C2 carbon.

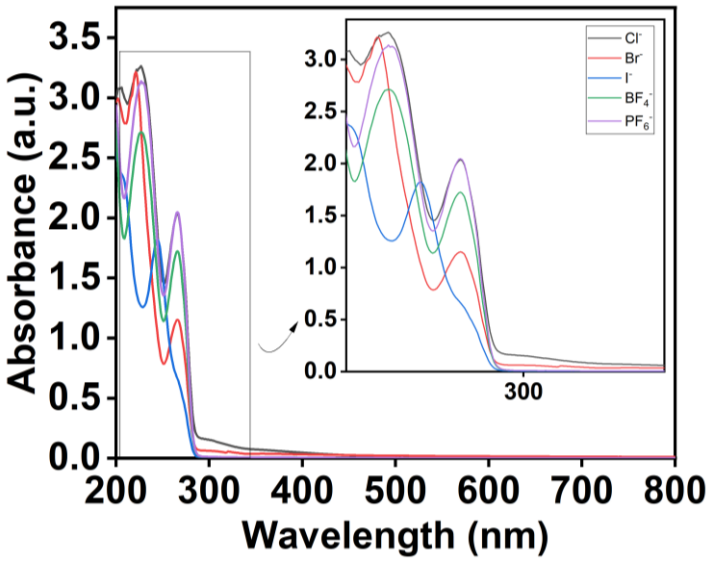

Figure 4.2. Plot of UV-Vis spectra of [3-isopropyl-1-(pyridine-2-yl)imidazolium]X (**L^2·HX**) where X = Cl, Br, I, BF_4, PF_6 recorded in CH_3CN. Inset showing the formation of charge transfer complex with I^- counter anion with a red shift in absorption maximum.

Figure 2 shows plots of UV-Vis spectra for [PyIm^{iPr}·HX] with X = Cl^-, Br^-, I^-, PF_6^-, and BF_4^-. The absorption spectra for imidazolium salts with PF_6^- and BF_4^- counter ions are identical, showing two absorption maxima at 227 nm ($\pi \rightarrow \pi^*$, imidazole ring) and 266 nm ($\pi \rightarrow \pi^*$, pyridine ring), respectively. While the absorption spectrum with chloride counter ions is nearly identical with those of BF_4^- and PF_6^-, those with bromide and iodide ions show a clear blue shift for the $\pi \rightarrow \pi^*$ transition in the imidazole ring from 227 nm to 221 nm and 206 nm, respectively. The absorption spectrum of the azolium salt with iodide counter ion also has another absorption centred around 244 nm, which is attributed to the CTTS (Charge-transfer-to-solvent) for iodide.[68,72] The very small blue shift from the literature-reported value of 246 nm for the CTTS of iodide in acetonitrile solvent has also been observed in earlier reports and attributed to the formation of a charge transfer complex with the imidazolium ion.[72] In addition, on increasing the concentration of the solution, a broad background absorption at 360 nm followed by a gradual rise in the curve from 326 nm was observed, which can be assigned as the CT band in ion pairs.[68,69,73] Similar to the previous reports, with increase in concentration, the intensity of CT band was also increased whereas the $\pi \rightarrow \pi^*$ bands at shorter wavelength were diminished.[72] Both, NMR and UV-Vis investigations confirm the ion-pair interactions and existence of contact ion-pairs in [PyIm^{iPr}·HX] in solutions.

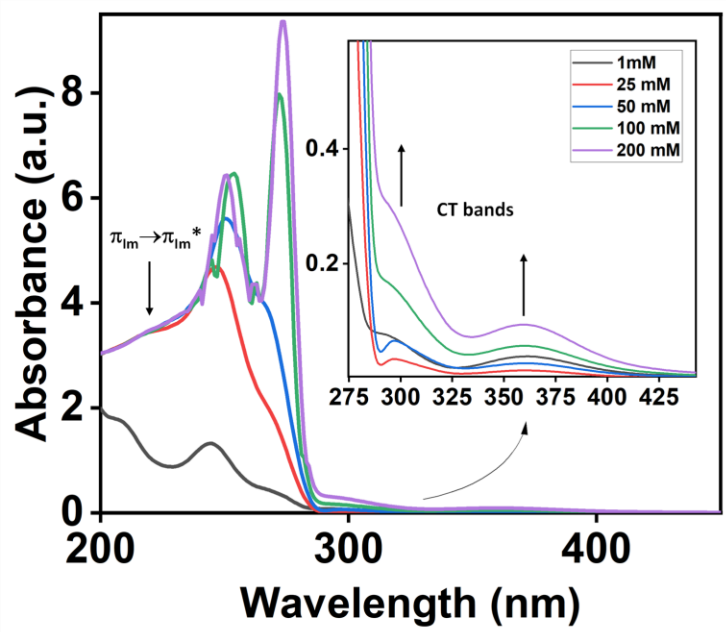

Figure 4.3. UV-vis spectra of **L^2·HI** recorded at various concentration in MeCN.

4.2.2 Computational Modelling

4.2.2 (i) Investigation of C2-H----X interaction in imidazolium salts

Interactions between azolium cations and anions such as halides and other bulkier anions have been studied by several groups, and previous reports suggest that halides develop stronger and more stable interactions with imidazolium proton compared to bulkier anions (BF_4^-, PF_6^-, BPh_4^-, etc.).[42–44] To investigate the structure of the $[PyIm^R][X]$ (R=Me, ^{i}Pr) based ion pairs, a stepwise optimization process was followed. Initially, we optimized the pyridine imidazolium ligand framework by considering two possible orientations of pyridine with respect to the C2-H of the imidazolium cation. In one orientation, pyridine-N remains *anti* to imidazolium C2-H, while in the other, it remains *syn* to C2-H. The optimized geometries of the ligand precursors $[PyIm^{Me/iPr}]^+$ with C2-H bond length and dihedral angle between the intersecting planes formed by atoms C2-N1-C5-N3 are shown in Figure 4.4.

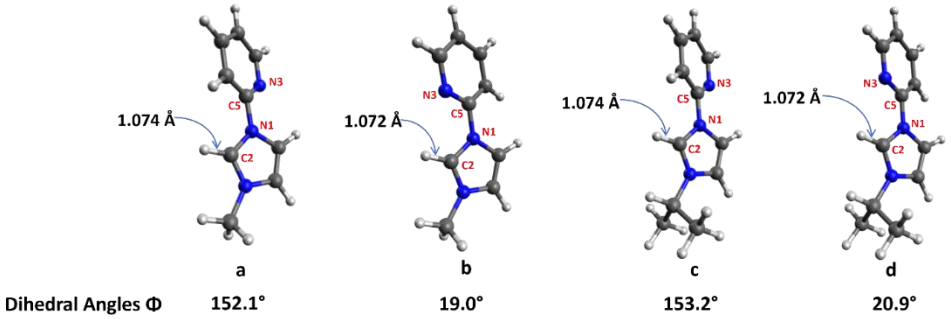

Figure 4.4. DFT-optimized structures of the ligand precursors $[PyIm^{Me}]^+$ and $[PyIm^{iPr}]^+$. The dihedral angle Φ between the intersecting planes formed by the azolium ring and pyridine ring is defined by four atoms, C2-N1-C5-N3.

Furthermore, halides or other counteranions were added to the optimized azolium cations, and the geometries were re-optimized to observe changes in the bond parameters and dihedral angles. In the case of methyl substituted azolium salts having the pyridine-N *anti* to C2-H (figure 4.5A), a linear hydrogen bonding interaction between the C2-H and X where X=Cl^-, Br^-, I^- and BF_4^- was observed.

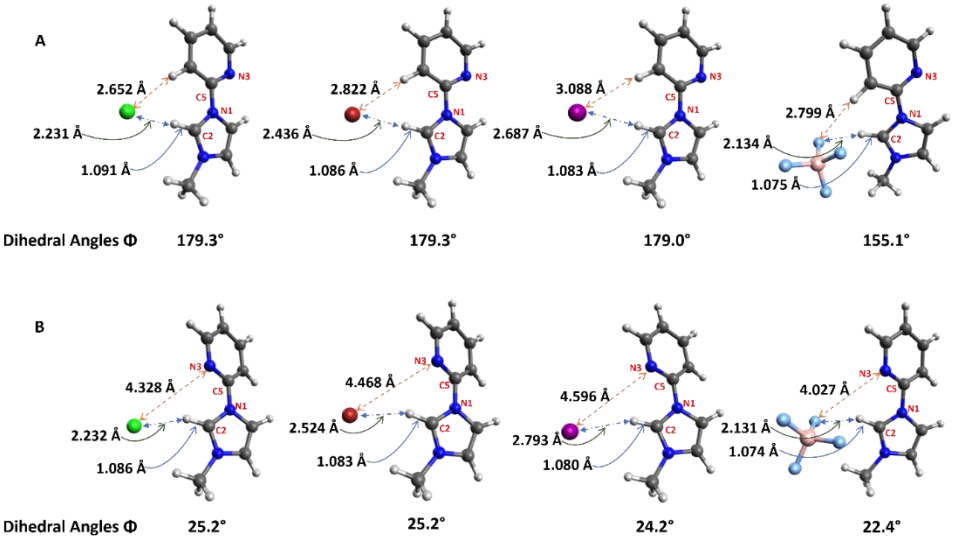

Figure 4.5. DFT-optimized structures of the ligand precursors $[PyIm^{Me}][X]$, where X= Cl (green), Br (red), and I (purple). (**A)** The Py-N

anti to C2-H of imidazoium. (**B)** The Py-N *syn* to C2-H of imidazolium. The dihedral angle (Φ) between the intersecting planes formed by the azolium ring and pyridine ring is defined by four atoms, C2-N1-C5-N3.

The increase in the C2-H bond length can be understood in terms of increasing polarization due to hydrogen bonding as experimentally validated by NMR (Table 1). The change in the dihedral angle is observed as a result of the interaction between PyC-H and the counteranion. In the case of structural optimization of methyl-substituted azolium salts with pyridine-N *syn* to the C2-H bond, repulsion between the lone pair of nitrogen and counteranions is apparent (Figure 4.5B). This repulsion affects the hydrogen bonding interaction between C2-H and X (X=Cl^-, Br^-, I^-, BF_4^-), making it bent and relatively weaker. The repulsion also forces the pyridine ring out of the plane, thereby increasing the dihedral angle between the intersecting planes formed by the atoms, as shown in figure 4.5B.

The stabilization energy due to hydrogen bonding in the solution was estimated by DFT calculations in a THF solution. As expected, the stabilization due to hydrogen bonding interaction between H---X was found to be in order Cl^- (-12.9 kcal)>Br^- (-11.9 kcal)>I^- (-9.9 kcal)> BF_4^- (-7.0 kcal) in case of pyridine-N *anti* to C2-H and for azolium salts with pyridine-N *syn* to C2-H the stabilization due to hydrogen bonding was found to be -10.2 kcal/mol, -9.4 kcal/mol, -8.8 kcal/mol, and -4.9 kcal/mol for Cl^-, Br^-, I^- and BF_4^- anion respectively. These values indicate the ion-pairing with BF_4^- can be easily broken due to solvation. Similarly, upon structural optimization and frequency calculation of isopropyl substituted azolium salts, identical results were obtained as their methyl substituted analogs (figure 4.6). Further investigation into the mechanistic pathway was conducted using methyl-based azolium salts with halides as counteranions.

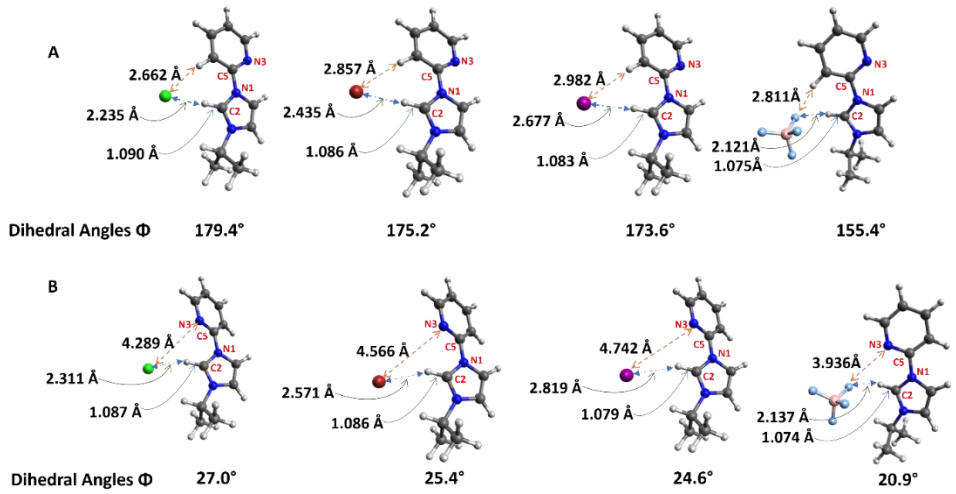

Figure 4.6. DFT-optimized structures of the ligand precursors [PyIm^{iPr}][X], where X= Cl (green), Br (red), and I (purple). (**A)** The Py-N trans to C2-H of imidazoium. (**B)** The Py-N cis to C2-H of imidazolium. The dihedral angle (Φ) between the intersecting planes formed by the azolium ring and pyridine ring is defined by four atoms, C2-N1-C5-N3.

4.2.2 (ii) Role of ion-pairs during synthesis of Ru(III)-NHC complexes

It has been reported that the addition of halide ions is required for the activation of C2-H for the generation of carbenes even in the presence of Ag_2O, facilitated by the precipitation of AgX in the transmetalation step.[76–78] The mechanism for the formation of **1a** was first investigated using PyIm^{Me}·HCl and $RuCl_3·3H_2O$ as the model reactions (scheme 4.1). For this reaction, two possible pathways were taken into consideration, first in which halide coordination to the ruthenium center takes place while the other in which halide doesn't coordinates to the ruthenium center. In the halide coordination path (Path-1), the coordination of the Cl^- ion and pyridine nitrogen to ruthenium leads to three isomeric intermediates, namely **A-Cl1**, **A-Cl2**, and **A-Cl3**. In **A-Cl1**, one remaining water molecule is trans to pyridine; in **A-Cl2**, the water is trans to the chloride, which leaves at the later stage, and in **A-Cl3**, water is cis to both the leaving chloride and pyridine. In Path-2, the chloride ion of the imidazolium salt does not

coordinate with the ruthenium center but remains hydrogen-bonded to imidazolium C2-H in intermediate **A'-Cl**. Of these four optimized intermediates, **A-Cl1**, with water trans to pyridine, was found to have the lowest energy. The relative energies for the other isomers were calculated w.r.t **A-Cl1** and found to be slightly higher as 3.0 kcal/mol, 2.3 kcal/mol and 4.9 kcal/mol for **A-Cl2**, **A-Cl3** and **A'-Cl** respectively. These energies were calculated for the doublet spin states. The DFT-optimized structures of **A-Cl1**, **A-Cl2**, **A-Cl3**, and **A'-Cl**, with important bond parameters, are shown in figure 4.7.

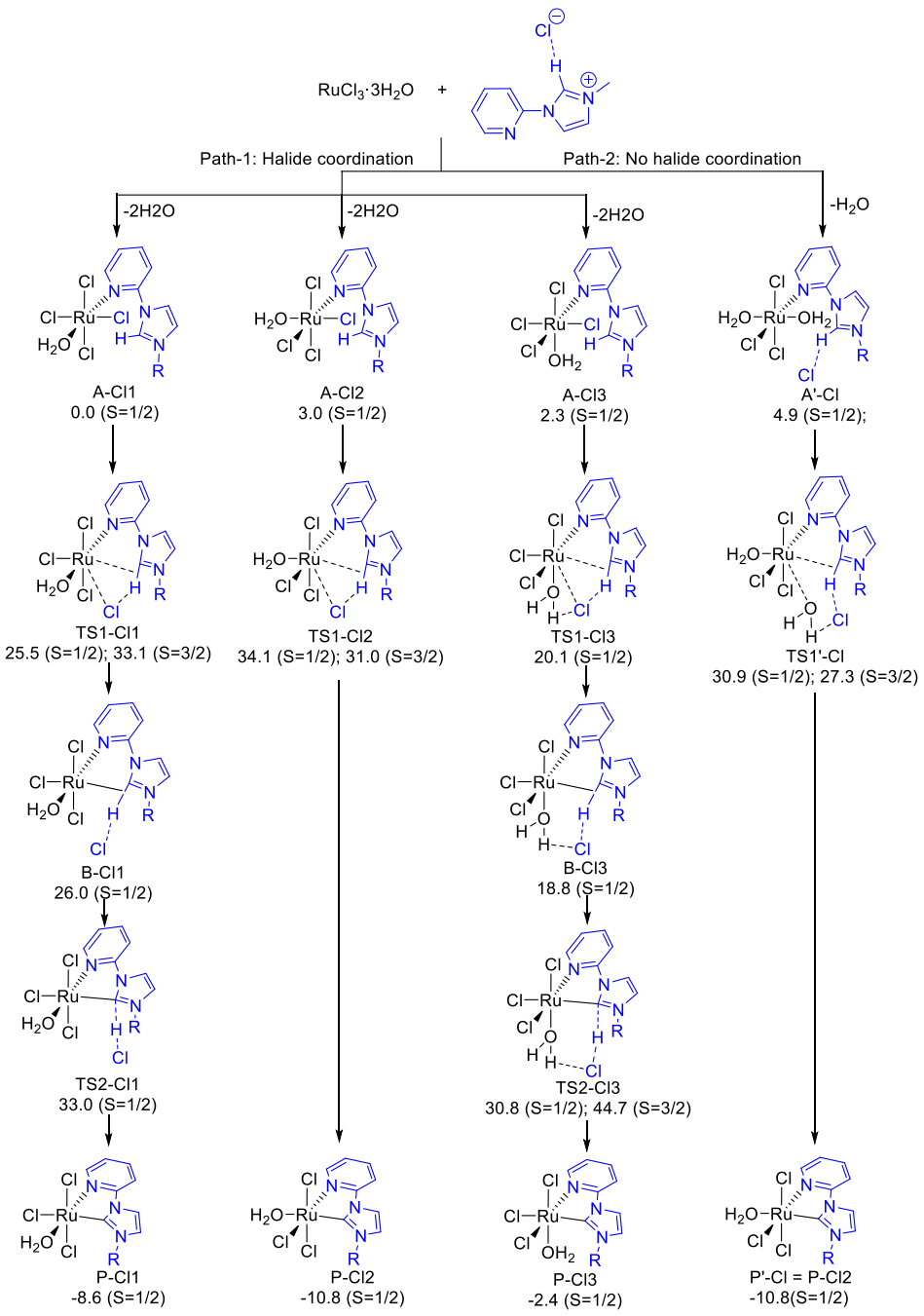

Scheme 4.1. Computational modelling of possible paths of formation of Ru(III)-NHC complexes. Gibbs free energies are reported in kcal/mol at 293.15 K, relative to the most stable intermediate **A-Cl1**.

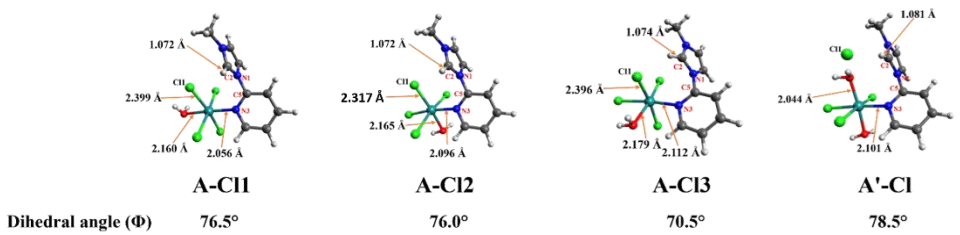

Figure 4.7. DFT optimized geometries of **A-Cl1**, **A-Cl2**, **A-Cl3** and **A'-Cl** along with the important bond lengths and the dihedral angle (Φ) between the intersecting planes defined by four atoms, C2-N1-C5-N3.

Further in the reaction following path 1, transition state **TS1** for all the isomers were located, in which the bond length between the leaving chloride and ruthenium increases while the imidazolium C2-H unit starts coming closer to the ruthenium. The transition state **TS1-Cl3** has the lowest energy, i.e., 20.1 kcal/mol, while the **TS1-Cl1** and **TS1-Cl2** have 25.5 kcal/mol and 34.1 kcal/mol energy respectively. This lowering in energy of the transition state **TS1-Cl3** can be attributed to the hydrogen bonding between the cis-water molecule, the leaving chloride, and the imidazolium C2-proton. The highest energy of **TS1-Cl2** is due to the presence of water trans to leaving chloride, which strengthens the ruthenium-chloride bond with a shorter bond length (2.317 Å in **A-Cl2** and 2.399 Å in **A-Cl1**), which requires more energy to cleave this bond. In the case of open-shell complexes, the involvement of species with higher spin states, especially in the transition states, cannot be ruled out. Therefore, attempts have been made to locate the transition states for the quartet (S=3/2) and sextet (S=5/2) spin states in both pathways.

During our attempt at sextet states, the molecule started to deform, and no suitable transition state could be located. In the case of **TS1-Cl1**, the Löwdin spin density localized on Ru was 0.85 in doublet spin state while in quartet spin state it becomes 2.43 on ruthenium. This spin densities gets distributed on the three chlorides viz 0.19 on Cl atom trans to leaving group and 0.20, 0.15 on two chlorides trans to each other and cis to the pyridine.

As the leaving chloride becomes free, new intermediate **B-Cl1** (26.0 kcal/mol) and **B-Cl3** (18.8 kcal/mol) are formed with the free Cl^- hydrogen bonded to the imidazolium C2-H. On the other hand, the **TS1-Cl2** transition state was found to form the product **P-Cl2** (-10.8 kcal/mol) directly. The lower energy of the intermediate **B-Cl3** than **B-Cl1** may be due to the additional hydrogen bonding between the cis-water molecule and free chloride. Next, **TS2-Cl1** and **TS2-Cl3** were located, involving C-H activation by ruthenium. The **TS2-Cl3** (30.8 kcal/mol) is 2.2 kcal/mol lower in energy than **TS2-Cl1** (33.0 kcal/mol). In case of **TS2-Cl3**, the Löwdin spin density located on ruthenium in doublet state was 0.90 while in the quartet state, the spin density become 2.43 on ruthenium and 0.27 on chloride atom trans to water molecule. The chloride ion, hydrogen bonded to the imidazolium C2 proton, then leaves as H-Cl, taking the proton and giving the final products **P-Cl1** (-8.6 kcal/mol) and **P-Cl3** (-2.4 kcal/mol). Among the three paths with isomeric structures, the one starting with **A-Cl3** gives the lowest energy route, with **TS2-Cl3** at 30.8 kcal/mol as the highest energy.

In Path-2, the chloride ion of the imidazolium salt does not coordinate with the ruthenium center but remains hydrogen-bonded to imidazolium C2-H in intermediate **A'-Cl** (4.9 kcal/mol). In the next step, the transition state **TS1'-Cl** (30.9 kcal/mol) was located, involving the dissociation of a water molecule and imidazolium C2-H coming closer to Ru. **TS1'-Cl** is directly converted to the final product **P'-Cl,** which is identical to that of **P-Cl2**.

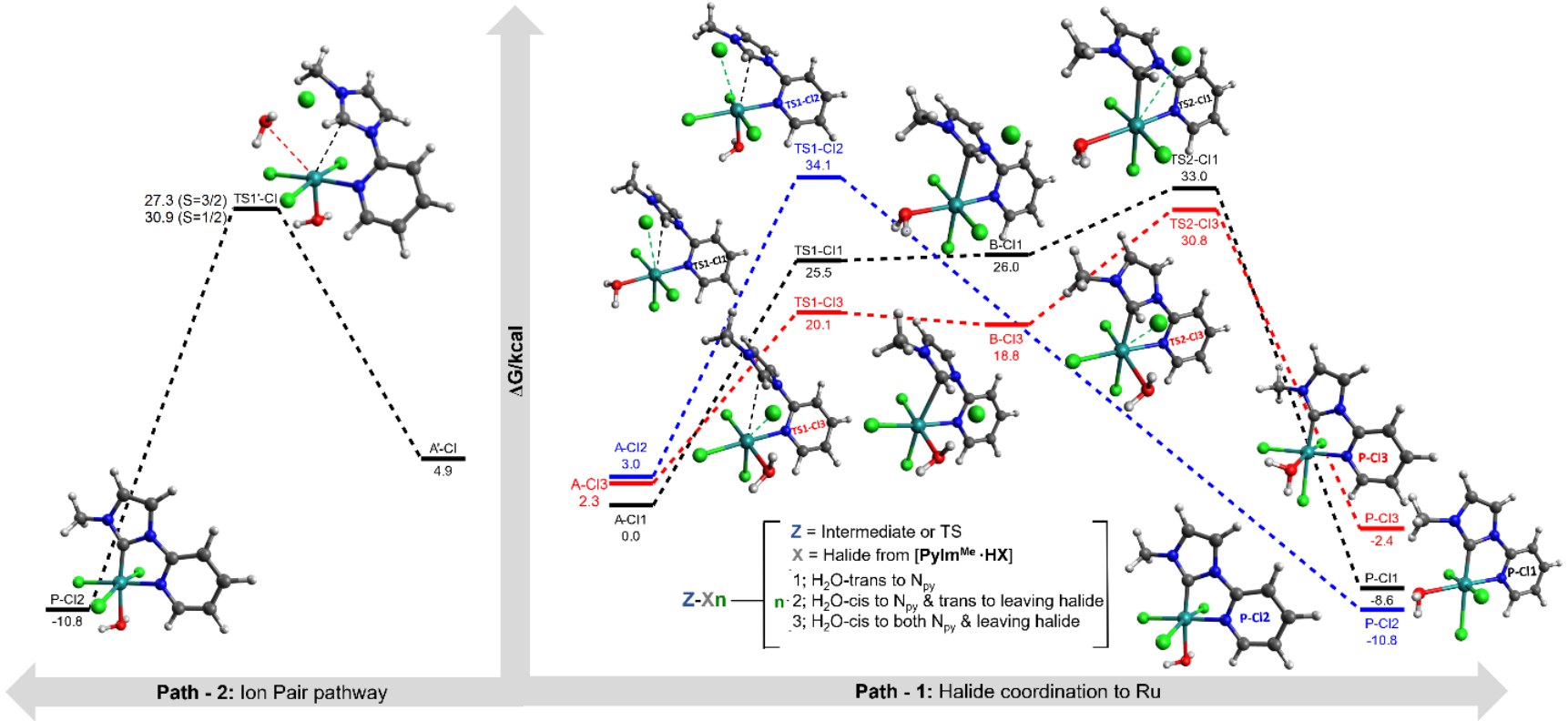

Figure 4.8. DFT computed energy profile diagram for the synthesis of Ru(III)-NHC complex from azolium salt with $\mathbf{Cl^-}$ ions. Gibbs free energies are reported in kcal/mol at 293.15 K, relative to the most stable intermediate **A-Cl1.** The geometries for A-Cl1, A-Cl2, A-Cl3 and A'-Cl have been shown in Figure 4.7.

For the quartet spin state, transition states **TS1-Cl1**, **TS1-Cl2**, **TS1'-Cl1,** and **TS2-Cl2** were located successfully, while **TS1-Cl3** and **TS2-Cl1** could not be found. The energy of transitions states with quartet spin was found lower than the doublet spin only for those transition states in which water molecule is present trans to the leaving group, i.e., **TS1-Cl2** (31.0 kcal/mol) and **TS1'-Cl** (27.3 kcal/mol) while in other cases higher energy for quartet transition state was observed. The energies calculated for the doublet spin states indicate the possibility of two channels, one starting from **A-Cl3** (halide coordination) and the other via **A'-Cl** (ion-pair path). However, considering the quartet spin state, the mechanism follows the ion pair path (Path-2) as it is the lowest energy route, with **TS1'-Cl** giving only 27.3 kcal/mol as the barrier height. The energy profile diagram for chloride salts following both the halide coordinated as well as ion-pair paths is shown in Figure 4.8.

In the case of reactions starting from imidazolium salts with bromide or iodide anions, for the halide coordinated pathway (Path-1), the number of possible isomeric forms will be doubled, depending on the type of leaving halide ion. For example, the corresponding intermediate, **A-Br1**, gives two possibilities denoted as **A-Br1a** (when it's the Br^- ultimately leaving the coordination sphere) or **A-Br1b** (when instead of the Br^-, one of the Cl^- ions leaves the coordination sphere and gives a mixed halide product). For bromide/iodide cases following the halide-coordinated pathway (Path-1), only the lowest energy path found for Cl^- starting from **A-X3a** and **A-X3b** (X = Br or I) was considered in addition to Path-2 (no Br^-/I^- coordination), starting from **A'-X** (X = Br or I).

The energy profile diagrams for the bromide and iodide salts following both pathways are shown in Figures 4.9 and 4.10, respectively. The energies of the intermediates and transition states for the doublet spin state were calculated for both pathways. The transition states in the quartet spin state were located for both pathways and for both halides. In case of

TS1-Br3a, the Löwdin spin population density located on the ruthenium in doublet spin state was 0.90 whereas in the quartet spin state, it is 2.51 on ruthenium and 0.23 on Cl trans to the leaving bromide. In **TS1-Br3b**, 0.90 Löwdin spin population density was located on ruthenium in doublet spin state, while in quartet spin state, 2.53 on ruthenium and 0.23 spin density on Cl trans to the leaving chloride was found. In the **TS2-Br3a** transition state, Löwdin spin density on ruthenium in doublet spin state was 0.90, on the other hand in the quartet state, 2.43 on ruthenium and 0.27 on Cl atom trans to water molecule coordinated to ruthenium. In case of **TS2-Br3b**, Löwdin spin density on ruthenium in doublet spin state was 0.90 while in quartet state, 2.41 on ruthenium and 0.30 on bromide was located. In **TS'-Br**, the Löwdin spin population density in the doublet spin state localized on ruthenium was 0.87, whereas in quartet state, 2.55 on ruthenium and 0.18, 0.15 on two chlorides trans to each other and cis to pyridine-N. Similarly for iodide salts, in **TS1-I3a** transition state, the 0.90 Löwdin spin density on ruthenium was found in doublet state, while in quartet spin state, 2.50 on ruthenium and 0.25 on Cl atom trans to leaving iodide. For **TS1-I3b**, the Löwdin spin population density localized on ruthenium 0.91 in doublet spin state, while in quartet spin state it becomes 2.55 on ruthenium and 0.24 on Cl atom trans to the leaving chloride. For **TS2-I3a**, the spin density observed on ruthenium quartet state was 0.90, which becomes 2.43 in quartet spin state along with 0.15, 0.21 spin population density on Cl atom trans to pyrdine-N and Cl atom cis to pyridine-N respectively. In case of **TS2-I3b** the Löwdin spin population density on ruthenium in doublet spin state was 0.90, while in quartet state, the spin density on ruthenium is 2.36 and 0.32 on iodide atom. The energy of the transition state for the quartet spin states was again found to be lower only for **TS'-X** of Path-2 (X = Br and I). For Path-1, only the energies for the doublet spin states are shown. In the case of iodide as leaving group, the reaction follows the ion pair pathway as it is the lowest energy route with **TS'-I** for doublet (24.7 kcal/mol) and quartet spin state (23.3 kcal/mol). However, in the case of

bromide, the lower energy route was found to be the halide coordination pathway, in which the transition state for chloride dissociation with **TS2-Br3b** (20.9 kcal/mol) is lower in energy, while **TS2-Br3a** (29.1 kcal/mol) involving dissociation of bromide requires higher energy. This is in line with the experimental observation that mixed halide complexes are formed starting from imidazolium salts with bromide ions but not with iodide ions. An intramolecular CMD route for the synthesis of Ru(III)-NHC complex in the presence of different halides is followed. In the case of I^- which follows ion pair pathway, the non-coordinated iodide abstracts the imidazolium C2-H proton of intermediate A'-I, and simultaneous bond formation between ruthenium and C2 carbon of imidazolium takes place via CMD transition state TS'-I. In case of Br^-, halide coordination route is followed which involves stepwise deprotonation and then metalation.

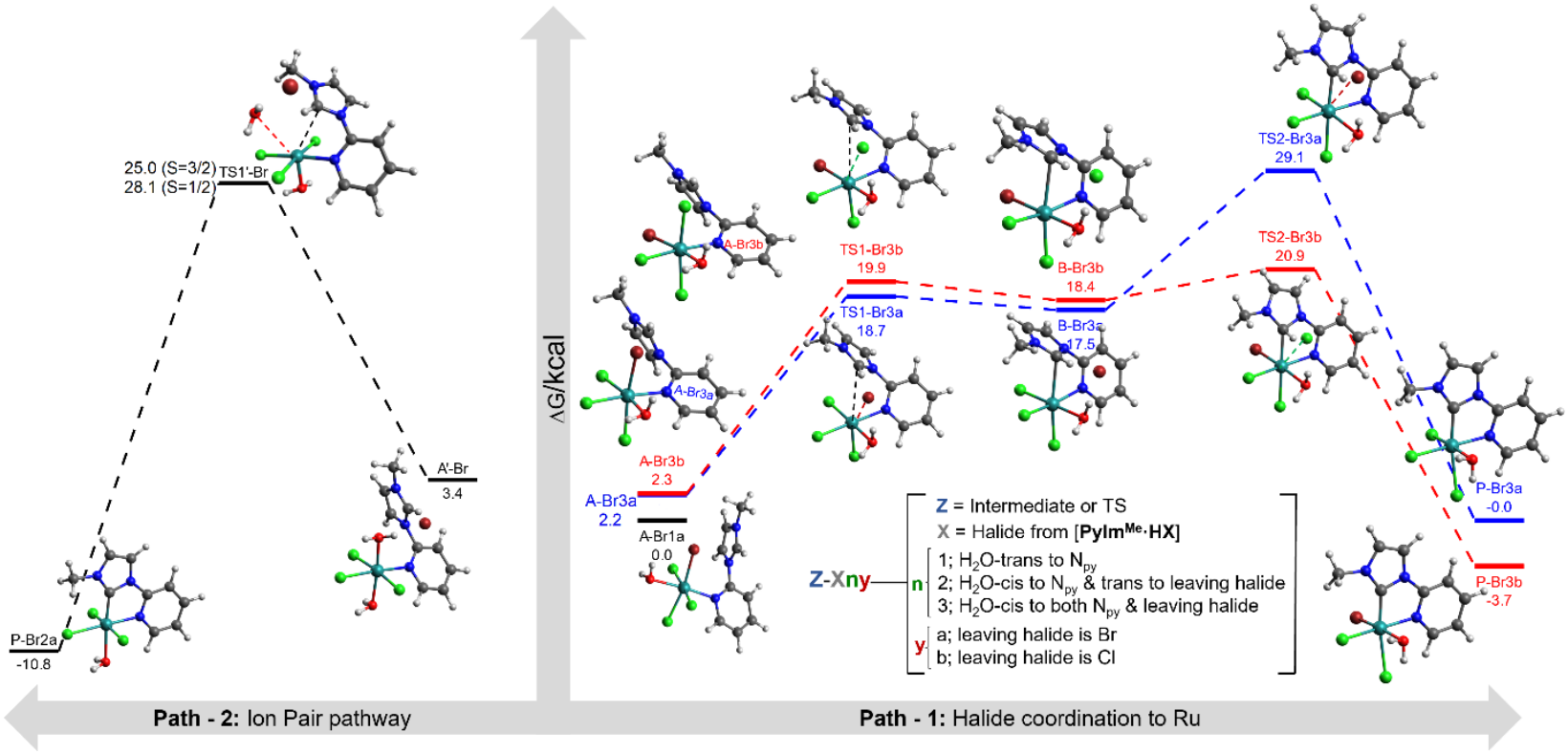

Figure 4.9. DFT computed energy profile diagram for the synthesis of Ru(III)-NHC complex from azolium salt with Br^- ion. Gibbs free energies are reported in kcal/mol at 293.15 K, relative to the most stable intermediate **A-Br1a**.

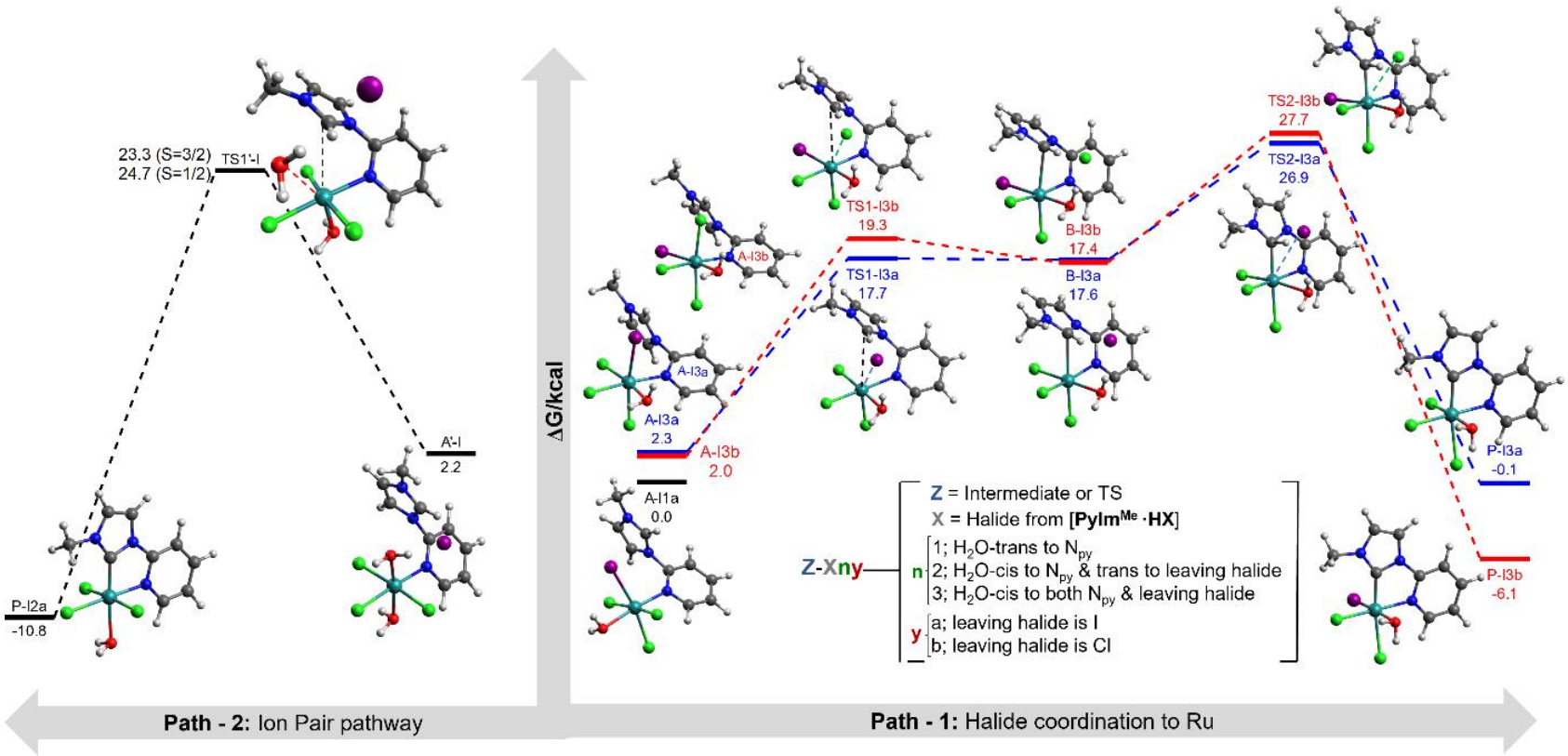

Figure 4.10. DFT computed energy profile diagram for the synthesis of Ru(III)-NHC complex from azolium salt with I^- ion. Gibbs free energies are reported in kcal/mol at 293.15 K, relative to the most stable intermediate **A-I1a**.

In contrast to the observations where rates of C2-H/D exchange were directly in line with the strengths of hydrogen bonding with the halide ions,[66,70] higher activation barrier was found in this study for Cl^- ions. To understand the reason for the high activation barrier in the reaction with imidazolium salts containing chloride anions, the stabilization effect of halide coordination and hydrogen bonding in ion pairs with different halides was calculated. The Intermediate **A'-NoX** and the transition state **TS'-NoX**, where the halides of imidazolium salt neither coordinate to the ruthenium nor remain hydrogen bonded (due to solvation), to the imidazolium C2-H were optimised, and their energies are compared to the corresponding species of the halide coordination (path 1) and ion-pairing (path 2) pathways with all three halides (Figure 4.11).

As can be seen in Figure 4.10, both the halide coordination as well as the hydrogen bonding with halides lower the energies of all transition states, thus making the halide-assisted C-H activation feasible. However, in case of X = Cl, the extent of stabilisation is significantly more for the intermediates **A-Cl1,** or **A'-Cl** compared to the corresponding transition states due to which the energy barriers become higher for the reaction with imidazolium salts having chloride anions. In the case of I^- ions, the stabilization of intermediates **A-I1a** (halide coordination) or **A'-I** (hydrogen bonding) is less than that of Cl^- analogs. This can be understood in terms of I^- being a soft ligand, while Cl^- is a hard ligand, which makes the latter a better ligand for the borderline acid Ru(III). The reaction involving Br^- presents an interesting scenario for the transition state **TS2-Br3b** having stabilisation due to Br^- coordination as well as the stabilisation due to relatively stronger hydrogen bonding of leaving halide, Cl^-, with the C-H group as well as the water molecule at cis position. The stabilisation of **TS2-Br3b** is nearly equal to the stabilisation of **A-Br3a** making the energy barrier lowest among all the three halides. A similar observation has been reported by Huynh et. al where the reactions with Br^- ions[76,78] proceed

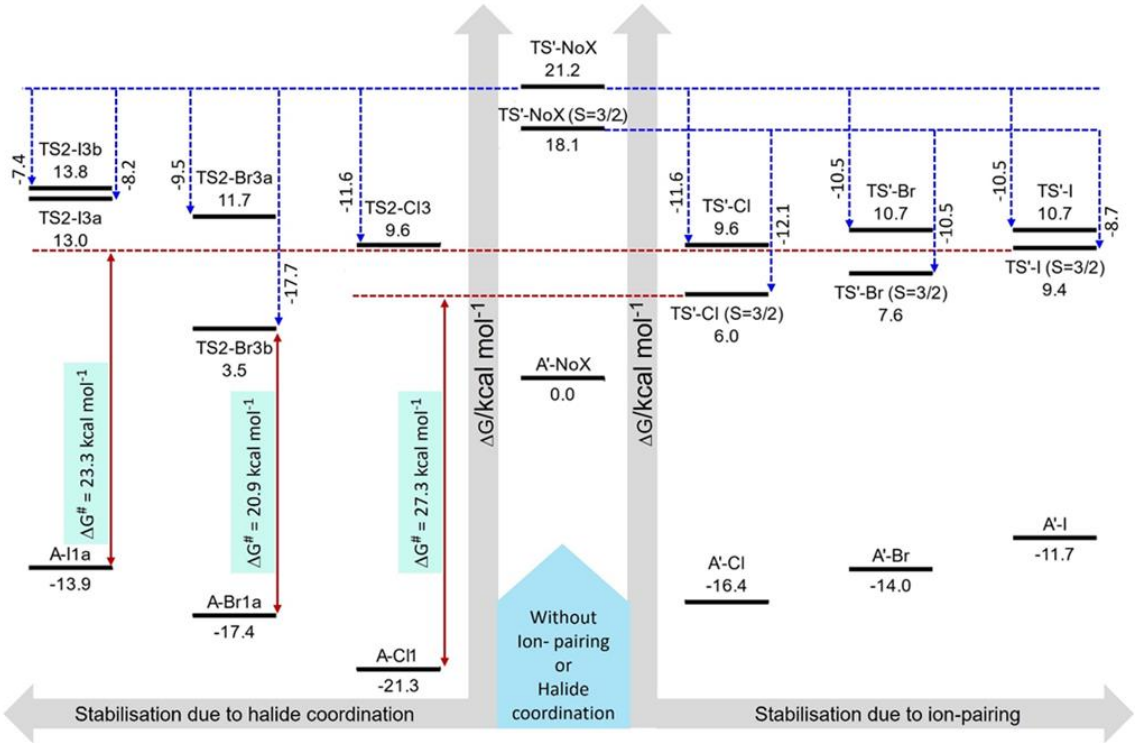

Figure 4.11. Stabilisation effect of halide coordination (left) and ion-pairing with halides (right) on intermediates and transition states. The $\Delta G^{\#}$ for the reaction with a particular halide is given as the difference between the most stable intermediate and the lowest energy transition state irrespective of the halide coordination or ion-pairing pathway. Energies of quartet spin states are shown only for species which are lower than doublet spin states.

at room temperature while the reaction with Cl^- ions[77] required a slightly elevated temperature. The DFT optimized structures for intermediates A'-NOX with different counteranions have been shown in Figure 4.12.

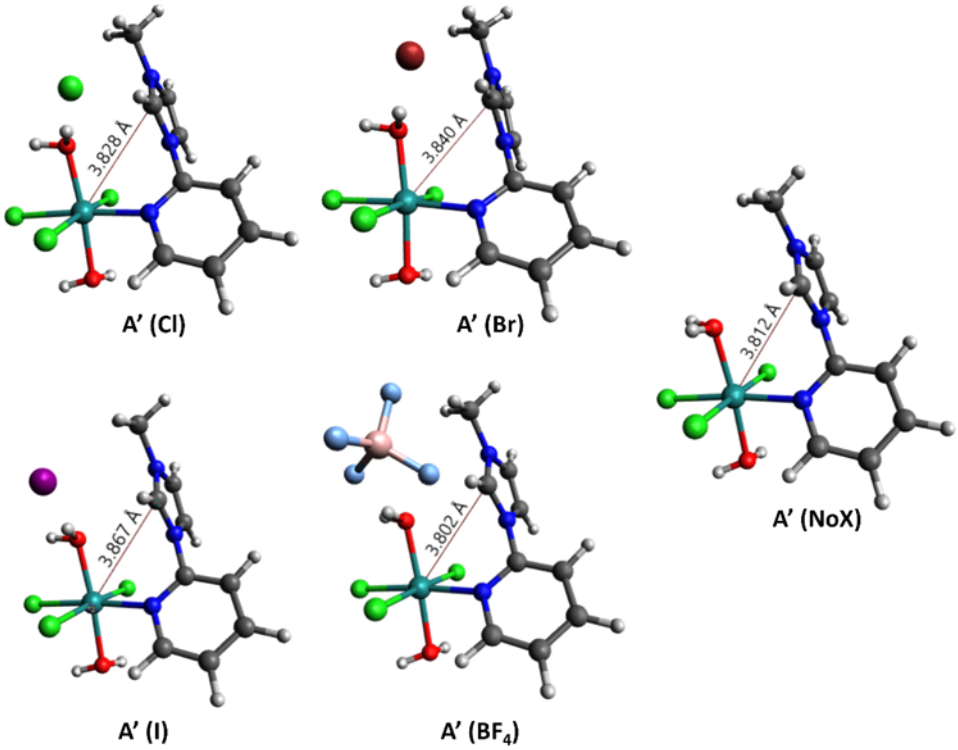

Figure 4.12. DFT optimized structures of intermediate A'-X where X= Cl, Br, I and BF_4 along with A'-NoX.

4.2.3 Synthesis of complex 1b from imidazolium salt with Chloride ions at elevated temperature

As indicated by computational analysis, a high activation barrier is required for the synthesis of complex in the presence of chloride counteranion. In order to achieve the higher activation barrier, we attempted the synthesis of complex **1b** using the corresponding imidazolium salt with chloride ions in dioxane solvent at elevated temperature (Scheme 4.2).

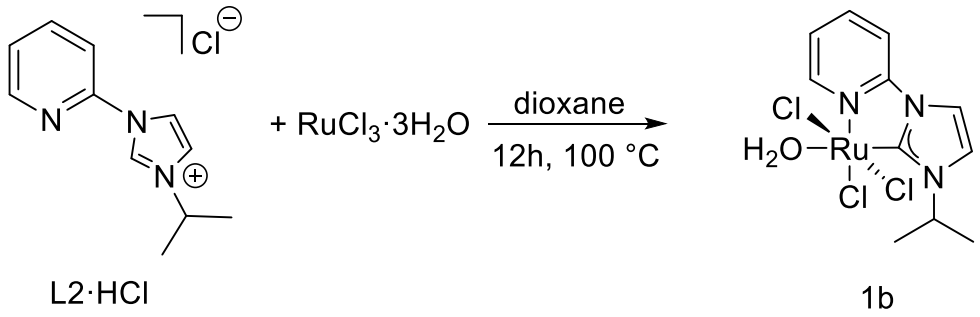

Scheme 4.2. Synthesis of complex **1b** in dioxane solvent at 100 ºC.

The successful synthesis of desired complex **1b** was confirmed by UV-Vis spectroscopy (Figure 4.13). The characteristic MLCT absorption maxima (λ_{max}) in UV-vis spectra for the Ru-NHC bond in complex **1b** was observed at 385 nm identical to the complex synthesized from corresponding imidazolium precursor with iodide counteranion. Despite poor yield, the successful synthesis of **1b** from imidazolium salt with chloride ions validates the findings of the computational study.

4.3 Conclusions

In this chapter, the role and effect of contact ion pairs for the synthesis of the Ru(III)-NHC complexes **1a** and **1b** have been investigated. To the best of our knowledge, this chapter describes the role of various halides and ion pairing in the C-H activation mediated by a Lewis acidic metal centre, for the first time. The existence of contact ion pairs in [PyIm^{iPr}·HX] ligand precursors was studied by NMR and UV-Vis spectroscopy. DFT modelling of possible paths for the formation of desired products suggests that the reaction follows the ion pair pathway when X = iodide in [PyIm^{Me}·HX] ligand precursor. Whereas in the case of Br^-, the reaction proceeds via a halide coordination pathway and yields mixed halide complexes. This synthetic route follows concerted metalation deprotonation (CMD) mechanism for ion pair route. The reaction could not be possible with Cl^- counterion under similar reaction conditions because of the higher

activation barrier resulting from the greater stabilisation of intermediates **A-Cl1** and **A'-Cl** compared to their corresponding transition states. This was further validated by the synthesis of complex **1b** using (**L^2·HCl**) at a higher temperature in refluxing dioxane.

4.4 Experimental Section

4.4.1 General Considerations

All reactions were performed in oven dried glassware under an inert atmosphere using Schlenk line technique. Azoles (1-H-imidazole and 1-H-benzimidazole) were purchased from Sisco Research Laboratories Pvt. Ltd. (SRL)-India. Solvents: dichloromethane (DCM), hexane, ethyl acetate (EtOAc), were purchased from S. D. Fine-Chem Limited and used after purification. Deuterated NMR solvent and $CDCl_3$, were purchased from Eurisotop and distilled from CaH_2 before use. 2-Bromopyridine was purchased from Spectrochem (India). Alkyl halides and $RuCl_3 \cdot 3H_2O$ were purchased from Spectrochem (India) and Sigma Aldrich respectivley. ESI^+-MS chromatograms were recorded using Bruker-Daltonics-MicroTOF-QII mass spectrometer for exact mass and true isotopic measurement. Electronic absorption spectra were recorded in a quartz cuvette using a Varian UV-vis spectrophotometer. A Bruker Avance NEO spectrometer operating at 500 MHz (^1H), and 126 MHz (^{13}C) were used to record the NMR spectra.

4.4.2 Synthesis of ligands

The synthesis of ligands was carried out by following the previously reported literature procedures.

4.4.3 Synthesis of complexes

4.4.3 (i) Synthesis of 1b using L^2·HCl at high temperature:

Following the synthetic procedure described for **1a**, L^2·HCl (1.85 mmol, 0.412 g) and $RuCl_3 \cdot 3H_2O$ (1.85 mmol, 0.485 g) were added in dioxane (7-8 ml). The reaction mixture was stirred for 12 hours at reflux temperature. Subsequently, the solid product was filtered and washed with dioxane. The sticky red-brown precipitate was obtained in a very small amount. Yield 2mg ≤ 5%. UV-vis λ_{max}/CH_3CN, nm: 432, 385 (Figure 4.13).

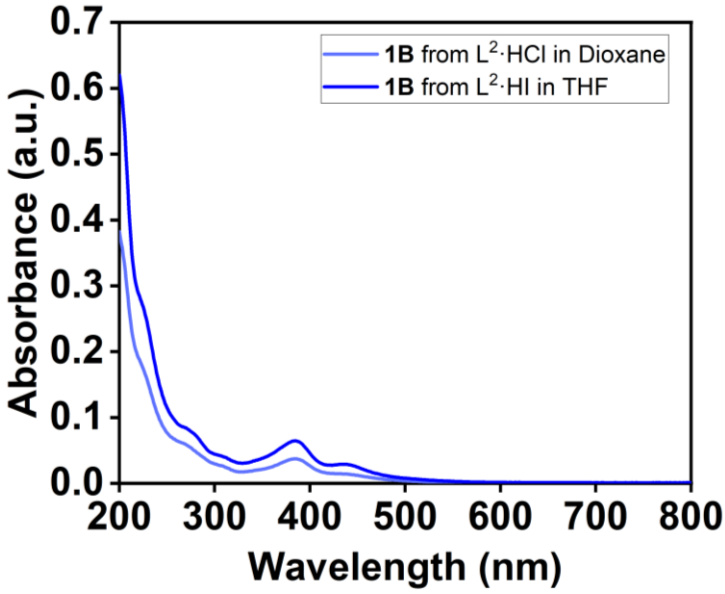

Figure 4.13. UV-vis spectra of **1b** synthesized from **L^2·HCl** in dioxane, recorded in MeCN at room temperature and its comparison with plot of **1b** synthesized from **L^2·HI** in THF.

4.4.4 DFT calculations

All DFT calculations were performed using the ORCA 5.0.3 program package developed by Neese and co-workers.[79–81] The geometry optimizations along with frequency calculations were carried out using B97-3c composite functional which is a low-cost method and is shown to produce excellent geometries for transition metal complexes and including open-shell complexes.[82] The B97-3c uses a modified, stripped-down triple-ζ basis, def2-mTZVP (BS1) along with auxiliary basis def2-mTZVP/J for Resolution of Identity (RI) approximation and def2-ECP[83–90] on

heavier elements (Ru and I), Grimme's atom-pairwise dispersion correction with the Becke-Johnson damping scheme (D3BJ),[91,92] and a short-range bond length adjustment.[82]. Tight SCF convergence criterion and a solvent model in which THF is described by an implicit conductor-like polarizable continuum medium (CPCM) was used during all calculations. Stationary points were confirmed to have either no imaginary frequency (for reactants and intermediates) or only one imaginary frequency along the reaction coordinates (for TS) by performing analytical frequency calculations at the same level of the DFT method. Transition states were confirmed to connect their respective intermediates via IRC calculations followed by geometry optimization in both directions. For final energies, single point calculations were performed using two of the most popular hybrid functionals shown to give excellent barrier heights for transition metal complexes; a hybrid meta-GGA functional M06-2X[93] of the Minnesota family developed by Donald G. Truhlar and coworkers; with Grimme's D3(zero) dispersion correction and another, range separated hybrid meta-GGA functional ωB97M-V[94] developed by Martin Head-Gorden and coworkers which includes VV10 non-local correlation. Larger basis set (BS2) def2-QZVP with def2-ECP on Ru, def2-TZVPD on halides (with def2-ECP on I) and def2-TZVP on all other atoms were used for single point energy calculations. To further check the reliability of the calculated energies with ωB97M-V and BS2 basis set, energies of few important intermediates and TS were recalculated with def2-QZVPPD on Ru and def2-TZVPPD on all other atoms (BS3) along with def2-ECP on Ru and I. ORCA's, inbuilt, finer integration grid "DEFGRID3" was used during all the single point calculations. The energies obtained from single point calculations were converted to Gibbs free energies using the total corrections obtained for the thermochemical calculations following the frequency calculations at the B97-3c level. To account for the entropy penalty during the change in number of components during a chemical change, MHP scheme proposed by Martin, Hay, and Pratt was applied which has also been used in several systems to produce

reasonable results.[95–97] According to this method, a correction of (n-m)× 4.3 kcal/mol is imposed whenever a reaction component changes from m components to n components. Gibbs free energies obtained from the single point calculations using BS2 or BS3 basis sets using M06-2X and ωB97M-V functionals after applying all the corrections mentioned above have been used to calculate the barrier heights and relative energies of various species. The energy profiles constructed using Gibbs free energies for both functionals follow similar pattern and give the same description of the possible paths, however ΔG values only for the ωB97M-V/BS2 are shown in figures throughout this paper. Gibbs free energies, ΔG are reported in Kcal/mol. The DFT calculated energies for all the species has been shown in Table 4.2.

Table 4.2. Energies of DFT optimized structures.

Species	**B97-3c**		**wB97M-V/BS2**	**M06-2X/BS2**	**wB97M-V/BS3**
	G	**G-E_{el}**	**E_{el}**	**E_{el}**	**E_{el}**
PATH-1					
A-Cl1 (S=1/2)	-2525.16779	0.16215422	-2525.498772	-2525.459053	*
A-Cl2 (S=1/2)	-2525.162533	0.16206776	-2525.493956	-2525.454397	*
A-Cl3 (S=1/2)	-2525.162168	0.16195382	-2525.494950	-2525.455593	*
TS1-Cl1 (S=1/2)	-2525.137867	0.16132721	-2525.457247	-2525.418869	*
TS1-Cl1 (S=3/2)	-2525.126486	0.16003194	-2525.443907	*	*
TS1-Cl2 (S=1/2)	-2525.122685	0.16173305	-2525.443982	-2525.405291	*
TS1-Cl2 (S=3/2)	-2525.128802	0.15804565	-2525.445240	*	*
TS1-Cl3 (S=1/2)	-2525.145587	0.16197066	-2525.466603	-2525.428898	*
TS1-Cl3 (S=3/2)	*	*	*	*	*
B-Cl1 (S=1/2)	-2525.145699	0.16140913	-2525.456526	-2525.417142	*
B-Cl2 (S=1/2)	-2525.191589	0.15566926	*	-2525.467176	*
B-Cl3 (S=1/2)	-2525.152265	0.16166784	-2525.468289	-2525.428763	*
TS2-Cl1 (S=1/2)	-2525.146445	0.15978579	-2525.443826	-2525.403452	*
TS2-Cl1 (S=3/2)	*	*	*	*	*
TS2-Cl2 (S=1/2)	*	*	*	*	*
TS2-Cl2 (S=3/2)	*	*	*	*	*
TS2-Cl3 (S=1/2)	-2525.151194	0.15861528	-2525.446109	-2525.405872	*
TS2-Cl3 (S=3/2)	-2525.126761	0.15147917	-2525.416815	*	*

P-Cl1 (S=1/2)	-2064.427007	0.15185753	-2064.703062	-2064.651387	
P-Cl2 (S=1/2)	-2064.43218	0.15108531	-2064.705817	-2064.655444	
P-Cl3 (S=1/2)	-2064.417785	0.15198211	-2064.693421	-2064.643702	
A-Br(1a) (S=1/2)	-4640.109977	0.16107424	-4639.321243	-4639.455738	-4639.331667
A-Br(3a) (S=1/2)	-4640.104486	0.16097371	-4639.317642	-4639.452403	*
A-Br(3b) (S=1/2)	-4640.104913	0.1607825	-4639.31732	-4639.451945	*
TS1-Br(3a) (S=1/2)	-4640.088026	0.16099068	-4639.291302	-4639.428628	*
TS1-Br(3a) (S=3/2)	*	*	*	*	*
TS1-Br(3b) (S=1/2)	-4640.088635	0.16093005	-4639.289423	-4639.425926	
TS1-Br(3b) (S=3/2)	-4640.080452	0.15888369	*	*	*
B-Br(3a) (S=1/2)	-4640.095049	0.16051554	-4639.29275	-4639.428263	*
B-Br(3b) (S=1/2)	-4640.096446	0.16042939	-4639.291228	-4639.425643	*
TS2-Br(3a) (S=1/2)	-4640.094952	0.15582251	-4639.269693	-4639.405155	-4639.280224
TS2-Br(3a) (S=3/2)	-4640.068552	0.14942345	-4639.239300	*	*
TS2-Br(3b) (S=1/2)	-4640.101093	0.15595918	-4639.282887	-4639.413625	-4639.2934
TS2-Br(3b) (S=3/2)	-4640.072387	0.15044113	*	*	*
P-Br(3a) (S=1/2)	-2064.417785	0.15198211	-2064.693421	-2064.643702	*
P-Br(3b) (S=1/2)	-4179.362257	0.15089766	-4178.517954	-4178.64221	*
A-I(1a) (S=1/2)	-2363.11112	0.16023252	-2362.995055	-2362.888953	-2363.005405
A-I(3a) (S=1/2)	-2363.105649	0.16045519	-2362.991544	-2362.885418	-2363.001801
A-I(3b) (S=1/2)	-2363.107098	0.15998201	-2362.991622	-2362.885198	-2363.001874
TS1-I(3a) (S=1/2)	-2363.088815	0.16004413	-2362.966728	-2362.864352	-2362.976957
TS1-I(3a) (S=3/2)	-2363.081752	0.1585561	-2362.955193	*	*
TS1-I(3b) (S=1/2)	-2363.091344	0.16022981	-2362.964286	-2362.859943	-2362.974572
TS1-I(3b) (S=3/2)	-2363.083492	0.15800292	-2362.953565	*	*
B-I(3a) (S=1/2)	-2363.095776	0.1598795	-2362.966662	-2362.862833	-2362.976956
B-I(3b) (S=1/2)	-2363.100823	0.15934497	-2362.966444	-2362.859621	-2362.976801
TS2-I(3a) (S=1/2)	-2363.096684	0.15412088	-2362.946018	-2362.841917	-2362.956349
TS2-I(3a) (S=3/2)	-2363.069614	0.14824267	-2362.911812	*	*
TS2-I(3b) (S=1/2)	-2363.101487	0.15744294	-2362.948066	-2362.840337	-2362.958464
TS2-I(3b) (S=3/2)	-2363.078061	0.14979873	-2362.919672	*	*
P-I(3a) (S=1/2)	-2064.417785	0.15198211	-2064.693421	-2064.643702	
P-I(3b) (S=1/2)	-1902.367069	0.14993832	-1902.195422	-1902.078296	-1902.204993
1A-tMeCN (P-Cl1) (S=1/2)	-2120.704885	0.17070198	-2121.027849	*	*
1A-tMeCN (P-Cl2) (S=1/2)	-2120.701544	0.17084844	-2121.027039	*	*

PATH-2					
A'-Cl (S = 1/2)	-2601.552585	0.18465754	-2601.942176	-2601.899481	*
A'-Cl (S = 3/2)	-2601.534712	0.17887917	-2601.908546	*	*
A'-Br (S = 1/2)	-4716.495264	0.1835744	-4715.767017	-4715.899089	*
A'-Br (S = 3/2)	-4716.478787	0.17739069	-4715.734415	*	*
A'-I (S = 1/2)	-2439.496832	0.18246485	-2439.442475	-2439.335023	-2439.455841
A'-I (S = 3/2)	-2525.149021	0.15631727	-2525.460817	*	*
A'-NOX (S=1/2)	-2141.206038	0.18718657	-2141.552584	2141.501809	*
A'-NOX (S=3/2)	-2141.194373	0.17938057	-2141.520481	2141.482045	
TS'-Cl (S = 1/2)	-2601.521165	0.18292754	-2601.89899	-2601.857485	*
TS'-Cl (S = 3/2)	-2601.528971	0.17895304	-2601.900755	*	*
TS'-Br (S = 1/2)	-4716.465606	0.18196658	-4715.726024	-4715.859705	*
TS'-Br (S = 3/2)	-4716.473345	0.17809265	-4715.727176	*	*
TS'-NOX (S=1/2)	-2141.185415	0.18532287	-2141.516976	-2141.466771	
TS'-NOX (S=3/2)	-2141.191886	0.18071929	-2141.517325	-2141.479116	
TS'-I (S = 1/2)	-2439.46951	0.18002361	-2439.404232	-2439.29812	-2439.418011
TS'-I (S = 3/2)	-2439.476349	0.17733296	-2439.40365	*	*
REAGENTS (S=1/2)					
H_2O	-76.40352788	0.00339891	-76.43894548	-76.43557981	-76.44477695
PyIm^{iPr+}	-591.2270077	0.19702956	-591.690388	-591.674402	*
$RuCl_3 \cdot 3(H_2O)$	-1704.920844	0.04054698	-1704.912061	-170.882904	*
Py(C)Im^{iPr}-Cl	-1051.564995	0.19270684	-1052.072783	-1052.064645	*
Py(N)Im^{iPr}-Cl	-1051.56098426	0.19320825	-1052.070069	*	
Py(C)Im^{iPr}-Br	-3166.509852	0.19204338	-3165.899889	-3166.066898	*
Py(N)Im^{iPr}-Br	-3166.50669973	0.19230995	-3165.897571	*	
Py(C)Im^{iPr}-I	-889.5124929	0.1912207	-889.577778	-889.505053	*
Py(C)Im^{iPr}-I	-889.50967490	0.19162308	-889.575888	*	
Py(C)Im^{iPr}-BF_4	-1015.721392	0.20197465	-1016.428726	-1016.378585	*
Py(C)Im^{iPr}-BF_4	-1015.71716036	0.20385645	-1016.426520	*	*
Py(C)Im^{Me}-Cl	-973.0224809	0.13963544	-973.456245	-1052.064645	*
Py(N)Im^{Me}-Cl	-973.01831085	0.14009591	-973.453374	-973.439778	*
Py(C)Im^{Me}-Br	-3087.967794	0.13842352	-3087.2833	-3166.066898	*
Py(N)Im^{Me}-Br	-3087.96402083	0.13906628	-3087.280767	-3087.442309	*
Py(C)Im^{Me}-I	-810.968701	0.1391813	-810.961028	-810.882933	*
Py(N)Im^{Me}-I	-810.96707716	0.13799415	-810.958892	-810.880713	*
Py(C)Im^{Me}-BF_4	-937.177151	0.14941301	-937.810888	-937.755133	*
Py(N)Im^{Me}-BF_4	-937.17488090	0.15010154	-937.809161	-937.7540187	*
$Ru(Cl)_3(H_2O)_2$(Cl)	-2088.863009	0.01572912	*	*	*
$Ru(Cl)_3(H_2O)_2$(Br)	-4203.806313	0.01448133	*	*	*
$Ru(Cl)_3(H_2O)_2$(I)	-1926.808559	0.01364238	*	*	*
HX (X=Cl)	-460.763282	-0.01143043	-460.7944947	-460.8033287	*
HX (X=Br)	-2575.700837	-0.01355368	-2574.612081	-2574.794669	*
HX (X=I)	-298.698248	-0.01517169	-298.2852921	-298.2266756	*
X=Cl	-460.32158648	-0.01504214	-460.3578120	*	*

X=Br	-2575.26994012	-0.01619296	-2574.186428	*	*
X=I	-298.27430763	-0.01684816	-297.8659268	*	*
X=BF_4	-424.49171522	-0.01409727	-424.7130312	*	*

4.5. References

[1] R. H. Crabtree, Alkane C–H activation and functionalization with homogeneous transition metal catalysts: a century of progress—a new millennium in prospect, J. Chem. Soc. Dalton Trans. 0 (2001) 2437–2450. https://doi.org/10.1039/B103147N.

[2] K.M. Altus, J.A. Love, The continuum of carbon–hydrogen (C–H) activation mechanisms and terminology, Commun. Chem. 4 (2021) 1–11. https://doi.org/10.1038/s42004-021-00611-1.

[3] B.A. Arndtsen, R.G. Bergman, T.A. Mobley, T.H. Peterson, Selective Intermolecular Carbon-Hydrogen Bond Activation by Synthetic Metal Complexes in Homogeneous Solution, Acc. Chem. Res. 28 (1995) 154–162. https://doi.org/10.1021/ar00051a009.

[4] K.I. Goldberg, A.S. Goldman, Large-Scale Selective Functionalization of Alkanes, Acc. Chem. Res. 50 (2017) 620–626. https://doi.org/10.1021/acs.accounts.6b00621.

[5] N.F. Dummer, D.J. Willock, Q. He, M.J. Howard, R.J. Lewis, G. Qi, S.H. Taylor, J. Xu, D. Bethell, C.J. Kiely, G.J. Hutchings, Methane Oxidation to Methanol, Chem. Rev. (2022). https://doi.org/10.1021/acs.chemrev.2c00439.

[6] S. Gaillard, C.S.J. Cazin, S.P. Nolan, N-Heterocyclic Carbene Gold(I) and Copper(I) Complexes in C–H Bond Activation, Acc. Chem. Res. 45 (2012) 778–787. https://doi.org/10.1021/ar200188f.

[7] A. Prades, M. Poyatos, J.A. Mata, E. Peris, Double C□H Bond Activation of C(sp3)H2 Groups for the Preparation of Complexes with Back-to-Back Bisimidazolinylidenes, Angew. Chem. 123 (2011) 7808–7811. https://doi.org/10.1002/ange.201101806.

[8] C. Wang, F. Chen, P. Qian, J. Cheng, Recent advances in the Rh-catalyzed cascade arene C–H bond activation/annulation toward diverse heterocyclic compounds, Org. Biomol. Chem. 19 (2021) 1705–1721. https://doi.org/10.1039/D0OB02377A.

[9] D. Munz, Pushing Electrons—Which Carbene Ligand for Which Application?, Organometallics 37 (2018) 275–289. https://doi.org/10.1021/acs.organomet.7b00720.

[10] R. Shang, L. Ilies, E. Nakamura, Iron-Catalyzed C–H Bond Activation, Chem. Rev. 117 (2017) 9086–9139. https://doi.org/10.1021/acs.chemrev.6b00772.

[11] J.A. Labinger, J.E. Bercaw, Understanding and exploiting C–H bond activation, Nature 417 (2002) 507–514. https://doi.org/10.1038/417507a.

[12] I. Hussain, T. Singh, Synthesis of Biaryls through Aromatic C□H Bond Activation: A Review of Recent Developments, Adv. Synth. Catal. 356 (2014) 1661–1696. https://doi.org/10.1002/adsc.201400178.

[13] T. Dalton, T. Faber, F. Glorius, C–H Activation: Toward Sustainability and Applications, ACS Cent. Sci. 7 (2021) 245–261. https://doi.org/10.1021/acscentsci.0c01413.

[14] J. Wencel-Delord, T. Dröge, F. Liu, F. Glorius, Towards mild metal-catalyzed C–H bond activation, Chem. Soc. Rev. 40 (2011) 4740–4761. https://doi.org/10.1039/C1CS15083A.

[15] A. Kasera, J.P. Biswas, A. Ali Alshehri, S. Ahmed Al-Thabaiti, M. Mokhtar, D. Maiti, Transition metal pincer complexes: A series of potential catalysts in CH activation reactions, Coord. Chem. Rev. 475 (2023) 214915. https://doi.org/10.1016/j.ccr.2022.214915.

[16] F. Roudesly, J. Oble, G. Poli, Metal-catalyzed CH activation/functionalization: The fundamentals, J. Mol. Catal. Chem. 426 (2017) 275–296. https://doi.org/10.1016/j.molcata.2016.06.020.

[17] M.T. Mihai, H.J. Davis, G.R. Genov, R.J. Phipps, Ion Pair-Directed C–H Activation on Flexible Ammonium Salts: meta-Selective Borylation of Quaternized Phenethylamines and Phenylpropylamines, ACS Catal. 8 (2018) 3764–3769. https://doi.org/10.1021/acscatal.8b00423.

[18] J. Wencel-Delord, F. Glorius, C–H bond activation enables the rapid construction and late-stage diversification of functional molecules, Nat. Chem. 5 (2013) 369–375. https://doi.org/10.1038/nchem.1607.

[19] A.J.I. Arduengo, R.L. Harlow, M. Kline, A stable crystalline carbene, J. Am. Chem. Soc. 113 (1991) 361–363. https://doi.org/10.1021/ja00001a054.

[20] C.M. Crudden, D.P. Allen, Stability and reactivity of N-heterocyclic carbene complexes, Coord. Chem. Rev. 248 (2004) 2247–2273. https://doi.org/10.1016/j.ccr.2004.05.013.

[21] M.N. Hopkinson, C. Richter, M. Schedler, F. Glorius, An overview of N-heterocyclic carbenes, Nature 510 (2014) 485–496. https://doi.org/10.1038/nature13384.

[22] F. Glorius, N-Heterocyclic Carbenes in Transition Metal Catalysis, Springer, 2007.

[23] E. Peris, R.H. Crabtree, New routes to carbene complexes for thermally and oxidatively robust homogeneous catalysts, Comptes Rendus Chim. 6 (2003) 33–37. https://doi.org/10.1016/S1631-0748(03)00003-1.

[24] F.E. Hahn, Introduction: Carbene Chemistry, Chem. Rev. 118 (2018) 9455–9456. https://doi.org/10.1021/acs.chemrev.8b00495.

[25] R. Jazzar, M. Soleilhavoup, G. Bertrand, Cyclic (Alkyl)- and (Aryl)-(amino)carbene Coinage Metal Complexes and Their Applications, Chem. Rev. 120 (2020) 4141–4168. https://doi.org/10.1021/acs.chemrev.0c00043.

[26] B.A. Vastine, M.B. Hall, The molecular and electronic structure of carbon–hydrogen bond activation and transition metal assisted

hydrogen transfer, Coord. Chem. Rev. 253 (2009) 1202–1218. https://doi.org/10.1016/j.ccr.2008.07.015.

[27] D.H. Ess, W.A.I. Goddard, R.A. Periana, Electrophilic, Ambiphilic, and Nucleophilic C−H Bond Activation: Understanding the Electronic Continuum of C−H Bond Activation Through Transition-State and Reaction Pathway Interaction Energy Decompositions, Organometallics 29 (2010) 6459–6472. https://doi.org/10.1021/om100879y.

[28] D. Balcells, E. Clot, O. Eisenstein, C—H Bond Activation in Transition Metal Species from a Computational Perspective, Chem. Rev. 110 (2010) 749–823. https://doi.org/10.1021/cr900315k.

[29] S. Winstein, T.G. Traylor, Mechanisms of Reaction of Organomercurials. II. Electrophilic Substitution on Saturated Carbon. Acetolysis of Dialkylmercury Compounds, J. Am. Chem. Soc. 77 (1955) 3747–3752. https://doi.org/10.1021/ja01619a021.

[30] D. Lapointe, K. Fagnou, Overview of the Mechanistic Work on the Concerted Metallation–Deprotonation Pathway, Chem. Lett. 39 (2010) 1118–1126. https://doi.org/10.1246/cl.2010.1118.

[31] B.S. Bouley, F. Tang, D.Y. Bae, L.M. Mirica, C–H bond activation via concerted metalation–deprotonation at a palladium(III) center, Chem. Sci. 14 (2023) 3800–3808. https://doi.org/10.1039/D3SC00034F.

[32] M. Simonetti, R. Kuniyil, S.A. Macgregor, I. Larrosa, Benzoate Cyclometalation Enables Oxidative Addition of Haloarenes at a Ru(II) Center, J. Am. Chem. Soc. 140 (2018) 11836–11847. https://doi.org/10.1021/jacs.8b08150.

[33] C. Athira, R. B. Sunoj, Role of Lewis acid additives in a palladium catalyzed directed C–H functionalization reaction of benzohydroxamic acid to isoxazolone, Org. Biomol. Chem. 15 (2017) 246–255. https://doi.org/10.1039/C6OB02318E.

[34] S. Ghosh, S. Shilpa, C. Athira, R.B. Sunoj, Role of Additives in Transition Metal Catalyzed C–H Bond Activation Reactions: A

Computational Perspective, Top. Catal. 65 (2022) 141–164. https://doi.org/10.1007/s11244-021-01527-9.

[35] T. Weskamp, V.P.W. Böhm, W.A. Herrmann, N-Heterocyclic carbenes: state of the art in transition-metal-complex synthesis, J. Organomet. Chem. 600 (2000) 12–22. https://doi.org/10.1016/S0022-328X(00)00035-8.

[36] E.C. Keske, O.V. Zenkina, R. Wang, C.M. Crudden, Synthesis and Structure of Silver and Rhodium 1,2,3-Triazol-5-ylidene Mesoionic Carbene Complexes, Organometallics 31 (2012) 456–461. https://doi.org/10.1021/om201104f.

[37] V. Karthik, V. Gupta, G. Anantharaman, Synthesis of Imidazole-Based Functionalized Mesoionic Carbene Complexes of Palladium: Comparison of Donor Properties and Catalytic Activity toward Suzuki–Miyaura Coupling, Organometallics 33 (2014) 6218–6222. https://doi.org/10.1021/om5009023.

[38] M.T. Zamora, M.J. Ferguson, R. McDonald, M. Cowie, Unsymmetrical Dicarbenes Based on N-Heterocyclic/Mesoionic Carbene Frameworks: A Stepwise Metalation Strategy for the Generation of a Dicarbene-Bridged Mixed-Metal Pd/Rh Complex, Organometallics 31 (2012) 5463–5477. https://doi.org/10.1021/om3004543.

[39] Y. Wang, B. Zhang, S. Guo, Transition Metal Complexes Supported by N-Heterocyclic Carbene-Based Pincer Platforms: Synthesis, Reactivity and Applications, Eur. J. Inorg. Chem. 2021 (2021) 188–204. https://doi.org/10.1002/ejic.202000911.

[40] Y. Wei, A. Petronilho, H. Mueller-Bunz, M. Albrecht, Mesoionic Triazolylidene Nickel Complexes: Synthesis, Ligand Lability, and Catalytic C–C Bond Formation Activity, Organometallics 33 (2014) 5834–5844. https://doi.org/10.1021/om500593s.

[41] K. F. Donnelly, A. Petronilho, M. Albrecht, Application of 1,2,3-triazolylidenes as versatile NHC-type ligands : synthesis, properties,

and application in catalysis and beyond, Chem. Commun. 49 (2013) 1145–1159. https://doi.org/10.1039/C2CC37881G.

[42] M. Baltrun, F. A. Watt, R. Schoch, C. Wölper, A. G. Neuba, S. Hohloch, A new bis-phenolate mesoionic carbene ligand for early transition metal chemistry, Dalton Trans. 48 (2019) 14611–14625. https://doi.org/10.1039/C9DT03099A.

[43] H. Vinh Huynh, T. Tien Lam, H.T. T. Luong, Anion influences on reactivity and NMR spectroscopic features of NHC precursors, RSC Adv. 8 (2018) 34960–34966. https://doi.org/10.1039/C8RA05839C.

[44] S. Sowmiah, V. Srinivasadesikan, M.-C. Tseng, Y.-H. Chu, On the Chemical Stabilities of Ionic Liquids, Molecules 14 (2009) 3780–3813. https://doi.org/10.3390/molecules14093780.

[45] C. Roth, T. Peppel, K. Fumino, M. Köckerling, R. Ludwig, The Importance of Hydrogen Bonds for the Structure of Ionic Liquids: Single-Crystal X-ray Diffraction and Transmission and Attenuated Total Reflection Spectroscopy in the Terahertz Region, Angew. Chem. Int. Ed. 49 (2010) 10221–10224. https://doi.org/10.1002/anie.201004955.

[46] Y. Gao, L. Zhang, Y. Wang, H. Li, Probing Electron Density of H-Bonding between Cation−Anion of Imidazolium-Based Ionic Liquids with Different Anions by Vibrational Spectroscopy, J. Phys. Chem. B 114 (2010) 2828–2833. https://doi.org/10.1021/jp910528m.

[47] K. Dong, S. Zhang, D. Wang, X. Yao, Hydrogen Bonds in Imidazolium Ionic Liquids, J. Phys. Chem. A 110 (2006) 9775–9782. https://doi.org/10.1021/jp054054c.

[48] K. Fumino, A. Wulf, R. Ludwig, The potential role of hydrogen bonding in aprotic and protic ionic liquids, Phys. Chem. Chem. Phys. 11 (2009) 8790–8794. https://doi.org/10.1039/B905634C.

[49] A. Wulf, K. Fumino, R. Ludwig, Spectroscopic Evidence for an Enhanced Anion–Cation Interaction from Hydrogen Bonding in Pure

Imidazolium Ionic Liquids, Angew. Chem. Int. Ed. 49 (2010) 449–453. https://doi.org/10.1002/anie.200905437.

[50] S. Cha, M. Ao, W. Sung, B. Moon, B. Ahlström, P. Johansson, Y. Ouchi, D. Kim, Structures of ionic liquid–water mixtures investigated by IR and NMR spectroscopy, Phys. Chem. Chem. Phys. 16 (2014) 9591–9601. https://doi.org/10.1039/C4CP00589A.

[51] S.K. Sinha, S. Guin, S. Maiti, J.P. Biswas, S. Porey, D. Maiti, Toolbox for Distal C–H Bond Functionalizations in Organic Molecules, Chem. Rev. 122 (2022) 5682–5841. https://doi.org/10.1021/acs.chemrev.1c00220.

[52] A. Fernández-Figueiras, M.A. Ravutsov, S.P. Simeonov, Site-Selective C–H Functionalization of Arenes Enabled by Noncovalent Interactions, ACS Omega 7 (2022) 6439–6448. https://doi.org/10.1021/acsomega.1c05830.

[53] N.Y.S. Lam, Z. Fan, K. Wu, H.S. Park, S.Y. Shim, D.A. Strassfeld, J.-Q. Yu, Empirical Guidelines for the Development of Remote Directing Templates through Quantitative and Experimental Analyses, J. Am. Chem. Soc. 144 (2022) 2793–2803. https://doi.org/10.1021/jacs.1c12654.

[54] M.T. Mihai, H.J. Davis, G.R. Genov, R.J. Phipps, Ion Pair-Directed C–H Activation on Flexible Ammonium Salts: *meta* -Selective Borylation of Quaternized Phenethylamines and Phenylpropylamines, ACS Catal. 8 (2018) 3764–3769. https://doi.org/10.1021/acscatal.8b00423.

[55] E. Clot, Ion-Pairing in Organometallic Chemistry: Structure and Influence on Proton Transfer from a Computational Perspective, Eur. J. Inorg. Chem. 2009 (2009) 2319–2328. https://doi.org/10.1002/ejic.200900151.

[56] K. Dong, S. Zhang, J. Wang, Understanding the hydrogen bonds in ionic liquids and their roles in properties and reactions, Chem.

Commun. 52 (2016) 6744–6764. https://doi.org/10.1039/C5CC10120D.

[57] L. Crowhurst, P.R. Mawdsley, J.M. Perez-Arlandis, P.A. Salter, T. Welton, Solvent–solute interactions in ionic liquids, Phys. Chem. Chem. Phys. 5 (2003) 2790–2794. https://doi.org/10.1039/B303095D.

[58] C. Roth, S. Chatzipapadopoulos, D. Kerlé, F. Friedriszik, M. Lütgens, S. Lochbrunner, O. Kühn, R. Ludwig, Hydrogen bonding in ionic liquids probed by linear and nonlinear vibrational spectroscopy, New J. Phys. 14 (2012) 105026. https://doi.org/10.1088/1367-2630/14/10/105026.

[59] H. Sivaram, J. Tan, H.V. Huynh, Syntheses, Characterizations, and a Preliminary Comparative Cytotoxicity Study of Gold(I) and Gold(III) Complexes Bearing Benzimidazole- and Pyrazole-Derived N-Heterocyclic Carbenes, Organometallics 31 (2012) 5875–5883. https://doi.org/10.1021/om300444c.

[60] J.C. Bernhammer, H.V. Huynh, Pyrazolin-5-ylidene Palladium(II) Complexes: Synthesis, Characterization, and Application in the Direct Arylation of Pentafluorobenzene, Organometallics 31 (2012) 5121–5130. https://doi.org/10.1021/om300464b.

[61] N. Đorđević, H.V. Huynh, Stereoelectronic Evaluation of Pyrazole- and Indazole-Derived N-Heterocyclic Carbenes, Organometallics 41 (2022) 335–344. https://doi.org/10.1021/acs.organomet.1c00675.

[62] N. Shahid, R.K. Singh, N. Srivastava, A.K. Singh, Base-free synthesis of benchtop stable Ru(III)-NHC complexes from RuCl3·3H2O and their use as precursors for Ru(II)-NHC complexes, Dalton Trans. (2023). https://doi.org/10.1039/D3DT00243H.

[63] A. G. Avent, P. A. Chaloner, M. P. Day, K. R. Seddon, T. Welton, Evidence for hydrogen bonding in solutions of 1-ethyl-3-methylimidazolium halides, and its implications for room-temperature halogenoaluminate(III) ionic liquids, J. Chem. Soc. Dalton Trans. 0 (1994) 3405–3413. https://doi.org/10.1039/DT9940003405.

[64] H.K. Stassen, R. Ludwig, A. Wulf, J. Dupont, Imidazolium Salt Ion Pairs in Solution, Chem. – Eur. J. 21 (2015) 8324–8335. https://doi.org/10.1002/chem.201500239.

[65] H. Wang, J. Wang, S. Zhang, Y. Pei, K. Zhuo, Ionic Association of the Ionic Liquids [C4mim][BF4], [C4mim][PF6], and [Cnmim]Br in Molecular Solvents, ChemPhysChem 10 (2009) 2516–2523. https://doi.org/10.1002/cphc.200900438.

[66] H. Vinh Huynh, T. Tien Lam, H.T. T. Luong, Anion influences on reactivity and NMR spectroscopic features of NHC precursors, RSC Adv. 8 (2018) 34960–34966. https://doi.org/10.1039/C8RA05839C.

[67] A. G. Avent, P. A. Chaloner, M. P. Day, K. R. Seddon, T. Welton, Evidence for hydrogen bonding in solutions of 1-ethyl-3-methylimidazolium halides, and its implications for room-temperature halogenoaluminate(III) ionic liquids, J. Chem. Soc. Dalton Trans. 0 (1994) 3405–3413. https://doi.org/10.1039/DT9940003405.

[68] R. Katoh, M. Hara, S. Tsuzuki, Ion Pair Formation in [bmim]I Ionic Liquids, J. Phys. Chem. B 112 (2008) 15426–15430. https://doi.org/10.1021/jp806578h.

[69] L.F.O. Faria, M.M. Nobrega, N. Falsini, S. Fanetti, M.L.A. Temperini, R. Bini, M.C.C. Ribeiro, Structure and Reactivity of the Ionic Liquid 1-Allyl-3-methylimidazolium Iodide under High Pressure, J. Phys. Chem. B 123 (2019) 1822–1830. https://doi.org/10.1021/acs.jpcb.8b10669.

[70] S. Cha, M. Ao, W. Sung, B. Moon, B. Ahlström, P. Johansson, Y. Ouchi, D. Kim, Structures of ionic liquid–water mixtures investigated by IR and NMR spectroscopy, Phys. Chem. Chem. Phys. 16 (2014) 9591–9601. https://doi.org/10.1039/C4CP00589A.

[71] M. Shukla, N. Srivastava, S. Saha, Theoretical and spectroscopic studies of 1-butyl-3-methylimidazolium iodide room temperature ionic liquid: Its differences with chloride and bromide derivatives, J.

Mol. Struct. 975 (2010) 349–356. https://doi.org/10.1016/j.molstruc.2010.05.003.

[72] T. Ogura, N. Akai, K. Shibuya, A. Kawai, Charge-Transfer Electronic Absorption Spectra of 1-Ethylpyridinium Cation and Halogen Anion Pairs in Dichloromethane and as Neat Ionic Liquids, J. Phys. Chem. B 117 (2013) 8547–8554. https://doi.org/10.1021/jp402329v.

[73] I. Tanabe, A. Suyama, T. Sato, K. Fukui, Potential Dependence of Electronic Transition Spectra of Interfacial Ionic Liquids Studied by Newly Developed Electrochemical Attenuated Total Reflectance Spectroscopy, Anal. Chem. 91 (2019) 3436–3442. https://doi.org/10.1021/acs.analchem.8b04931.

[74] B. A. Marekha, O. N. Kalugin, A. Idrissi, Non-covalent interactions in ionic liquid ion pairs and ion pair dimers: a quantum chemical calculation analysis, Phys. Chem. Chem. Phys. 17 (2015) 16846–16857. https://doi.org/10.1039/C5CP02197A.

[75] Y. Umebayashi, H. Hamano, S. Tsuzuki, J.N. Canongia Lopes, A.A.H. Pádua, Y. Kameda, S. Kohara, T. Yamaguchi, K. Fujii, S. Ishiguro, Dependence of the Conformational Isomerism in 1-n-Butyl-3-methylimidazolium Ionic Liquids on the Nature of the Halide Anion, J. Phys. Chem. B 114 (2010) 11715–11724. https://doi.org/10.1021/jp1044755.

[76] H. Sivaram, J. Tan, H.V. Huynh, Syntheses, Characterizations, and a Preliminary Comparative Cytotoxicity Study of Gold(I) and Gold(III) Complexes Bearing Benzimidazole- and Pyrazole-Derived N-Heterocyclic Carbenes, Organometallics 31 (2012) 5875–5883. https://doi.org/10.1021/om300444c.

[77] J.C. Bernhammer, H.V. Huynh, Pyrazolin-5-ylidene Palladium(II) Complexes: Synthesis, Characterization, and Application in the Direct Arylation of Pentafluorobenzene, Organometallics 31 (2012) 5121–5130. https://doi.org/10.1021/om300464b.

[78] N. Đorđević, H.V. Huynh, Stereoelectronic Evaluation of Pyrazole- and Indazole-Derived N-Heterocyclic Carbenes, Organometallics 41 (2022) 335–344. https://doi.org/10.1021/acs.organomet.1c00675.

[79] F. Neese, F. Wennmohs, U. Becker, C. Riplinger, The ORCA quantum chemistry program package, J. Chem. Phys. 152 (2020) 224108. https://doi.org/10.1063/5.0004608.

[80] F. Neese, The ORCA program system, WIREs Comput. Mol. Sci. 2 (2012) 73–78. https://doi.org/10.1002/wcms.81.

[81] F. Neese, Software update: The ORCA program system—Version 5.0, WIREs Comput. Mol. Sci. 12 (2022) e1606. https://doi.org/10.1002/wcms.1606.

[82] J.G. Brandenburg, C. Bannwarth, A. Hansen, S. Grimme, B97-3c: A revised low-cost variant of the B97-D density functional method, J. Chem. Phys. 148 (2018) 064104. https://doi.org/10.1063/1.5012601.

[83] M. Dolg, H. Stoll, H. Preuss, Energy-adjusted ab initio pseudopotentials for the rare earth elements, J. Chem. Phys. 90 (1989) 1730–1734. https://doi.org/10.1063/1.456066.

[84] D. Andrae, U. Häußermann, M. Dolg, H. Stoll, H. Preuß, Energy-adjustedab initio pseudopotentials for the second and third row transition elements, Theor. Chim. Acta 77 (1990) 123–141. https://doi.org/10.1007/BF01114537.

[85] B. Metz, H. Stoll, M. Dolg, Small-core multiconfiguration-Dirac–Hartree–Fock-adjusted pseudopotentials for post-d main group elements: Application to PbH and PbO, J. Chem. Phys. 113 (2000) 2563–2569. https://doi.org/10.1063/1.1305880.

[86] K.A. Peterson, D. Figgen, E. Goll, H. Stoll, M. Dolg, Systematically convergent basis sets with relativistic pseudopotentials. II. Small-core pseudopotentials and correlation consistent basis sets for the post-d group 16–18 elements, J. Chem. Phys. 119 (2003) 11113–11123. https://doi.org/10.1063/1.1622924.

[87] T. Leininger, A. Nicklass, W. Küchle, H. Stoll, M. Dolg, A. Bergner, The accuracy of the pseudopotential approximation: non-frozen-core effects for spectroscopic constants of alkali fluorides XF (X = K, Rb, Cs), Chem. Phys. Lett. 255 (1996) 274–280. https://doi.org/10.1016/0009-2614(96)00382-X.

[88] M. Kaupp, P. v. R. Schleyer, H. Stoll, H. Preuss, Pseudopotential approaches to Ca, Sr, and Ba hydrides. Why are some alkaline earth MX2 compounds bent?, J. Chem. Phys. 94 (1991) 1360–1366. https://doi.org/10.1063/1.459993.

[89] M. Dolg, H. Stoll, Pseudopotential study of the rare earth monohydrides, monoxides and monofluorides, Theor. Chim. Acta 75 (1989) 369–387. https://doi.org/10.1007/BF00526695.

[90] X. Cao, M. Dolg, Valence basis sets for relativistic energy-consistent small-core lanthanide pseudopotentials, J. Chem. Phys. 115 (2001) 7348–7355. https://doi.org/10.1063/1.1406535.

[91] S. Grimme, S. Ehrlich, L. Goerigk, Effect of the damping function in dispersion corrected density functional theory, J. Comput. Chem. 32 (2011) 1456–1465. https://doi.org/10.1002/jcc.21759.

[92] S. Grimme, J. Antony, S. Ehrlich, H. Krieg, A consistent and accurate ab initio parametrization of density functional dispersion correction (DFT-D) for the 94 elements H-Pu, J. Chem. Phys. 132 (2010) 154104. https://doi.org/10.1063/1.3382344.

[93] Y. Zhao, D.G. Truhlar, The M06 suite of density functionals for main group thermochemistry, thermochemical kinetics, noncovalent interactions, excited states, and transition elements: two new functionals and systematic testing of four M06-class functionals and 12 other functionals, Theor. Chem. Acc. 120 (2008) 215–241. https://doi.org/10.1007/s00214-007-0310-x.

[94] N. Mardirossian, M. Head-Gordon, ωB97M-V: A combinatorially optimized, range-separated hybrid, meta-GGA density functional with

VV10 nonlocal correlation, J. Chem. Phys. 144 (2016) 214110. https://doi.org/10.1063/1.4952647.

[95] R.L. Martin, P.J. Hay, L.R. Pratt, Hydrolysis of Ferric Ion in Water and Conformational Equilibrium, J. Phys. Chem. A 102 (1998) 3565–3573. https://doi.org/10.1021/jp980229p.

[96] J. Zhang, Q. Zhang, Z. Zhu, B. Wang, Theoretical investigation on the palladium-catalyzed selective formation of spirocyclenes from dienallenes, J. Organomet. Chem. 912 (2020) 121173. https://doi.org/10.1016/j.jorganchem.2020.121173.

[97] J. Ariai, U. Gellrich, The entropic penalty for associative reactions and their physical treatment during routine computations, Phys. Chem. Chem. Phys. 25 (2023) 14005–14015. https://doi.org/10.1039/D3CP00970J.

Chapter 5

Ru(III)-aNHC to Ru(III)-NHC conversion: A Computational Study

5.1 Introduction

NHCs have been used as ancillary ligands for over five decades and are considered to be stronger electron donors than phosphines and pyridines.[1,2] N-heterocyclic carbenes have garnered significant attention over the past two decades due to their remarkable σ-donating capabilities and steric tunability, facilitating the stabilization of various metal centers and the subsequent utilization of the resultant NHC compounds in numerous applications, particularly in homogeneous catalysis.[3–13] Imidazol-2-ylidene-type N-heterocyclic carbenes (NHCs) typically coordinate to metal centers or heteroatoms via the C2 carbon, resulting in "normal" NHC (nNHC). However, Crabtree and colleagues first demonstrated that these NHCs could bind to a metal center through the C4/C5 carbon, yielding the corresponding "abnormal" or mesoionic NHC species (aNHC).[14,15] In comparison to nNHCs, aNHCs demonstrate a more pronounced σ-donating ability, attributed to the partial vinylic character of the C4/C5-bonding, resulting in higher basicity at the metal center, making them good candidates for achieving highly active homogeneous catalysts for T.H. and Oppenauer-type oxidations. [16–22] Additionally, aNHC exhibits reduced steric hindrance due to the proximity of a single nitrogen and its corresponding N-substituent altering the reactivity from NHC, increasing the stability of aNHC more than NHC.[23–25] Despite the higher reactivity, the aNHC complexes have been less explored.

The formation of M-aNHC complexes is kinetically more favorable[26] and is influenced by various parameters, including the steric bulk at the N-wingtip of the azolium ring, [27–31]the impact of counter anions from the ligand precursors, [32–35] and the solvent's effect[36].

These factors may also prompt the inversion of the ring and the establishment of the stable isomer following rearrangement. [37–41]

The normal to abnormal NHC rearrangement in transition metal chemistry has recently been reported.[42–46] These rearrangements readily occur due to steric congestion, thus overcoming the electronic preference for *n*NHC versus *a*NHC ligation.[46] It has been reported that the free NHC is more stable than the free aNHC; however, the DFT calculations suggest that the abnormal binding through C4/C5 can be thermodynamically much less favored (23.3 kcal/mol) than normal C2-binding ($ML_n = PtCl_3^-$).[15,47] Energy decomposition calculations indicate that the energy gap between the parent nNHC and aNHC is approximately 19 kcal/mol.[47,48] High activation barrier for the metalation with aNHC than NHC was found by the pK_a values for the C2 bound and C5 bond proton, i.e., for the C2 bound proton pK_a = 24.9, while for the C5 bound proton pK_a = 33.0.[49–54]

High valent metal-NHC complexes have always been a subject of interest due to the limited work done in this field. Prior to our group's work,[55] few Ru(III)-NHC-based complexes were reported to be obtained either from a Ru(II) precursor oxidation or identified as intermediate during the electrochemical reaction.[56–59] Ever since the isolation of the first abnormal-NHC carbene complexes by Crabtree and *coworkers* in 2002,[60] a series of transition metal complexes with aNHC have been reported. The conversion of normal-NHC to abnormal-NHC has also been found to occur due to steric congestion.[46] However, the conversion of abnormal-NHC to normal-NHC has not been observed. In our recent work, we observed this unusual phenomenon.

Our group has recently reported the synthesis of Ru(III)-NHC (**1B**) complex by the reaction of $RuCl_3 \cdot 3H_2O$ with $PyNHC^{Me}$.X (where X= Cl, Br, I) bidentate ligand framework.[55] This complex (**1B**) was utilized as a precursor in the synthesis of phosphine-free Ru(II)-CNC pincer complexes shown in Chapter 3. Theoretical investigations in the previous chapter

described the halide-assisted electrophilic C-H activation of imidazolium salts ($PyNHC^{Me}$·X (where X= Cl, Br, I)), following the concerted-metalation-deprotonation (CMD) mechanism in the synthesis of our Ru(III)-NHC complexes. Recently, our group, in the hunt to design a high valent Ru-NHC complex, reported a new synthetic route for the synthesis of kinetic product Ru(III)-aNHC (**1A**) *via* electrophilic C-H bond activation in an aqueous solution of acid.[62] An *in situ* conversion of the kinetic product **1A** to the thermodynamic product **1B** was observed. Several controlled experiments were performed to predict the mechanism of this conversion.[62]

In this chapter, we describe the computational study for the mechanistic pathway leading to the conversion of kinetic product **1A** to the thermodynamic product **1B** (Scheme 5.1) and also validate the experimentally predicted pathway by our DFT computed mechanism.

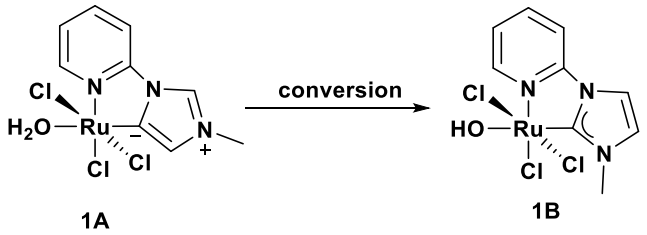

Scheme 5.1. The recently reported Ru(III)-aNHC and Ru(III)-NHC complexes by our group.

5.2 Results and Discussion

In the previous chapter, we described the role of halides in the synthesis of Ru(III)-NHC complex (**1B**). The experimental investigation suggests that the conversion of **1A** to **1B** takes place with time in the reaction medium (water solvent) and is effected by several factors, like the concentration of chloride in solution and the occupancy of the $C3_{Py}$ position. To gain mechanistic insight into the *in situ* conversion of Ru(III)-aNHC (**1A**) to Ru(III)-NHC (**1B**), DFT investigations were performed at 293.15 K

temperature in water solvent. Initially, the geometries of **1A** and **1B** were optimized, and their energies were calculated. The relative Gibbs free energy energy of **1B** w.r.t to **1A** was calculated and found to be -8.8 kcal/mol (Figure 5.1).

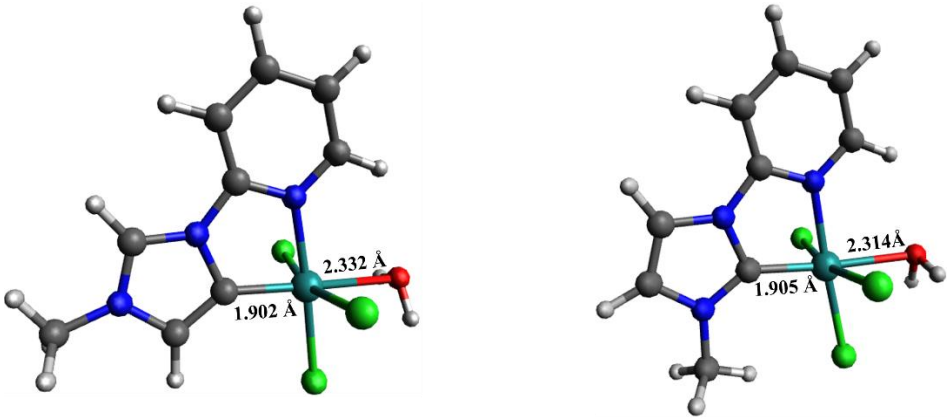

Figure 5.1. DFT optimized structures of **1A** and **1B** with Gibbs free energies w.r.t. **1A**.

The bond length for the Ru-OH_2 bond in **1A** was found to be 2.332 Å, while the bond length for the Ru-OH_2 bond in 1B was 2.314 Å (Figure 5.1). The longer Ru-OH_2 bond in **1A** suggests stronger σ-donation and a greater trans effect. The bond length of the Ru-carbene($C5_{Im}$) for **1A** is 1.902 Å, while for **1B**, the Ru-carbene($C2_{Im}$) appears to be 1.905 Å in the DFT optimized structures (Figure 5.1).

In the experimental study, control experiments have been performed to predict the plausible pathway for the conversion of **1A** to **1B**.[62] In one of the experiments., the C3 position of the pyridine ring of the azolium salt was substituted by the methyl group and reacted under the reaction condition with $RuCl_3 \cdot 3H_2O$ to give the corresponding products. The kinetic product **3A** and the thermodynamic product **3B** were observed (Figure 5.2). Upon substitution of the C3Py proton by methyl, it was observed that the conversion of abnormal **3A** to normal **3B** slowed down drastically. This

experiment indicated the role of $C3_{Py}$-H in the in situ conversion of **1A** to **1B**.

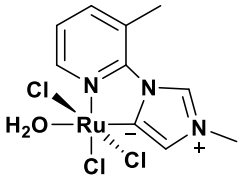

3A

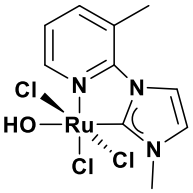

3B

Figure 5.2. Recently reported complexes **3A** and **3B** by our group.

Based on the experimental findings and literature survey, it can be assumed that the proton required for the conversion may be coming from $C3_{Py}$. Taking this into account, we initially propose a very common cyclometallation pathway involving the $C3_{Py}$-H called the pyridine roll-over pathway.

5.2.1 Pyridine roll-over pathway-

Roll-over cyclometallation is a common and widely studied pathway for Pd and Pt metals and bipyridine as ligands.[63–71] Choudhury and *coworkers* reported C-H functionalization of alkynes via the bimodal flip-flop roll-over of pyridine and NHC in Rh(III)-NHC complex via a proto-demetalation step.[72,73]. Serrano and *coworkers* reported a roll-over complex *via* C-H bond activation from a new bromide 2-(pyridin-2-yl)imidazo[1,2-a]pyridine ligand and $IrCl_3$.[74]

In the first step, starting from **1A**, dissociation of hemilabile Ru-N_{Py} followed by a roll-over of pyridine along the C-N bond takes place to give intermediate **A** vis transition state **TS1**. In intermediate **A**, the bond length for the Ru-carbene(C5) increases to 1.932 Å (1.902 Å for **1A**) while the bond length for the trans Ru-OH_2 decreases to 2.317 Å (2.332 for **1A**). The $C3_{Py}$-H comes in close proximity to the ruthenium, with the bond distance between Ru-H($C3_{Py}$) appearing 2.228 Å in the optimized geometry. In the case of **TS1**, the Löwdin spin density localized on Ru was 0.82.

In the subsequent step, C-H bond activation of $C3_{Py}$ by ruthenium occurs, followed by intramolecular proton transfer to imidazolium-C5. This C-H proton transfer may proceed through two different routes. If the C-H proton transfer occurs *via the* ruthenium center, this is called the oxidative addition pathway. On the other hand, when the Cl coordinated to the ruthenium center acts as a proton carrier, this pathway is called Cl assisted pathway. After the proton transfer to $C5_{Im,}$ both routes follow same pathway.

5.2.1.a Oxidative Addition pathway (Path 1)

This pathway involves the ruthenium center for the proton transfer from $C3_{Py}$ to $C5_{Im}$. In this pathway, the C-H bond activation of the $C3_{Py}$ takes place by the Ru(III)-Lewis acidic metal center followed by the transfer of proton to imidazolium-C5 to give intermediate **B** with the cleavage of the Ru-$C5_{Im}$ bond via **TS2** (51.5 kcal/mol). The bond length between Ru-$C3_{Py}$ in intermediate **B** appears as 2.040 Å (Ru-N_{Py} bond length for **1A** = 2.061 Å), and the bond length of the Ru-OH_2 decreases drastically to 2.147 Å. The Löwdin spin density for **TS2** localized on Ru increases to 0.86. As the proton transfer and the cleavage of the Ru-$C5_{Im}$ bond occurs, the imidazolium ring undergoes rotation along the C-N bond. This rotation of the imidazolium ring occurs through transition state **TS3**, such that the imidazolium-C2 proton comes close to the Ru(III) center, resulting in intermediate **C**. The bond of Ru-OH_2 in **C** becomes 2.151 Å while the Ru-$C3_{Py}$ becomes 2.056 Å. The Löwdin spin density in the case of **TS3** localized on ruthenium increases to 0.88.

In the next step, C-H bond activation of the $C2_{Im}$ proton occurs by the Lewis acidic Ru(III) center, followed by proton transfer to $C3_{Py}$, leading to intermediate **D** via transition state **TS4**. The intermediate **D** closely resembles **A** but with the $C2_{Im}$ coordination i.e., normal coordination. The bond length of Ru-$C2_{Im}$ appears to be 1.929 Å while the Ru-OH_2 bond

becomes 2.292 Å. The Löwdin spin density localized on ruthenium for TS4 becomes 0.86.

In the final step, the pyridine roll-over happens again via **TS5** to give the Ru(III)-NHC (**1B**). The Löwdin spin density localized on ruthenium for **TS5** becomes 0.83. The energy profile diagram for the pyridine rotation involving the oxidative addition route with DFT-optimized structures of intermediates and their corresponding Gibbs free energies calculated in kcal/mol are shown in Figure 5.3. The important bond lengths of intermediates and their dihedral angles are shown in Figure 5.4.

The transition state **TS2** involves the proton transfer *via* ruthenium from $C3_{Py}$ of intermediate **A** to $C5I_m$ of intermediate **B**. This proton transfer requires 51.5 kcal/mol energy, which is higher; therefore, another route for the proton transfer was proposed, which involves the participation of chloride coordinated to ruthenium.

5.2.1.b Chloride-assisted pathway (Path 2)

This route was proposed as an alternative to intramolecular proton transfer from $C3_{Py}$ of **A** to $C5I_m$ of **B** via the metal center. This route proposes proton transfer via nearby chloride coordinated with the ruthenium center. The chloride becomes free and acts as a carrier of proton. Starting from intermediate **A**, the chloride coordinated to ruthenium dissociates and abstracts the $C3_{Py}$ proton, forming a free H-Cl molecule and giving intermediate **P1** via transition state **TS2a** (45.0 kcal/mol). The Ru-$C5_{Im}$ bond of P1 upon chloride dissociation becomes 1.936 Å while the Ru-OH_2 bond becomes 2.319 Å. The Löwdin spin density localized on ruthenium for **TS2a** is 0.86. In the following steps, the intramolecular rearrangement of H-Cl occurs before transferring the proton to the $C5_{Im,}$ forming intermediate **B**. Next, the free H-Cl rearranges its orientation such that its proton comes in the vicinity of the other chloride, forming an intermediate **P2**. The proton from the H-Cl is transferred to another chloride, regenerating a new H-Cl

free molecule, giving an intermediate **P3**. Later, this proton from the free H-Cl is transferred to the $C5_{Im}$ via transition state **TS2c** (46.1 kcal/mol), giving the intermediate **B**. The Löwdin spin density localized on ruthenium for **TS2a** is 0.84. The next steps from **B** to **1B** follow the same route as the oxidative addition pathway (*wide supra*). The energy profile diagram for the pyridine rotation pathway following the chloride-assisted route with DFT-optimized geometries and their corresponding Gibbs free energies are shown in Figure 5.5. The critical bond length of intermediates and their dihedral angles are shown in Figure 5.6.

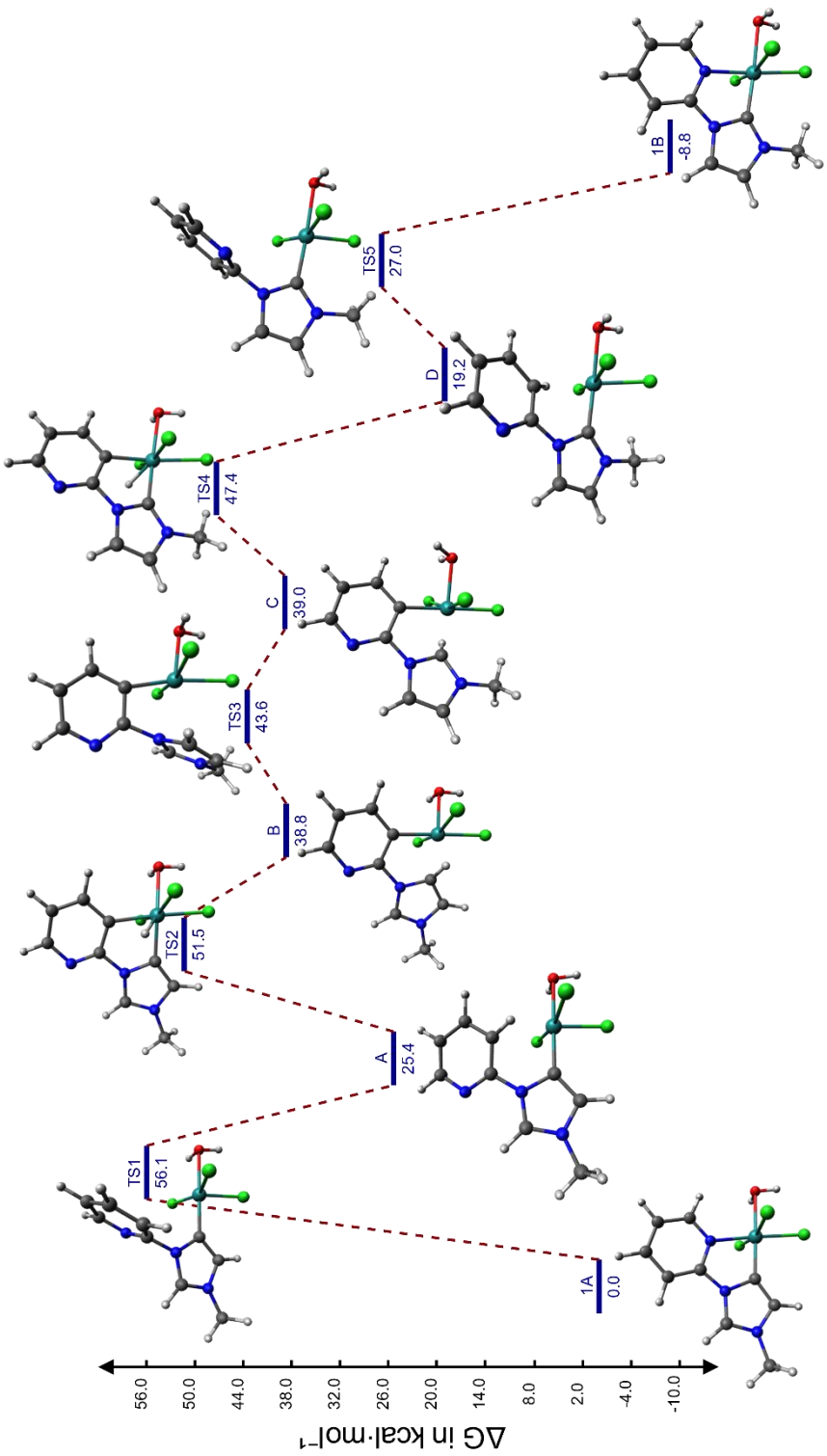

Figure 5.3. DFT computed energy profile diagram for the conversion of Ru(III)-aNHC (**1A**) to Ru(III)-NHC (**1B**) by pyridine roll-over oxidative addition pathway (Path 1). Gibbs free energies are reported in kcal/mol at 293.15 K, relative to the **1A**

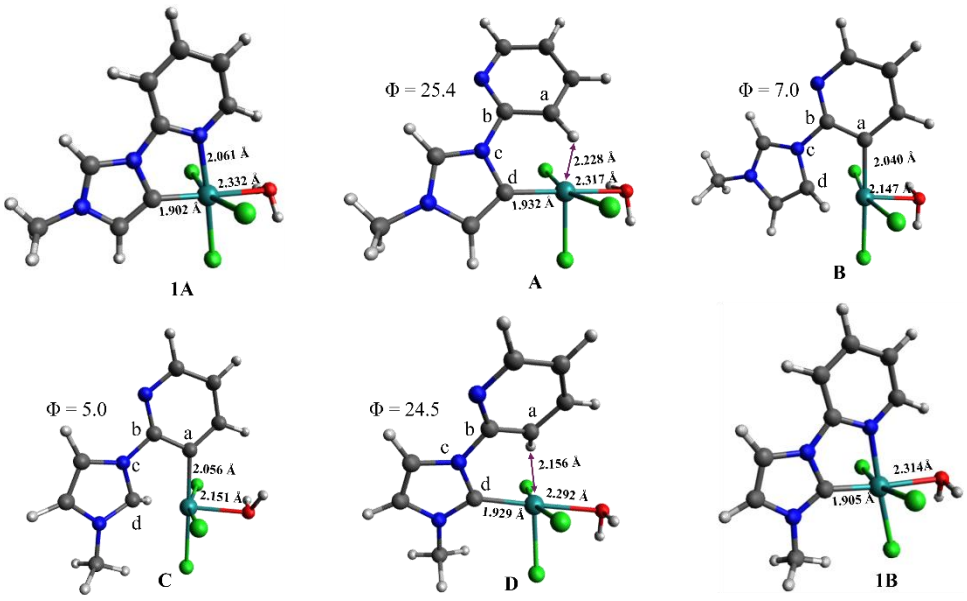

Figure 5.4 DFT optimized intermediates with important bond lengths and dihedral angle (Φ) for Path 1.

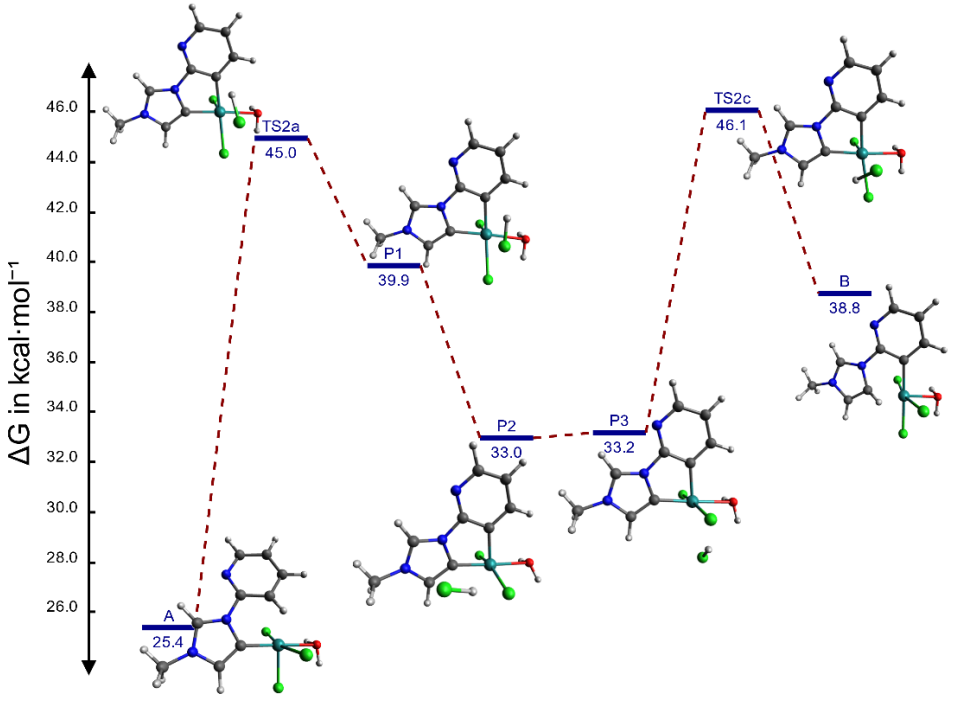

Figure 5.5. DFT computed energy profile diagram for the conversion of Ru(III)-aNHC (**1A**) to Ru(III)-NHC (**1B**) by pyridine roll-over chloride assisted pathway. Gibbs free energies are reported in kcal/mol at 293.15 K, relative to the **1A**.

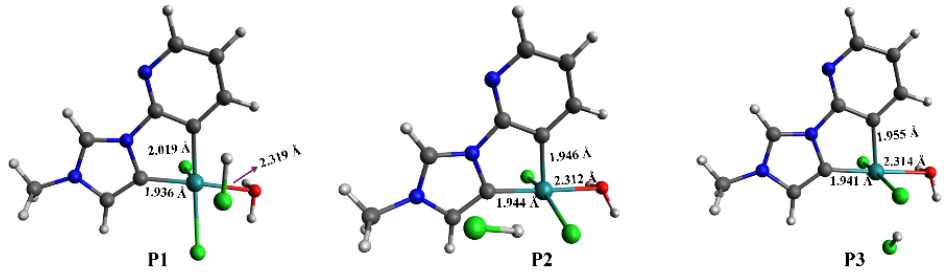

Figure 5.6. DFT optimized intermediates with important bond lengths and dihedral angle (Φ) for Path 2.

The experimental study observed that the complex **3A** remained as abnormal-NHC and did not convert to its normal-NHC analog **3B** even after 15 days, which supports the pyridine roll-over mechanism.

Through the DFT study, we could observe that the pyridine roll-over mechanism is still a high-energy pathway as the dissociation of the Ru-N_{Py} bond of **1A** requires 56.1 kcal/mol of energy. This indicates that the $C3_{Py}$ is not a feasible source of proton. Therefore, an alternative source of proton was required for intramolecular proton transfer to $C5_{Py}$ following a lower energy pathway. We propose that the intramolecular proton transfer may occur either from an external proton source or from the water coordinated to ruthenium trans to the aNHC. The experimental investigations rejected the possibility of the proton coming from an external source. [62] Therefore, the coordinated water molecule is the only possible source of proton. When the coordinated water acts as the proton source, the pathway is called a water-assisted pathway.

5.2.2 Water assisted pathway

The aNHC coordinated trans to the water molecule makes the Ru-OH_2 bond elongated, hence labile (Figure 5.1). Figure 5.7 shows the energy profile diagram for the water-assisted pathway with DFT-optimized geometries of the transition state and intermediates and their corresponding Gibbs free energies, calculated in kcal/mol. In the first step, a dynamic intramolecular

exchange between the H_2O and one of the axially coordinated chloride occurs *via* berry pseudo rotation, making the H_2O molecule *cis*- to the aNHC, resulting in intermediate **A**. In this geometry, the water molecule is not trans to another axial chloride, while the aNHC is also trans to chloride. The bond length of the Ru-OH_2 in **A** becomes 2.234 Å, while the bond length for Ru-$C5_{Im}$ becomes 1.939. The Ru-Cl bond length for trans to carbene Cl is 2.463 Å. In the next step, protonation of the carbene carbon by one of the protons of the H_2O molecule, followed by cleavage of the Ru-aNHC bond, takes place via the transition state **TS2** to give the intermediate **B** having free imidazolium ring. This proton transfer requires 38.4 kcal/mol energy, much lower than the energy needed for proton transfer by pyridine rotation (51.5 kcal/mol for oxidative addition and 45.0 for chloride-assisted pathway). The Ru-OH bond length in **B** is 1.926 Å while the Ru-Cl trans to dissociated carbene becomes 2.261. The Löwdin spin density localized on ruthenium for **TS2** is 0.87.

Ananikov and *coworkers* reported 2015 that Ni(II)-NHC complexes tended to undergo hydrolysis and cleavage of Ni-NHC bonds under mild conditions due to water in organic solvents.[75] The nature of halogen influences this hydrolytic ability, which is coordinated to the metal center and follows the order Cl > Br > I.[75] This indicates that the chloride coordinated to the metal center facilitates the proton-assisted dissociation of the Ru(III)-aNHC bond.

In the next step, the rotation of the imidazolium ring, along with the rotation of the Ru-N_{Py} bond, takes place via transition state **TS3** such that the $C2_{Im}$ proton comes in the vicinity of the OH coordinated to ruthenium, resulting in intermediate **C**. The Ru-OH bond length after rotation along the single bond becomes 1.946 Å, and the Ru-Cl bond trans to carbene becomes 2.340 Å. The Löwdin spin density localized on ruthenium for transition state **TS2** decreases to 0.82. This step is followed by $C2_{Im}$-H bond activation

by ruthenium *via* transition state **TS4** and reprotonation of OH to form H_2O, resulting in intermediate **D.** The intermediate **D** is similar to **A** but with

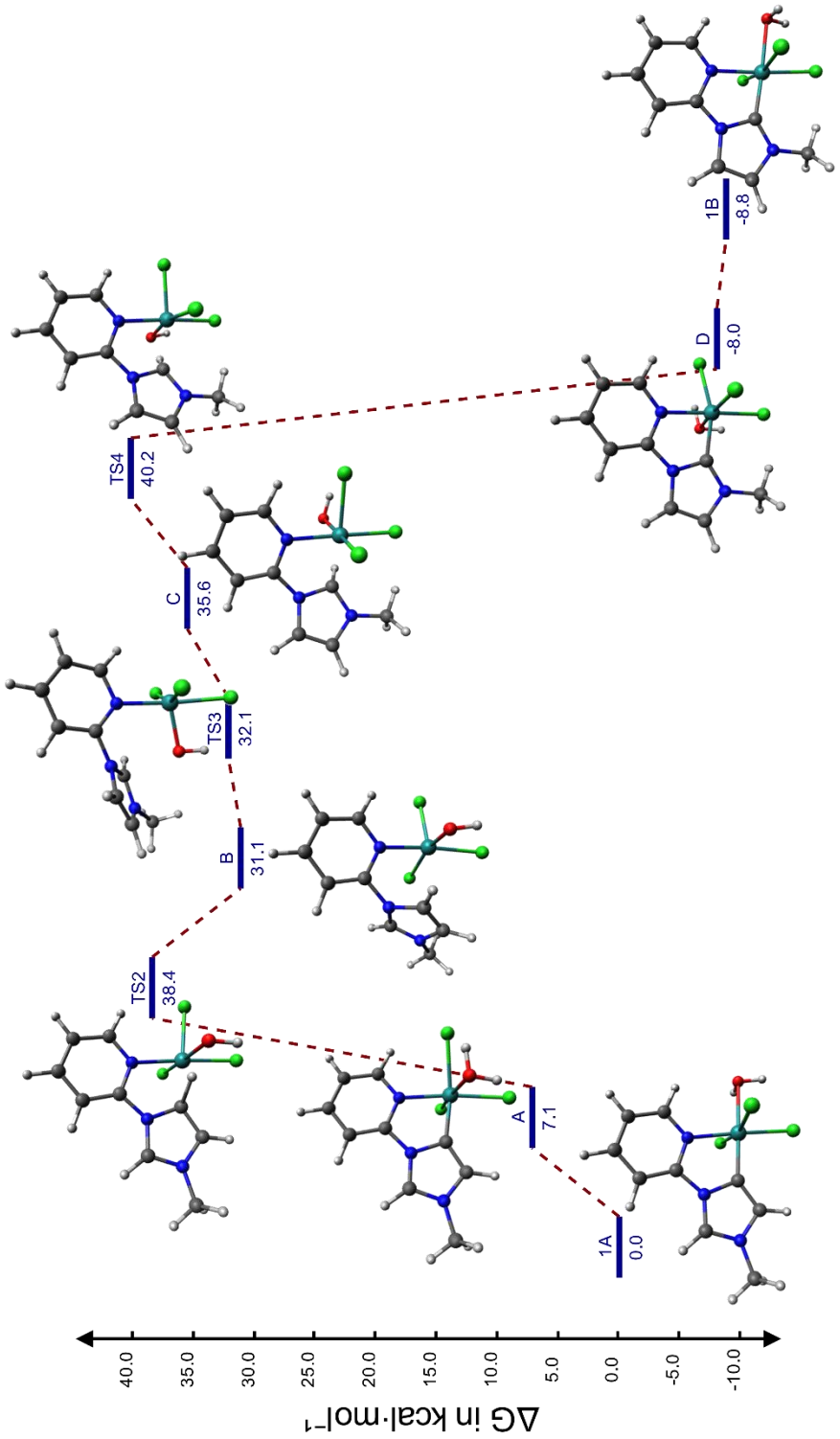

Figure 5.7. DFT computed energy profile diagram for the conversion of Ru(III)-aNHC (**1A**) to Ru(III)-NHC (**1B**) by water-assisted pathway (Path 3). Gibbs free energies are reported in kcal/mol at 293.15 K, relative to the **1A**

coordination of normal NHC to ruthenium. The Ru-OH_2 bond length becomes 2.209 Å with Ru-$C2_{Im}$ bond length 1.933 Å and Ru-Cl trans to carbene as 2.497 Å. The Löwdin spin density localized on ruthenium for **TS4** becomes 0.85. The water molecules rearrange back to the trans-to-carbene orientation, giving the Ru(III)-NHC **1B**. The important bond lengths of intermediates and their dihedral angles are shown in Figure 5.8.

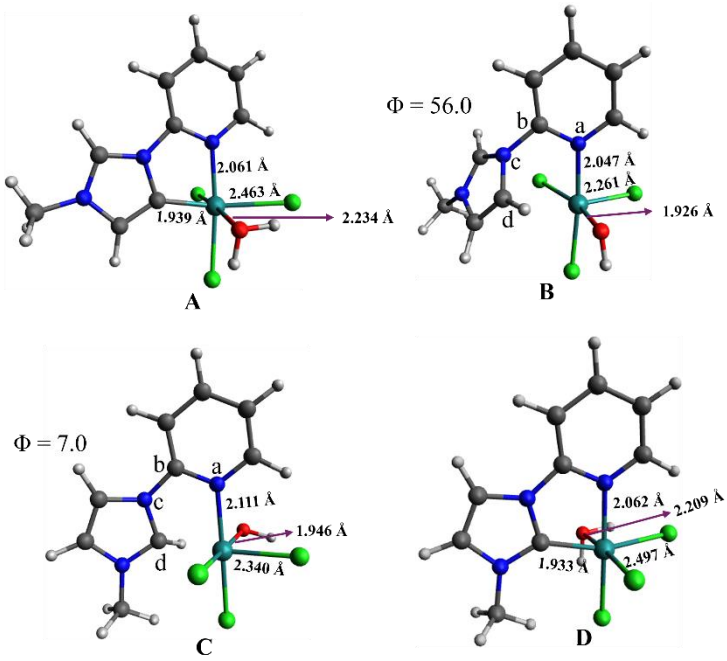

Figure 5.8. DFT optimized intermediates with important bond lengths and dihedral angle (Φ) for Path 3.

5.3 Conclusion

In this chapter, we report the DFT computed plausible pathways for the conversion of our recently reported complexes **1A** to **1B**. This is the first report in which the mechanism for the abnormal-NHC conversion to normal-NHC conversion is given. We propose three possible routes, i.e., pyridine roll-over oxidative addition pathway (**Path 1**), pyridine roll-over chloride-assisted pathway (**Path 2**), and Water-assisted pathway (**Path 3**).

Path 2 differs from **path 1** in that chloride plays a role in transferring a proton from $C3_{Py}$ to $C5_{Im}$ instead of ruthenium. This proton transfer via chloride lowers the transition state, making the conversion more feasible. The DFT study proposed a pyridine rotation pathway, which is also supported by the experimental results from our recent work, where the importance of $C3_{Py}$-H was observed. The dissociation of Ru-N_{Py} requires high energy, i.e., 56.1 kcal/mol; therefore, a Water-assisted pathway was proposed where the coordinated Water trans to the aNHC takes part in the proton transfer to $C5_{Im}$. The water-assisted pathway follows the lowest energy route, and therefore, it is the most feasible pathway for the conversion of R(III)-aNHC (**1A**) to Ru(III)-NHC (**1B**).

5.4 DFT experimental

All DFT calculations were performed using the ORCA 5.0.3 program package developed by Neese and coworkers.[76–78] The geometry optimizations along with frequency calculations were carried out using B97-3c composite functional which is a low-cost method and is shown to produce excellent geometries for transition metal complexes.[79] The B97-3c uses a modified, stripped-down triple-ζ basis, def2-mTZVP (BS1) along with auxiliary basis def2-mTZVP/J for Resolution of Identity (R.I.) approximation and def2-ECP[80–87] on heavier elements (Ru), Grimme's atom-pairwise dispersion correction with the Becke-Johnson damping scheme (D3BJ),[88,89] and a short-range bond length adjustment.[79]. Tight SCF convergence criterion and a solvent model in which "water" is described by an implicit conductor-like polarizable continuum medium (CPCM) was used during all calculations. Stationary points were confirmed to have either no imaginary frequency (for reactants and intermediates) or only one imaginary frequency along the reaction coordinates (for T.S.) by performing analytical frequency calculations at the same level of the DFT method. Transition states were confirmed to connect their respective intermediates via IRC calculations followed by geometry optimization in

both directions. For final energies, single point calculations were performed using one of the most popular hybrid functionals shown to give excellent barrier heights for transition metal complexes i.e., range separated hybrid meta-GGA functional ωB97M-V[90] developed by Martin Head-Gorden and coworkers which includes VV10 non-local correlation. Larger basis set (BS2) def2-QZVP with def2-ECP on Ru, def2-TZVPD with def2-ECP on Cl and def2-TZVP on all other atoms were used for single point energy calculations. ORCA's, inbuilt, finer integration grid "DEFGRID3" was used during all the single point calculations. The energies obtained from single point calculations were converted to Gibbs free energies using the total corrections obtained for the thermochemical calculations following the frequency calculations at the B97-3c level. Gibbs free energies, ΔG are reported in Kcal/mol.

Table 5.1 Energies of DFT optimized structures.

Pyridine roll-over oxidative addition pathway

Species	**B97-3c**			**wB97M-V/BS2**
	G	**G-E_{el}**	**E_{el-sol}**	**E_{el}**
1A	-2064.37497144	0.15022775	-2064.56706761106	-2064.63967119191
TS1	-2064.33397893	0.1491613	-2064.51743721883	-2064.5977182342
A	-2064.34621983	0.1487541	-2064.52678130367	-2064.6076912328
TS2	-2064.31058476	0.14638638	-2064.48945244956	-2064.563175201
B	-2064.32285555	0.14950082	-2064.51044937949	-2064.58085655618
TS3	-2064.29750904	0.15057737	-2064.48479966948	-2064.57575622285
C	-2064.32692447	0.1490242	-2064.51254892314	-2064.58157033306
TS4	-2064.32584349	0.14665609	-2064.49627371897	-2064.57868970987
D	-2064.3646773	0.15040937	-2064.53789187214	-2064.62836340731
TS5	-2064.34947592	0.15073098	-2064.52424843749	-2064.61488171521
1B	-2064.40062608	0.15125834	-2064.57942721576	-2064.66911915847

Pyridine roll-over chloride assisted pathway

Species	B97-3c			**wB97M-V/BS2**
	G	**G-E_{el}**	**E_{sol}**	**E_{el}**
TS2a	-2064.31562603	0.14354065	-2064.48591149929	-2064.57639956203
P1	-2064.3174592	0.14496128	-2064.49143280199	-2064.58364035952
P2	-2064.34358167	0.14392903	-2064.51380428983	-2064.59628498811
P3	-2064.34388071	0.14411396	-2064.5135297492	-2064.59689507899
TS2c	-2064.31421595	0.14355533	-2064.48429012136	-2064.57494284887

Water-assisted pathway

Species	B97-3c			**wB97M-V/BS2**
	G	**G-E_{el}**	**E_{sol}**	**E_{el}**
A	-2064.35974336	0.15100476	-2064.55638557673	-2064.62541714709
TS2	-2064.29865168	0.14657542	-2064.49939864294	-2064.56251972698
B	-2064.32330871	0.15140566	-2064.52422677391	-2064.58362130908
TS3	-2064.31505602	0.15149583	-2064.51915911728	-2064.57906935579
C	-2064.33200656	0.15050813	-2064.52620706835	-2064.58132560486
TS4	-2064.3175608	0.14687234	-2064.50841771288	-2064.57013162903
D	-2064.38196901	0.15213944	-2064.56595032553	-2064.65288885124

5.5 References

[1] S. Zhao, Z. Yang, G. Jiang, S. Huang, M. Bian, Y. Lu, W. Liu, An overview of anticancer platinum *N*-heterocyclic carbene complexes, Coord. Chem. Rev. 449 (2021) 214217. https://doi.org/10.1016/j.ccr.2021.214217.

[2] S.Y. Hussaini, R.A. Haque, M.R. Razali, Recent progress in silver(I)-, gold(I)/(III)- and palladium(II)-*N*-heterocyclic carbene complexes: A review towards biological perspectives, J. Organomet. Chem. 882 (2019) 96–111. https://doi.org/10.1016/j.jorganchem.2019.01.003.

[3] P. de Frémont, N. Marion, S.P. Nolan, Carbenes: Synthesis, properties, and organometallic chemistry, Coord. Chem. Rev. 253 (2009) 862–892. https://doi.org/10.1016/j.ccr.2008.05.018.

[4] V. César, S. Bellemin-Laponnaz, L. H. Gade, Chiral N-heterocyclic carbenes as stereodirecting ligands in asymmetric catalysis, Chem. Soc. Rev. 33 (2004) 619–636. https://doi.org/10.1039/B406802P.

[5] P.L. Arnold, I.J. Casely, F-Block N-Heterocyclic Carbene Complexes, Chem. Rev. 109 (2009) 3599–3611. https://doi.org/10.1021/cr8005203.

[6] S. Bellemin-Laponnaz, S. Dagorne, Group 1 and 2 and Early Transition Metal Complexes Bearing N-Heterocyclic Carbene Ligands: Coordination Chemistry, Reactivity, and Applications, Chem. Rev. 114 (2014) 8747–8774. https://doi.org/10.1021/cr500227y.

[7] A.J. Arduengo, Looking for Stable Carbenes: The Difficulty in Starting Anew, Acc. Chem. Res. 32 (1999) 913–921. https://doi.org/10.1021/ar980126p.

[8] D. Pugh, A.A. Danopoulos, Metal complexes with 'pincer'-type ligands incorporating *N*-heterocyclic carbene functionalities, Coord. Chem. Rev. 251 (2007) 610–641. https://doi.org/10.1016/j.ccr.2006.08.001.

[9] S.P. Nolan, N-Heterocyclic Carbenes in Synthesis, John Wiley & Sons, 2006.

[10] W.A. Herrmann, N-Heterocyclic Carbenes: A New Concept in Organometallic Catalysis, Angew. Chem. Int. Ed. 41 (2002) 1290–1309. https://doi.org/10.1002/1521-3773(20020415)41:8<1290::AID-ANIE1290>3.0.CO;2-Y.

[11] S.P. Nolan, N-Heterocyclic Carbenes: Effective Tools for Organometallic Synthesis, John Wiley & Sons, 2014.

[12] D. Bourissou, O. Guerret, F.P. Gabbaï, G. Bertrand, Stable Carbenes, Chem. Rev. 100 (2000) 39–92. https://doi.org/10.1021/cr940472u.

[13] L. Benhamou, E. Chardon, G. Lavigne, S. Bellemin-Laponnaz, V. César, Synthetic Routes to N-Heterocyclic Carbene Precursors, Chem. Rev. 111 (2011) 2705–2733. https://doi.org/10.1021/cr100328e.

[14] Abnormal binding in a carbene complex formed from an imidazolium salt and a metal hydride complex - Chemical Communications (RSC Publishing), (n.d.). https://pubs.rsc.org/en/content/articlelanding/2001/cc/b107881j (accessed September 11, 2024).

[15] S. Gründemann, A. Kovacevic, M. Albrecht, J.W. Faller, R.H. Crabtree, Abnormal Ligand Binding and Reversible Ring Hydrogenation in the Reaction of Imidazolium Salts with IrH5(PPh3)2, J. Am. Chem. Soc. 124 (2002) 10473–10481. https://doi.org/10.1021/ja026735g.

[16] L. Benhamou, J. Wolf, V. César, A. Labande, R. Poli, N. Lugan, G. Lavigne, Chelation-Assisted Reactions of Phosphine- and Olefin-Tethered Imidazolium Derivatives and Their Affiliated N-Heterocyclic Carbenes with Roper's Complex Ru(CO)2(PPh3)3, Organometallics 28 (2009) 6981–6993. https://doi.org/10.1021/om900813p.

[17] S. Saha, T. Ghatak, B. Saha, H. Doucet, J.K. Bera, Steric Control at the Wingtip of a Bis-N-Heterocyclic Carbene Ligand: Coordination Behavior and Catalytic Responses of Its Ruthenium Compounds, Organometallics 31 (2012) 5500–5505. https://doi.org/10.1021/om300469n.

[18] A. Prades, E. Peris, M. Albrecht, Oxidations and Oxidative Couplings Catalyzed by Triazolylidene Ruthenium Complexes, Organometallics 30 (2011) 1162–1167. https://doi.org/10.1021/om101145y.

[19] P. Mathew, A. Neels, M. Albrecht, 1,2,3-Triazolylidenes as Versatile Abnormal Carbene Ligands for Late Transition Metals, J. Am. Chem. Soc. 130 (2008) 13534–13535. https://doi.org/10.1021/ja805781s.

[20] F.P. Malan, E. Singleton, P.H. van Rooyen, M. Albrecht, M. Landman, Synthesis, Stability, and (De)hydrogenation Catalysis by Normal and Abnormal Alkene- and Picolyl-Tethered NHC Ruthenium Complexes, Organometallics 38 (2019) 2624–2635. https://doi.org/10.1021/acs.organomet.9b00178.

[21] L. Bernet, R. Lalrempuia, W. Ghattas, H. Mueller-Bunz, L. Vigara, A. Llobet, M. Albrecht, Tunable single-site ruthenium catalysts for efficient water oxidation, Chem. Commun. 47 (2011) 8058–8060. https://doi.org/10.1039/C1CC12615F.

[22] A. D. Both, M. J. Sauer, W. Baratta, F. E. Kühn, Abnormal NHC ruthenium catalysts: mechanistic investigations of their preparation and steric influence on catalytic performance, Catal. Sci. Technol. 12 (2022) 5597–5603. https://doi.org/10.1039/D2CY01036D.

[23] R.H. Crabtree, Abnormal, mesoionic and remote N-heterocyclic carbene complexes, Coord. Chem. Rev. 257 (2013) 755–766. https://doi.org/10.1016/j.ccr.2012.09.006.

[24] K.F. Donnelly, A. Petronilho, M. Albrecht, Application of 1,2,3-triazolylidenes as versatile NHC-type ligands: synthesis, properties, and application in catalysis and beyond, Chem. Commun. 49 (2013) 1145–1159. https://doi.org/10.1039/C2CC37881G.

[25] Beyond Conventional N-Heterocyclic Carbenes: Abnormal, Remote, and Other Classes of NHC Ligands with Reduced Heteroatom Stabilization | Chemical Reviews, (n.d.). https://pubs.acs.org/doi/10.1021/cr8005087# (accessed September 11, 2024).

[26] O. Schuster, L. Yang, H.G. Raubenheimer, M. Albrecht, Beyond Conventional *N* -Heterocyclic Carbenes: Abnormal, Remote, and Other Classes of NHC Ligands with Reduced Heteroatom Stabilization, Chem. Rev. 109 (2009) 3445–3478. https://doi.org/10.1021/cr8005087.

[27] S. Ataie, A. Khanzadeh, L.P. Mangin, M.I. Lohoar, B. Fitchett, R.T. Baker, Bifunctional Hydroboration Catalyst Activation Using a Co SNS Amido Complex Bearing an Abnormal-NHC Ligand, Organometallics (2023). https://doi.org/10.1021/acs.organomet.3c00348.

[28] S. Byun, S. Park, Y. Choi, J.Y. Ryu, J. Lee, J.-H. Choi, S. Hong, Highly Efficient Ethenolysis and Propenolysis of Methyl Oleate Catalyzed by Abnormal N-Heterocyclic Carbene Ruthenium Complexes in Combination with a Phosphine–Copper Cocatalyst, ACS Catal. 10 (2020) 10592–10601. https://doi.org/10.1021/acscatal.0c02018.

[29] A. Das, S. Chakraborty, S.K. Mandal, Abnormal N-heterocyclic Carbene Based Ni(II) π-allyl Complex towards Molecular Oxygen Activation, Chem. – Asian J. 16 (2021) 2257–2260. https://doi.org/10.1002/asia.202100568.

[30] M. Bhunia, P.K. Hota, G. Vijaykumar, D. Adhikari, S.K. Mandal, A Highly Efficient Base-Metal Catalyst: Chemoselective Reduction of Imines to Amines Using An Abnormal-NHC–Fe(0) Complex, Organometallics 35 (2016) 2930–2937. https://doi.org/10.1021/acs.organomet.6b00478.

[31] M.J. Bitzer, A. Pöthig, C. Jandl, F.E. Kühn, W. Baratta, Ru–Ag and Ru–Au dicarbene complexes from an abnormal carbene ruthenium system, Dalton Trans. 44 (2015) 11686–11689. https://doi.org/10.1039/C5DT01914A.

[32] L.N. Appelhans, D. Zuccaccia, A. Kovacevic, A.R. Chianese, J.R. Miecznikowski, A. Macchioni, E. Clot, O. Eisenstein, R.H. Crabtree, An Anion-Dependent Switch in Selectivity Results from a Change of C−H Activation Mechanism in the Reaction of an Imidazolium Salt with $IrH_5(PPh_3)_2$, J. Am. Chem. Soc. 127 (2005) 16299–16311. https://doi.org/10.1021/ja055317j.

[33] B. Eguillor, M.A. Esteruelas, M. Oliván, M. Puerta, Abnormal and Normal N-Heterocyclic Carbene Osmium Polyhydride Complexes Obtained by Direct

Metalation of Imidazolium Salts, Organometallics 27 (2008) 445–450. https://doi.org/10.1021/om7010722.

[34] L. Cancela, M.A. Esteruelas, M. Oliván, E. Oñate, Azolium Control of the Osmium-Promoted Aromatic C–H Bond Activation in 1,3-Disubstituted Substrates, Organometallics 40 (2021) 3979–3991. https://doi.org/10.1021/acs.organomet.1c00565.

[35] M. Baya, B. Eguillor, M.A. Esteruelas, M. Oliván, E. Oñate, Influence of the Anion of the Salt Used on the Coordination Mode of an N-Heterocyclic Carbene Ligand to Osmium, Organometallics 26 (2007) 6556–6563. https://doi.org/10.1021/om700746h.

[36] A. Kovacevic, K.R. Meadows, M. Counts, D.J. Arthur, Solvent influence in the formation of normal and abnormal carbene complexes in reactions of imidazolium salts with [Ir(H)2(PPh3)2(OCMe2)2]BF4, Inorganica Chim. Acta 373 (2011) 259–261. https://doi.org/10.1016/j.ica.2011.01.046.

[37] J.-Y. Lee, J.-Y. Lee, Y.-Y. Chang, C.-H. Hu, N.M. Wang, H.M. Lee, Palladium Complexes with Tridentate N-Heterocyclic Carbene Ligands: Selective "Normal" and "Abnormal" Bindings and Their Anticancer Activities, Organometallics 34 (2015) 4359–4368. https://doi.org/10.1021/acs.organomet.5b00586.

[38] A.M. Chernysheva, M. Weinhart, M. Scheer, A.Y. Timoshkin, Normal to abnormal I^{t}Bu·AlH$_3$ isomerization in solution and in the solid state, Dalton Trans. 49 (2020) 4665–4668. https://doi.org/10.1039/C9DT04698D.

[39] R.S. Ghadwal, D. Rottschäfer, D.M. Andrada, G. Frenking, C.J. Schürmann, H.-G. Stammler, Normal-to-abnormal rearrangement of an N-heterocyclic carbene with a silylene transition metal complex, Dalton Trans. 46 (2017) 7791–7799. https://doi.org/10.1039/C7DT01199G.

[40] R.A. Layfield, J.J.W. McDouall, M. Scheer, C. Schwarzmaier, F. Tuna, Structure and bonding in three-coordinate N-heterocyclic carbene adducts of iron(ii) bis(trimethylsilyl)amide, Chem. Commun. 47 (2011) 10623. https://doi.org/10.1039/c1cc14576b.

[41] T. Pugh, R.A. Layfield, Reactivity of three-coordinate iron–NHC complexes towards phenylselenol and lithium phenylselenide, Dalton Trans. 43 (2014) 4251–4254. https://doi.org/10.1039/C3DT53203H.

[42] P.L. Arnold, S.T. Liddle, Deprotonation of N-Heterocyclic Carbenes to Afford Heterobimetallic Organolanthanide Complexes, Organometallics 25 (2006) 1485–1491. https://doi.org/10.1021/om050895u.

[43] C.E. Cooke, M.C. Jennings, R.K. Pomeroy, J.A.C. Clyburne, Normal and Abnormal NHC Coordination in [Os4(μ-H)4(CO)11(IMes)] and Exhaustive Dehydrogenation of an IMes Methyl Group, Organometallics 26 (2007) 6059–6062. https://doi.org/10.1021/om7007293.

[44] R.A. Musgrave, R.S.P. Turbervill, M. Irwin, J.M. Goicoechea, Transition Metal Complexes of Anionic N-Heterocyclic Dicarbene Ligands, Angew. Chem. Int. Ed. 51 (2012) 10832–10835. https://doi.org/10.1002/anie.201206100.

[45] B.M. Day, T. Pugh, D. Hendriks, C.F. Guerra, D.J. Evans, F.M. Bickelhaupt, R.A. Layfield, Normal-to-Abnormal Rearrangement and NHC Activation in Three-Coordinate Iron(II) Carbene Complexes, J. Am. Chem. Soc. 135 (2013) 13338–13341. https://doi.org/10.1021/ja408589p.

[46] G. Schnee, O. Nieto Faza, D. Specklin, B. Jacques, L. Karmazin, R. Welter, C. Silva López, S. Dagorne, Normal-to-Abnormal NHC Rearrangement of AlIII, GaIII, and InIII Trialkyl Complexes: Scope, Mechanism, Reactivity Studies, and H2 Activation, Chem. – Eur. J. 21 (2015) 17959–17972. https://doi.org/10.1002/chem.201503000.

[47] G. Sini, O. Eisenstein, R.H. Crabtree, Preferential C-Binding versus N-Binding in Imidazole Depends on the Metal Fragment Involved, Inorg. Chem. 41 (2002) 602–604. https://doi.org/10.1021/ic010714q.

[48] R. Tonner, G. Heydenrych, G. Frenking, Bonding Analysis of N-Heterocyclic Carbene Tautomers and Phosphine Ligands in Transition-Metal Complexes: A Theoretical Study, Chem. – Asian J. 2 (2007) 1555–1567. https://doi.org/10.1002/asia.200700235.

[49] A.M. Magill, B.F. Yates, An Assessment of Theoretical Protocols for Calculation of the pKa Values of the Prototype Imidazolium Cation, Aust. J. Chem. 57 (2004) 1205–1210. https://doi.org/10.1071/CH04159.

[50] A.M. Magill, K.J. Cavell, B.F. Yates, Basicity of Nucleophilic Carbenes in Aqueous and Nonaqueous SolventsTheoretical Predictions, J. Am. Chem. Soc. 126 (2004) 8717–8724. https://doi.org/10.1021/ja038973x.

[51] K. Denk, P. Sirsch, W.A. Herrmann, The first metal complexes of bis(diisopropylamino)carbene: synthesis, structure and ligand properties, J. Organomet. Chem. 649 (2002) 219–224. https://doi.org/10.1016/S0022-328X(02)01133-6.

[52] P. Bazinet, G.P.A. Yap, D.S. Richeson, Constructing a Stable Carbene with a Novel Topology and Electronic Framework, J. Am. Chem. Soc. 125 (2003) 13314–13315. https://doi.org/10.1021/ja0372661.

[53] M. Mayr, K. Wurst, K.-H. Ongania, M.R. Buchmeiser, 1,3-Dialkyl- and 1,3-Diaryl-3,4,5,6-tetrahydropyrimidin-2-ylidene Rhodium(i) and Palladium(II) Complexes: Synthesis, Structure, and Reactivity, Chem. – Eur. J. 10 (2004) 1256–1266. https://doi.org/10.1002/chem.200305437.

[54] A.R. Chianese, A. Kovacevic, B.M. Zeglis, J.W. Faller, R.H. Crabtree, Abnormal C5-Bound N-Heterocyclic Carbenes: Extremely Strong Electron Donor Ligands and Their Iridium(I) and Iridium(III) Complexes, Organometallics 23 (2004) 2461–2468. https://doi.org/10.1021/om049903h.

[55] N. Shahid, R.K. Singh, N. Srivastava, A.K. Singh, Base-free synthesis of benchtop stable Ru(III)–NHC complexes from RuCl3·3H2O and their use as precursors for Ru(II)–NHC complexes, Dalton Trans. 52 (2023) 4176–4185. https://doi.org/10.1039/D3DT00243H.

[56] S. Hitzel, C. Färber, C. Bruhn, U. Siemeling, Reactions of [RuCl2(PPh3)3] with Nitron and with the “Enders Carbene”: Access to Ruthenium(III) NHC Complexes, Organometallics 33 (2014) 425–428. https://doi.org/10.1021/om401058e.

[57] P.L. Arnold, A.C. Scarisbrick, Di- and Trivalent Ruthenium Complexes of Chelating, Anionic N-Heterocyclic Carbenes, Organometallics 23 (2004) 2519–2521. https://doi.org/10.1021/om0498091.

[58] Y. Shimoyama, T. Ishizuka, H. Kotani, Y. Shiota, K. Yoshizawa, K. Mieda, T. Ogura, T. Okajima, S. Nozawa, T. Kojima, A Ruthenium(III)–Oxyl Complex Bearing Strong Radical Character, Angew. Chem. 128 (2016) 14247–14251. https://doi.org/10.1002/ange.201607861.

[59] F. Chen, G.-F. Wang, Y.-Z. Li, X.-T. Chen, Z.-L. Xue, Syntheses, structures and electrochemical properties of homoleptic ruthenium(III) and osmium(III) complexes bearing two tris(carbene)borate ligands, Inorg. Chem. Commun. 21 (2012) 88–91. https://doi.org/10.1016/j.inoche.2012.04.020.

[60] S. Gründemann, A. Kovacevic, M. Albrecht, J.W.F. Robert, H. Crabtree, Abnormal binding in a carbene complex formed from an imidazolium salt and a metal hydride complex, Chem. Commun. (2001) 2274–2275. https://doi.org/10.1039/B107881J.

[61] N. Srivastava, N. Shahid, A.K. Singh, Insights into the effect of contact ion-pairs on C.H. bond activation for the synthesis of Ru(III)-NHC complexes: A combined experimental and computational study, J. Organomet. Chem. 998 (2023) 122802. https://doi.org/10.1016/j.jorganchem.2023.122802.

[62] N. Shahid, V. Budhija, A. K Singh,. Halide assisted electrophilic C-H activation in aqueous acid and salt solutions for the synthesis of Ru(III)-abnormal-NHC complexes, Organometallics 43 (2024) 2243-2255. https://doi.org/10.1021/acs.organomet.4c00273.

[63] G. Minghetti, A. Doppiu, A. Zucca, S. Stoccoro, M.A. Cinellu, M. Manassero, M. Sansoni, Palladium(II) and platinum(II)-C(3)-substituted 2,2′-bipyridines, Chem. Heterocycl. Compd. 35 (1999) 992–1000. https://doi.org/10.1007/BF02252169.

[64] A. Zucca, G.L. Petretto, S. Stoccoro, M.A. Cinellu, M. Manassero, C. Manassero, G. Minghetti, Cyclometalation of 2,2′-Bipyridine. Mono- and

Dinuclear C,N Platinum(II) Derivatives, Organometallics 28 (2009) 2150–2159. https://doi.org/10.1021/om801033g.

[65] Cyclopalladation of 6-Substituted-2,2‘-bipyridines. Metalation of Unactivated Methyl Groups vs Aromatic C−H Activation | Organometallics, (n.d.). https://pubs.acs.org/doi/10.1021/om000239o (accessed September 11, 2024).

[66] A. Zucca, S. Stoccoro, M.A. Cinellu, G. Minghetti, M. Manassero, M. Sansoni, Metallation of Unactivated Methyl Groups − Platinum(II) Derivatives with 6-Alkyl-2,2′-bipyridines, Eur. J. Inorg. Chem. 2002 (2002) 3336–3346. https://doi.org/10.1002/1099-0682(200212)2002:12<3336::AID-EJIC3336>3.0.CO;2-Z.

[67] S. Stoccoro, L. Maidich, T. Ruiu, M.A. Cinellu, G.J. Clarkson, A. Zucca, Chiral cyclometalation of 6-(1-phenylbenzyl)-2,2′-bipyridine, Dalton Trans. 44 (2015) 18001–18011. https://doi.org/10.1039/C5DT02483H.

[68] G. Minghetti, S. Stoccoro, M.A. Cinellu, B. Soro, A. Zucca, Activation of a C−H Bond in a Pyridine Ring. Reaction of 6-Substituted 2,2‘-Bipyridines with Methyl and Phenyl Platinum(II) Derivatives: N ',C(3)-"Roll-over" Cyclometalation, Organometallics 22 (2003) 4770–4777. https://doi.org/10.1021/om0301583.

[69] A. Zucca, D. Cordeschi, S. Stoccoro, M.A. Cinellu, G. Minghetti, G. Chelucci, M. Manassero, Platinum(II)-Cyclometalated “Roll-over” Complexes with a Chiral Pinene-Derived 2,2′-Bipyridine, Organometallics 30 (2011) 3064–3074. https://doi.org/10.1021/om200172h.

[70] A. Zucca, D. Cordeschi, L. Maidich, M.I. Pilo, E. Masolo, S. Stoccoro, M.A. Cinellu, S. Galli, Rollover Cyclometalation with 2-(2′-Pyridyl)quinoline, Inorg. Chem. 52 (2013) 7717–7731. https://doi.org/10.1021/ic400908f.

[71] S. Stoccoro, G. Chelucci, M.A. Cinellu, A. Zucca, G. Minghetti, Cyclometallated derivatives of palladium(II) and platinum(II) derived from 6-t-butyl-2,2′-bipyridine, J. Organomet. Chem. 450 (1993) C15–C16. https://doi.org/10.1016/0022-328X(93)80172-8.

[72] C. Dutta, D. Ghorai, J. Choudhury, To "Roll-over" or Not? Stereoelectronically Guided C–H Functionalization Pathways from Rhodium–Abnormal NHC Intermediates, ACS Omega 3 (2018) 1614–1620. https://doi.org/10.1021/acsomega.7b01846.

[73] D. Ghorai, C. Dutta, J. Choudhury, Switching of "Roll-over Pathway" in Rhodium(III)-Catalyzed C–H Activation of Chelating Molecules, ACS Catal. 6 (2016) 709–713. https://doi.org/10.1021/acscatal.5b02540.

[74] Y. Varela, G. Ramírez-García, J.O. C. Jimenez-Halla, M. Segovia-Mendoza, H. Prado-Garcia, K. Wrobel, K. Wrobel, S. Gutiérrez-Granados, C. Lemini, O. Serrano, A roll-over Ir(iii) complex of 2-(6-bromopyridin-2-yl)imidazo[1,2- a]pyridine, New J. Chem. 47 (2023) 5625–5633. https://doi.org/10.1039/D2NJ06026D.

[75] A.V. Astakhov, O.V. Khazipov, E.S. Degtyareva, V.N. Khrustalev, V.M. Chernyshev, V.P. Ananikov, Facile Hydrolysis of Nickel(II) Complexes with N-Heterocyclic Carbene Ligands, Organometallics 34 (2015) 5759–5766. https://doi.org/10.1021/acs.organomet.5b00856.

[76] F. Neese, F. Wennmohs, U. Becker, C. Riplinger, The ORCA quantum chemistry program package, J. Chem. Phys. 152 (2020) 224108. https://doi.org/10.1063/5.0004608.

[77] F. Neese, The ORCA program system, WIREs Comput. Mol. Sci. 2 (2012) 73–78. https://doi.org/10.1002/wcms.81.

[78] F. Neese, Software update: The ORCA program system—Version 5.0, WIREs Comput. Mol. Sci. 12 (2022) e1606. https://doi.org/10.1002/wcms.1606.

[79] J.G. Brandenburg, C. Bannwarth, A. Hansen, S. Grimme, B97-3c: A revised low-cost variant of the B97-D density functional method, J. Chem. Phys. 148 (2018) 064104. https://doi.org/10.1063/1.5012601.

[80] M. Dolg, H. Stoll, H. Preuss, Energy-adjusted ab initio pseudopotentials for the rare earth elements, J. Chem. Phys. 90 (1989) 1730–1734. https://doi.org/10.1063/1.456066.

[81] D. Andrae, U. Häußermann, M. Dolg, H. Stoll, H. Preuß, Energy-adjustedab initio pseudopotentials for the second and third row transition elements, Theor. Chim. Acta 77 (1990) 123–141. https://doi.org/10.1007/BF01114537.

[82] B. Metz, H. Stoll, M. Dolg, Small-core multiconfiguration-Dirac–Hartree–Fock-adjusted pseudopotentials for post-d main group elements: Application to PbH and PbO, J. Chem. Phys. 113 (2000) 2563–2569. https://doi.org/10.1063/1.1305880.

[83] K.A. Peterson, D. Figgen, E. Goll, H. Stoll, M. Dolg, Systematically convergent basis sets with relativistic pseudopotentials. II. Small-core pseudopotentials and correlation consistent basis sets for the post-d group 16–18 elements, J. Chem. Phys. 119 (2003) 11113–11123. https://doi.org/10.1063/1.1622924.

[84] T. Leininger, A. Nicklass, W. Küchle, H. Stoll, M. Dolg, A. Bergner, The accuracy of the pseudopotential approximation: non-frozen-core effects for spectroscopic constants of alkali fluorides X.F. (X = K, Rb, Cs), Chem. Phys. Lett. 255 (1996) 274–280. https://doi.org/10.1016/0009-2614(96)00382-X.

[85] M. Kaupp, P. v. R. Schleyer, H. Stoll, H. Preuss, Pseudopotential approaches to Ca, Sr, and Ba hydrides. Why are some alkaline earth MX2 compounds bent?, J. Chem. Phys. 94 (1991) 1360–1366. https://doi.org/10.1063/1.459993.

[86] M. Dolg, H. Stoll, Pseudopotential study of the rare earth monohydrides, monoxides and monofluorides, Theor. Chim. Acta 75 (1989) 369–387. https://doi.org/10.1007/BF00526695.

[87] X. Cao, M. Dolg, Valence basis sets for relativistic energy-consistent small-core lanthanide pseudopotentials, J. Chem. Phys. 115 (2001) 7348–7355. https://doi.org/10.1063/1.1406535.

[88] S. Grimme, S. Ehrlich, L. Goerigk, Effect of the damping function in dispersion corrected density functional theory, J. Comput. Chem. 32 (2011) 1456–1465. https://doi.org/10.1002/jcc.21759.

[89] S. Grimme, J. Antony, S. Ehrlich, H. Krieg, A consistent and accurate ab initio parametrization of density functional dispersion correction (DFT-D) for the 94 elements H-Pu, J. Chem. Phys. 132 (2010) 154104. https://doi.org/10.1063/1.3382344.

[90] N. Mardirossian, M. Head-Gordon, ωB97M-V: A combinatorially optimized, range-separated hybrid, meta-GGA density functional with VV10 nonlocal correlation, J. Chem. Phys. 144 (2016) 214110. https://doi.org/10.1063/1.4952647.

Chapter 6

Conclusions and Future Scope

6.1 Conclusions

In summary, my thesis primarily focuses on the synthesis, characterization, and applications of Ru(II)-NHC complexes, followed by theoretical investigations of Ru(III)-NHC complexes. These Ru(III)-NHC complexes have been used for the synthesis of phosphine-free Ru(II)-NHC complexes having mixed protic- and classical-NHC in one molecule.

In ***chapter 1****,* we briefly describe the structural and electronic study on the NHCs and its ruthenium complexes. Factors effecting the synthesis of NHCs and the importance of protic-NHCs have been discussed.

In ***chapter 2***, we briefly describe the synthesis of Ru(II)-CNC pincer complexes **1** and **2** having protic- or anionic-NHC and classical-NHC in one molecule. These complexes directly compare the structural and electronic properties of protic- or anionic-NHC with the classical NHC ligands. A comparison of molecular structures indicated the metal carbene bond length for anionic-NHC > protic-NHC > classical-NHC. The electrochemical investigation revealed the electron donation tendency for classical-NHC > protic-NHC and anionic-NHC > protic-NHC. The cooperative nature of anionic-NHC ligand was shown by heterolytic H_2 splitting to give the Ru(II)-pNHC hydride complex **3**.

In ***chapter 3,*** we report the synthesis of new phosphine-free Ru(II)-NHC complexes (**3**-**6**) having mixed protic- and classical-NHC in one molecule. These complexes were synthesized from our in-house reported Ru(III)-NHC precursor complex. The new complexes were explored for the catalytic application in the oxidant-free acceptorless dehydrogenation of benzyl alcohol to benzoic acid. The catalytic activity of the phosphine-

based (**1**, **2**) and phosphine-free complexes (**3-6**) was compared. The best results were shown by catalyst **4,** and a maximum TON up to 20000 has been observed.

In ***chapter 4,*** we describe the role of halides in the synthesis of our in-house reported Ru(III)-NHC complexes. We performed experimental and theoretical investigations. The existence of ion-pair interaction was confirmed by the UV-vis and NMR study. At the same time, the DFT calculations were performed to understand the mechanism involved in the synthesis of complexes with different halides. Two plausible pathways were proposed, i.e., the ion-pair pathway and halide coordination pathway. The azolium salts with Cl^- and I^- counteranions follow the ion-pair pathway. In the case of Br^- counteranion, the halide coordination pathway is followed, which results in the mixed halide complex as observed in the experimental study. The DFT result was also validated by an experiment where the Ru(III)-NHC complex could be prepared at a higher temperature by the azolium salt with chloride counteranion.

In ***Chapter 5,*** we describe the DFT-computed mechanistic pathway for the *in situ* conversion of kinetic product Ru(III)-aNHC (**1A**) to Ru(III)NHC (**1B**). We proposed three possible pathways for this conversion, i.e., the pyridine roll-over oxidative addition pathway, pyridine rotation chloride-assisted pathway, and the water-assisted pathway. The water-assisted pathway is the most feasible as it follows a lower-energy route.

6.2 Future Scope

The NHCs known for their stability and strong electron donation tendency make the transition metal complexes highly stable and electron-rich. The protic-NHC ligands provide the metal with a proton-delivering site at the β-position. This β-functionality may provide hydrogen bonding for recognition and orientation of substrates at the metal center. The complexes reported can therefore be further utilized for small molecule activation like CO_2, H_2, CO, etc., and the cooperativity between metal and ligand can be explored. The catalysts, being electron-rich, can also be utilized for water oxidation catalysis.

The synthetic strategy can be utilized for the design of a new series of complexes that provide a comparison between cyclic(alkyl)(amino)carbenes (CAACs), protic-NHCs, anionic NHCs, and classical NHCs.

APPENDIX 1

Table A1

Table A1. Permissions for re-producing the materials

Figure 1.12	Sphere dimensions for steric parameter determination (%V_{Bur}) of NHC ligands	Reproduced from Ref. [40]: Chapter 1, with permission from the American Chemical Society